

# THÈSE

Pour obtenir le grade de  
Docteur

Délivrée par **Montpellier SupAgro**

Préparée au sein de l'école doctorale **GAIA**  
et des unités de recherche **AMAP** et **AGAP**

Spécialité: **Biologie, Interactions,  
Diversité Adaptative des Plantes (BIDAP)**

Présentée par **Raphaël PEREZ**

**Analyzing and modelling the genetic variability  
of aerial architecture and light interception of  
the oil palm (*Elaeis guineensis* Jacq)**

Soutenue le 3 janvier 2017 devant le jury composé de

**M. Gerhard BUCK-SORLIN**  
Professeur, IRHS AgroCampus Ouest

Rapporteur

**M. Christophe PLOMION**  
Directeur de recherche, INRA

Rapporteur

**M. Eric DUFRÊNE**  
Directeur de recherche, CNRS

Examineur

**M. Alain RIVAL**  
Professeur, CIRAD

Examineur & Président du jury

**Mme Evelyne COSTES**  
Directrice de recherche, INRA

Directrice de thèse

**M. Jean DAUZAT**  
Chercheur, CIRAD

Co-directeur de thèse

**M. Jean-Pierre CALIMAN**  
Directeur de recherche, SMARTRI

Invité





*A ma grand-mère*



*The formulation of a problem is often more essential than its solution, which may be merely a matter of mathematical or experimental skill. To raise new questions, new possibilities, to regard old problems from a new angle requires creative imagination and marks real advances in science.*

*Albert Einstein*  
Evolution of Physics (1938)



## Remerciements

Une thèse n'est pas uniquement l'aboutissement d'un travail personnel, mais plutôt le fruit de réflexions et d'interactions avec les personnes qui nous encadrent et nous entourent. Durant ces trois années de thèse, j'ai eu la chance d'avoir un environnement professionnel et personnel optimal, et je tiens ici à remercier toutes les personnes qui y ont contribué et sans qui ce travail n'aurait pu être réalisé.

Mes premiers remerciements s'adressent à Evelyne et Jean, pour la qualité avec laquelle ils ont dirigé ce travail, ainsi que pour toutes les connaissances et compétences qu'ils m'ont apportées, chacun à leur manière. Un grand merci aussi pour la confiance qu'ils m'ont accordée et la liberté avec laquelle j'ai pu entreprendre mes travaux. Ce fut un plaisir de travailler avec vous deux et j'espère sincèrement avoir l'occasion de travailler avec vous à nouveau. Evelyne, merci pour ta disponibilité tout au long de ma thèse, malgré ton emploi du temps toujours très chargé. Merci pour la rigueur scientifique avec laquelle tu as supervisé ce travail, tes conseils, ton efficacité pour me pousser toujours plus loin dans mes réflexions et ton aide précieuse pour la rédaction de ce manuscrit. Jean, un grand merci pour ta gentillesse et ton investissement au quotidien dans ce projet. Merci pour tout le temps que tu as passé dans l'implémentation des modules de simulation, pour les innombrables discussions que nous avons eues autour des résultats et pour tes nombreuses relectures de mes articles. Tes idées sans fin m'ont vraiment poussé à aller explorer de multiples hypothèses et avoir un point de vue critique sur mon travail. Je pense que cela a vraiment été scientifiquement très formateur pour moi, et je t'en remercie profondément.

Je tiens aussi à vivement remercier Benoît, sans qui ce projet de thèse n'aurait jamais vu le jour. J'ai vraiment pris plaisir à interagir avec toi, aussi bien lors de ma précédente expérience au Cirad que tout au long de cette thèse. Merci pour la pertinence de tes remarques et la pédagogie avec laquelle tu as su m'encadrer, tu m'as vraiment donné goût à la modélisation.

Jean-Pierre, je te suis profondément reconnaissant de m'avoir toujours fait confiance au travers de nos différentes collaborations. Un grand merci pour ta disponibilité lors de mes visites en Indonésie et pour m'avoir permis de mener à bien mes expérimentations. Merci aussi pour ton expertise sur le palmier à huile, ta gentillesse et ton sens de l'humour. J'espère vivement que nous pourrions continuer à travailler ensemble.

Merci à toi Hervé, "Monsieur palmier", pour le travail de terrain acharné que nous avons réalisé pour mettre en place le protocole expérimental sous cette chaleur équatoriale, j'en garde un très bon souvenir. Merci aussi pour ta disponibilité et pour les réponses aux multiples questions que j'ai pu te poser sur la culture du palmier à huile.

Gilles, merci pour ton aide précieuse en statistique et la manière avec laquelle tu as su me faire comprendre certains aspects délicats de cette discipline qui en a fait fuir plus d'un.

Merci à Thierry Simonneau, Robert Faivre et Gaëtan Louarn pour l'intérêt que vous avez porté à mon travail aux travers de mes deux comités de thèse. Merci pour vos remarques pertinentes et vos conseils avisés. Robert, merci pour ton investissement dans ce projet et l'aide précieuse que tu m'as apportée dans l'analyse de sensibilité.

Un grand merci à Christophe Plomion et Gerhard Buck-Sorlin pour avoir accepté de rapporter ce manuscrit. Je remercie également vivement Alain Rival et Eric Dufrêne d'avoir accepté d'être examinateurs de cette thèse. Merci notamment à Gerhard et Alain pour les corrections qu'ils ont apportées à mon

manuscrit et qui ont permis d'améliorer la qualité écrite de ce rapport. Enfin merci à l'ensemble des membres du jury pour la qualité de leurs interventions durant ma soutenance.

Ungkapan terima kasih juga saya tujukan kepada rekan-rekan saya di Indonesia atas perhatian dan kerjasama yang menyenangkan. Terima kasih banyak Pak Doni, Pak Fadhli, Pak Bengki, Pak Muklis, Pak Koko, Pak Putra, Pak Zulham atas bantuannya selama proses pengambilan data di lapangan. Terima kasih pula saya sampaikan kepada Ibu Reni, Ibu Eva, Ibu Putri, Ibu Ribka, Ibu Eti, Pak Yong, Pak Pujianto, Pak Sudarto, Pak Wahyu, Pak Naim, Pak Prapto, Pak Farhi, Pak Dedi *my love*, Pak Divo *the rockstar* dan Pak Bram untuk sambutannya yang sangat hangat selama di Libo. Terima kasih juga untuk semua pegawai di kantor Sawit Mas estate dan Libo. Ungkapan terima kasih yang khusus saya sampaikan kepada pondok Libo volley-ball team. Tak lupa ungkapan terima kasih kepada Ibu Rita untuk masakannya yang sangat lezat dan Pak Uli untuk sambutannya yang hangat dan penuh senyuman selama saya tinggal di mess.

Merci à mes deux formidables ex-collocs Ensato-Cirado-docteurs: Hermine et Guillaume. Merci à vous deux pour les supers repas passés à la maison et nos profondes discussions (n'est ce pas Hermine!), sans compter les multiples soirées qui nous replongeaient dans nos années Toulousaines. J'espère que nous pourrons continuer à constamment nous retrouver comme ces deux dernières années.

Merci à Julien pour tous les bons moments passés en ta compagnie lors de notre mission à Palembang, j'espère que nous pourrons un jour nous retrouver de nouveau là bas et partager un bon *rendang* avec un délicieux *sirsak juice*. Raphaël, merci pour les bons moments partagés lors de mes visites à Libo et nos sessions de pêche si fructueuses...

Je voudrais aussi profondément remercier mes collègues et amis d'AMAP. Mat, merci pour ces deux ans passé dans ce si grand bureau, tu as vraiment su me faire partager ta passion pour la botanique, grâce à toi je ne regarde plus les plantes uniquement de mon point de vue d'agronome. Merci aussi pour ces parties de pêche qui nous auront offert de bonnes kefta. Merci à Patoch *le liberao* pour ton sens de l'humour et tes expressions toujours aussi originales, sans compter nos multiples discussions sur les scripts Ru. Merlino, merci pour ta bonne humeur au quotidien et pour ton formidable travail de réparation de la cafetière! Merci aussi à Jimmy l'expert en pêche pour toutes nos virées matinales à Carnon. Muchas gracias a todos mis amigos hispanicos Narco, Luis y Santiago. Narco gracias por los cafes con tus chocolates, las cervezas y tu frances perfecto. Luis *el papito* gracias por tu generosidad y espero que podremos hacer kite-surf juntos el proximo verano. Santiago gracias por los buenos momentos y no olvides Trumping Donald en los EU. Thank you Emil for those 3 years together, I was sure you would finally use R. Merci à tous les autres camarades d'AMAP: Diane, Emilie, Rinny, Awaz, Artémis, Yan, Charlene, Amandine, Valaire, Alexis, Oumarou, Stephane, Jérôme, Yogan, Pierre C., Pierre P., Lorenzo et Bastien. Merci à Fabien pour ta constante bonne humeur, j'étais ravi de partager le bureau avec toi cette dernière année de thèse. Merci aux informaticiens qui m'ont beaucoup aidé durant cette thèse: Sébastien Griffon, François de Coligny, Julien Heurtebize et Philippe Verley. Un grand merci à Nathalie, Nora, Noémie pour leur aide administrative et Yannick pour les recherches bibliographiques. Merci à tous les autres collègues d'AMAP avec qui j'ai pu interagir: Thierry Fourcaud, Jean-François Barczy, Yves Caraglio, Philippe Borianne, Nick Rowe, Yves Dumont et Stéphane Guitet.

Merci aux collègues de l'équipe AFEF pour leur accueil lors de mes nombreuses visites: Alix, Véronique, Isabelle, Lamia, Sébastien, Gerardo, David, Pierre-Éric, Bouhaïde et Jean-Luc. Merci aussi aux autres collègues d'AGAP avec qui j'ai pu interagir avant et durant cette thèse: Anne Clément-Vidal, Sandrine Roques, Serge Braconnier, Marcel de Raissac, Denis Fabre, Sébastien Tisné et David Cross.

Merci à la Z team du Cirad pour ces trois années de compétition intense (et ce titre tant attendu!) et les bons moments passés ensemble: Captain' Momo, Stéphanie, Claire, Gilles, Cricri, Riton, Slo, Renaud, Marc, François et Christophe.

Mes derniers remerciements vont à ma famille, sans qui je n'aurais pu entreprendre un doctorat. Tout d'abord un grand merci à mes parents pour m'avoir toujours soutenu et épaulé durant toutes ces années d'études, et surtout pour m'avoir fait comprendre que le plus important c'est de faire ce que l'on aime. Un grand merci à ma grand mère qui m'a toujours beaucoup encouragé dans mes études. Merci également à mon frangin pour être venu "subir" cette soutenance de thèse. Enfin un immense merci à ma femme Cláudia, avec qui je partage le goût pour la recherche depuis notre rencontre. Merci pour ton soutien, pour les nombreuses discussions que nous avons eues ensemble et qui m'ont souvent débloqué, pour le travail ingrat de relecture de mon anglais et enfin pour les multiples conseils que tu as su m'apporter. Enfin merci pour t'être si bien occupé de notre petite Gabi, qui elle aussi m'a soutenu à sa manière, en faisant très vite toutes ses nuits pour me laisser finir cette thèse, à tête reposée.





## Abstract

The development of new breeding strategies to find more sustainable and productive systems is a major challenge to cope with ceaseless increasing demands for vegetable oils, notably palm oil. Optimizing plant architecture to increase radiation interception efficiency could be an option for enhancing potential oil palm production. Indeed, studies in cereals showed great improvement of yields by altering plant architecture, in combination with agronomic practices. By analogy, we proposed to investigate the influence of oil palm architecture on the capacity of the plant to intercept light, by using 3D reconstructions and model-assisted evaluation of radiation-use efficiency. The first objective of this study was to analyse and model oil palm architecture and light interception taking into account genetic variability. A second objective was to explore the potential improvement in light capture and carbon assimilation by manipulating oil palm leaf traits and propose architectural ideotypes.

Data were collected in Sumatra, Indonesia, on five progenies (total of 60 palms), in order to describe the aerial architecture from leaflet to crown scales. Allometric relationships were applied to model these traits according to ontogenetic gradients and leaf position within the crown. The methodology allowed reconstructing virtual oil palms at different stages over plant development. Additionally, the allometric-based approach was coupled to mixed-effect models in order to integrate inter and intra progeny variability through progeny-specific parameters. The model thus allowed simulating the specificity of plant architecture for a given progeny while including observed inter-individual variability. The architectural model, once parameterized for the different progenies, was then implemented in AMAPstudio to generate 3D mock-ups and estimate light interception efficiency, from individual to stand scales.

Model validations were performed at different scales. Firstly at organ scale, the geometry of the stem, the leaves and the leaflets were compared between virtual mock-ups and actual plants measured in the field. Secondly, at plant scale with indicators derived from terrestrial laser scanning (TLS) to assess crown dimensions and porosity. These indicators integrated topological and geometrical information related to the amount of light intercepted by an individual. Finally, validations were performed at plot scale using hemispherical photographs (HP) to assess the variability of canopy openness for the five studied progenies.

Significant differences in leaf geometry (petiole length, density of leaflets and rachis curvature) and leaflets morphology (gradients of leaflets length and width) were detected between and within progenies, and were accurately simulated by the modelling approach. The comparison of plant area obtained from TLS and virtual TLS highlighted the capacity of the model to generate realistic 3D mock-ups. The architectural variabilities observed at plot scale between and within progenies were also satisfactory simulated. Finally, light interception estimated from the validated 3D mock-ups showed significant variations among the five progenies.

Sensitivity analyses (Morris method and metamodeling approach) were then performed on a subset of architectural parameters in order to identify the architectural traits impacting light interception efficiency and potential carbon assimilation over plant development. Daily carbon assimilation was estimated with a photosynthesis model coupled to the radiative balance model, which enabled to integrate the temporal and spatial variations of photosynthetic organ irradiances.

The most sensitive parameters over plant development were those related to leaf area (rachis length, number of leaflets, leaflets morphology), although fine attribute related to leaf geometry showed increasing influence when canopy got closed. In adult stand, optimized carbon assimilation was estimated on plants presenting a leaf area index (LAI) between 3.2 and 5.5  $\text{m}^2.\text{m}^{-2}$ , with erect leaves, short rachis and petiole and high number of leaflet on rachis. Four ideotypes were identified with respect to carbon assimilation, exhibiting specific geometrical features that optimize light distribution within plant crown and reduce mutual shading among plants.

In conclusion, this study highlighted how a functional-structural plant model (FSPM) can be used to virtually explore plant biology. In our case, the 3D model of oil palm, in its conception and its application, enabled the detection of the architectural traits genetically determined and influencing light

interception. The limited number of traits revealed in the sensitivity analysis and the combination of traits proposed through ideotypes could guide future breeding programs. Forthcoming work will be dedicated to integrate in the modeling approach other physiological processes such as stomatal conductance and carbon partitioning. The improved FSPM could then be used to test different scenarios, for instance in climate change context with low radiations or frequent drought events. Similarly, the model could be used to investigate different planting patterns and intercropping systems and propose new multi-criteria ideotypes of oil palm.

**Keywords:** carbon assimilation, FSPM, hemispherical photographs, ideotype, light interception efficiency, mixed-effect model, plant architecture, progeny, terrestrial LiDAR, three-dimensional reconstruction, sensitivity analysis

## Résumé

Le développement de nouvelles voies d'amélioration génétique vers des systèmes plus productifs et respectueux de l'environnement est un défi majeur pour répondre à la demande croissante en huiles végétales, notamment en huile de palme. L'une des options pour améliorer la performance de ces systèmes agricoles serait d'optimiser l'architecture des plantes pour augmenter l'efficacité de l'interception du rayonnement. En effet, des études menées sur les céréales ont permis d'améliorer les rendements en utilisant des architectures spécifiques de plantes en association avec des techniques culturales. Suivant une stratégie similaire, cette étude propose d'analyser l'influence de l'architecture du palmier à huile sur sa capacité à intercepter la lumière, en se basant sur des reconstructions 3D de palmiers et en établissant un bilan radiatif sur ses structures végétales reconstruites *in silico*. Le premier objectif de l'étude était de caractériser et modéliser la variabilité génétique de l'architecture du palmier à huile et de son interception lumineuse. Dans un deuxième objectif l'amélioration potentielle de l'interception de la lumière et de l'assimilation carbonée a été évaluée en modifiant les traits morphologiques et géométriques des feuilles et des idéotypes architecturaux de palmiers à huile ont été proposés.

Les données ont été recueillies à Sumatra (Indonésie) pour décrire l'architecture aérienne à différentes échelles (des folioles jusqu'à la couronne foliaire) sur cinq descendances de palmiers, ou progénies (60 individus). Des relations allométriques ont été utilisées pour modéliser les traits architecturaux en fonction de gradients ontogénétique et de topologie des feuilles dans la couronne. La méthode permet de reconstruire des palmiers à huile virtuels à différents âges au cours du développement. De plus, l'approche allométrique a été couplée à des modèles à effets mixtes pour intégrer au travers de paramètres la variabilité entre et au sein des cinq progénies. Le modèle permet ainsi de simuler les spécificités architecturales des cinq progénies en incluant les variabilités entre individus observés. Le modèle architectural, paramétré pour les différentes progénies, a ensuite été implémenté dans AMAPstudio pour générer des maquettes 3D de palmiers et ainsi estimer leur interception lumineuse, de l'individu à la parcelle entière.

La validation du modèle a été réalisée à différentes échelles. Dans un premier temps, à l'échelle des organes, les géométries du stipe, des feuilles et des folioles ont été comparées entre les plantes virtuelles et les plantes observées sur le site d'étude. Dans un deuxième temps, à l'échelle de la plante à partir d'indicateurs liés aux dimensions et aux porosités des couronnes, établis à partir de mesures de LiDAR terrestre (TLS). Ces indicateurs ont permis d'intégrer les informations topologiques et géométriques liées à la quantité de lumière interceptée par individu. Enfin, à l'échelle du couvert, des photographies hémisphériques (HP) ont été collectées pour évaluer la variabilité de la fermeture des canopées des cinq progénies étudiées, puis comparées à des estimations de fractions de trouées calculées sur les maquette reconstruites.

Les résultats de ces analyses ont révélé des différences significatives entre et au sein des progénies, dans la géométrie des feuilles (longueur du pétiole, densité de folioles sur le rachis, et courbure du rachis) et dans la morphologie des folioles (gradients de longueurs et largeurs le long du rachis). La comparaison des indicateurs estimés par TLS et TLS virtuels réalisés *in silico* souligne la capacité du modèle à générer correctement la surface d'interception de la couronne. Les comparaisons ces caractéristiques entre plantes virtuelles et plantes observées montrent que les maquettes 3D sont comparables aux observations menées sur le site d'étude. Les variabilités architecturales observées en champ entre et au sein des progénies sont aussi correctement simulées. Enfin, les différentes progénies montrent des efficacités distinctes de l'interception lumineuse.

Des analyses de sensibilité (méthode de Morris et approche de méta-modélisation) ont ensuite été réalisées pour identifier les traits architecturaux influençant l'interception lumineuse et l'assimilation potentielle à différents âges de la plante. L'assimilation journalière de carbone a été estimée à l'aide d'un modèle de photosynthèse couplé au modèle de bilan radiatif, et a ainsi permis d'intégrer à l'échelle de la plante entière les variations temporelles et spatiales de l'éclairement des organes photosynthétiques.

Les paramètres les plus sensibles au cours du développement furent ceux reliés à la surface totale foliaire

(longueur des rachis, nombre de folioles, morphologie des folioles), mais les attributs géométriques plus fins de la feuille ont montré un effet croissant avec la fermeture de la canopée. Sur un couvert adulte, l'optimum en assimilation carbonée est atteint pour des indices de surfaces foliaires (LAI) entre 3,2 et 5,5  $\text{m}^2 \cdot \text{m}^{-2}$ , avec des feuilles érigées, de courts pétioles et rachis et un nombre important de folioles sur le rachis. Quatre idéotypes architecturaux pour l'assimilation carbonée ont été proposés et présentent des combinaisons spécifiques de traits géométriques, limitant l'ombrage mutuel des plantes et optimisant la distribution de la lumière dans la couronne.

En conclusion, cette étude met en évidence comment un modèle structure-fonction de plante (FSPM) peut être utilisé pour explorer virtuellement la biologie des plantes. Dans notre cas d'étude, le modèle 3D de palmiers à huile, dans sa conception et son application, a permis de détecter les traits architecturaux génétiquement déterminés et influençant l'interception lumineuse. Ainsi, le nombre limité de traits dégagés par l'analyse de sensibilité ainsi que les combinaisons de traits révélées au travers des idéotypes pourraient être pris en compte dans de futurs programmes de sélection. En perspective, des travaux dédiés à intégrer dans ce modèle d'autres processus physiologiques, tels que la régulation de la conductance stomatique et le partitionnement du carbone dans la plante, sont à envisager. Ce nouvel FSPM pourrait alors être utilisé pour tester différents scénarii, comme par exemple dans un contexte de changement climatique avec de faibles radiations et des périodes de sécheresse fréquentes. De même, ce modèle pourrait être utilisé pour étudier différentes configurations de plantation et des systèmes de cultures intercalaires, et ainsi proposer de nouveaux idéotypes multicritères.

**Mots clés :** assimilation carbonée, FSPM, photos hémisphériques, idéotype, efficience d'interception de la lumière, modèles à effets mixtes, architecture végétale, progénie, LiDAR terrestre, reconstruction 3D, analyse de sensibilité

# Contents

<b>I</b>	<b>Introduction</b>	<b>17</b>
1	Oil palm: state of the art . . . . .	17
1.1	Botanical description . . . . .	17
1.2	Geographical distribution and global production . . . . .	19
1.3	Ecophysiology . . . . .	19
1.4	Selection and breeding . . . . .	21
1.5	Palm oil among vegetable oils . . . . .	22
1.6	Future demand . . . . .	22
2	Scientific context . . . . .	23
2.1	Plant breeding and quantitative genetics . . . . .	23
2.2	The ideotype concept . . . . .	23
2.3	Plant architecture: description and modelling . . . . .	24
2.4	Using plant modelling to evaluate and predict plant performances . . . . .	26
2.5	Retrospect of oil palm models and their applications . . . . .	29
3	Objectives and approaches of the thesis . . . . .	31
4	Experimental site and plant material . . . . .	33
4.1	Experimental site . . . . .	33
4.2	Plant material . . . . .	33
<b>II</b>	<b>The Architectural Model</b>	<b>37</b>
1	Introduction . . . . .	38
2	Material and methods . . . . .	39
2.1	Architectural description . . . . .	39
2.2	Model description . . . . .	40
2.3	Model calibration . . . . .	43
2.4	Model simulation and validations . . . . .	46
3	Results . . . . .	46
3.1	Progeny effect at 47 months after planting . . . . .	46
3.2	Progeny and individual effects on allometry . . . . .	47
3.3	Assessment of model reconstruction . . . . .	50
4	Discussion . . . . .	50
4.1	Genetic control of plant architecture . . . . .	50
4.2	Using allometry to analyse genotypic variability . . . . .	54
4.3	Model simulation and accuracy of 3D reconstruction . . . . .	55
4.4	Exploration of genotypic performance using 3D reconstruction . . . . .	55
5	Supplementary material . . . . .	57

<b>III</b>	<b>Model validation and light interception efficiency among oil palm progenies</b>	<b>61</b>
1	Introduction . . . . .	63
2	Material and Method . . . . .	65
2.1	Experimental site and plant material . . . . .	65
2.2	Data collection . . . . .	65
2.3	Virtual palms modelling . . . . .	65
2.4	Generating virtual TLS (VTLS) and virtual hemispherical photographs (VHP) . .	66
2.5	Validation procedure using indicators related to plant and canopy structure . . . .	67
2.6	Assessment of light interception efficiency per progeny . . . . .	69
2.7	Statistical analyses . . . . .	70
3	Results . . . . .	71
3.1	Validation of 3D reconstructions at plant scale with TLS-derived indicators . . . .	71
3.2	HP-derived indicators to evaluate and validate architectural variabilities at plot scale	73
3.3	Correlation between simulated light interception and VTLS- and VHP-derived indicators . . . . .	75
4	Discussion . . . . .	78
4.1	Scope of TLS and HP indicators for the assessment of 3D models . . . . .	78
4.2	Using HP and TLS indicators to validate the architecture modelling approach with respect to light interception . . . . .	79
4.3	Genetic effect on light interception . . . . .	80
4.4	Conclusion . . . . .	81
5	Supplementary Material . . . . .	82
<b>IV</b>	<b>Sensitivity analysis and Ideotype design</b>	<b>87</b>
1	Introduction . . . . .	89
2	Material and Method . . . . .	90
2.1	Overall strategy . . . . .	90
2.2	Architectural model . . . . .	90
2.3	Radiative balance model . . . . .	92
2.4	Carbon assimilation model . . . . .	94
2.5	Sensitivity analyses . . . . .	95
3	Results . . . . .	97
3.1	Sensitivity of architectural parameters over plant age . . . . .	97
3.2	Comparing experimental vs. field calibrated mock-ups . . . . .	99
3.3	Sensitivity analysis on adult stand . . . . .	99
3.4	Ideotyping architecture (architectural traits) with regards to carbon assimilation .	102
4	Discussion . . . . .	106
4.1	Viability, benefits and limitations of the modelling approach . . . . .	106
4.2	Designing architectural ideotypes for oil palm . . . . .	108
4.3	Perspectives for oil palm breeding . . . . .	109
5	Supplementary Material . . . . .	111
<b>V</b>	<b>General discussion</b>	<b>117</b>
1	Retrospect on the general problematic . . . . .	117
1.1	Scientific framework . . . . .	117
1.2	Conceptual basis of an oil palm ideotype . . . . .	118
2	Three-dimensional representations of oil palm . . . . .	118
2.1	Conception and formalism of the 3D modelling approach . . . . .	118
2.2	Assessing 3D mock-up of oil palm . . . . .	120

3	Enhancing light interception and potential carbon acquisition of oil palm . . . . .	121
3.1	Difference in light interception efficiency among progenies . . . . .	121
3.2	Designing ideotypes to optimise light interception and carbon assimilation . . . . .	122
3.3	Improving the carbon assimilation model . . . . .	123
3.4	Genetic control of oil palm architecture . . . . .	124
4	Towards a FSPM simulating yield of oil palm . . . . .	125
5	Conclusions . . . . .	126
<b>A</b>	<b>Protocol for measuring aerial architectural traits of <i>Elaeis guineensis</i> Jacq.</b>	<b>129</b>
<b>B</b>	<b>Field replicates comparison and sampling assessment</b>	<b>143</b>
	<b>Bibliography</b>	<b>149</b>





# Chapter I

## Introduction

### 1 Oil palm: state of the art

#### 1.1 Botanical description

The African oil palm (*Elaeis guineensis* Jacq.) belongs to the monocotyledonous family of Arecaceae, together with the coconut palm (*Cocos nucifera*) and the date palm (*Phoenix dactylifera*), and it was first described by Nicholas Joseph Jacquin in 1763. It is one of the two species composing the genus *Elaeis*, the other being the American oil palm, *E. oleifera*. Oil palm is a perennial plant which architecture follows the Corner model [Hallé and Oldeman, 1970], which is characterized by a mono-axial shoot (the stem) that produces phytomers in regular succession (Fig. I.1). The phytomer consists of a node to which a leaf and an inflorescence (male or female, when abortion does not occur) are attached [Henry, 1958]. The number of phytomers produced annually varies from 30 to 40 for young palms and 20 to 25 for mature palms. The crown is made of 60 expanded leaves for young palms and 30 to 45 for adult oil palms. More than 50 hidden leaves are developing underneath a unique apical meristem (Fig. I.2 A). Leaves are disposed according to a radial symmetry with a phyllotaxis varying from 135.7 to 137.5 degrees. Due to this regular phyllotaxis, it is possible to distinguish spirals of leaves (parastichies) and determine the order (rank) with which leaves were emitted. The order 8 parastichy is the reference to identify leaf rank (Fig. I.2 B). Leaf rank 1 is the youngest leaf fully open (unfolded) leaf at the top of the stem (leaves below rank one are called spears). As a result, the topological position of a leaf within the crown can be used to estimate its age.

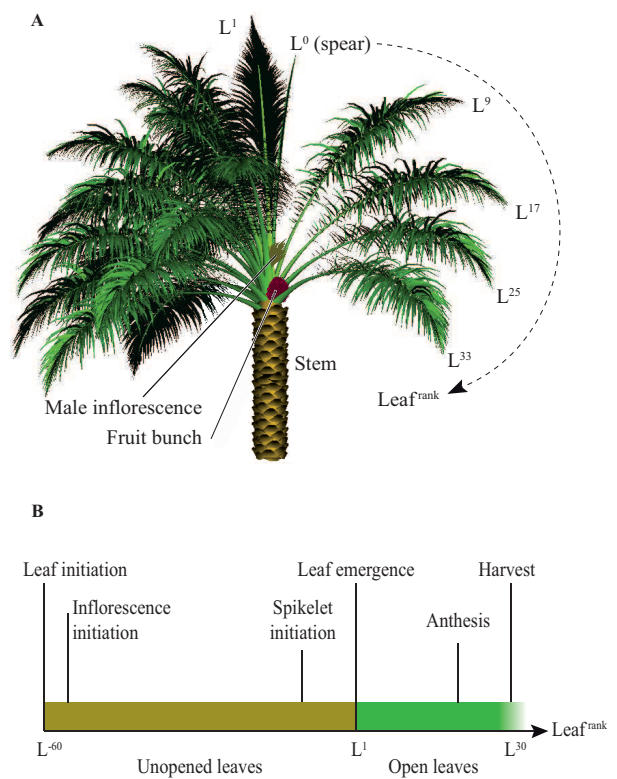


Figure I.1: A) Representation of oil palm architecture following the Corner model. B) Development stages of oil palm leaves and inflorescences at mature stage. (credits R. Perez and J. Dauzat)

One month after germination, two cataphylls are produced before the first green leaf appears. During the following five months, seedlings emit about one leaf with a unique lamina per month. Pro-

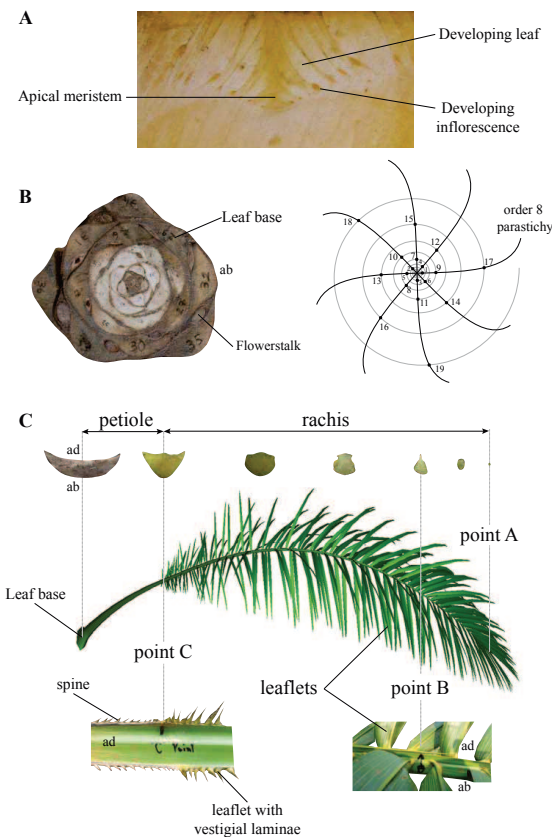


Figure I.2: A) Longitudinal section of apical dome of the stem where leaves and inflorescences are initiated by the apical meristem. B) Cross section of apical dome of the stem. Leaves are organized with a radial phyllotaxy as represented on the right scheme. Numbers represent ranks of the expended leaves. C) Oil palm leaf with detailed evolution of cross-sections along petiole and rachis (top) and zoom on leaf at reference points (bottom). ad: adaxial face, ab: abaxial face. (credits H. Rey and R. Perez)

gressively, leaf shape changes to become pinnate. Mature oil palm leaves are compound leaves with an even-pinnate arrangement. The leaf is composed by a petiole and a rachis that bears leaflets, also called pinnae (Fig. I.2C). Both sides of the leaves have almost a similar number of leaflets but their disposition along the rachis is irregular. Pinnae are clustered along the rachis and spreading in different planes. Leaflets belonging to a same cluster can be either pendulous, horizontal or erect [Henderson,

2002]. [Lecoustre and Jeager, 1989] observed that leaflets can be alone or gathered by groups of 2 to 4. At adult stage, leaf length can reach 10 meters and bears approximately 250 to 350 leaflets [Corley and Tinker, 2016]. Four years separate leaf initiation from senescence, with two years during which the leaf is emerged and can photosynthesize (Fig. I.1B).

The root system of oil palm is fasciculate, i.e. thousands of adventitious roots are spreading from a bole at stem basis. Initially, oil palm seedling presents an orthotropic tap root, or radicle, which will progressively disappear to establish structured and hierarchized roots [Jourdan and Rey, 1997a]. Four levels of root differentiation were described (RI to RIV), the two firsts order playing a role of anchorage and lateral spreading while the finer roots (RIII and RIV) exploit soil resources.

The oil palm is monoecious, i.e. male and female inflorescences occur separately in the same plant. Reproduction is thus allogamous with cross-pollination. First inflorescences produced by young palms are mainly male before female inflorescence production occurs in smaller proportions than male inflorescences (female inflorescences representing around 30% to 50% of total inflorescences on adult plants [Corley and Tinker, 2016]). For both sexes, the development of oil palm inflorescences lasts around 2 to 3 years from initiation to maturity [Adam et al., 2011]. Each inflorescence is composed of spikelets spirally disposed around a flowerstalk and enclosed in two fibrous spathes before anthesis (Fig. I.3). The number of spikelets increases with plant age from 60 at 3-year-old up to 150 at 10-year-old, and high variation exists between palms. A male spikelet may bear up to 785 flowers while a female spikelet bears less than 30 flowers. A female inflorescence requires 4.5 to 6 months after anthesis to reach maturity, i.e. a fruit bunch. Fruit-set is generally low (30% to 60% of the flowers developed into fruit) and well-set bunches carry on average 1500 to 2000 fruits [Corley and Tinker, 2016].

A fruit bunch (fresh fruit bunch: FFB) weighs around 12 kg and approximately 10 bunches can be produced for a mature palm per year in optimal conditions. Fruits represent 60% to 70% of the FFB and are sessile drupes with a mesocarp and a kernel from which two kinds of oils are extracted.

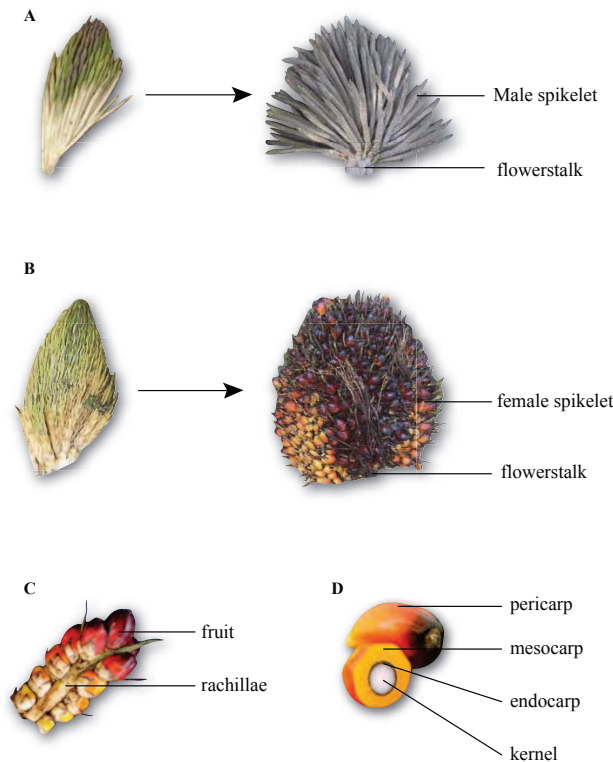


Figure I.3: A) Male inflorescence before anthesis (left) and after anthesis (right). B) Female inflorescence before anthesis (left) and fruit bunch at harvest (right). C) Spikelet of female inflorescence. D) Oil palm fruit. (credits H. Rey and R. Perez)

The oil content in the mesocarp represents 40% to 60% and constitutes the main source of oil palm designated as crude palm oil (CPO). The kernel contains around 50 % of oil, called palm kernel oil (PKO), which presents a different composition than the CPO and is comparable to coconut oil in fatty acid composition.

## 1.2 Geographical distribution and global production

*E. guineensis* is a tropical plant originated from the Gulf of Guinea and is naturally abundant in African rainforest. Due to its high productivity, oil palm is now largely exploited in all the regions that offer suitable conditions for its cultivation. Oil

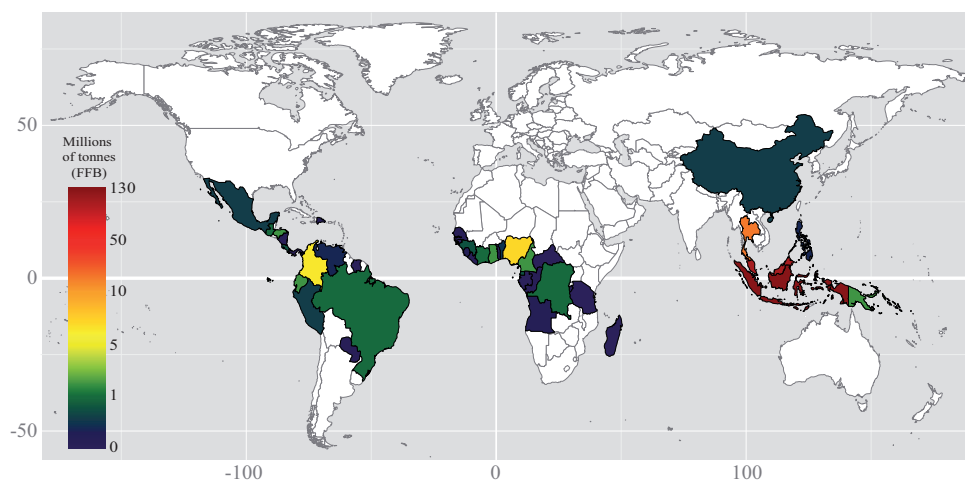
palm plantations are geographically distributed in tropical lowlands in Africa, South-East Asia and South and Central America (Fig.I.4). *E. guineensis* is exploited in Africa and South East Asia while *E. oleifera* is exploited in Latin America as it has demonstrated resistance to local diseases (such as bud rot). Optimal growing conditions of oil palm correspond to 2000-2500 mm of annual rainfall with no or limited dry seasons; mean annual temperature between 26-29°C and 16-17 MJ.m<sup>-2</sup> of daily solar radiation [Corley and Tinker, 2016].

Plantations of oil palm are usually established following an equilateral design at a density of 130-150 trees per hectare, and are maintained for 25-30 years on average. Seedlings are grown in nursery for 12 to 18 months before field planting. In industrial plantation, legume cover (mainly *Pueraria phaseoloides* and *Mucuna pruriens*) is established before planting to avoid soil erosion, fix nitrogen in soils and protect young palms from harmful weeds. Cover plants remain in young plantation until the available light under the canopy is insufficient for their growth. During the six first months of production, bunches removal is often recommended to enhance vegetative growth and allow larger bunches yield starting from three years-old plants [Corley and Tinker, 2016]. The main producing countries are Indonesia, Malaysia, Thailand, Nigeria and Colombia, which produce for their own consumption as for the main consumer countries (Fig. 4B). In 2013, the production reached 54 million tonnes of oil, Indonesia and Malaysia representing 85% of this production. At global scale, almost half of palm oil production comes from smallholders; some countries producing almost exclusively from smallholding (90% in Ghana), while others countries are dominated by industrial production (60% in Indonesia) [Rival and Levang, 2014]. The main consumers are India, Indonesia, China and Europe, which represented 65% of the global consumption in 2013.

## 1.3 Ecophysiology

As for the majority of crops, the main factors limiting oil palm growth are light, water and nutrients. Oil palm is a perennial crop and, as a result, variation in microclimatic events, resources availability and occurrences of abiotic and biotic stresses during

A



B

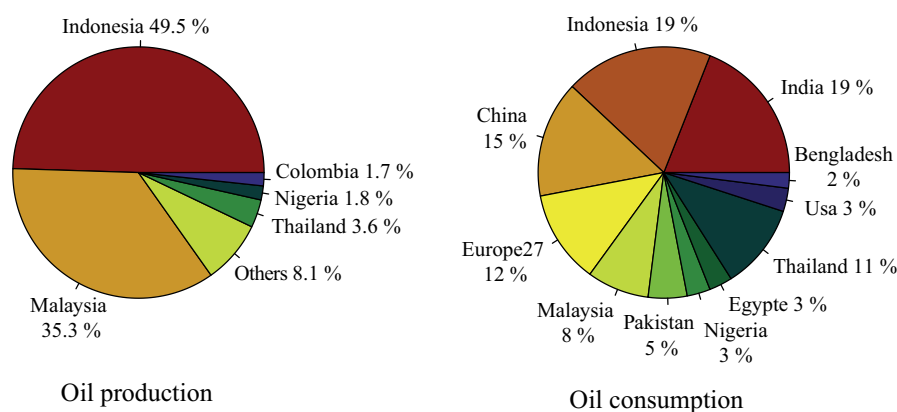


Figure I.4: A) Geographical distribution of oil palm production in the world (FAOSTAT 2014). B) Distribution of the main producing and consuming countries of palm oil in the world. (FAOSTAT 2013).

a given period may induce fluctuation of production afterwards [Legros et al., 2009a, Legros et al., 2009b, Legros et al., 2009c]. Oil palm is sensitive to insufficient water supply or dry periods, mainly when the vapour pressure deficit (VPD) rises above 1.8 kPa, which leads to stomata closure, and subsequently reduces carbon assimilation [Dufrêne and Saugier, 1993]. Oil palm limits transpiration during water stress period by decreasing new leaves appearance and inducing quick stomatal closure [Dufrêne et al., 1992]. The mobilisation of non-structural carbohydrate (NSC) reserves [Legros et al., 2009c]

also allows oil palm to control seasonal source-sink imbalances. As a result, oil palm can be cultivated in suboptimal regions, but the physiological adjustments involved in buffering environmental constraints cause limitation in oil palm productivity. Indeed, several studies pointed out variations in sex ratio (number females inflorescences to total inflorescences) and inflorescence abortion rate in relation with water stress and assimilates availability [Durand-Gasselin et al., 1999, Pallas et al., 2013b], resulting in a lower number of bunches produced annually.

## 1.4 Selection and breeding

Genetic origins of the cultivated *Elaeis guineensis* Jacq are very narrow. Three main morphotypes have been identified thanks to the distinct morphology of their fruit: *dura*, *pisifera* and *tenera*, the latter being a *dura* x *pisifera* intraspecific hybrid (Fig. I.5).

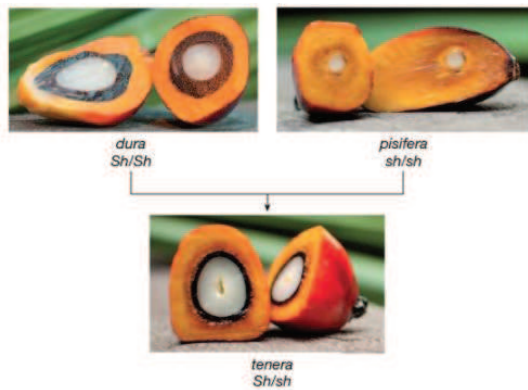


Figure I.5: *dura*, *pisifera* and *tenera* fruit forms with the corresponding allele of the Shell gene (credit: Singh *et al.*, 2013).

The *dura* type bears fruits with a thick endocarp while *pisifera* has no endocarp resulting in important pulp to fruit ratio and infertility. *Dura* types were historically selected and improved from four palms introduced in South-East Asia (called Deli *dura*) while the African *pisifera* were originated from only two palms and improved in Africa. The discovery of the inheritance of *shell* thickness gene [Beirnaert and Vanderweyen, 1941, Singh *et al.*, 2013a] lead to the exploitation of the *tenera* cross as it presents 30% more oil content than *duras*. Since then breeding programs have been mainly based on reciprocal recurrent selection (RRS) between Deli and African material [Cochard *et al.*, 2009] (Fig. I.6). Such strategy implies keeping and improving *dura* and *pisifera* populations separately and requires testing populations of full sib family. A full sib family, also called progeny, is obtained from a unique bunch pollinated by the same male inflorescence. Biparental crosses between heterozygous parents conduct breeders to deal with progenies presenting large intra-genotypic variability. Development of clones could reduce the time needed

in breeding schemes but still face some difficulties for large-scale propagation [Corley and Tinker, 2016]. Indeed, during plant tissue culture, changes in DNA methylation cause developmental abnormalities. This epigenetic phenomenon produces clones with phenotypes which differ from the single donor genotype (also called ortet), characterized by abnormal feminization of male flowers leading to partial or complete flower sterility. This abnormality, called the 'mantled' phenotype, represents in oil palm around 5% of somatic embryo-derived clones [Jaligot and Rival, 2015].

Selection is mainly based on integrative traits related to yield components so far, such as weight and number of bunches, and tolerance to biotic and abiotic stresses (diseases, drought, nutrients). *E. oleifera* x *E. guineensis* interspecific hybrids are likely to enlarge agronomic potential of oil palm cultivation [Barcelos *et al.*, 2015], and the rapid evolution of genomic technics together with the recent oil palm genome sequencing [Singh *et al.*, 2013b] would probably pave the way to develop new breeding criteria.

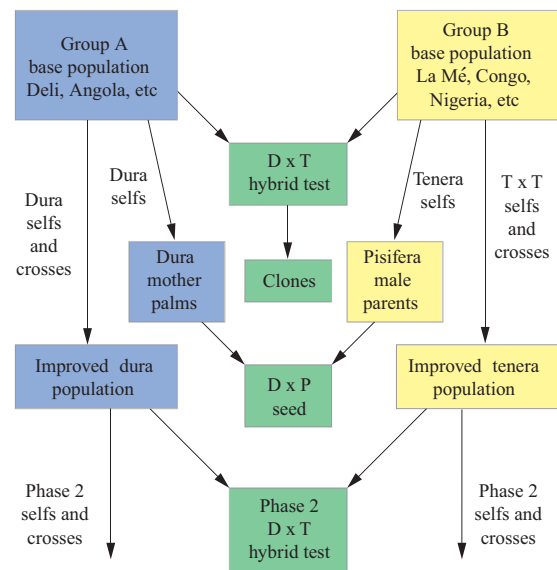


Figure I.6: Schema of the reciprocal recurrent selection applied on oil palm (source: [Corley and Tinker, 2016] redrawn from [Baudouin *et al.*, 1997])



## 1.5 Palm oil among vegetable oils

Oil palm (*E. guineensis*) has the highest productivity among cultivated oil crops, with a global average oil yield of 3.8 tonnes.ha<sup>-1</sup> compared to less than 1 tonne.ha<sup>-1</sup> for the others leading oilseeds crops (Rival and Levang, 2014). As a result, although it occupies less than 7% (19 Mha) of agricultural land dedicated to vegetable oil, oil palm is the first source of vegetable oils in the world, representing more than a third of global production (Fig. I.7). Oil palm has the lowest cost of production among vegetable oils even if it requires relatively intensive labour (labour costs being low in South East Asia). The low cost of its production also remains in the limited amount of pesticide applied in comparison to other crops such as soybean. Palm oil composition is balanced between saturated (mainly palmitic acid) and unsaturated fatty acids, making it solid at ambient temperature. This property has raised interest in agri-food industries to limit the harmful effect of partial hydrogenation of vegetable oils. The chemical properties of palm oil (together with palm kernel oil) also raised interest for oleochemical industries. Contrarily to other vegetable oils, the part of palm oil used in biodiesel remains lower than 10%, although it is growing fast [Corley and Tinker, 2016].

## 1.6 Future demand

Vegetable oil production has continuously increased thanks to cropland development, agronomical practices and genetic improvement. Even so, future global demand, estimated to reach 240 million tonnes by 2050 [Barcelos et al., 2015], needs to be fulfilled. Developing countries have known rapid expansion of their crops to satisfy not only their own consumption but also to supply global demand (Fig. I.8). The crops mainly cultivated in such developing countries were soybean in South America and oil palm in South East Asia. Malaysia first developed oil palm at large scale in the 60's, followed by Indonesia which became the first palm oil producer, reaching nowadays half of the global production. To cope with steadily increasing consumer demand, Indonesia and Malaysia have thus implemented a rapid expansion of oil palm plantations, often to the detriment of vulnerable forestry system and/or

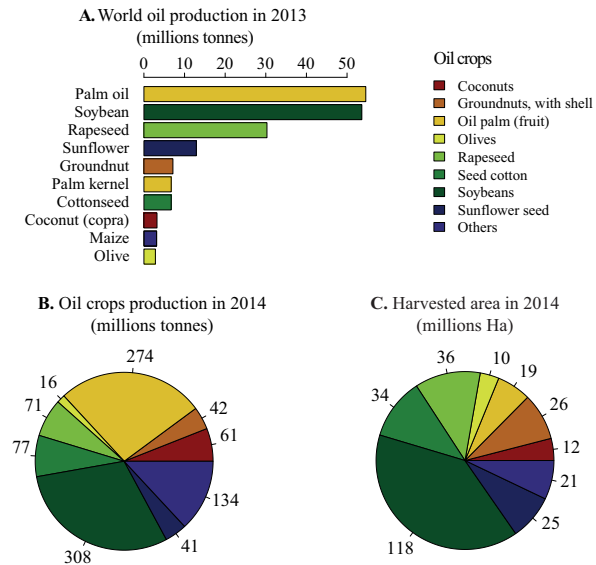


Figure I.7: Oil and crops production and harvested area of the principal vegetable oil crops in the world (source: FAOSTAT 2014).

sometimes in unsuitable lands. The production of

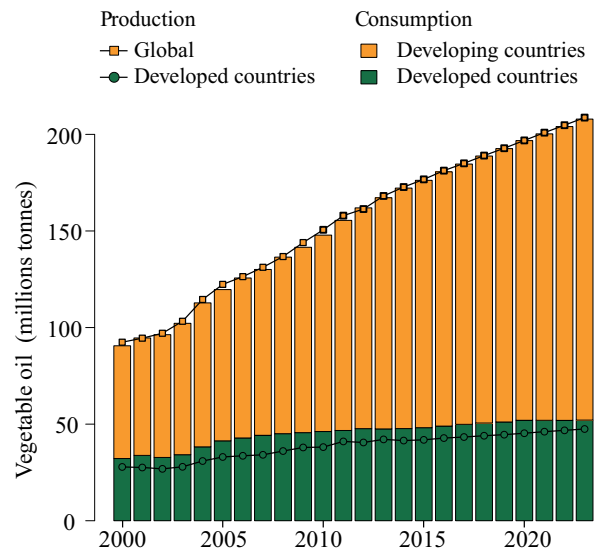


Figure I.8: Production and consumption of vegetable oils (Source: OECD-FAO Agricultural Outlook 2014-2023).

the two world leaders is projected to grow by 1.9%

per year on average, which is a slower rate compared to the last 30 years, as a result of land restrictions, environmental constraints and labour costs becoming more constraining [OECD/FAO, 2014]. In addition, recent but recurrent manifestations of extreme climate phenomena in South East Asia, like drought, result in high variation in oil palm production over years [Corley and Tinker, 2016]. As a matter of fact, Indonesian and Malaysian authorities now face the challenge of developing strategies which allow oil production growth while limiting environmental damages.

## 2 Scientific context

### 2.1 Plant breeding and quantitative genetics

Quantitative genetics is the study of the genetic control of quantitative characters, i.e. complex characters that, conversely to qualitative characters, present a continuous range of values (yield for instance). Quantitative characters are controlled by several genes with relatively low effect on the phenotype when analyzed separately [Hill, 2010]. Whatever the effect of a gene on the phenotype, the segregation of its alleles must follow Mendel laws. The effect of the variation of a unique gene is hardly perceptible on the phenotype. However, when considering the segregation of all the genes controlling a quantitative character within a population, it is possible, using statistical methods, to explain the part of phenotypic variation due to genotypic variation. For an individual  $i$ , the value of a quantitative character, or phenotype ( $P_i$ ), results from its genotype ( $G_i$ ), its environment ( $E_i$ ) and the interaction between them ( $G_i \times E_i$ ):

$$P_i = \mu + G_i + E_i + G_i \times E_i \quad (\text{I.1})$$

with  $\mu$  being the expected phenotypic value of the population.  $G_i$  corresponds to the genotypic value of the individual  $i$ . The value of  $G_i$  depends on the studied population and is the sum of the additive ( $A_i$ ), the dominant ( $D_i$ ) and epistatic effects ( $I_i$ ) of the individual:

$$G_i = A_i + D_i + I_i \quad (\text{I.2})$$

$A_i$  is also called the breeding value, and represents the mean effect of an individual on its descendants (progeny).  $D_i$  is the interaction effect between the alleles of a same gene and  $I_i$  is the interaction effect between alleles of two different genes. Based on this general genetic model, it is possible to estimate the genetic value of a genotype considering both additive and dominant effects. Under hypotheses of independency between  $A$ ,  $D$  and  $E$ , the phenotypic variance equals  $\sigma_p^2 = \sigma_g^2 + \sigma_e^2$  with  $\sigma_g^2 = \sigma_a^2 + \sigma_d^2$ . Hence, by characterizing both phenotype and genotype of all the individuals of a population, it is thus possible to estimate the broad-sense heritability of a character ( $H^2$ ), which is defined as the fraction of the genotypic variance to phenotypic variance, and narrow-sense heritability ( $h^2$ ) when considering only the additive part of the genetic variance :

$$H^2 = \frac{\sigma_g^2}{\sigma_p^2} \quad (\text{I.3})$$

$$h^2 = \frac{\sigma_a^2}{\sigma_p^2} \quad (\text{I.4})$$

Heritabilities can be estimated by statistical analyses, by analysis of variance (ANOVA), but mixed-effect models with restricted maximum likelihood (REML) method are usually applied when dealing with complex pedigree (see [Cros, 2015] for a review).

Quantitative genetics thus offers the possibility to investigate the influence of genotype on phenotype, and to identify the plants that present interesting breeding values to integrate them in breeding programs. However, such strategy relies on the possibility of clearly characterizing both genotype and phenotype. Biotechnological tools now enable a rapid and complete description of genotypes, but characterizing phenotypes (phenotyping) is presently a bottleneck, due to the complexity of measuring some phenotypic traits.

### 2.2 The ideotype concept

The notion of ideotype was first proposed by Donald [Donald, 1968] as an alternative to empirical selection relying on yield. An ideotype is thus a conceptual plant characterized by sets of traits that confer interests in a given agronomical context. An

ideotype must be designed for a targeted environment as the morphological and physiological traits composing the ideotype are specific to particular environmental conditions and management practices [Martre et al., 2014]. According to ideotype breeding, breeders select phenotypes close to the ideotype rather than for yield. This approach was initially developed in cereals [Khush, 2001, Peng et al., 2008] and was later applied on perennial plants [Lauri and Costes, 2005, Cilas et al., 2006]. In any case, the capacity to finely quantify phenotypic traits is a critical point in the conception of ideotype.

## 2.3 Plant architecture: description and modelling

### Describing plant architecture

Plant architecture results from a equilibrium between endogenous growth process and environmental constraints [Barthélémy, 1991]. The study of plant architecture at a given time relies on the description of the topology and the geometry of plant organs [Godin et al., 1999]. Topology refers to the physical connections between plant components while geometry includes the shape, size, orientation and spatial location of the components. A plant can be decomposed as a sum of elementary structures that are repeated during growth and specifically organized into different levels of organization [Barthélémy, 1991]. Hallé et al. [Hallé and Oldeman, 1970, Hallé et al., 1978] proposed the notion of *architectural model* to describe the different types of plant architecture and their growing strategies. This concept of *architectural model* was essentially based on the recognition of successive patterns of branching over plant development. The definition of these growth strategies is however too large to classify species according to their architecture [Barthélémy, 1991]. Hence other architectural studies [Edelin, 1977, Barthélémy, 1991, Barthélémy and Caraglio, 2007] were set up in order to establish a conceptual framework of plant architecture based on four concepts: the category of axis, the architectural unit, the reiteration and the ontogenetic stages of a plant.

A plant is made of axes that can be categorized according to their morphological, anatomical or func-

tional distinctive features (trunk, branch, shoot). For each species the number of categories of axes is finite and relatively low [Barthélémy and Caraglio, 2007]. The notion of *architectural unit* was introduced by Edelin [Edelin, 1977] to qualitatively describe the hierarchy and spatial arrangement of these categories of axes. The spatial arrangement of axes refers to the notion of branching order, which is the topological description of axes according to their relative establishment in space. The *architectural unit* constitutes the level of organization that enables to specifically describe species, and it is characterized by traits related to growth and branching processes, morphological differentiation of axes and position of reproductive structures [Barthélémy and Caraglio, 2007]. Branching process includes the orientation of branches (e.g orthotropic or plagiotropic), the type of branching (monopodial or sympodial), the persistence of branches (indefinite, long or short), the organization of lateral development around mother branch (acrotony, mesotony and basitony), the type of meristematic activity (rhythmic or continuous) and leaf arrangement (phyllotaxis). Conversely to monocaulous plants like oil palm that conserve a single architectural unit over time, other plants can repeat their architectural unit during their lifespan. This morphogenetic process through which the organism duplicates its own elementary architecture is called reiteration [Barthélémy and Caraglio, 2007]. Finally, the notion of plant ontogeny accounts for the dynamics of plant architecture and refers to particular developmental stages of the plant. Ontogenetic gradients can be identified through changes in the morphology of shoots or leaves (or morphogenetic gradients), the apparition of new category of axes, and finally the apparition and degree of repetition of reiteration process.

### 3D representation of plants

Plant architectural models can be developed by many different ways that mainly depends on the purpose underlying their practical applications. Such models can thus be static, describing plant form at a given time, or developmental, including the evolution of the form with time [Prusinkiewicz, 2004]. Developmental models can be either descriptive (representing acquired data relative to plant archi-



texture and called virtual reconstruction) or mechanistic (integrating physiological mechanisms). In both models, plants are considered as an association of discrete components (modules) specifically arranged in space according to plant topology. These modules can represent different components of the plant with various scales (branch, metamers, internodes, leaves, flowers, buds) and can be functionally interconnected when using mechanistic developmental models.

Architectural models were developed using different formalisms. Lindenmayer developed the L-system formalism for simulating the development of multicellular organisms [Lindenmayer, 1968] that was later applied in plants and enabled to account for change in plant topology and geometry over time [Prusinkiewicz and Lindenmayer, 1990]. Further extension of L-systems were designed in order to couple developmental rules to functional processes [Kurth and Sloboda, 1997]. Other formalisms more dedicated to plant simulation were developed for specifically simulating forest trees [Perttunen et al., 1996] or any plant on the basis of elementary processes involved in building plant architecture such as bud break, bud growth and mortality with views on the plant organization [Prusinkiewicz and Lindenmayer, 1990, Perttunen et al., 1996, De Reffye et al., 1997, Barczy et al., 2008].

The 3D representation of plants required quantitative data that enable to retrieve plant topology and geometry of organs. First descriptions of plant topology were obtained by considering plants as strings of characters [Prusinkiewicz and Lindenmayer, 1990]. Later, graphs have been proposed to account for the different level of organization within a plant (organ, growth unit, shoot, branch), like the multi scale tree graph (MTG) [Godin and Caraglio, 1998]. Different methods have been developed to measure the spatial orientation and shape of plant organs, either measured with simple equipment such as rulers and protractors [Takenaka et al., 1998, Casella and Sinoquet, 2003, Rey et al., 2008] or obtained from digitizers that record directly the 3D points of interest (e.g position of internode, insertion of leaves) [Sinoquet et al., 1997, Louarn et al., 2008, Yang et al., 2016]. This latter method can be time consuming and is hardly practicable on large plants. A more recent method consists in using terrestrial LiDAR scans (TLS) which have

the advantage of quickly collecting a very large amount of 3D data related to plant topology and organ geometry [Côté et al., 2009, Raunonen et al., 2013, Hackenberg et al., 2014]. This method is particularly adequate for the reconstruction of tree skeleton but self-occlusion problems limit its potential to fully describe plant architecture.

All these methods enable *in silico* generation of static or dynamic 3D representation of a given plant (called mock-up), that can be used as a support to study the relationships between plant structure and function. The use of 3D representation to assess physiological processes raises the question about the capacity of virtual plants to accurately reproduce observed plant architecture. Indeed, the main difficulty relies on modeling the interaction between plant architecture and the environment. Modelling studies now aim at introducing feedbacks between physiological processes driven by the environment and the morphogenesis processes building plant architecture [Fourcaud et al., 2008]. When these interactions are not completely decoded, 3D model usually invokes statistical approach to simulate architectural variations.

To our knowledge validation processes on virtual plants mostly relies on the quantitative comparison between mean observed and simulated values for geometrical and topological descriptors [Sonohat et al., 2006, Costes et al., 2008]. Validations are also based on the comparison of more integrative variables related to ecophysiological processes, typically light interception [Casella and Sinoquet, 2003, Louarn et al., 2008].

Previous studies carried out in the AMAP (Botany and modelling of plant architecture and vegetation) joint research unit [Lecoustre and Jeager, 1989, Dauzat, 1990, Julia, 2007] were aimed at characterizing and representing oil palm architecture. Results of these studies and the expertise developed in AMAP (H. Rey, personal communication) were used to support the present study.

## 2.4 Using plant modelling to evaluate and predict plant performances

### Conceptual framework

Different approaches can be involved to address limitations of crop production, such as improving plant yield by the development of new varieties or/and the implementation of innovative crop management technics. One hypothesis underlying oil palm yield variation is that plants do not fully express their production potential when resources are limited. Testing such hypothesis is not straightforward and requires a detailed comprehension of plant physiology. Understanding how plants use and transform resources is crucial to enhance their performance. The three main resources of interest are water, soil nutrients and light. Plant performance can thus be conceptualized as the succession of critical physiological processes from light resource captured to yield of the harvested product. [Monteith, 1977] suggested that the total dry biomass produced is closely correlated to accumulated solar radiation following the equation:

$$Y = \underbrace{PAR \times \epsilon_i \times \epsilon_c}_{\text{Total biomass}} \times \epsilon_p \quad (\text{I.5})$$

where:

Y: yield (g.m<sup>-2</sup> or tonnes.ha<sup>-1</sup>)

PAR: photosynthetically active radiation (MJ.m<sup>-2</sup> or MJ.ha<sup>-1</sup>)

$\epsilon_i$ : light interception efficiency

$\epsilon_c$ : photosynthetic conversion efficiency (g.MJ<sup>-1</sup> or tonnes.MJ<sup>-1</sup>)

$\epsilon_p$ : partitioning efficiency

Light interception efficiency ( $\epsilon_i$ ) reflects the capacity of the canopy to capture light and is often defined as the fraction of incident PAR intercepted by the foliage. The photosynthetic conversion coefficient or radiation use efficiency ( $\epsilon_c$ ), represents dry matter produced per unit of radiation absorbed and is usually defined as the slope of the linear relationship between plant biomass production and the accumulated intercepted PAR. Studying carbon

assimilation implies a detailed analysis of complex physiological mechanisms and trade-off between photosynthetic capacity and stomatal conductance. Partitioning efficiency ( $\epsilon_p$ ) or harvest index represents the fraction of total dry matter allocated to the harvested product, i.e. for oil palm, the fruit dry matter or, more precisely, the quantity of extractable oil. The study of  $\epsilon_p$  relies on the comprehension of the mechanisms involved in the flux of carbon assimilates in the different compartments of the plant (vegetative organs or reproductive organs).

Following Monteith' concept, three potential ways of improving plant yield can be investigated which act either on  $\epsilon_i$ ,  $\epsilon_c$  or  $\epsilon_p$ , PAR being inevitably imposed by climatic conditions. An interesting question is to what extent increasing light interception by modifying morphological traits may improve plant yield.

### Process-based models and Functional-structural plant models

Different methods for modelling plants exist and the choice of using one or another depends on the addressed scientific issue. A first approach, called Process-based models (PBM), is classically used in agriculture and aims at simulating plant functioning at the crop scale, without taking into account the individual structure of the plant, but rather considering the amount of crop per unit of surface area. Conversely, functional-structural plant models (FSPM) are based on the explicit description of plant topology and organ geometry [Vos et al., 2010]. FSPMs explore the relationship between plant structure and the processes that underlie growth and development [DeJong et al., 2011], i.e how plants react to the environment by adapting their functions (photosynthesis, transpiration, biomass allocation) and their structure. The advantage of FSPM over PBM relies on its capacity to model functioning processes at organ scale (e.g. photosynthesis) and then to explicitly integrate them at plant scale, but generally implies additional computational cost. Conversely, PBM propose an integrative vision of plant functioning that can lead to the identification of the main processes involved in the comprehension of a particular problems. Modelling plant structure and physiological processes is also a practical tool to

test hypotheses and set up virtual experiments concerning processes that could otherwise take years in field conditions [Fourcaud et al., 2008], especially for perennial crops like oil palm. FSPM allows testing the influence of structural traits (separately or in combination) on processes such as light interception [Sarlikioti et al., 2011, Da Silva et al., 2014] and carbon assimilation [Song et al., 2013, Chen et al., 2014]. As a result FSPM can be an efficient tool to design ideotypes.

### Modelling light interception

Several methods can be used to evaluate light interception, and their practicability depends on the scale of evaluation (stand, plant or organ scale). Indirect methods such as Plant Canopy Analyzer (PCA) or hemispherical photographs (HP) have been commonly used to describe the radiation distribution in the canopy [Frazer et al., 2001, Jonckheere et al., 2004]. Those methods are based on estimations of gap fraction, i.e. gaps through the canopy, from which light interception efficiency can be derived. Methods based on canopy reflectance measurements (Ratio Vegetation Index (RVI)) can also be applied to estimate interception efficiency [Jørgensen et al., 2003]. PCA, HP and reflectance methods allow the calculation of light interception efficiency at plot scale, commonly defined as the fraction of incident PAR intercepted ( $f_{PAR}$ ).

Direct light measurements are precise and may be used to quantify light interception efficiency at organ scale. However, direct measurements require handling very large numbers of light sensors [Xue et al., 2015] and may modify plant architecture when disposed on organs [Sonohat et al., 2002]. Apart from being fastidious, the application of such radiometric measurements is poorly reproducible and highly depends on field radiative conditions. Alternatively, simulations of light interception on plant representations can be easily reproduced for various radiative conditions. Simulations can also provide very detailed and comprehensive data that would require a huge number of sensors for direct measurements. As a result modelling approaches on virtual plants have been proposed to estimate the capacity of plants to intercept light, whatever the scale of study.

In FSPM, light interception is simulated using radiative transfer models combined with three-dimensional representations of plants [Dauzat and Eroy, 1997, Chelle and Andrieu, 1998, Sinoquet et al., 2001]. One approach to model light is to consider foliage as a turbid medium [Sinoquet et al., 2001]. Under such assumption one can apply the Beer-Lambert's law (Equation I.6) like in PBMs, assuming that light interception through a homogeneous vegetation layer is an exponential function of leaf area index (LAI) [Monsi and Saeki, 2005]:

$$I_c = I^{-k \times LAI_c} \quad (I.6)$$

where:

$I_c$ : Radiation measured within the canopy at a given depth

$I$ : Incident radiation above canopy

$k$ : extinction coefficient which is generally calibrated through measurements

$LAI_c$ : Cumulated LAI in the layer of vegetation

For trees, canopy space is divided into volume elements (voxels), each one being characterized by mean properties as leaf area density and leaf inclination distribution [Sinoquet et al., 2001]. Alternatively, the canopy is represented by a detailed collection of geometric primitives (polygons) of which spatial coordinates are known. Two main methods are commonly used for estimating the radiative balance of each element of the canopy (voxel or geometric primitives): the radiosity method and ray tracing. The radiosity method is based on mutual light exchanges factors between all the canopy components [Chelle and Andrieu, 1998]. Ray tracing models, commonly referred as Monte Carlo models (or quasi Monte Carlo models), stochastically simulate light rays coming from light sources (e.g sun) and the rays that are scattered within the canopy [Buck-Sorlin et al., 2011, Song et al., 2013]. Alternatively, rapid simulations can be performed through the calculation of multiple Z-buffer images that applied on both volume and surface canopy representations [Dauzat and Eroy, 1997, Rey et al., 2008]. A similar approach is used in the discrete anisotropic radiative transfer (DART)

model [Gastellu-Etchegorry et al., 1996] with application in remote sensing studies. The principle of this method is the discretization of the incident radiation into directional fluxes accounting for direct and diffuse radiation, estimated via clearness index ( $K_t$ ), which is defined as the ratio of the measured global irradiance to the corresponding irradiance above the atmosphere [Bristow and Campbell, 1984]. Then, for each direction, plant components are projected on an image plane with a Z-Buffer. Counting the visible pixels on resulting images finally allows assessing the quantity of light intercepted by each plant component from each direction.

### **Influence of plant architecture on light interception**

The way plant intercepts light is strongly related to the degree of canopy closure and plant leaf area, often expressed per unit of ground area and defined as leaf area index (LAI; [Bréda, 2003]). At stand scale, light interception is thus conditioned by the distance between plants (planting density) and the vertical and lateral extension of individual crowns. At plant scale, a fine description of canopy structure is essential to quantify and understand the variation of light interception. Several studies investigated how different combinations of these morphological traits (mostly traits related to foliage) can explain variation in light capture, and aimed at identifying the main traits involved in light interception efficiency [Chazdon, 1985, Takenaka, 1994, Valladares et al., 2002, Pearcy et al., 2005, Da Silva et al., 2014].

Two key components control the quantity of light intercepted at plant scale: leaf dispersion and leaf area density [Duursma et al., 2012]. Leaf dispersion characterizes the spatial distribution of leaves within the crown, i.e. if leaves tend to be clumped or regularly arranged. Leaf dispersion partly depends on the structure of shoots and/or petioles that support leaves. Shoot number and internode length [Percy et al., 2005, Dauzat et al., 2008] as well as petiole length [Takenaka et al., 2001, Niinemets et al., 2004a, Chenu et al., 2005] can modulate leaf aggregation and consequently light interception. Phyllotaxis significantly influences light capture efficiency but inefficient phyllotactic patterns (e.g. decussate) can be compensated by leaf morphological plasticity [Niklas, 1988, Valladares

and Brites, 2004]. Shoots and petiole with elevation angle that confer horizontal and flat position of leaves can optimize leaf irradiance [Niinemets et al., 2004b]. The disposition and angles of leaves on shoots have consequences on plant self-shading and therefore can also alter light interception efficiency [Falster and Westoby, 2003, Pearcy et al., 2005, Parveaud et al., 2008].

Leaf area density determines the quantity of leaf area contained in crown volume. Leaf area density is a function of number, shape, size and individual area of leaves. All these traits have been shown to greatly influence light interception efficiency [Chazdon, 1985, Pearcy et al., 2004, Da Silva et al., 2014]. Optimal leaf geometry also depends on the light environment of plant habitat. Under strong light intensity, high number of small and narrow leaves with steep elevation angle can be favourable to reduce exposure to excessive light intensity [Takenaka, 1994, Falster and Westoby, 2003] and limit transpiration losses. The strategy of shade tolerant plants is different; few broad leaves with horizontal positioning confer high level of light interception efficiency by limiting self-shading [Percy et al., 2004].

### **Enhancing plant performance by optimising light interception efficiency**

Crop improvement in the last century was partly a consequence of the augmentation of light capture by plants in combination with agronomic practices [Khush, 2001]. For instance great improvements in cereals yield were obtained with smaller and more erect leaves, allowing planting at higher density [Murchie et al., 2009, Kumar et al., 2017]. Evidence of genetic variation in light interception efficiency was established for different species such as miscanthus [Jørgensen et al., 2003] and soybean [Koester et al., 2014]. These studies highlighted that the improvement of yield provided by a given genotype was closely linked to higher values of  $\epsilon_i$ . Given the close relationship between plant structure and light capture, the augmentation of  $\epsilon_i$  with genetic improvement requires the heritability of some of the architectural traits described in the previous section. Hence, other studies investigated more deeply the relationships between genetic and  $\epsilon_i$  by quantifying architectural differences between

genotypes. Genetic control of tillering and consequences on light interception was demonstrated in cereals [Sakamoto and Matsuoka, 2004, Yang and Hwa, 2008, Moeller et al., 2014]. Heritability of branching pattern [Wu and Stettler, 1998, Segura et al., 2008a] and plant height [Plomion et al., 1996, Barcelos et al., 2015] were also established on perennial species. At leaf scale, genetic analysis pointed the possibility to guide breeding towards leaf morphology [Serrano-Cartagena et al., 1999, Frary et al., 2004] and leaf orientation and angles [Li et al., 2015, Truong et al., 2015].

The close relationship between light interception and yield can be empirically demonstrated. [Koester et al., 2014] found significant correlation between  $\epsilon_i$  and yield examining several cultivars of soybean. For oil palm, a linear relationship between individual light interception and fruit yields has been established with experiments based on high planting density and leaf pruning treatments [Corley and Tinker, 2016]. High planting density is beneficial at the young stage to maximize light interception by the canopy, but it lowers the yield of mature palm. Such results indicate that yield per plant drops when inter-palm competition increases, and highlights the importance of light accessibility.

Beyond maximizing light capture, it is important to consider the intensity of light reaching leaves since excessive irradiance can lead to photoinhibition. Photosynthesis is positively correlated to leaf irradiance, but above a certain limit (estimated at  $1100 \mu\text{mol}_{PFD} \text{ m}^{-2} \text{ s}^{-1}$  for oil palm [Dufrène and Saugier, 1993]), excessive irradiance saturates carbon assimilation. This non-linear relationship between light interception and carbon assimilation can vary among plants and is defined as the photosynthetic conversion coefficient ( $\epsilon_c$ ) in Monteith' formalism. Finally, the partitioning coefficient ( $\epsilon_p$ ) may also limit direct correlation between light interception and yield. Considering a linear relationship between carbon assimilates and fruit yield would results in some oversimplification. Complex processes between sources and sinks of carbon are likely to occur [Pallas et al., 2013a], especially in perennial plants capable to store carbon reserves in order to buffer trophic imbalances.

## Modelling carbon assimilation

Estimating the potential of carbon assimilation versus leaf irradiance and micrometeorological factors requires modelling physiological process of photosynthesis. [Farquhar et al., 1980] developed the reference model to estimate carbon net assimilation ( $A_n$ ) as a function of photon flux density (PFD) and  $\text{CO}_2$  concentration in the mesophyll. Further works were undertaken in order to couple this model with a stomatal conductance model [Baldocchi, 1994, Leuning, 1995]. Methods were proposed to calibrate the parameters of Farquhar model related to maximum catalytic rate of the enzyme Rubisco ( $V_{\text{cmax}}$ ) and the maximum electron transport rate ( $J_{\text{max}}$ ) [Bernacchi et al., 2001, Leuning, 2002]. These methods were applied on response curves to variables such as PFD, partial pressure of intracellular  $\text{CO}_2$  ( $C_i$ ) and temperature.

In parallel, a simplified model was also proposed using a non-rectangular hyperbola function to predicted photosynthesis response to irradiance with four biologically meaningful parameters [Marshall and Biscoe, 1980] and was later updated to account for  $\text{CO}_2$  concentration and nitrogen dependencies [Thornley, 1998].

## 2.5 Retrospect of oil palm models and their applications

Originally oil palm models were developed with the objective to forecast yield. The first modelling approaches were based on the relationship between total dry matter produced and yield, i.e. the partitioning efficiency ( $\epsilon_p$ ). Corley [Corley et al., 1971] suggested, from experimental figures, that vegetative growth might take priority when assimilate supplies are limiting. Other models were later developed focussing essentially on physiological processes like photosynthesis, respiration and assimilate partitioning among plant organs. Dufrène et al. [Dufrène et al., 1990, Dufrène et al., 1992, Dufrène and Saugier, 1993] calibrated a carbon model on oil palm and linked productivity to climatic factors with special attention to water stress. Van Kraalingen et al. [Van Kraalingen et al., 1989] developed a canopy assimilation model (OPSIM) by estimating photosynthesis and assimilates partitioning. Outputs from this



model suggested that improvement of yield could be reached by enhancing crop photosynthesis. Jones [Jones, 1997] proposed a model that enables the prediction of seasonal variations in the number of bunches in relation with the trophic status of the palm trees (through experiments with bunch ablation and fruit pruning treatments). These studies predicted short-term yield based on the number of bunches to harvest.

Combres et al. [Combres et al., 2013] developed a model (ECOPALM) with the objective of obtaining a reliable prediction of oil palm production and its variations over seasons in order to better organize production and transformation chains. Calibrated against studies on the seasonal rhythm of bunch production in relation to drought period, photoperiod and carbon sink-source imbalances on palm oil [Legros, 2008], this model was able to operate at large plot level and simulated the monthly number of harvested bunches for a mature palm plantation (13 to 20 years old). ECOPALM reproduced production cycle observed at population scale for a given progeny but stressed the need to develop an individual-based approach to deal with inter-tree production variability. In complement to ECOPALM, another modelling approach (X-palm) was developed to model the behavior of the plantation as a sum of individual trees [Pallas et al., 2013c]. This functional model aims at representing the topology of the tree as well as organs growth dynamic, and integrates biological processes to simulate plant production. X-palm relies on the concept of competition between sinks that drives carbon partitioning between the different organs of the plant [Luquet et al., 2006, Pallas et al., 2013a]. A competition index ( $I_c$ ) is established through a carbon demand/supply ratio at the plant level. Estimation of organ assimilate demand is based on organ potential growth according to its physiological age and on its biomass composition. Assimilate supply is estimated using the Monteith formalism [Monteith, 1977] and the Beer-Lambert law [Monsi and Saeki, 2005].

Other models were developed with the purpose to better assess the sustainability of oil palm production. Hoffmann et al. [Hoffmann et al., 2014] proposed an integrative approach (PALMSIM) to

predict oil palm potential yield, on a monthly basis, for several sites across Indonesia and Malaysia. The model provided a map of potential yield which, combined with existing maps of land use, could identify degraded lands suitable for oil palm cultivation. A comparable approach was developed to predict oil palm growth and yield over various sites in Papua New Guinea, integrating fertiliser managements (nitrogen treatments) [Huth et al., 2014]. The model accurately predicted vegetative growth and bunch production over the sites in relation to nitrogen supply and highlighted the possibility of using a modelling framework to test sustainable production system. The authors nevertheless stressed the need to enlarge the range of environments and plant ages investigated before using the model as a decision-making tool. Fan et al. [Fan et al., 2015] developed a sub-canopy model for oil palm (CLM-Palm), in order to allow the comparison of carbon, water and energy cycles between natural ecosystems and oil palm plantation. The model allows simulating plant growth and yields at the phytomer scale, and shows the difficulty to predict inter-site variabilities.

All these models developed on oil palm offer the possibility to predict oil palm yield according to environmental conditions, but none of them were designed to address the influence of genetic variability (except for the X-palm model). Sensitivity analyses of these models can bring valuable information. For instance in CLM-Palm, the most sensitive parameters related to cumulative yields were the ones related to the allocation of nitrogen and carbon toward leaves, acting, respectively, on photosynthetic capacity and leaf biomass. The analysis of PALMSIM sensitivity highlighted that parameters linked to light use efficiency had the strongest impact on bunch yield. In an ideotype design context, those results highlight the functioning processes that should be optimized. However, although both Xpalm and CLM-Palm models integrate plant topology, none of these models explicitly represent the structure of oil palm. Given the close relationships between plant architecture, light interception and physiological processes, an FSPM dedicated to oil palm appears to be a powerful approach for the identification of the key morphological traits of interest for breeding.

### 3 Objectives and approaches of the thesis

Oil palm production has continuously increased over the past 50 years thanks to breeding programs based on fruit yield (bunch production and oil extraction rate) [Corley and Tinker, 2016], but a yield ceiling tends to be reached under actual agronomic practices, even in regions where conditions are optimal for its cultivation like Indonesia (<http://faostat3.fao.org>, Fig. I.9 ).

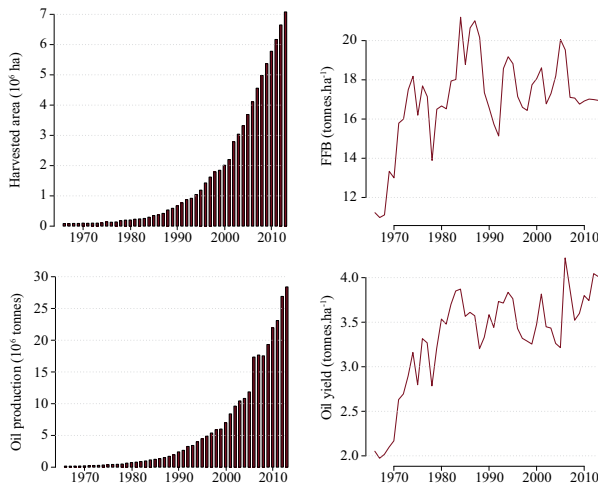


Figure I.9: Production, harvested area and average fresh fruit bunch (FFB) and oil yields of oil palm in Indonesia since 1966 (source: FAOSTAT 2014).

In this thesis we propose to explore an alternative way for improving oil palm performances based on 3D reconstructions and model assisted evaluation of radiation-use efficiency. The main assumption underlying this thesis is the possibility to improve oil palm potential yield via plant breeding, selecting phenotypic traits that optimize light interception efficiency ( $\epsilon_i$ ). This hypothesis raises the following questions:

- To what extent does oil palm architecture vary and is it genetically determined?
- How does light interception efficiency vary among progenies?

- Which architectural traits do impact light interception the most?

So far, there is no research paying attention to the architectural traits involved in the light capture and subsequent carbon assimilation in oil palm. Such an issue remains hardly achievable directly through field experiments and we thus proposed to follow a modelling approach. The existing oil palm models (section 2.5) do not explicitly represent plant architecture, thus hampering their use for tackling the questions addressed in this study. Hence we proposed to develop a FSPM of oil palm which could be able to quantify and analyse the impact of architectural traits on light interception and potential carbon assimilation. In this study, abiotic constraints linked to water and soil nutrients will not be considered so plant performance will be only evaluated according to the acquisition and use of the light resource. In this context, the main objectives of the thesis are:

- To characterize the architectural variability of oil palm and reconstruct 3D mock-ups accordingly
- To evaluate light interception efficiency of 3D mock-ups simulated for different oil palm progenies
- To propose architectural ideotypes optimising light interception and carbon assimilation

These three objectives will be addressed separately in three chapters presented in a scientific paper format (see thesis framework Fig. I.10). First a new modelling approach able to simulate oil palm architecture is presented in chapter II. Beyond model formalism, this chapter presents a comparison of the architectural traits between progenies and the estimations of heritabilities associated to the architectural traits investigated. In the third chapter we propose to evaluate the accuracy of the architectural model through comparisons of model simulations with field data obtained by hemispherical photographs and terrestrial LiDAR. Then we investigate the efficiency of studied progenies to capture light, by applying a light interception model on simulated mock-ups. In chapter IV, a sensitivity analysis is performed to detect the main architectural traits affecting light interception and carbon

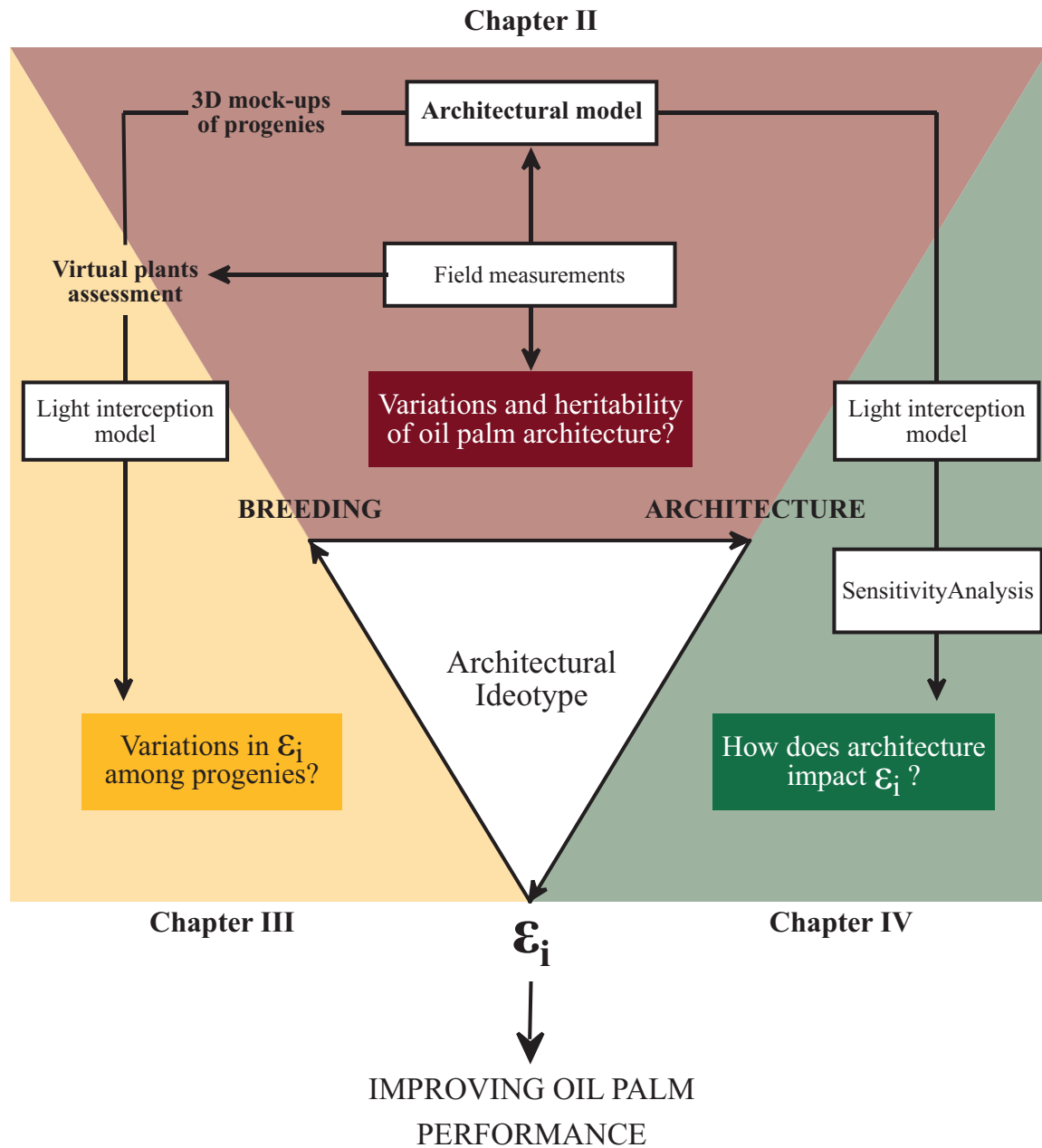


Figure I.10: Thesis conceptual and methodological framework

acquisition. Architectural ideotypes are suggested from these results. Finally, in a last chapter we discuss the overall approach followed in the present study and consider the perspectives offered by the

work initiated during this thesis.



## 4 Experimental site and plant material

### 4.1 Experimental site

Data were collected from an experimental plantation of the SMART Research Institute (SMARTRI, Smart Tbk.) located in South Sumatra, near Palembang (Fig. I.11 A). The trial has been set up under the framework of a breeding program aiming at studying environment and genotype interaction on 25 progenies (Compréhension des Interactions Génotype Environnement or CIGE project). Seedlings were planted in 2010, approximately 18 months after germination. The experimental design is a Fisher block design of five blocks. Each block is subdivided in 25 elementary parcels, where 25 trees of the same progeny compose each parcel. The planting density is 136 plants  $\text{ha}^{-1}$ , in a 9.2 m equilateral triangular pattern.

The experimental site is under sub-optimal climatic conditions for oil palm growth, with temperature varying from 23 to 29 °C, relative humidity between 60 to 98% and daily global radiation between 12 and 17  $\text{MJ.m}^{-2}$  (Fig. I.11 B). However the region is not optimal in terms of rainfall since a dry season usually occurs from July to September. Annual rainfall varied between 2000 and 2800 mm except in years 2014 and 2015 for which annual rainfall drops under 1800 mm.

### 4.2 Plant material

The plants used in the experimental site were *tenera* hybrids (*dura* x *pisifera* cross). The genetic origin of the planting material was from Africa or from Asia. African materials were from three origins: Deli x La Mé (DL), Deli x (La Mé x Sibiti) (DS) and Deli x Yangambi (DY). One progeny, identified as Deli x Unknown (DU) refers to an undetermined origin, either Yangambi or La Mé, and was added to the trial because of its putative tolerance to drought. Deli names make reference to the origin of efficient material used before the appearance of *tenera* hybrids and which are now used as female in crossings (*deli dura*). African origins refer to the regions where the material was selected from (Yangambi and Sibiti in the Democratic Republic of the Congo and La Mé in Côte d'Ivoire). Asian

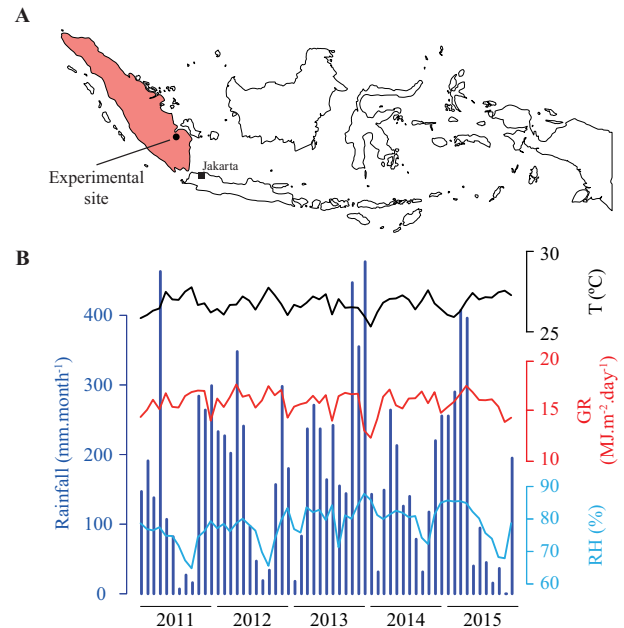


Figure I.11: A) Location of the experimental site in South Sumatra. B) Monthly climatic data in the experimental site from January 2011 to November 2015 (T: daily mean temperature; GR: daily mean global radiation; RH: daily mean relative humidity)

material are Deli x Avros (DA), AVROS (Algemene Vereniging van Rubber planters ter Oostukut van Sumatra) referring to the name of the company that selected plant material in trials set up in Sumatra. A total of 25 progenies were studied in this trial, 16 selected in Africa by the PalmElit company according to several criteria such as: fresh fruit bunch (FFB) production, oil yield, stem growth, precocity of production and parents origin (female origin *dura* and male origin *pisifera*). Those progenies were chosen to maximize the diversity of genetic backgrounds as well as variations in yield components characteristics. The eight other progenies were Deli x AVROS material originated from PT Smart breeding programs. The genetic material under study is interesting as it presents resources independently selected in different world regions and form different breeding programs.

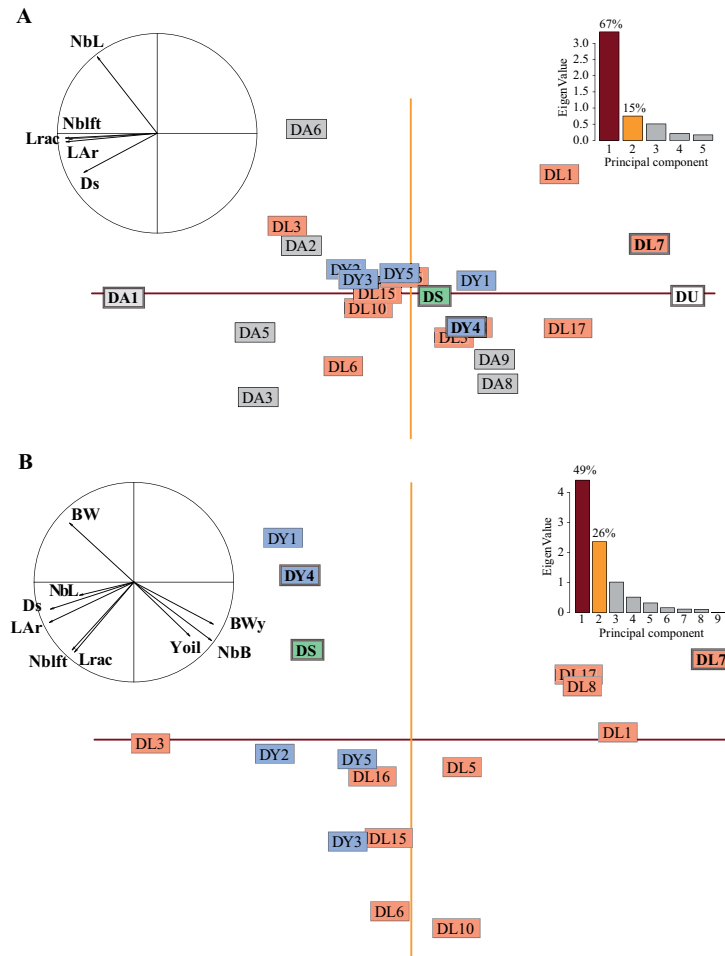


Figure I.12: A) Principal component analysis based on vegetative measurements on the studied site. B) Principal component analysis based on vegetative measurements and production data from mature plants of the same progenies. NbL: number of green leaves on the crown; NbLft: number of leaflets on leaf rank 17; Lrac: rachis length of leaf rank 17; LAr: relative leaf area; Ds: stem basis diameter; BW: average bunch weight; BWy: total bunches weight per plant per year. NbB: annual bunches number; Yoil: Oil yield per year.

### Selection of progenies for the study

For the development of this project, long periods dedicated to measurements of plant architecture were needed, consequently architectural description could not be performed on the 25 progenies and only some contrasted progenies had to be considered. The strategy adopted to select the progenies was thus established from four criteria based on data available before the beginning of the thesis: genetic origins, coarse architectural differences, the

production of similar progenies at mature stage and the availability of seeds for further trials if needed (e.g. observations in nursery).

Coarse architectural traits (number of leaves, rachis length, number of leaflets on rachis, stem basis diameter and relative leaf area) were collected three years after planting (2013) on the 25 progenies cultivated in the experimental site and were used to perform a principal component analysis (PCA) (Fig. I.12 A). The correlation circle points out high

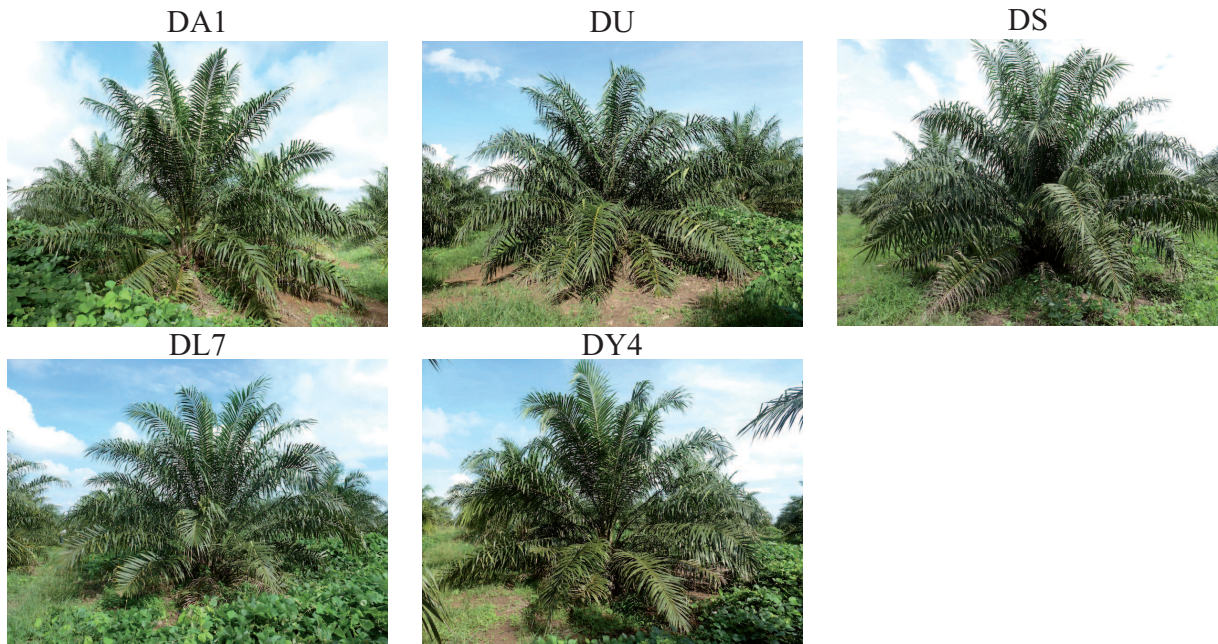


Figure I.13: Pictures of the studied progenies three years after planting (November 2013).

contribution of leaves dimensions to the first components while the second principal component is more linked to stem diameter and number of leaves. The first component explains 67% of total variance and allows discerning progenies depending on the vigor of their vegetative part. The projection of progenies on the two first components revealed differences between genetic origins, mainly for DA progenies which bear more vigorous crown compared to other progenies. The DA1, DL7 and DU progenies proved to be the most interesting according to the distribution of the associated projections on the principal axis. However, many progenies are gathered near axes origin, which indicates that the information given by those data presents some limits to discriminate progenies (mainly DY). A second PCA was then initiated after integrating production data of mature plants available from a previous breeding trial (genetic material from which the CIGE progenies were selected) (Fig. I.12 B). Individual production variables (average bunch weight, total bunch weight per year, annual bunch number and oil yield per year) enabled to better decipher progenies characteristics. The first principal component

opposes vegetative growth performances to yield performances while the second component is based on the opposition between production types (high number of light bunches versus small number of heavy bunches). The DY1, DY4, DS, DL3, DL10, DL6 and DL7 progenies showed the most contrasted production. Finally, the selection was performed by combining genetic origins, the projections of progenies on the two PCAs and the availability of the material for further studies. Eventually, DA1, DL7, DS, DU and DY4 were the five progenies chosen to carry out field measurements and explore the variability of oil palm architecture (Fig. I.13).



## Chapter II

# The Architectural Model

## Integrating mixed-effect models into an architectural plant model to simulate inter and intra-progeny variability: a case study on oil palm (*Elaeis guineensis* Jacq.)

Raphaël P.A. Perez, Benoît Pallas, Gilles Le Moguédec, Hervé Rey, Sébastien Griffon, Jean-Pierre Caliman, Evelyne Costes and Jean Dauzat.

Published in *Journal of Experimental Botany* (2016) doi:10.1093/jxb/erw203

### Abstract

**Background and Aims:** Three-dimensional (3D) reconstruction of plants is time-consuming and involves considerable levels of data acquisition. This is possibly one reason why the integration of genetic variability into 3D architectural models has so far been largely overlooked.

**Methods:** In this study, an allometry-based approach was developed to account for architectural variability in 3D architectural models of oil palm (*Elaeis guineensis* Jacq.) as a case study. Allometric relationships were used to model architectural traits from individual leaflets to the entire crown while accounting for ontogenetic and morphogenetic gradients. Inter and intra-progeny variabilities were evaluated for each trait and mixed-effect models were used to estimate the mean and variance parameters required for complete 3D virtual plants.

**Key results:** Significant differences in leaf geometry (petiole length, density of leaflets, and rachis curvature) and leaflet morphology (gradients of leaflet length and width) were detected between and within progenies and were modelled in order to generate populations of plants that were consistent with the observed populations.

**Conclusions:** The application of mixed-effect models on allometric relationships highlighted an interesting trade-off between model accuracy and ease of defining parameters for the 3D reconstruction of plants while at the same time integrating their observed variability. Future research will be dedicated to sensitivity analyses coupling the structural model presented here with a radiative balance model in order to identify the key architectural traits involved in light interception efficiency.

**Key words:** Allometric relationship, *Elaeis guineensis*, genetic variability, mixed-model, plant architecture, three-dimensional reconstruction.

## 1 Introduction

Understanding how plants intercept and use solar radiation is a necessary step for enhancing their performance. Plant architecture, defined as the combination of plant topology and organ geometry [Godin et al., 1999], plays a key role in collecting light. Many aerial architectural traits have been shown to influence light interception, such as internode and petiole length [Takenaka, 1994, Sarlikioti et al., 2011], and leaf area density and spatial distribution of leaves [Falster and Westoby, 2003, Willaume et al., 2004, Parveaud et al., 2008]. Plant architecture also affects microclimatic conditions (organ temperature, hygrometry, and light environment), which are known to influence biological and physiological processes such as photosynthesis and leaf transpiration [Niinemets, 2007, Vos et al., 2010]. Moreover, since plant architecture changes over time, the relevant developmental stages along with temporally variable aspects of morphology and topology must be taken into account when describing plant architecture [Barthélémy and Caraglio, 2007].

Biophysical models (e.g. light interception models, energy balance models) can be applied to three-dimensional (3D) plant representations to evaluate the influence of architectural traits on plant performance. These models can be built from explicit descriptions of plant topology and organ geometry [Vos et al., 2010]. One strategy is to record 3D points of interests using digitizing methods [Sinoquet et al., 1997, Godin et al., 1999, Sonohat et al., 2006, Louarn et al., 2008]; however, digitizing whole-plant architecture is time-consuming and is not adapted to fully describe large plants [Parveaud et al., 2008] or many individuals. Alternatively, allometric relationships combined with sampling strategies can be used to reconstruct plant architecture from the scale of the single organ to the entire plant stand [Casella and Sinoquet, 2003, Rey et al., 2008]. Such allometric relationships reflect the morphological relationships between plant components at different scales of organization. Recent methods based on image processing or 3D LiDAR scanning are likely to improve data collection efficiency in the future [Phattaralerphong and Sinoquet, 2005, Côté et al., 2009, Hackenberg et al., 2014].

Reducing the time needed for data acquisition is crucial for quantitative genetic studies or plant

breeding programmes aiming to study architectural traits [Sakamoto and Matsuoka, 2004, Segura et al., 2006]. Studies on different species have demonstrated large genotypic variability in architectural traits and revealed genetic polymorphism associated with this variability [Bradshaw and Stettler, 1995, Plomion et al., 1996, Wu and Stettler, 1998, Wang and Li, 2005, Segura et al., 2008b, Ben Sadok et al., 2013, Li et al., 2015]. Inter and intra-genotypic variability can be estimated by quantitative genetic models. These models allow the estimation of (co)variance components, that is, partitioning of the total observed variance into its causal components, in particular variance due to genetic and environmental effects [Gallais, 1990, Smith et al., 2005]. These analyses are mainly based on mixed-effect models and allow the estimation of genotypic values, trait heritability, and genetic correlations between variables [Segura et al., 2008a]. Currently, several crop models integrate genotype-dependent parameters related to plant phenology, light interception, light conversion efficiency, or responses to abiotic conditions [Hammer et al., 2010, Casadebaig et al., 2011]. In such approaches, genotypes are represented by a set of parameters estimated directly through dedicated experiments and, for the most part, independently of each other [Tardieu, 2003, Lecoeur et al., 2011]. Other studies also include genetic parameters, combining allelic effects from quantitative trait loci (QTL) with model parameters [Chenu et al., 2009, Letort et al., 2008]. Pioneering studies were dedicated to simple plant functions, such as leaf expansion rate [Reymond et al., 2003] or specific leaf area [Yin et al., 1999]. More recently, marker-based crop models, estimating values of ecophysiological parameters from genetic markers, were used to explore potential yield improvement and support breeding strategies [Gu et al., 2014]. Regarding 3D representations of plants, few models have been calibrated for different genotypes [Casella and Sinoquet, 2003, Rey et al., 2008]; so far, none of them have dealt with the genetic control of architectural variability.

Usually, models integrate genotypic differences by quantifying genetic parameters via phenotypic mean values, thus neglecting inter-individual variability [Louarn et al., 2008]. Such an approach can be applied when plants are genetically fixed, as in the case of many annual crops or some tree clones



(e.g. rubber trees, *Eucalyptus*), but this might lead to oversimplification when progenies have been subjected to large genetic segregation and grown directly in field conditions [e.g. oil palm (*Elaeis guineensis*), maize (*Zea mays*) or *Coffea*]. In such case, the use of mixed-effect models is particularly interesting because they take account of both inter and intra-progeny variability.

The principal goal of this study was to account for the architectural variability among individuals and among progenies in a 3D modelling approach. Oil palm (*Elaeis guineensis* Jacq.) is a convenient model for such a study because it exhibits a simple architectural topology following the Corner model, characterized by a mono-axial shoot producing phytomers in regular succession [Hallé and Oldeman, 1970]. An adult oil palm bears 3050 opened leaves disposed in a radial symmetry [Rees, 1964]. Its structural complexity results from its leaf geometry: each leaf is pinnate, being divided into a petiole and a rachis bearing leaflets. The junction of the petiole and rachis (called point C) is recognizable from the presence of small leaflets with vestigial laminae. The rachis cross section is wide and asymmetrical at point C (with a flat adaxial side and a convex abaxial side) and becomes gradually circular from so-called point B (mid-rachis) and point A (rachis extremity). In optimal growing conditions, the number of leaves produced per year varies from 30 to 40 in plants of 24 years of age and then declines to 20-25 leaves per year from 8 years old onwards [Corley and Tinker, 2003]. Leaf size increases up to the adult stage (8 years) with the result that, for a given individual, leaf size is observed to increase distally along the stem.

The long duration between consecutive generations of oil palm together with the difficulty of producing clonal plants prevents the generation of fixed lines and thus obliges breeders to adopt complex breeding schemes based on biparental crosses between heterozygous parents. Hence, most oil palms cultivated in the world are *dura* x *pisifera* crosses, displaying large intra-genotypic variability. Genetic analyses of oil palm have been mainly carried out on yield components or on traits involved in oil and fruit quality [Billotte et al., 2010]. High heritabilities have been found for quantitative traits related to bunch components and many QTL associated with these traits have been detected [Rance et al.,

2001]. Moreover, several characters controlled by a single gene have been reported, such as shell thickness, leaflet lamina development [Corley and Tinker, 2003], and, more recently, oil deterioration [Morcillo et al., 2013]. Nevertheless, except for coarsely defined traits related to characteristics such as leaf area, rachis length, or stem height [Rance et al., 2001, Corley and Tinker, 2003], no detailed analysis combining genotypic variability and architectural traits of oil palm has been performed up to now. The modelling approach presented here couples mixed-effect models with a 3D architectural model based on oil palm. The major architectural traits that are likely to govern light interception (leaf and leaflet geometries) were studied and analysed in terms of their variability between and within progenies. Observations were performed on 60 individuals among five progenies of different genetic origins. Linear and nonlinear allometric relationships were designed for modelling the selected traits and combined with mixed-effect models to explore the significance of intra- and inter-progeny effects. The trait variabilities estimated by these models were finally used to parameterize the reconstruction of 3D mock-ups representative of the variability observed in the field between individuals and between progenies.

## 2 Material and methods

### 2.1 Architectural description

The description of the geometry of plant components and their topological arrangement was carried out at two scales of organization: plant scale and leaf scale (Table II.1). At the plant scale, attributes related to stem (height  $H$  and basal diameter  $D$ ) and crown (number of leaves and phyllotaxis  $\phi$ ) were defined. At the leaf scale, petiole, rachis, and leaflet geometry was characterized as well as the spatial organization of leaflets along the rachis. Leaves were topologically positioned along the stem depending on their insertion rank, where leaf rank 1 corresponded to the youngest leaf displaying fully unfolded leaflets [Corley and Tinker, 2003]. Three types of attributes were considered to account for leaf geometry: i) dimensional attributes (rachis length  $L_{rac}$  and petiole length  $L_p$ ); ii) structural

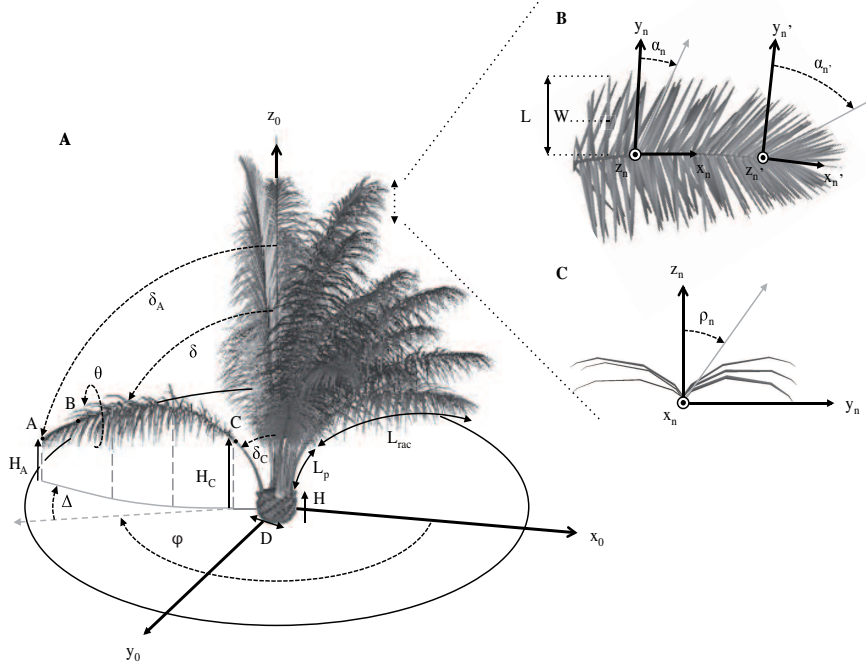


Figure II.1: Geometric variables for assessing and generating 3D oil palm architecture. (A) Variables at the plant and leaf scale. Elevation angles ( $\delta$ ) are measured from the vertical reference  $z_C$ . Rachis azimuth ( $\Delta$ ) is measured through the projected points along the rachis on  $(x_C, y_C)$  plane. Phyllotaxis ( $\phi$ ) is measured as the azimuth angle from one leaf insertion relatively to the following one. Rachis twist ( $\theta$ ) is measured as the rotation angle of the rachis local plane from a vertical plane. (B) Detailed top view of a leaf in horizontal plane. Leaflet lengths ( $L$ ) and widths ( $W$ ) are measured in a sample of 10 leaflets per leaf. Axial insertion (azimuth angles  $\alpha_n$ ) is measured with reference to local rachis planes  $(x_n, y_n)$ . (C) Detailed front view of a leaf in a transverse plane to the rachis axis. Radial insertion (elevation angle  $\rho_n$ ) is measured with reference to local rachis planes  $(z_n, y_n)$ . Definitions and symbols are given in Table II.1.

attributes (number of leaflets  $NbLft$ ); and (iii) attributes related to leaf orientation and angle along the rachis. Leaf curvature, deviation, and twist were described respectively by functions of the elevation angle ( $\delta$ ), azimuth angle ( $\Delta$ ), and twist angle ( $\theta$ ) along consecutive segments of rachis (see Fig. II.1A). Leaflets were characterized by their dimensions (length  $L$  and width  $w$ ) and their insertion angles on rachis ( $\alpha$  and  $\rho$ ; see Fig. II.1B).

## 2.2 Model description

In this experiment, plants had not yet reached the mature stage so leaf size was still increasing along the stem with plant age. The methodology used to describe organ geometry and their changes within the plant topology was based on positional informa-

tion [Prusinkiewicz et al., 2001]. We assumed that, over the considered developmental stage (3-4 years after planting), the allometric relationships governing the shape of the leaf and leaflets were invariant and that only their dimensions evolved with plant age. Conversely, the ratio of petiole length to rachis length ( $ratio_L$ ), the relative position of point B on the rachis ( $Pos_{Brel}$ ), and the gradients of leaflet geometry (shape and angles) along the rachis were assumed to be identical for all the leaves of a given individual, at least for the studied plant ages.

**Modelling morphogenetic gradients** Linear, logistic, and polynomial functions were used to model geometric gradients of plant components according to temporal or spatial variables (Tables II.2 and II.3).



Table II.1: Symbols and abbreviations

Field observations	
Plant scale	
$\Sigma leaves$	Plant age expressed as the number of leaves emitted since planting date
$H_C^*$	Height of rachis point C from the ground (cm)
$H_A^*$	Height of rachis point A from the ground (cm)
$H$	Stem height (cm)
$D$	Stem basal diameter (cm)
$\phi$	Phyllotaxis (degrees)
Leaf scale	
$Rk$	Leaf rank: spatial position of the leaf on stem (leaf rank 1 at stem top)
$L_{rac}$	Rachis length (cm)
$L_p$	Petiole length (cm)
$NbLft$	Number of leaflets per leaf
$Pos$	Metric position on rachis
$\delta_C$	Declination at point C: angle from the vertical axis to rachis axis at petiole tip (degrees)
$\delta_A$	Declination at point A: angle from the vertical axis to rachis axis at rachis tip (degrees)
$\delta$	Rachis curvature: evolution of declination along rachis (degrees)
$\Delta$	Rachis deviation: projection angle of rachis in an horizontal plane (degrees)
$\theta$	Rachis twist: rotation angle of rachis from the horizontal plane (degrees)
$Area^*$	Leaf area (m <sup>2</sup> )
$RkLft$	Leaflet rank: rank of leaflet along the rachis (leaflet rank 1 at point C)
$L_B$	Leaflet length at point B (cm)
$W_B$	Leaflet maximum width at point B (cm)
$L$	Leaflet length (cm)
$W$	Leaflet maximum width (cm)
$w$	Leaflet width (cm)
$\alpha$	Leaflet axial insertion: azimuth angle of leaflet midrib projected on the local rachis plan (degrees)
$\rho$	Leaflet radial insertion: elevation angle of leaflet midrib projected on the local rachis plan (degrees)
$Area_{Lft}^*$	Leaflet area (cm <sup>2</sup> )
Calculated variables	
$ratio_L$	Ratio of petiole length to rachis length
$FreqLft$	Ratio of leaflets number to rachis length
$Pos_{rel}$	Relative metric position on rachis
$PosB_{rel}$	Relative metric position of point B on rachis
$PosLft_{rel}$	Relative metric position on leaflet midrib
$RankLft_{rel}$	Relative leaflet rank
$L_{rel}$	Relative leaflet length (relative to all leaflets on rachis)
$W_{rel}$	Relative leaflet maximum width (relative to all leaflets on rachis)
$w_{rel}$	Relative leaflet width (relative to all positions along leaflet midrib)

\*variables used to assess model reconstruction

Table II.2: Allometric relationships (functions  $f_1$  to  $f_{10}$  refer to the functions presented in Table II.3). See Table II.1 for variable meanings

Predicted variables	Explanative variables	Equation	Parameters meaning
<b>Stem scale</b>			
$H$ (cm)	$\Sigma leaves$	(eq1) $H = f_3(\Sigma leaves)$	$h_0$ : stem height at planting date
$D$ (cm)	$L_{rac}$ (cm)	(eq2) $D = f_2(L_{rac})$	$h_g$ : growth rate factor $D_{max}$ : maximum basis diameter $D_{slp}$ : slope factor at inflexion point $L_{Dinfl}$ : rachis length at inflexion point
<b>Leaf scale</b>			
$L_{rac}$ (cm)	$\Sigma leaves$	(eq3) $L_{rac} = f_1(\Sigma leaves)$	$L_{rac_{int}}$ : intercept $L_{rac_{slp}}$ : slope
$L_p$ (cm)	$L_{rac}$ (cm)	(eq4) $L_p = ratio_L \cdot L_{rac}$	$ratio_L$ : ratio of petiole length to rachis length
$NbLft$	$L_{rac}$ (cm)	(eq5) $NbLft = f_2(L_{rac})$	$Nb_{max}$ : maximum number of leaflets per leaf $Nb_{slp}$ : slope factor at inflexion point $L_{Nb_{infl}}$ : rachis length at inflexion point
$\delta_C$ (°)	$Rk$	(eq6) $\delta_C = f_1(Rk)$	$\delta_{C_{int}}$ : intercept $\delta_{C_{slp}}$ : slope
$\delta_A$ (°)	$\delta_C$ (°)	(eq7) $\delta_A = f_2(\delta_C)$	$\delta_{A_{max}}$ : maximum declination at point A $\delta_{A_{slp}}$ : slope factor at inflexion point $\delta_{infl}$ : $\delta_C$ angle at inflexion point
$\delta$ (°)	$Pos_{rel}$	(eq8) $\delta = \delta_C + f_4(Pos_{rel})(\delta_A - \delta_C)$	$\delta_{sf}$ : evolution of curvature along the rachis
$\Delta$ (°)	$Pos_{rel}$	(eq9) $\Delta = \Delta_a \cdot f_4(Pos_{rel})$	$\Delta_a$ : Deviation angle at point A $\Delta_{sf}$ : evolution of deviation along the rachis
$\theta$ (°)	$Pos_{rel}$	(eq10) $\theta = f_5(Pos_{rel})$	$\theta_a$ : Twist angle at point A $\theta_s$ : evolution of twist along the rachis
$PosLft_{rel}$	$RankLft_{rel}$	(eq11) $PosLft_{rel} = f_4(RankLft_{rel})$	$d_{Lft}$ : evolution of inter-leaflets distance along the rachis
$L_B$ (cm)	$L_{rac}$ (cm)	(eq12) $L_B = f_1(L_{rac})$	$L_{B_{int}}$ : intercept $L_{B_{slp}}$ : slope
$W_B$ (cm)	$L_{rac}$ (cm)	(eq13) $W_B = f_1(L_{rac})$	$W_{B_{int}}$ : intercept $W_{B_{slp}}$ : slope
$L_{rel}$	$Pos_{rel}$	(eq14) $L_{rel} = f_6(Pos_{rel})$	$l_c$ : $L_{rel}$ at point C $p_L$ : position of the longest leaflet on rachis $l_a$ : $L_{rel}$ at A point
$W_{rel}$	$Pos_{rel}$	(eq15) $W_{rel} = f_7(Pos_{rel})$	$w_c$ : $W_{rel}$ at point C $p_W$ : position of the largest leaflet on rachis $w_a$ : $W_{rel}$ at point A
$L$ (cm)	$Pos_{rel}$	(eq16) $L = L_{rel} \frac{L_B}{f_6(Pos_{B_{rel}})}$	
$W$ (cm)	$Pos_{rel}$	(eq17) $W = W_{rel} \frac{W_B}{f_7(Pos_{B_{rel}})}$	$Pos_{B_{rel}}$ : Relative metric position of point B on rachis
$w_{rel}$	$Pos_{rel}, PosLft_{rel}$	(eq18) $w_{rel} = f_8(Pos_{rel}, PosLft_{rel})$	$p_w$ : relative position of maximum width on leaflet $sl$ : leaflet shape factor
$\alpha$ (°)	$Pos_{rel}$	(eq19) $\alpha = f_9(Pos_{rel})$	$\alpha_c$ : leaflet axial insertion angle at point C $\alpha_s$ : decreasing-factor of axial angle along rachis $\alpha_a$ : leaflet axial insertion angle at A point
$\rho$ (°)	$Pos_{rel}$	(eq20) $\rho = f_{10}(Pos_{rel})$	$\rho_c$ : leaflet radial insertion angle at point C $\rho_{0.5}$ : radial insertion angle on middle rachis length

Table II.3: Functions used in the allometric relationships

$$f_1(x) = int + x \cdot slp \quad (II.1)$$

$$f_2(x) = \frac{max}{1 + e^{4slp(x_{inf} - x)}} \quad (II.2)$$

$$f_3(x) = h_0 \cdot e^{hg \cdot x} \quad (II.3)$$

$$f_4(x) = \frac{(1 + sf)x^2}{1 + sf \cdot x^2} \quad (II.4)$$

$$f_5(x) = \theta_a \cdot x^{3\theta_s} \quad (II.5)$$

$$f_6(x) = \begin{cases} l_c + 2\frac{1-l_c}{p_L}x + \frac{l_c-1}{p_L^2}x^2, & \text{if } x \leq p_L \\ 1 + \frac{l_a-1}{(1-p_L)^2}(x-p_L)^2, & \text{if } x > p_L \end{cases} \text{ and } p_L \in ]0, 1[ \quad (II.6)$$

$$f_7(x) = \begin{cases} w_c + \frac{1-w_c}{p_W}x, & \text{if } x \leq p_W \\ \frac{1-w_a \cdot p_W + (w_a-1)x}{1-p_W}, & \text{if } x > p_W \end{cases} \text{ and } p_W \in ]0, 1[ \quad (II.7)$$

$$f_8(u, v) = \frac{v^{p-1}(1-v)^{q-1}}{p_w}$$

where:

$$\begin{aligned} p & \text{ and } q \text{ are function of } p_W \text{ and } sl \\ p_w & = f_1(u) \\ sl & = f_1(u) \end{aligned} \quad (II.8)$$

$$f_9(x) = \sqrt{\alpha_c^2 + 2\alpha_c \cdot \alpha_s \cdot x + (\alpha_a^2 - \alpha_c^2 + 2\alpha_c \cdot \alpha_s)x^3} \quad (II.9)$$

$$f_{10}(x) = \begin{cases} \rho_c + 4x(\rho_{0.5} - \rho_c)(1-x), & \text{if } x \leq 0.5 \\ \frac{\rho_c}{4b} \cdot x(x-1), & \text{if } x > 0.5 \end{cases} \quad (II.10)$$

As far as possible, functions were designed parsimoniously (low number of parameters), with parameters related to the observable geometrical properties and minimizing mean square error and bias between observed and simulated values. At the plant scale, two variables were introduced to account for morphogenetic gradients of leaves in the crown: the number of leaves emitted from planting date ( $\Sigma leaves$ ) and the leaf rank ( $Rk$ ) (Table II.1 and Fig. II.2). The evolution of rachis length ( $L_{rac}$ ) over time was estimated as a linear function of  $\Sigma leaves$  (eq3 in Table II.2 and Table II.3).  $Rk$  was used to model the evolution of rachis declination at point C along the stem [ $\delta_C$  (eq6)]. At the leaf scale, the relative metric position on the rachis ( $Pos_{rel} = Pos/L_{rac}$ ) was used to describe the evolution of the rachis segment angles [elevation  $\delta$  (eq6, eq7, and eq8); azimuth  $\Delta$  (eq9); and twist

$\theta$  (eq10)]. Similarly, geometrical attributes [length (eq14), width (eq15), and insertion angle (eq19 and eq20)] of leaflets were determined according to their relative position along the rachis ( $Pos_{rel}$ ). Finally, the relative metric position of the leaflet midrib [ $PosLft_{rel}$  (eq11)] was introduced for modelling leaflet shape [evolution of width (eq18)].

**Modelling organ dimensions** Once organ geometry was modelled by allometric functions describing relative proportions (variables with subscript 'rel'), 'scaling' functions were applied to estimate their absolute value (variables expressed as a function of  $\Sigma leaves$  or  $L_{rac}$ ; Table II.2). The number of leaflets borne by the rachis was predicted by a logistic function of rachis length (eq5; Table II.2).

Leaflet dimensions were estimated from linear relationships between rachis length and leaflet dimension at point B (eq12 and eq13). Absolute dimensions of leaflets ( $L$ ,  $W$ ) along the rachis were estimated using their relative values ( $L_{rel}$ ,  $W_{rel}$ ), that is, relative to the longest (largest) leaflets on the rachis, and rescaling them using the absolute values  $L_B$  and  $W_B$  (eq14 and eq15).

## 2.3 Model calibration

### *Plant material and growing conditions*

Measurements were performed at an experimental plantation of the SMART Research Institute (SMARTRI, Smart Tbk.) located in South Sumatra province, Indonesia (2°59' 27.99" S, 104°45' 24.24" E). The trial was set up in 2010, 18 months after seedling germination. The genetic material studied was composed of 25 progenies of *tenera* hybrids selected by the PalmElit Company and SMARTRI using several criteria: production of fresh fruit bunches, oil yield, stem growth, precocity of production, and parent origins. The experimental design was a Fisher block design of five blocks subdivided into 25 elementary parcels, each parcel including 25 trees of the same progeny (see Supplementary Fig. II.7 page 57). The planting density was 136 plants ha<sup>-1</sup> in a 9.5 m equilateral triangular pattern whatever the progeny. For this study, we selected five progenies (hereafter referred to as DA1, DL7, DS, DU, and DY4) in view of their different morphologies, diversity of origins (Asian and African origins), and their architecture. All progenies were

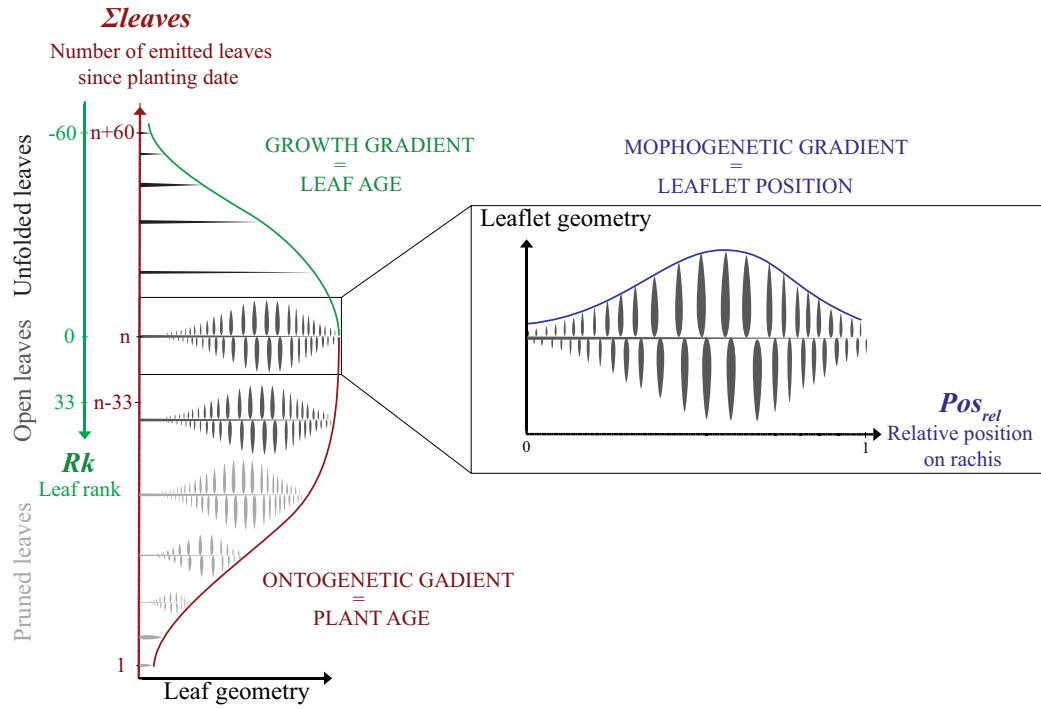


Figure II.2: Variables used to model morphogenetic gradients at leaf and leaflet scale.

known to have a good production performance (see Supplementary Table II.7 page 57). The site is characterized by a tropical humid climate, considered as optimal conditions for oil palm cultivation.

**Data collection** Architectural measurements were performed on plants located in the same experimental block in order to reduce sources of heterogeneity (see Supplementary Fig. II.7 page 57 and protocol appendix A page 129). Every 6 months from December 2010 to November 2014, coarse-scale measurements (rachis length, stem basal diameter, and number of leaflets) were made for each individual (5 progenies x 25 plants x 6 dates). The number of observations per progeny was dependent on the type of measurements (see Supplementary Table II.8). Numerous detailed measurements were subsequently collected 39 months after planting (MAP; April 2014) and used to define the allometric relationships. A second set of data was collected 47MAP (November 2014) for a larger number of individuals (between 6 and 12 plants per progeny)

for a more detailed assessment of trait variability among progenies. For allometric relationships related to ontogenetic gradients, that is, dependent on plant age, model calibration was performed on data collected from 6 to 47 MAP.

**Estimated variables** Analyses of data collected at 39 MAP showed that sampling 10 leaflets was sufficient to simulate accurately the leaf area and the leaf shape (see Supplementary Fig. II.7 page 57). Similarly, the marked leaf symmetry observed meant that we could limit measurements to only one side of the leaf (see Supplementary Figs II.8 and II.9 page 58-59). Each leaf was labelled as soon as it was fully open, thus enabling us to count the leaves emitted per plant since planting date ( $\Sigma leaves$ ). Leaf area (*Area*) was estimated by dividing the leaf into 10 equal sections along the rachis. On each section, the number of leaflets was counted on both sides and a median leaflet was chosen for which length and width of segments (in five regular intervals along the leaflet midrib) were measured to

estimate the entire individual leaflet area ( $Area_{Lft}$ ). This approach considered the leaflet as a sum of trapezes. For each rachis section, total leaflet area was approximated by multiplying the individual leaflet area by the number of leaflets on the corresponding section. Leaf area was finally obtained as the combined sum area of the 10 sections [Talliez and Koffi, 1992].

Leaf curvature and deviation along the rachis were estimated by measuring distances between control points along the rachis and their projections on a horizontal plane (10 points per leaf). Projection distances were used afterwards to estimate deviation and elevation angles of leaves along the stem.

**Analyses of inter-individual variability and differences among progenies** A first analysis was aimed at assessing architectural variability between and within progenies at 47 MAP (Fig. II.1). For the variables not related to rachis length ( $\Sigma leaves$ ,  $\phi$ ,  $H$ , and  $\delta_C$ ), oneway ANOVA were performed with progeny effect. Conversely, when variables were correlated with rachis length, analyses of covariance (ANCOVA) were performed without interaction but considering a genotype and a rachis length effect. For all the variables, Tukeys tests were used for post hoc comparisons. The homoscedasticity of variables and normality of model residuals were verified using Levene's and Shapiro-Wilks' tests respectively.

For evaluating the variability of a trait within a progeny and comparing it to the variability between progenies, we defined an interfamily broad-sense heritability ( $h^2$ ) as the ratio of progeny variance to total variance ( $h^2 = \sigma_{progeny}^2 / \sigma_{total}^2$ ) [Gallais, 1990]. This index was calculated for each phenotypic trait at 47 MAP, using the restricted maximum likelihood method [Corbeil and Searle, 1976] to estimate progeny and residual variances (the total variance being given by the sum of both progeny and residual variances). In a second step, the study focused on variables affected by ontogenetic and morphogenetic gradients. Because these variables change over time and space, statistical analyses were performed directly on the allometric relationships to test for differences among and within progenies. Allometric relationships were adjusted on different data sets: all data gathered (null model), data sorted

per progeny (progeny model), and data sorted per plant (individual model). A likelihood ratio test was then carried out using a Chi-squared test ( $\chi^2$ ) to compare models (null, progeny, and individual) and to assess inter-progeny and intra-progeny effects. Likelihoods of progeny models were calculated in reference to the total variance, whereas likelihoods of individual models were calculated in reference to the intra-progeny variance for each progeny.

The number of estimated parameters varied depending on the considered function and the significance of progeny and individual effects. If both progeny and individual effects were significant, model parameters were then estimated by performing hierarchical mixed-effects models, considering the individual plant (intra-progeny) effect as a random effect nested within a fixed progeny effect, expressed as a matrix [Pinheiro and Bates, 2000] as:

$$y_{ijk} = f(x_{ijk}; \phi_{ij}) + \epsilon_{ijk}, \epsilon_{ijk} \hookrightarrow \mathcal{N}(0, \sigma^2)$$

$$\phi_{ij} = A_{ij}\beta_i + B_{ij}b_{ij}, b_{ij} \hookrightarrow N(0, \Psi_i)$$

where  $f$  represents one of the allometric relationships presented (Table II.2),  $y_{ijk}$  labels the  $k^{th}$  observation of the  $j^{th}$  individual of the  $i^{th}$  progeny,  $x_{ijk}$  is the covariate vector related to this observation, and  $\epsilon_{ijk}$  represents model residuals (assumed to be independent and identically distributed). The vector  $\phi_{ij}$  represents the model parameters associated with the  $j^{th}$  individual of the  $i^{th}$  progeny,  $\beta_i$  is the vector of fixed effects related to the  $i^{th}$  progeny, and  $b_{ij}$  is the random effect vector associated with the  $j^{th}$  individual of progeny  $i$ . In other words,  $b_{ij}$  represents the deviation of the  $\phi_{ij}$  from the mean parameter  $\beta_i$  due to the  $j^{th}$  individual.  $A_{ij}$  and  $B_{ij}$  are incidence matrices and  $\Psi_i$  is the variance-covariance matrix associated with the progeny  $i$ . Consequently, for each function used to predict trait values, the progeny effect is related to the mean parameter ( $\beta_i$ ) of the model whereas the individual effect defines variance parameters ( $\Psi_i$ ) of the model. In cases where only the inter-progeny effect was significant, only mean parameters and model residuals were estimated for each progeny.

The inter-progeny coefficient of variation (CV) was calculated by dividing the SD of the mean values of each progeny by the overall mean. The intra-progeny CV was calculated for each progeny as the SD of individual parameters estimated by the

mixed-effect model ( $\sqrt{\Psi_i}$ ) divided by the corresponding mean value.

## 2.4 Model simulation and validations

**Simulations of palm mock-up** A dedicated oil palm simulation model (VPalm) was developed using the basis of a former simulator of coconut palms [Dauzat and Eroy, 1997]. VPalm was written using object-oriented programming in Java language as an application of the AMAPstudio software suite [Griffon and de Coligny, 2014]. The VPalm simulator enabled us to rebuild the topological structure of the palm through decomposition into elementary components organized along a multiscale tree graph [Godin and Caraglio, 1998]. The simulator was designed for integrating the allometric relationships (Table II.2) needed to render the plant topology and its 3D geometry. Each individual palm was reconstructed from an input file generated to account for the progeny parameterization as well as individual variability. The random sampling procedure of R [R Core Team, 2015] was used to generate random individual parameters by combining estimated mean parameters associated with progeny effect ( $\beta_i$ ) with variance-covariance matrices associated with individual effect ( $\Psi_i$ ) when significant. Even if significant, individual effects were not considered if the explanatory variables of the allometric relationship were estimated using individual effects (like *NbLft* for instance) to avoid any over-parameterization. In other words, we assumed that the variance component linked to the explanatory variable (e.g. rachis length) was sufficiently spread into the response and consequently did not require the estimation of individual variance components. Twenty five random VPalm parameters files were created in this way to generate 25 virtual individuals for each progeny that were subsequently laid out to reproduce the experimental parcels at 47 MAP.

**Assessing model reconstruction** Different variables were extracted from the 3D simulated mock-ups with the Xplo software of AMAPstudio to compare their value with field observations in terms of root mean square error (RMSE), normal-

ized RMSE (NRMSE), and bias, defined as follows:

$$RMSE = \sqrt{\frac{\sum_{i=1}^n (s_i - m_i)^2}{n}}$$

$$NRMSE = \frac{RMSE}{\frac{\sum_{i=1}^n (m_i)}{n}}$$

$$Bias = \frac{\sum_{i=1}^n (s_i - m_i)}{n}$$

with  $s_i$  and  $m_i$  the  $i^{th}$  simulated and measured values and  $n$  the number of observations.

The accuracy of model prediction was evaluated for variables related to leaf and leaflet geometry (rachis and petiole lengths, leaflet length and width, leaf and leaflet angles). Inspecting the potential errors resulting from the successive assembly of allometric relationships was crucial. As an example, the area of leaflets along the rachis (*AreaLft*) combined several allometric relationships (eq3, eq5, and eq11-18 in Table II.2) needed to reproduce accurately morphogenetic gradients. Similarly, the height of the rachis tip ( $H_A$ ; Fig. II.1) depended on many intermediate variables (stem height, leaf length, and leaf curvature) and we therefore checked the simulated values against measurements for different leaf ranks. Finally, the simulated variances computed after running 25 random simulations were compared to the observed variances using Fishers test. All statistical analyses presented above were performed with R software and the parameters of mixed-effect models were estimated using the nlme package of R.

## 3 Results

### 3.1 Progeny effect at 47 months after planting

At the plant scale, progeny effect was highly significant ( $P < 0.001$ ) for the number of leaves emitted since planting date ( $\Sigma leaves$ ) and stem basal diameter (D). However, no effect was found for phyllotaxis nor stem height ( $P > 0.05$ ; Table II.4). Stem diameter was significantly smaller for the progeny DU, which also emitted a lower number of leaves from planting date. Important and significant variability was observed in the number of emitted leaves between progenies (103-121 leaves between



Table II.4: Mean and standard deviation (in parentheses) observed per progeny and estimated heritability (broad sense) for the variables (data collected 47 MAP). Leaf rank refers to the ranks on which observations were done. Significance levels of progeny effects correspond to the P-value of ANOVA and ANCOVA

Variables	Leaf rank	Progeny					Heritability
		DA1	DL7	DS	DU	DY4	
<b>Plant scale</b>							
$\Sigma leaves$	-	116 (3) a	111 (2) b	115 (2) a	108 (4) c	109 (3) bc	0.58 ***
$\phi$ (°)	-	136.7 (0.5)	137.1 (1)	136.9 (1)	137.0 (0.7)	136.6 (0.4)	< 0.01 n.s
$H$ (cm)	-	90 (9)	84 (13)	86 (9)	78 (13)	84 (20)	0.02 n.s
$D$ (cm)	-	75 (6) a	78 (7) a	74 (6) a	63 (4) b	80 (7) a	0.53 ***†
<b>Leaf scale</b>							
$L_{rac}$ (cm)	32 ± 6	340 (28) b	326 (18) b	340 (20) c	343 (23) ab	352 (34) a	0.21 ***
$ratio_L$	32 ± 6	0.32 (0.03) a	0.25 (0.02) b	0.23 (0.02) c	0.27 (0.02) b	0.25(0.03) b	0.63 ***†
$L_p$ (cm)	32 ± 6	96 (18) a	73 (16) b	71 (15) c	76 (21) bc	87 (13) ab	0.29 ***†
$NbLft$	34 ± 6	247 (7) bc	243 (10) c	263 (16) a	244 (16) c	255 (8) ab	0.26 ***†
$FreqLft$	34 ± 6	0.72 (0.03) c	0.76 (0.05) ab	0.79 (0.07) a	0.73 (0.05) b	0.73 (0.06) b	0.28 ***†
$\delta_C$ (°)	17 ± 2	34 (5) a	38 (4) a	35 (7) a	39 (5) a	37 (5) a	0.12 *
$L_B$ (cm)	31 ± 6	79 (6) a	69 (4) c	77 (5) ab	75 (3) b	76 (5) b	0.41 ***†
$W_B$ (cm)	31 ± 6	4.3 (0.4) bc	4.1 (0.3) c	4.4 (0.3) b	5.0 (0.3) a	4.4 (0.4) b	0.44 ***†
$Area$ (m <sup>2</sup> )	30 ± 4	3.7 (0.2) a	2.7 (0.2) b	3.3 (0.4) a	3.5 (0.1) a	3.6 (0.3) a	0.65 ***†

†Progeny with different letters are significantly different (Tukeys test  $P < 0.05$ ). For variable abbreviations see Table II.1.

†Variable on which an ANCOVA is performed with progeny factor and rachis length as covariable. n.s., non-significant;

\* $P < 0.05$ ; \*\* $P < 0.01$ ; \*\*\* $P < 0.001$

plants), with DA1 and DS developing significantly more leaves than other progenies. At the leaf scale, differences between progenies were significant ( $P < 0.05$ ) for all variables. Leaf area and the ratio of petiole length to rachis length showed the most important variability between progenies and the highest inter-family heritabilities (0.63 for the ratio and 0.65 for leaf area, Table II.4). DA1 developed leaves with a petiole accounting for a third of the total leaf length ( $ratio_L = 0.32$ ) whereas DS displayed the smallest petioles ( $ratio_L = 0.23$ ). The highest density of leaflets ( $FreqLft$ ) was observed for progeny DS (0.79 leaflet cm<sup>-1</sup>) and progeny DL7 displayed the lowest leaf area. Finally,  $\delta_C$  displayed large intra-progeny variability (CV = 0.15), leading to a weak inter-family heritability estimated for this trait ( $h^2 = 0.12$ ).

For leaflet dimensions ( $L_B$  and  $W_B$ ), progenies exhibited significant differences and high heritabilities were observed ( $h^2 > 0.4$ ). Progeny DU had

the largest leaflets whereas the longest ones were observed for progeny DA1.

### 3.2 Progeny and individual effects on allometry

Likelihood ratio tests between nested models (null model, progeny model, individual model) highlighted the significance ( $P < 0.001$ ) of progeny effects for all the studied variables. For instance, at the plant scale, the growth rate parameter  $h_g$  was significantly different between progenies ( $h_g = 0.021$  for DA1 and  $h_g = 0.025$  for the other progenies). At the leaf scale, the tendency to increase leaf length during plant development ( $L_{racslp}$ ) displayed low variability between progenies (Fig. II.3A; CV = 0.06). The variability in the declination of the leaf at point C ( $\delta_C$ ) with leaf rank indicated that trends in leaf bending along the stem varied by progeny (Fig. II.3B). The progeny DU presented

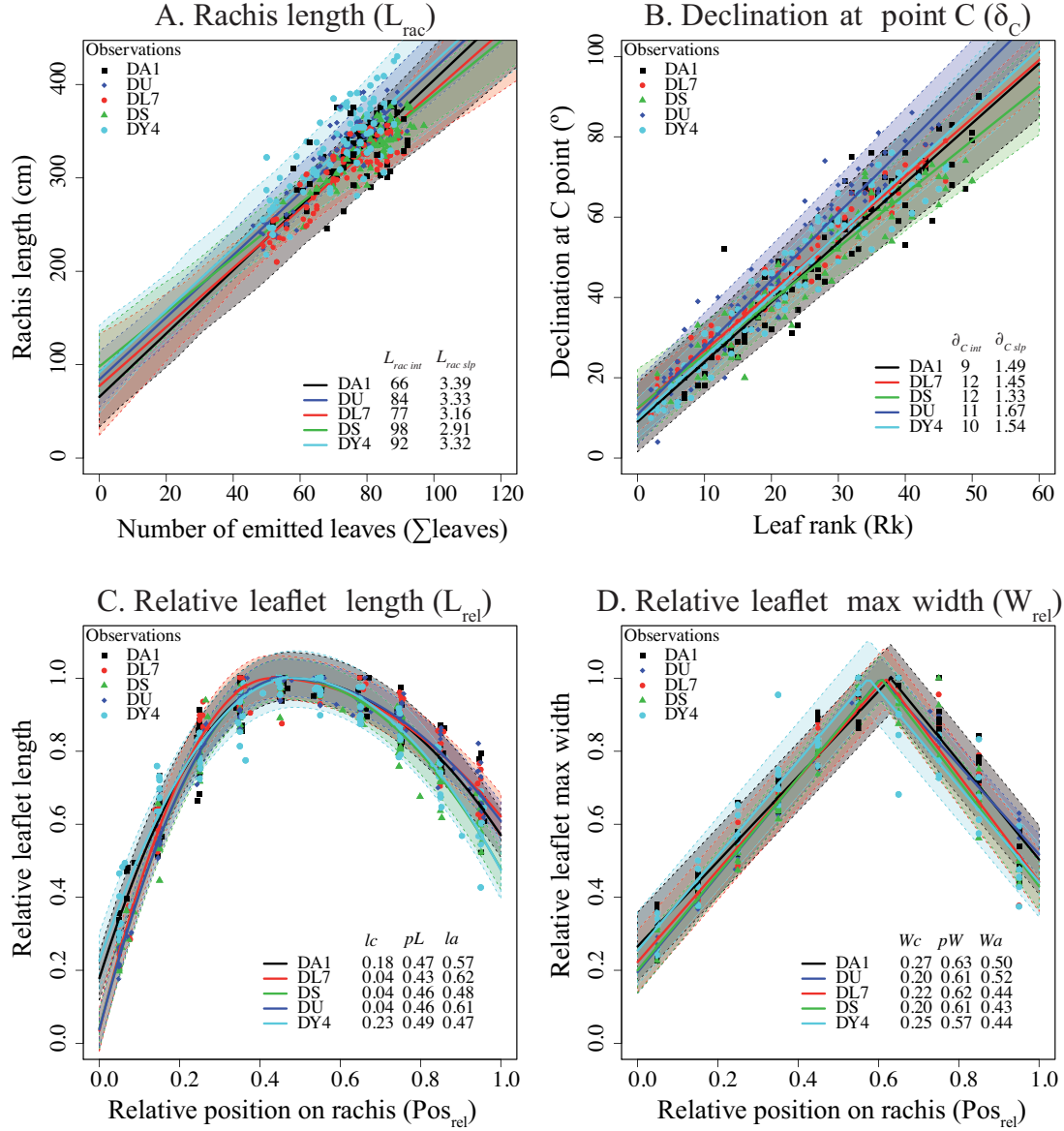


Figure II.3: Comparison of fitted curve per progeny (solid lines) for the rachis length ( $L_{rac}$ ) (A), the declination at point C ( $\delta_C$ ) (B), the relative leaflet length ( $L_{rel}$ ) (C), and the relative leaflets width ( $W_{rel}$ ) (D). Limits represent the distribution of individual effects (95% confidence intervals estimated from 100 simulations for each progeny). Mean values of parameters are presented at the lower right of each graphic. See Table II.1 for variable abbreviations, Table II.2 for parameter abbreviations, and Table II.3 for the equation used for fittings.

a steep increase in  $\delta_C$  with leaf rank ( $\delta_{C\ slp} = 1.67^\circ \text{ rank}^{-1}$ ) whereas DS displayed a slower increase in  $\delta_C$  ( $\delta_{C\ slp} = 1.33^\circ \text{ rank}^{-1}$ ). For leaflet shape, the relative position of the longest leaflet ( $p_L$ ) and the relative position of the largest leaflet ( $p_w$ ) pre-

sented low variabilities between progenies compared to leaflet length and width at rachis extremities ( $l_c$ ,  $l_a$ ,  $w_c$ , and  $w_a$ ) (Fig. II.3C, D). Parameter values per progeny for all the allometric relationships are summed up in Supplementary Table II.9.



Table II.5: Coefficient of variation per progeny and within progenies of variables and parameters associated with allometric relationships. Significance levels of progeny correspond to the P-value of the likelihood ratio tests between null and progeny models. Significance levels of individual effect correspond to the P-value of the likelihood ratio tests between progeny and individual models

Variables	Parameters	Progeny effect	Individuals effect				
			DA1	DL7	DS	DU	DY4
<b>Plant scale</b>							
<i>H</i>		***	*	*	n.s	*	n.s
	$h_0^a$	-	-	-	-	-	-
	$h_g$	0.07	0.07	0.05	0.03	0.05	0.08
<i>D</i>		***	n.s	n.s	n.s	n.s	n.s
	$D_{max}$	0.05	0.06	0.10	0.06	0.19	0.11
	$D_{slp}$	0.18	0.17	0.50	0.34	0.21	0.31
	$L_{Dinfl}$	0.04	0.07	0.07	0.07	0.13	0.13
<b>Leaf scale</b>							
<i>Lrac</i>		***	***	***	***	***	***
	$Lrac_{int}$	0.15	0.78	0.65	0.72	0.39	0.52
	$Lrac_{slp}$	0.06	0.20	0.25	0.26	0.15	0.24
<i>NbLfl</i>		***	**	n.s	n.s	n.s	n.s
	$Nb_{max}$	0.04	0.16	0.07	0.13	0.18	0.08
	$Nb_{slp}$	0.21	0.42	0.30	0.34	0.25	0.23
	$L_{Nbinfl}$	0.01	0.15	0.05	0.13	0.18	0.07
$\delta_C$		***	***	***	***	***	***
	$\delta_{Cint}$	0.13	0.42	0.29	0.41	0.45	0.25
	$\delta_{Cslp}$	0.09	0.09	0.08	0.15	0.09	0.10
$L_B$		***	***	*	**	n.s	**
	$L_{Bint}$	0.16	0.48	0.36	0.31	0.58	0.20
	$L_{Bslp}$	0.11	0.21	0.25	0.28	0.17	0.33
$W_B$		***	n.s	*	n.s	n.s	*
	$W_{Bint}$	0.18	0.16	0.33	0.18	0.40	0.16
	$W_{Bslp}$	0.31	0.23	0.34	0.64	0.34	0.68
$L_{rel}$		***	***	***	***	***	***
	$l_c$	0.84	0.21	0.67	0.92	0.92	0.51
	$p_l$	0.05	0.16	0.11	0.07	0.04	0.13
	$l_a$	0.13	0.14	0.12	0.13	0.14	0.13
$W_{rel}$		***	***	***	**	***	***
	$w_c$	0.18	0.09	0.13	0.17	0.13	0.22
	$pW$	0.02	0.05	0.06	0.03	0.03	0.07
	$w_a$	0.09	0.15	0.16	0.08	0.12	0.14

<sup>a</sup> Stem height at planting date ( $h_0$ ) was fixed at 5 cm for all progenies. n.s., non-significant; \* $P < 0.05$ ; \*\* $P < 0.01$ ; \*\*\* $P < 0.001$ ). See Table II.1 for variable abbreviations and Table II.2 for parameter abbreviations.

Likelihood ratio tests revealed significant individual effects for all variables except for stem basal diameter (Table II.5). Some variables ( $L_{rac}$ ,  $\delta_C$ ,  $L_{rel}$ , and  $W_{rel}$ ) showed a highly significant individual effect for all progenies, contrary to other variables ( $NbLft$ ,  $L_B$ ,  $W_B$ ) for which intra-progeny differences were only significant for some progenies. The highest intra-progeny variability was detected for the leaflet relative length at point C ( $l_c$ ), which exhibited a CV varying from 0.21 to 0.92 within progenies.

### 3.3 Assessment of model reconstruction

#### Assessment of mean prediction per progeny

As expected, when data were used directly to calibrate the model (Fig. II.4A), the predictions were close to observations with a NRMSE  $< 0.08$  and a low bias. Simulated petiole length ( $L_p$ ) was slightly overestimated (bias = 5.79 cm), probably because the ratio of petiole to rachis length was calibrated using older leaves that were more accessible for measurements than those used for model validation. Regarding the variables simulated from a combination of various allometric relationships (Fig. II.4B), greater discrepancies were noted, with greater NRMSE values ranging from 0.09 to 0.19. The most important differences between observations and simulations were observed for rachis heights at points A and C. Leaf area at rank 17 was overestimated on average (bias = 0.23 m<sup>2</sup>), mainly due to progeny DU showing important dissimilarities with observations (NRMSE = 0.16 for this progeny).

#### Simulation of morphogenetic gradients within the canopy

The average predictions of leaflet area along the rachis were in accordance with observations, with an RMSE varying from 19 to 27 cm<sup>2</sup> and with a bias  $< 16$  cm<sup>2</sup> (Fig. II.5A).

Predictions of leaf areas according to their position on the stem were accurate (NRMSE = 0.16) and with low bias except for progeny DU, which displayed, on average, a larger simulated leaf area than observed (bias = 0.57; Fig. II.5B).

Regarding the development of rachis height at point C ( $H_C$ ) and point A ( $H_A$ ) with leaf rank,  $H_A$  was slightly underestimated on average (bias =

-13.52 cm) with an NRMSE  $< 0.2$  (Fig. II.4B). Similarly, the decrease in HC (Fig. II.5D) was correctly simulated, particularly for progenies DA1 and DY4, but more errors were detected for progeny DL7 and DS (bias  $> 10$  cm).

#### Assessment of variance prediction per progeny

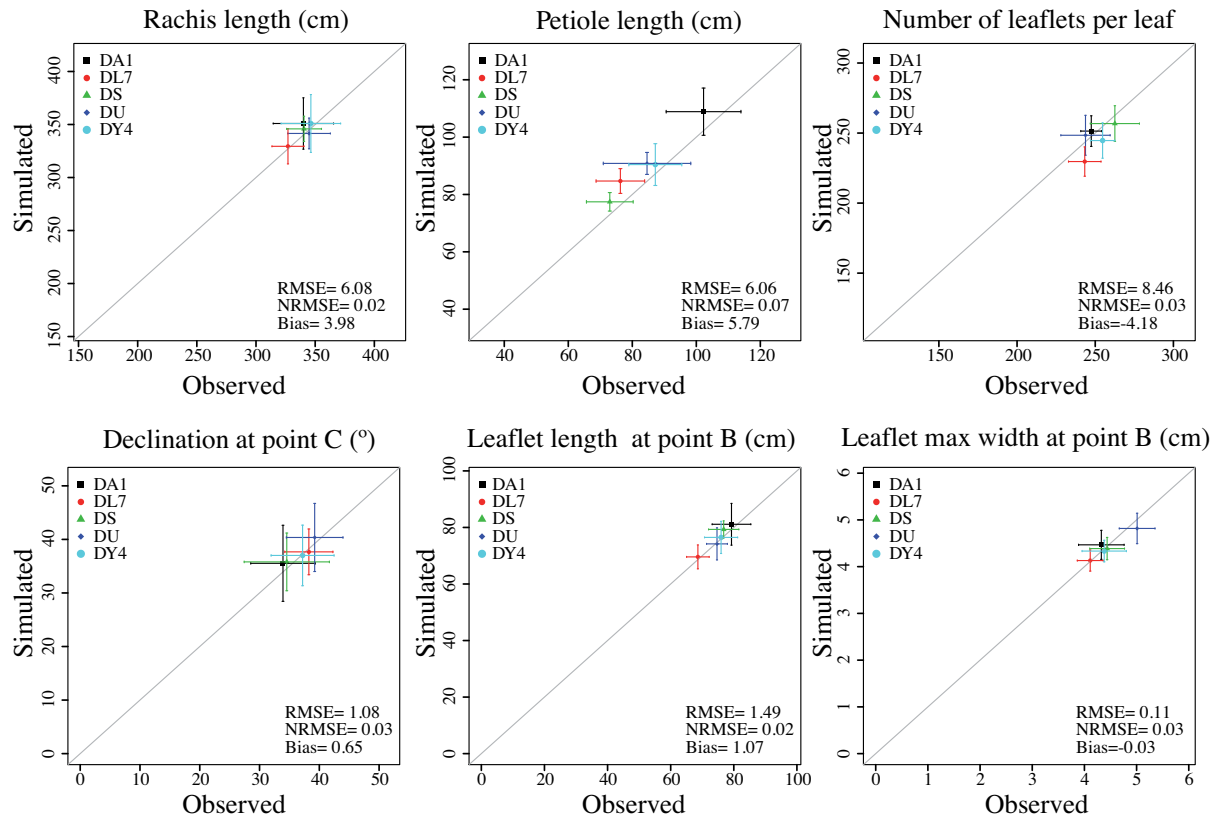
3D mockups of each studied progeny (Fig. II.6) revealed the capacity of the modelling approach to simulate the architectural genotypic characteristics described above. The quality of variance prediction was assessed for each trait by analysing the ratio of simulated SD from 25 mock-ups to the observed SD (Table II.6). No significant difference was reported between observed and simulated SD for rachis length and the declination at point C. Likewise, no difference was noticed for HA and HC (ratio varying from 0.83 to 1.85). Slight differences were observed for the number of leaflets for which the predicted SD was higher than that observed for progenies DA1 and DY4 (ratio = 1.63). Conversely, simulated variances were lower than observed for petiole length and leaflet width (Fig. II.4A); however, these differences were nonsignificant for all progenies.

Finally, the simulated leaf area SD was higher than that observed for all progenies except for progeny DS. This difference was only significant for progeny DU, in which the simulated SD was more than three times higher than the observed SD.

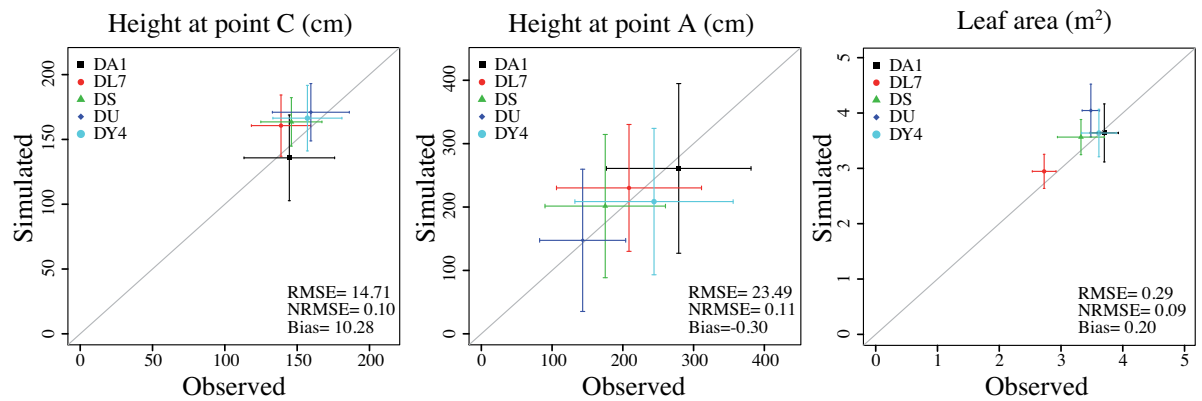
## 4 Discussion

### 4.1 Genetic control of plant architecture

The present study highlighted significant progeny effect for all studied architectural traits of young plants except for phyllotaxis and stem height (Table II.4). These results are in accordance with a study by [Billotte et al., 2010] on adult oil palms. These authors did not detect a significant difference in stem height among 15 crosses, whereas high genetic variability was highlighted for leaf and leaflet dimensions (rachis length, number of leaflets, leaflet length, and leaflet width). In other species, high heritabilities of plant height and diameter have been



#### A. Traits simulated from allometric relationship



#### B. Traits integrating successive allometric relationships

Figure II.4: Comparison between measured and simulated variables for each progeny 47 MAP (points represent mean values, crossed bars represent the range of standard deviation around mean value). Simulated variables are extracted from 25 mock-ups generated by VPalm. Declination angle at point C are represented for leaves located at rank  $17 \pm 2$ . For the other variables, the ranks of simulated leaves correspond to the ranks of observed leaves ( $30 \pm 5$  in average). Solid line represents the 1:1 line.

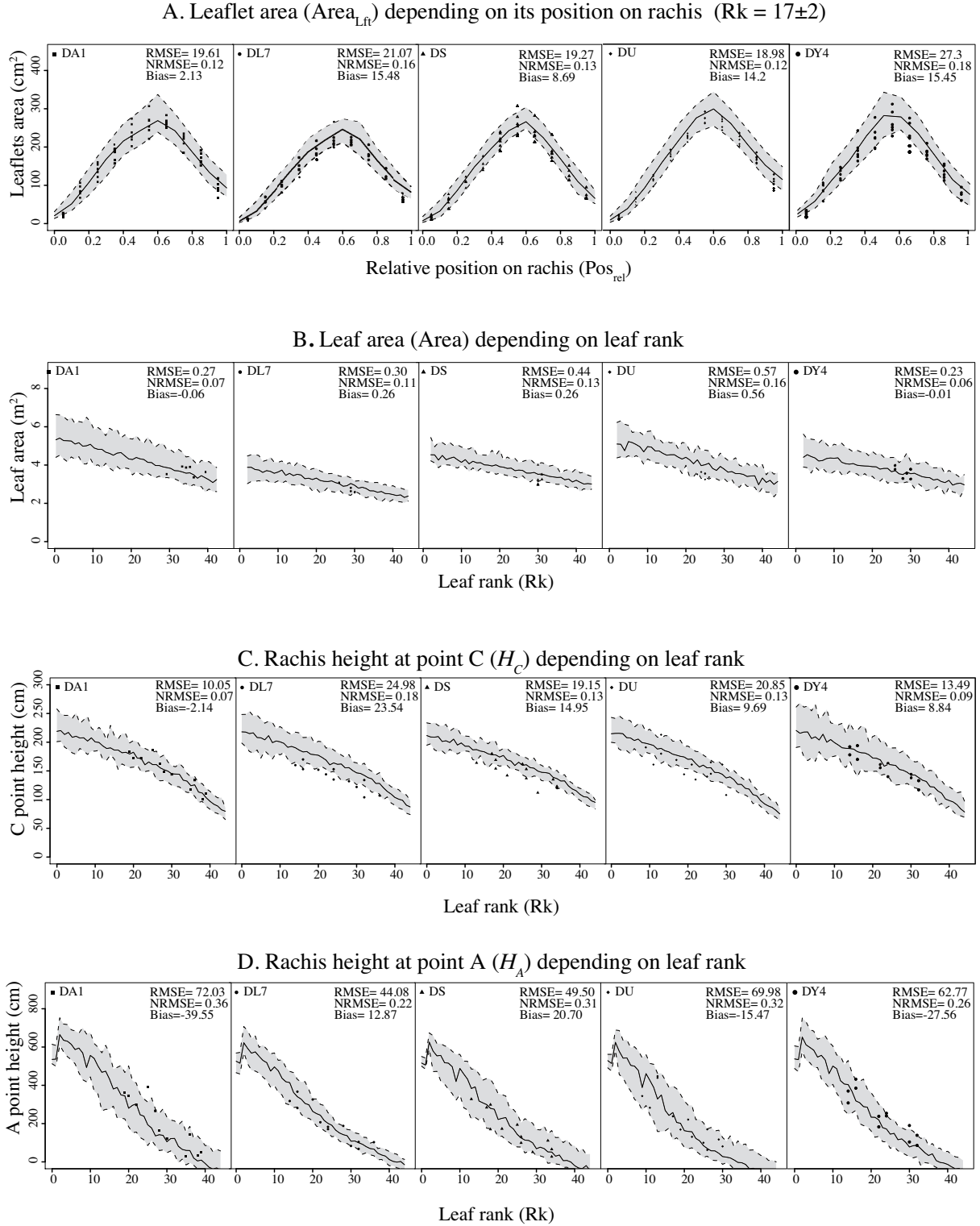


Figure II.5: Evaluation of model reconstruction for five progenies. Mean (continuous lines) and 95% confidence interval (envelopes) of predictions are calculated from 25 plants simulated with VPalm for each progeny. Points represent observed values.

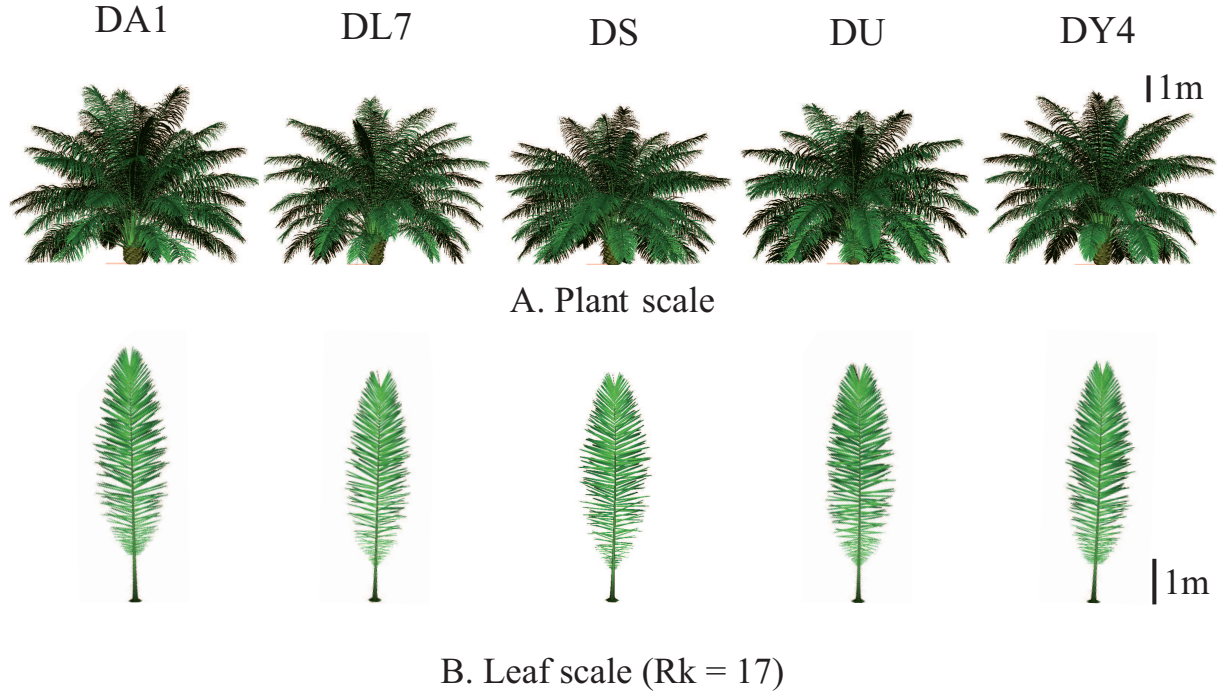


Figure II.6: Three-dimensional mock-ups simulated with VPalm. (A) Representation of an average plant for each progeny (generated from parameters mean values per progeny). (B) Top view of the 17th expanded leaf taken from the plant in panel (A).

Table II.6: Comparison between observed and simulated variances 47 MAP. The table shows the ratio of simulated standard deviation to observed standard deviation. Leaf rank refers to the ranks on which observations were done. Significance levels correspond to the P-value of the Fisher test between observed and simulated variance

Variables	Leaf rank	Progeny				
		DA1	DL7	DS	DU	DY4
<i>Lrac</i>	$32 \pm 6$	0.95 n.s	1.23 n.s	0.81 n.s	0.81 n.s	1.08 n.s
<i>Lp</i>	$32 \pm 6$	0.70 n.s	0.57 *	0.44 **	0.28 ***	0.88 n.s
<i>NbLft</i>	$34 \pm 6$	1.63 *	1.01 n.s	0.81 n.s	0.90 n.s	1.62 *
$\delta_C$	$17 \pm 2$	1.32 n.s	1.06 n.s	0.76 n.s	1.34 n.s	1.07 n.s
$L_B$	$31 \pm 6$	1.20 n.s	1.18 n.s	0.63 ***	1.72 **	1.08 n.s
$W_B$	$31 \pm 6$	0.71 **	0.91 n.s	0.72 **	0.95 n.s	0.54 ***
$H_C$	$24 \pm 8$	1.06 n.s	1.15 n.s	0.89 n.s	0.83 n.s	1.06 n.s
$H_A$	$24 \pm 8$	1.31 n.s	0.98 n.s	1.33 n.s	1.85 n.s	1.03 n.s
<i>Area</i>	$30 \pm 4$	2.29 n.s	1.61 n.s	0.83 n.s	3.38 *	1.53 n.s

n.s., non-significant; \* $P < 0.05$ ; \*\* $P < 0.01$ ; \*\*\* $P < 0.001$ . For variable abbreviations see Table II.1

previously observed in several dicotyledons, such as *Populus*, *Eucalyptus*, and apple trees (*Malus domestica*) [Bradshaw and Stettler, 1995, Byrne et al., 1997, Wu and Stettler, 1998, Osorio et al., 2001, Segura et al., 2006], and monocotyledons, such as rice (*Oryza sativa*) and maize [Hung et al., 2012, Yang and Hwa, 2008]. In these studies, heritability values were computed as the ratio of genotypic variance to phenotypic variance. In our study, the same estimation of heritability was not possible because progenies were grown without any replicate of each genotype. An inter-family broad-sense heritability (ratio of progeny variance to phenotypic variance) was thus presented as an index to estimate the stability of the architectural traits within families. This inter-family broad-sense heritability estimated at a given plant age was high for stem diameter but close to zero for stem height. Stem height was, however, significantly different between progenies when taking into account the number of leaves produced since planting date (Table II.5), suggesting potential differences in internode lengths.

At the leaf scale, the main difference among progenies was the length of the petiole relative to leaf length ( $ratio_L$ ), and this ratio was found to be the most stable trait within progenies ( $h^2 = 0.63$ ) together with leaf area ( $h^2 = 0.65$ ). Interestingly,  $ratio_L$  was much higher for the progeny DA1, which was the only family selected from an Asian pedigree. Such results indicate the importance of genetic control on leaf morphology, as has been observed in other species for leaf length and width [Frary et al., 2004, Hung et al., 2012] and leaf area [Byrne et al., 1997, Wu and Stettler, 1998]. Conversely, the low heritability found for the declination at point C contrasts with previous studies that showed high heritability of leaf angle in a maize population [Hung et al., 2012] and genetic control of leaf curvature in *Arabidopsis thaliana* [Serrano-Cartagena et al., 1999] and rice based on analyses of mutants [Yang and Hwa, 2008].

In the present study, the significant intra-progeny variability may be explained by genetic segregation and/or by soil and resource heterogeneity within the field [Welham et al., 2002]. Indeed, even if all plants were grown in the same block, the environmental variability between parcels could be confused with an inter-progeny genetic effect on the architecture due to the experimental design. The

absence of a linked pedigree between the studied families, and the lack of genetic information as well as information on soil characteristics, meant that we were not able to separate genetic effect from environmental effect. In the future, the integration of architectural phenotypic data in an experimental design involving crosses with known pedigree or clones could lead to a better depiction of the genetic control (QTL analysis) of architectural traits as previously performed for production variables in oil palm [Tisné et al., 2015].

## 4.2 Using allometry to analyse genotypic variability

The use of distinct response curves has been proposed as a way to account for the genetic variability of responses to environmental conditions in plant models [Tardieu, 2003]. Likewise allometric relationships have been used for modelling the architecture of different genotypes [Casella and Sinoquet, 2003, Rey et al., 2008]. Our allometry-based approach was particularly appropriate for oil palm because it displays a very simple branching pattern. Indeed, the regular succession of phytomers in a single axis allowed us to study and describe the whole plant architecture solely with allometric relationships based on leaf position on the stem or leaflet position on the rachis. However, allometric rules may not be sufficient to describe plants that exhibit a complex branching pattern [Lopez et al., 2008, Costes et al., 2008]. Nonetheless, the principle of coupling mathematical functions describing the relationships between plant variables (allometric relationships or response curves to environmental variables) with a mixed-effect model, as proposed here, remains relevant to any modelling approach that aims to describe genotypic behaviours.

Mixed-effect models have mainly been used in descriptive modelling approaches that deal with genotype-environment interactions [Smith et al., 2005] or, more recently, to enhance the predictive capacity of agronomic and forest growth models [Hall and Bailey, 2001, Nothdurft et al., 2006, Baey et al., 2013, Le Bec et al., 2015]. Characterizing genetic behaviour through mixed-effects models is nevertheless possible when data are available for a large number of individuals. 3D plant reconstructions based on allometric relationships were thus pre-



ferred to digitizing because of the significant time saving.

In this study, the allometric relationships selected had the benefit of using model parameters linked to geometrical and topological properties. Consequently, parameters could be directly measured in future studies (using these already defined allometric relationships) to avoid having to make exhaustive measurements to estimate parameters from curve fitting. This trade-off between model accuracy and sampling effort is fully justified in cases of quantitative genetics and studies on plant architecture that require a large number of individuals to be phenotyped.

Another advantage of using an allometric approach is the possibility of characterizing contrasting profiles of ontogenetic and morphogenetic gradients between progenies (Table II.1 and Fig II.3). Hence, not only could we compare plant architecture at a given time, we could also examine the temporal variability of architectural traits. This allowed us to detect features such as differential stem growth that were not identified at 47 MAP.

Progeny effects were, however, estimated trait by trait, without considering correlations between traits. Correlations between traits could be considered in further studies on the genetic determinism of plant architecture as a whole. From this perspective, methods discriminating classes of architecture from similarity indices between structures [Segura et al., 2008b, Kawamura et al., 2013] could be relevant. However, the classes mainly reflect the variation in the object sizes or number of components. In addition, in the absence of a genetic interaction between architectural components, such an approach may lead to a loss of important phenotypic information for breeding. Alternatively, a system of equations representing the trait dynamics or co-variations of trajectories, as proposed by Wu et al. (2011) could be used to study the genetic determinants of developmental processes of plant architecture.

### 4.3 Model simulation and accuracy of 3D reconstruction

In most modelling approaches, the general assessment of plant reconstruction relies on quantitative comparisons between means observed and simulated values for geometrical [Sonohat et al., 2006]

or topological descriptors [Costes et al., 2008], or for more integrative features related to ecophysiological variables such as light interception [Casella and Sinoquet, 2003, Louarn et al., 2008]. In the current study, the quality of plant reconstruction was evaluated both in terms of mean and variance. The overall comparison showed the accuracy of the model reconstruction because it reproduced the main differences in architectural traits between progenies (Fig. II.4 and Table II.6). Nevertheless, model simulation accuracy tended to decrease when considering integrative variables simulated by a set of equations (e.g. leaf area for progeny DU).

Contrary to the variables simulated only through direct allometric relationships ( $L_{rac}$  or  $L$ ), assessing the general quality of the 3D mock-ups generated by VPalm was not straightforward. An initial validation of the quality of the simulated 3D mock-ups was performed for the height of the rachis extremity but further investigations need to be carried out for the intra-canopy structure of plants, for instance, by using hemispherical photographs [Louarn et al., 2008] or terrestrial LiDAR [Côté et al., 2009].

### 4.4 Exploration of genotypic performance using 3D reconstruction

The architectural dissimilarities reported here between progenies, such as the number of leaflets per leaf, leaf curvature, and leaf shape, confer different spatial arrangements of leaves that likely influence light capture efficiency at the plant and leaf scale [Takenaka, 1994, Takenaka et al., 2001, Falster and Westoby, 2003, Dauzat et al., 2008]. The combination of the reconstruction model proposed here with a radiative balance model would enable us to address the influence of plant architecture on light interception, considering not only inter-progeny variability but also intra-progeny variability. One originality of our approach was to integrate differences in ontogenetic gradients among plants, which increases the potential to generate plant architecture at different stages over a plants lifetime. However, the conservation of constant allometric relationships related to plant components and morphologies during development is questionable and would need further investigation [Niklas, 1995].

The integration of inter-progeny and inter-individual variability in plant architecture is a first

step towards investigating the impact of the architecture of oil palms on their performance in the field. Forthcoming work will be dedicated to sensitivity analyses coupling our structural model with a radiative balance model to identify the key architectural traits involved in light interception efficiency. Further research could also include a transition from the static model proposed here to a dynamic model with a trade-off between 3D architecture, light interception, photosynthesis, and plant growth over time [Vos et al., 2010]. Such prospects would involve coupling this architectural model with a dedicated plant growth simulator [Pallas et al., 2013a], allowing the simulation of retroactions between plant functioning, growth, and production.

## Acknowledgements

This work was financially supported by the SMART Research Institute (SMARTRI, Smart Tbk.). The authors make special thanks to the SMARTRI staff for the logistic and technical assistance, in particular to Mr Doni A. Raharjo, Mr Fadhli, Mr Bengki, and Mr Muklis for their much valued help in the field data acquisition. We also greatly thank Nick Rowe for his help in English revision.



## 5 Supplementary material

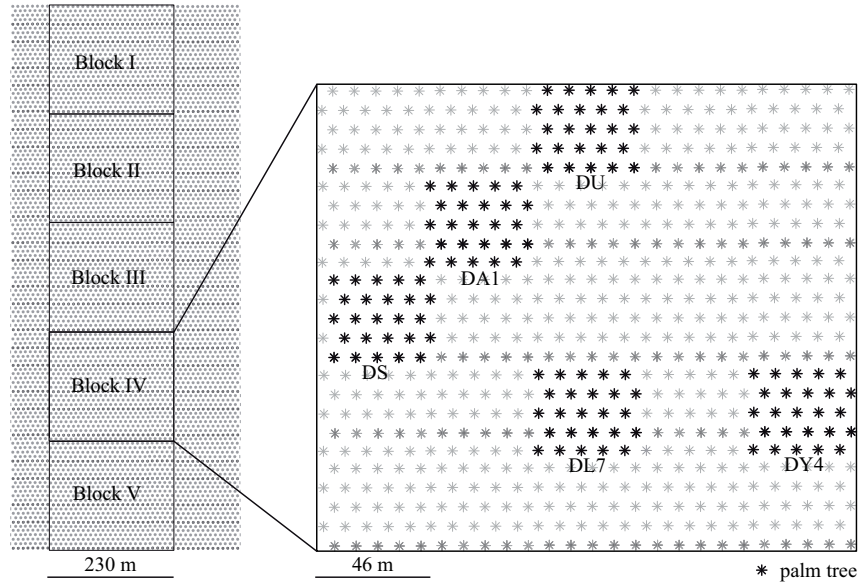


Figure II.7: Experimental design with the location of the 5 elementary parcels of the studied progenies (in black). Measurements were done on a single block to limit environmental variations.

Table II.7: Progenies description

Reference	Progeny	Origin	Characteristics
DA1	Deli x Avros	South East Asia	Large vegetative apparatus
DL7	Deli x La Mé	Africa	Low vegetative apparatus High yield
DS	Deli x (La Mé x Sibiti)	Africa	Medium vegetative apparatus Medium yield
DU	Deli x Unknown	Africa	Medium vegetative apparatus Drought tolerance
DY4	Deli x Yangambi	Africa	Medium vegetative apparatus Medium yield

Table II.8: Monitoring of data collection

Variables	Number of observations per progeny		
	Every 6 months from planting	39 months after planting	47 months after planting
Leaf Number ( $\Sigma leaves$ )	25 plants		
Stem height ( $H$ )		9 plants	12 plants
Stem basis diameter ( $D$ )	25 plants	9 plants	12 plants
Declination $C$ ( $\delta_C$ )		5 leaves x 4 plants	10 leaves x 9 plants
Rachis angles ( $\delta, \Delta, \theta$ )		5 leaves x 4 plants	3 leaves x 4 plants
Leaf length ( $L_{rac}$ ) (rank17)	25 plants	6 plants	
Leaf length ( $L_{rac}$ ) (other ranks)		6 leaves x 4 plants	4 leaves x 12 plants
Number of leaflets ( $NbLft$ )	25 plants	6 plants	12 plants
Leaf area ( $Area$ )		1 leaf x 4 plants	1 leaf x 6 plants
Leaflets length ( $L$ )	4 leaflets x 1 leaf x 25 plants	10 leaflets x 1 leaf x 4 plants	10 leaflet x 1 leaf x 6 plants
Leaflets width ( $W$ )	4 leaflets x 1 leaf x 25 plants	10 leaflets x 1 leaf x 4 plants	10 leaflet x 1 leaf x 6 plants
Leaflets angles ( $\alpha, \rho$ )		10 leaflets x 1 leaf x 4 plants	

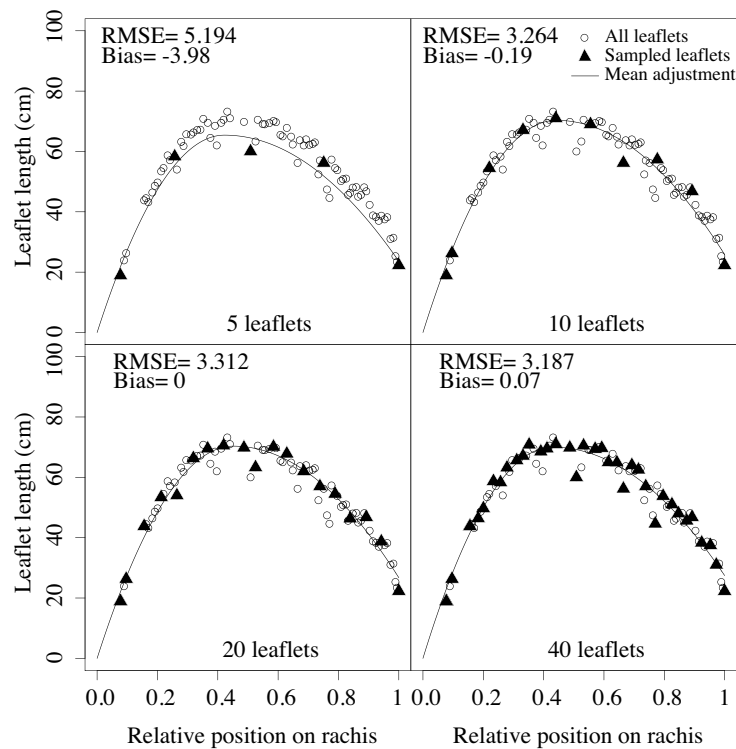


Figure II.8: Leaflet length adjustment (lines) with different sample size from observed data (circles). For each subsample (black triangles), leaflets were selected at constant intervals along the rachis. (RMSE: root mean square error).

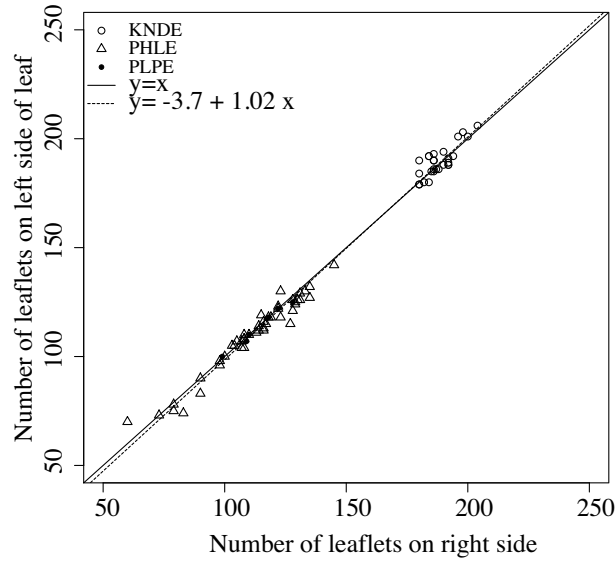


Figure II.9: Comparison of the number of leaflets on each side of rachis. Data were collected in 93 leaves in three different trials (KNDE: Deli x Avros, adult plants; PHLE: Deli x Avros, young plants; PLPE: Deli x Lam, young plants).

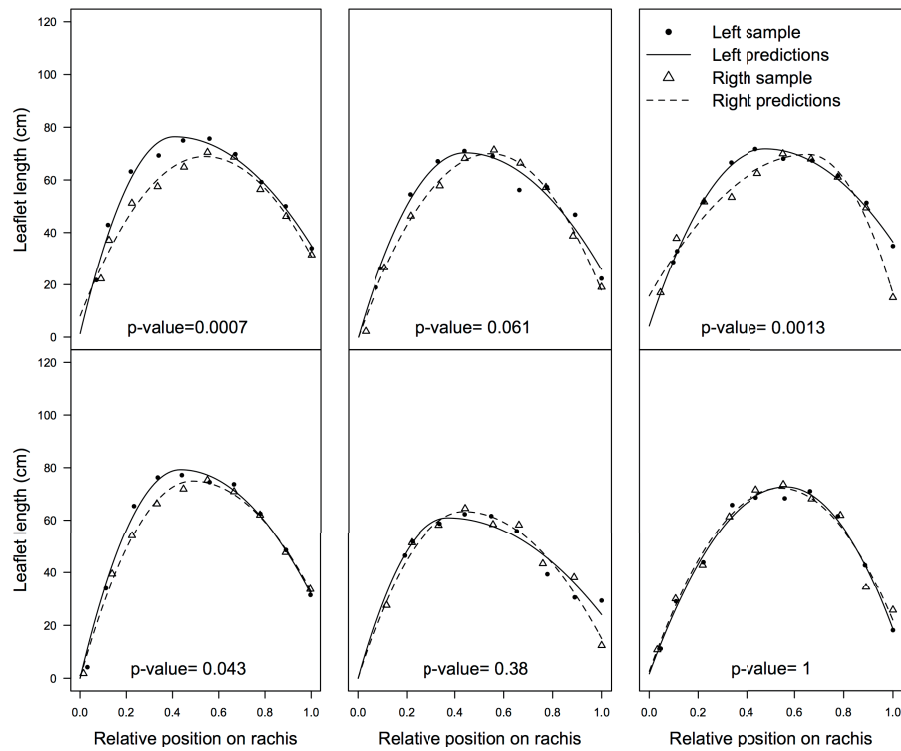


Figure II.10: Length of leaflets along the rachis measured on each side of leaf. P-value corresponds to the likelihood ratio test performed on fitted parameters for the right and left sides of the leaf (leaf is considered symmetric when P-value > 0.05).

Table II.9: Mean and standard deviation (in parentheses) of parameters used in allometric relationships for the 5 studied progenies (covariance between parameters are not presented).

Variables	Parameters	Progeny				
		DA1	DL7	DS	DU	DY4
$H$	$h_0$	5	5	5	5	5
	$h_g$	0.021	0.025	0.025	0.025	0.026
$D$	$D_{max}$	77.5	76.0	76.9	70.5	81.7
	$D_{slp}$	0.007	0.005	0.007	0.007	0.005
	$L_{Dinfl}$	168.8	153.1	165.1	160.8	175.4
$\phi$	$\phi$	136.9(0.73)	136.9(0.73)	136.9(0.73)	136.9(0.73)	136.9(0.73)
$Lrac$	$lrac_{int}$	65.5 (20.2)	77.2 (33.0)	98.0 (18.61)	84.1 (12.872)	91.8 (21.113)
	$lrac_{slp}$	3.39 (0.31)	3.16 (0.60)	2.91 (0.25)	3.33 (0.32)	3.32 (0.47)
$Lp$	$ratio_L$	0.32 (0.03)	0.26 (0.02)	0.23 (0.02)	0.27 (0.02)	0.26 (0.03)
$NbLft$	$Nb_{max}$	134	124	138	132	130
	$Nb_{slp}$	0.003	0.005	0.004	0.004	0.005
	$L_{Nbinfl}$	151.3	153.1	152.0	153.0	155.0
$\delta_C$	$\delta_{Cint}$	9.1 (2.0)	12.3 (3.0)	12.5 (3.4)	10.8 (3.4)	9.7 (0.8)
	$\delta_{Cslp}$	1.49 (0.07)	1.45 (0.09)	1.33 (0.13)	1.67 (0.05)	1.54 (0.13)
$\delta_A$	$\delta_{Amax}$	180	143	146	134	141
	$\delta_{Aslp}$	0.007	0.018	0.017	0.012	0.016
	$\delta_{Ainfl}$	40.2	24.6	19.7	12.3	15.1
$\delta$	$\delta_{sf}$	1.739 (1.61)	1.343 (0.571)	3.855 (2.856)	2.566 (2.626)	2.012 (0.634)
$\Delta$	$\Delta_a$	8.4 (9.3)	5.0 (4.8)	4.8 (6.2)	3.4 (2.8)	5.5 (6.8)
	$\Delta_{sf}$	2	2	2	2	2
$\theta$	$\theta_a$	19.6(10.8)	15.5 (12.8)	16.9 (12.2)	15.6 (12.1)	18.8 (10.4)
	$\theta_s$	3	3	3	3	3
$PosLft_{rel}$	$d_{Lft}$	2.21	2.32	2.31	2.36	2.41
$L_B$	$LB_{int}$	17.75 (3.2)	25.45 (3.15)	28.84 (4.61)	23.49 (3.60)	28.78 (0.72)
	$LB_{slp}$	0.18 (0.02)	0.13 (0.01)	0.14 (0.01)	0.15 (0.01)	0.13 (0.01)
	$PosB_{rel}$	0.63	0.60	0.608	0.624	0.62
$W_B$	$WB_{int}$	2.6 (0.1)	2.2 (0.1)	2.9 (0.1)	2.2 (0.2)	3.1 (0.0)
	$WB_{slp}$	0.005 (0.000)	0.006 (0.001)	0.005 (0.000)	0.008 (0.001)	0.004 (0.000)
$L_{rel}$	$l_c$	0.18 (0.02)	0.04 (0.01)	0.04 (0.04)	0.04 (0.05)	0.23 (0.09)
	$p_L$	0.47 (0.06)	0.43 (0.03)	0.49 (0.02)	0.46 (0.02)	0.49 (0.06)
	$l_a$	0.57 (0.08)	0.62 (0.05)	0.48 (0.04)	0.61 (0.06)	0.47 (0.07)
$W_{rel}$	$w_c$	0.27 (0.02)	0.22 (0.00)	0.20 (0.02)	0.20 (0.02)	0.25 (0.03)
	$pW$	0.63 (0.01)	0.62 (0.02)	0.61 (0.02)	0.61 (0.01)	0.57 (0.03)
	$w_a$	0.50 (0.04)	0.44 (0.03)	0.43 (0.03)	0.52 (0.05)	0.44 (0.06)
$\alpha$	$\alpha_c$	78.2 (0.1)	90.0 (2.8)	86.8 (3.4)	96.9 (2.8)	82.2 (1.7)
	$\alpha_a$	10.4 (4.8)	25.9 (0.0)	23.6 (11.7)	21.9 (1.5)	15.9 (6.3)
	$\alpha_s$	-4.69 (0.85)	-29.15 (2.43)	-12.77 (0.89)	-24.90 (4.18)	-21.04 (2.77)
$\rho_{Up}$	$\rho_{CUp}$	26.3	41.9	26.4	27.5	20.2
	$\rho_{0.5Up}$	60.5	51.3	52.5	61.5	46.3
$\rho_{MedUp}$	$\rho_{CMedUp}$	16.7	10.5	42.9	-2.9	17.3
	$\rho_{0.5MedUp}$	9.1	15.2	16.0	32.5	15.5
$\rho_{MedDwn}$	$\rho_{CMedDwn}$	-7.9	-2.0	-14.0	2.2	-10.6
	$\rho_{0.5MedDwn}$	-4.8	-3.7	-5.5	-11.8	-8.1
$\rho_{Dwn}$	$\rho_{CDwn}$	-12.3	-25.5	-2.3	-28.6	-24.0
	$\rho_{0.5Dwn}$	-34.3	-16.7	-22.9	-19.7	-15.7

## Chapter III

# Model validation and light interception efficiency among oil palm progenies

## 3D plant model assessed by T-LiDAR and hemispherical photographs: a useful tool to compare light interception among oil palm progenies

Raphaël P.A. Perez, Jean Dauzat, Frédéric Théveny, Sébastien Griffon, Jean-Pierre Caliman and Evelyne Costes

Submitted to *Agricultural and Forest Meteorology*

### Abstract

*Background and Aims:* The paradigm of functional-structural models (FSPM) assumes that entering into detail of plant structure allows a better understanding of functional processes and in particular the way plants capture light for performing photosynthesis. However, a deep attention must be paid to the consistency between virtual plants and plants in the field in terms of size and geometry to accurately evaluate light interception. This paper thus aimed at i) assessing the capacity of an architectural 3D model for oil palm (*Elaeis guineensis*) to accurately represent plants structural characteristics at both plant and plot scales and ii) using the validated 3D mock-ups to investigate how light interception efficiency varies among progenies which exhibit contrasting architectures.

*Methods:* Innovative indicators related to plant geometry and topology, were derived from terrestrial LiDAR scanners (TLS) and hemispherical photographs (HP) in order to assess a 3D plant model. Such indicators were established from field measurements and were compared to equivalent indicators extracted from virtual TLS (VTLS) and virtual HP (VHP) simulated on 3D mock-ups. Indicators were then evaluated for their significance in terms of virtual light interception at plant and plot scales. Progeny effect on light interception efficiency was finally evaluated on five different progenies.

*Key results:* The structural indicators estimated from VTLS and VHP were significantly correlated with their equivalent estimated from TLS and HP, respectively and with simulation outputs related to light interception. Light interception efficiencies estimated from the validated 3D mock-ups significantly

differed among the five progenies under study, notably from a dynamic point of view.

**Conclusions:** Our results highlight the relevance of using TLS- and HP-derived indicators to evaluate the consistency of virtual 3D reconstruction of plants in relation with light capture, at both plant and plot scales. This study paves the way for further investigations aiming at unravelling the relationships between oil palm architecture and the physiological processes driving its production.

**Key words:** 3D mock-up, *Elaeis guineensis*, genetic variability, hemispherical photographs, light interception, terrestrial LiDAR, validation.

# 1 Introduction

Functional-structural plant models (FSPM) are efficient tools for exploring plants performances [Vos et al., 2010]. They are particularly suitable for investigating how plant architecture may alter light interception efficiency or carbon assimilation, either for perennial [Lamanda et al., 2008, Louarn et al., 2008, Da Silva et al., 2013] or for annual species [Rey et al., 2008, Song et al., 2013, Barillot et al., 2014, Chen et al., 2014]. With the development of structural models able to generate genetics-dependent architecture [Kang et al., 2014, Xu et al., 2011], there is an increasing interest in using FSPM to compare genetic materials.

In this context, special care must be taken when modelling plant geometry as it influences the light captured by plants and the subsequent physiological processes such as carbon assimilation and plant transpiration. But assessing 3D architectural characteristics on virtual plants in comparison with plants observed in field still remains complex. Overcoming the methodological difficulty to assess 3D plant representations is thus a crucial point when designing FSPM for the assessment of plant performances.

FSPM validations with respect to light interception can be performed at canopy scale by different measurement methods which can provide spatialized information on either the transmitted light or leaf area distribution. Spatial information on the light transmitted can be obtained from radiometric measurements using light sensors positioned within the plant itself [Sinoquet et al., 2001], under forest canopy [Onoda et al., 2014] or field crops [Madonni et al., 2001, Xue et al., 2015]. However such measurements are quite tedious and only a small number of locations can be sampled. Besides, the installation of sensors on leaves may alter canopy structure and thus the way light penetrates the canopy [Sonohat et al., 2002]. In any case, validations are hampered by the fact that simulations must be done under the same radiative conditions as in the field, in terms of sun position as well as direct and diffuse components of incident radiation. Alternatively, measurements using the Plant Canopy Analyzer (PCA) or hemispherical photographs (HP) can provide information which is independent from radiative conditions. HPs and PCA measurements

were mostly intended to estimate leaf area index (LAI) at plot scale [Bréda, 2003, Jonckheere et al., 2004, Roupsard et al., 2008]. Both PCA and HP provide canopy “gap fractions” which are directly related to light interception since they represent the path for light rays to penetrate the canopy [Monsi and Saeki, 2005]. PCA acquisitions require nevertheless a reference sensor, positioned either above the canopy or far away from it, making it tedious to operate in case of tall canopies. Terrestrial LiDAR scanners (TLS) have been used at plot scale as an indirect ground-based method to estimate canopy gap fractions similarly to HPs [Danson et al., 2007, Ramirez et al., 2013, Seidel et al., 2015]. LiDAR-based canopy gap fraction estimation revealed some benefits compared to HPs due to its insensitivity to sky illumination, although other sources of errors have been reported [Vaccari et al., 2013]. The major limitation of point-based gap fraction is the difficulty to analyze partial-return of laser beams at the edges of vegetation components (e.g. leaves), leading to an underestimation of gap fractions [Vaccari et al., 2013, Woodgate et al., 2015].

Even if these methods are useful for getting valuable information at plot scale and can be used to validate virtual scenes, the validation of 3D geometry at individual scale requires more detailed information. In this perspective, TLS opens new prospects for characterizing single plant structure, as it allows quick and effective way of in situ collection of 3D information at plant scale, in either natural or planted stands. TLS-derived information opens new prospects for breaking through the lack of methods for characterizing single plant structure. Several studies have shown the usefulness of TLS to retrieve individual crown structure [Moorthy et al., 2011] LAI [Moorthy et al., 2008, Lin and West, 2016] or leaf area density (LAD; [Hosoi and Omasa, 2007], or to rebuild accurately tree structure from 3D point clouds [Côté et al., 2009, Hackenberg et al., 2014, Raunonen et al., 2013]. Also, Van der Zande et al [Van der Zande et al., 2011] have proposed a methodology to estimate light interception of heterogeneous forest canopy directly from TLS data (Voxel-based Light Interception Model), revealing the practical use of LiDAR for evaluating plants radiative environment.

In a previous study, a structural model of oil palm

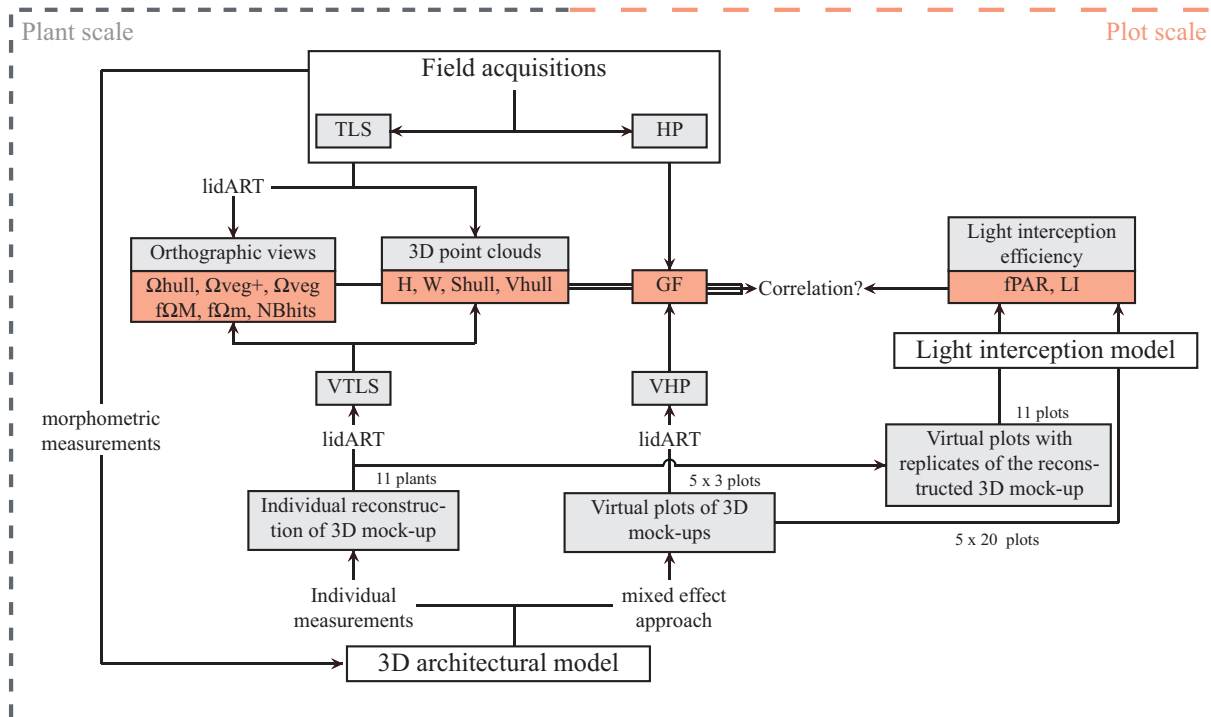


Figure III.1: Procedure to assess the quality of the 3D modeling approach in relation with light interception. The indicators and variables investigated are in red boxes (see Table III.1 page 68 for abbreviations;  $f_{PAR}$ : fraction of incident PAR intercepted;  $LI$ : Leaf irradiance).

(Vpalm) was developed to generate specific architecture of different progenies [Perez et al., 2016], able to reconstruct static mock-ups of plants derived from field measurements. The combination of this model with the radiative balance model MMR [Dauzat and Eroy, 1997, Dauzat et al., 2008] allows comparing *in silico* progenies according to their efficiency to intercept light. At plant scale, a first assessment of the developed oil palm architectural model was achieved by comparing model predictions with field observations for variables at organ scale, related to leaf and leaflets geometry (e.g. rachis and petiole length, leaflet length and shape, leaf and leaflet angles or leaf area), both in terms of progeny mean and inter-individual variance [Perez et al., 2016]. The quality of 3D mock-ups was also partially evaluated at plant scale considering the height of rachis tips. Nonetheless, the assessment of both the integrative structure and the intra-canopy structure of 3D plants, notably with respect to light interception remains to be carried out.

In the present study we propose an innovative way of using TLS to validate individual oil palm mock-ups that were independently reconstructed with the structural model and from direct morphometric measurements and allometric relationships. Integrative indicators of single plant architecture, derived from TLS, were compared to similar indicators extracted from virtual TLS performed on 3D mock-ups. At plot scale, hemispherical photographs were used to assess the quality of virtual plot representation, by comparing the variations of gap fractions between and within plots of five different progenies. The TLS and HP-derived indicators were subsequently confronted with variables related to light interception efficiency in order to evaluate the relevance of the proposed indicators for assessing the virtual 3D reconstruction of plants in relation with light capture (Fig. III.1). In a second step we use the validated mock-ups in combination with a light interception model [Dauzat and Eroy, 1997, Dauzat et al., 2008] to investigate how



light interception efficiency may vary between oil palm progenies which exhibit contrasting architecture. As the 3D model allowed simulating inter- and intra- progeny architectural variability, variations of light interception among progenies were evaluated both at individual and plot scales.

## 2 Material and Method

### 2.1 Experimental site and plant material

Field measurements were performed in experimental plots at the SMART Research Institute (SMARTRI, Smart Tbk.) located in Palembang (South Sumatra province, Indonesia). The trial was set up in 2010, 18 months after seedlings germination and growth in nursery. In this study, we focused on five elementary plots, planted with 25 plants belonging to the same progeny. Five progenies (namely DA1, DL7, DS, DU, and DY4) were selected to encompass a wide genetic background (Asian and African origins) and architectures while presenting good production performance. The planting density was  $136 \text{ plants.ha}^{-1}$  in a 9.5 m equilateral triangular pattern. TLS and hemispherical photographs were both collected between November and December 2014, i.e. approximately 4 years after planting date.

### 2.2 Data collection

#### T-LiDAR scans

A total of 11 oil palms (3 DL7, 3 DS, 3 DU and 2 DY4) were scanned with a RIEGL VZ400 terrestrial laser scanner (RIEGL Laser Measurement Systems GmbH, Horn, Austria). Each scan was centred on a single palm at a distance from its stem comprised between 6m and 8m in order to obtain a full view without occlusion from other palms in the foreground. Scans were performed with an angular resolution of 0.02 degrees in elevation and azimuth.

Recorded 3D point clouds were manually cleaned using Riegl software (RiSCAN PRO v2.0.1) in order to suppress the points belonging to weeds, soil or other palms. Because scans were collected on immature palms at a stage where the canopy was not yet closed, the surrounding 3D points of selected

palms were easily cleaned out from a zenithal viewpoint. A second filter was performed from lateral viewpoints that enabled to delete points related to weeds and soil, except around the base of the trees where weeds and lower leaves were penetrating each other.

#### Hemispherical photographs

Hemispherical photographs were recorded using a Nikon Coolpix 4.5 mega pixel digital camera with a Fish-eye lens (Nikon Tele Converter TC-E2 2X 62mm, Japan). Pictures were taken at dusk under overcast sky conditions in order to get the best conditions for images post-processing. Twenty-six images (A-Z) were collected in the inter- and intra-rows of each elementary parcel for each of the five progenies leading to a total of 130 images (see experimental design in supplementary material Fig. III.10 page 82).

### 2.3 Virtual palms modelling

The structural model that was developed to generate 3D mock-ups of oil palm [Perez et al., 2016] was built from several campaigns of data collection undertaken on 60 oil palms (12 plants x 5 progenies), from 2012 to 2016. In order to assess the evolution of plants architecture over time, allometric relationships were designed to simulate the morphogenetic gradients of architectural traits within the crown at leaf and leaflet scales. Additionally, mixed-effect models were combined with allometric relationships to account for inter- and intra-progeny variability through progeny-specific parameters. This methodology allowed the simulation of plant architecture for a given progeny while including inter-individual variability, and to generate 3D mock-ups of oil palms at different stages of their development. Virtual stands could thus be set up *in silico* composed by as many plants as desired, using the random parameters of the mixed model approach associated to inter-individual variability.

## 2.4 Generating virtual TLS (VTLS) and virtual hemispherical photographs (VHP)

### Simulation of virtual palms and virtual plots

Vpalm model [Perez et al., 2016] was used to generate two sets of virtual palms. In the first set, we used individual field measurements (leaf dimensions and curvature, leaflets dimensions) to the reconstruct 3D mock-ups of the 11 plants that were scanned in the field, in order to assess the quality of individual 3D reconstruction. The second set was designed to evaluate the capacity of the model to render intra-plot variability. For this, we simulated a plot of 16 palms per progeny consistently with the estimated variability of both topology and geometry among individuals and arranged them in a quincunx planting pattern (supplementary material Fig. III.10 page 82). For each progeny, three replicates of plots composed of different virtual palms were generated to account for inter-individual variability in further statistical comparisons with virtual hemispherical photographs. Either individual 3D mock-ups or plots were simulated within 3D scenes built in the AMAPstudio platform [Griffon and de Coligny, 2014], which enabled to extract various data (e.g leaf area) according to the topology and/or the typology of plant components. Each plot was virtually duplicated limitless (leading to an infinite canopy) in order to prevent border effects in raytracing processes.

### Raytracing simulation of VTLS and VHP

Individual 3D mocks were used to generate virtual LiDAR scans (VTLS) (Fig. III.2A) whereas plots of 16 simulated palms were used to generate virtual hemispherical photographs (VHP) (Fig. III.2B). Both VTLS and VHP were generated according to the field positions recorded for the associated TLS and HP (Fig. III.2). For VTLS, the position of the scanner relatively to the tree position was determined for each TLS acquisition by manually retrieving the direction and distance of the base of the trunk in the point cloud. The raytracing software AMAPstudio-lidART (<http://amap.cirad.fr/fr/plateformes.php>) was used for generating VTLS from individual 3D mock-up and VHP from virtual plots. First, the

scene was divided into voxels and the list of plants components (e.g. leaflets or petiole/rachis segments) that were partially or totally included in each voxel was built. Each plant component was represented by 3D mesh decomposed in triangular facets. The raytracing process was then run with the following steps for each ray: (i) find the first voxel crossed, (ii) check the intersection with triangles of plant component mesh (iii) if no intersection, record the position of the nearest hit or find the next voxel, (iv) when the ray exit the voxel space, generate the next ray in the case of VTLS or transpose the ray in the virtual neighbour duplicated plot in case of VHP. At the end of the process a virtual 3D point cloud was generated, each point corresponding to a hit of the virtual laser beam on a component of a 3D mock-up. Raytracing simulations were performed with a constant angular step for rays elevation and azimuth, consistently with Riegl VZ400 device but with lower resolution (0.1°) for minimizing computation time.

### Processing TLS and HP orthographic views for comparing virtual vs. field acquisitions

In order to generate indicators related to areas of plants that could intercept light from a given viewpoint, 3D point clouds of VTLS and TLS were represented in 2D using an orthographic projection mode generating circular images in which the distance of pixels to the image centre was linearly related to their elevation. We used orthographic projection because it allowed analysing images independently of their resolution by using solid angles. Indeed, all pixels of the projected images subtended a same solid angle which was given by:

$$\Omega_{pix} = 2\pi(1 - \cos(\frac{\delta_a}{2})) \quad (III.1)$$

with  $\Omega_{pix}$  being the solid angle of one pixel in steradians (sr) and  $\delta_a$  the angular step of the LiDAR beam, either in elevation or in azimuth. VHP were also displayed in orthographic projection for comparison with HP. It is noteworthy that such projection would be comparable to images produced by a perfect fisheye lens.

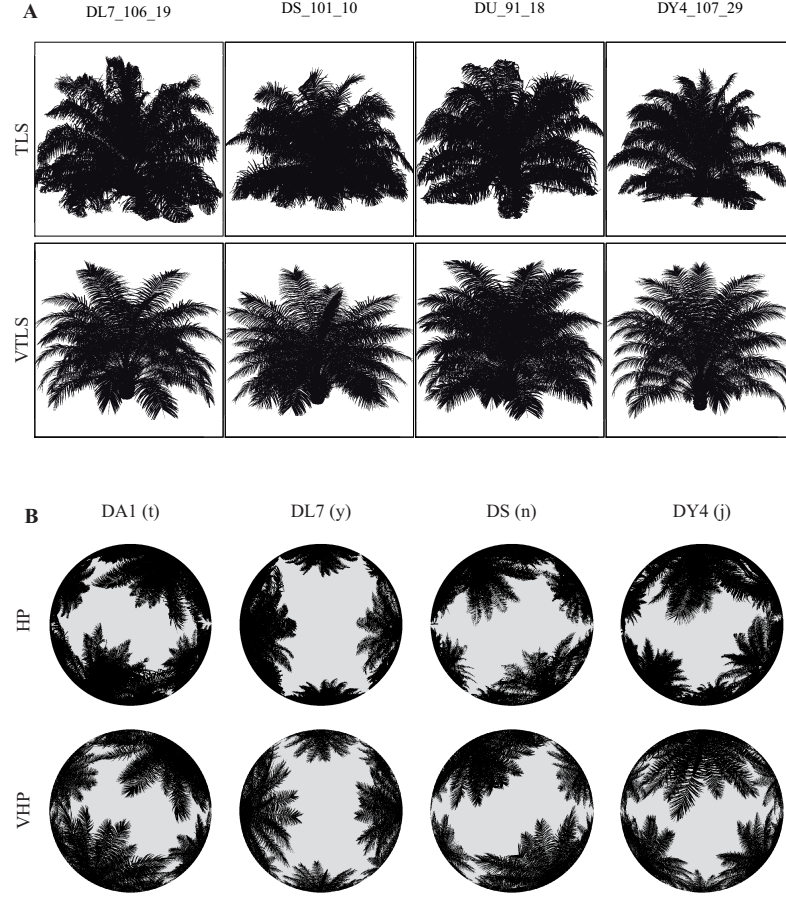


Figure III.2: A) Comparison of field TLS with virtual LiDAR scans (VTLS) obtained with AMAPstudio lidART software. B) Comparison of field hemispherical photographs (HP) and virtual hemispherical photographs (VHP) generated with lidART.

## 2.5 Validation procedure using indicators related to plant and canopy structure

### TLS-derived indicators for validations at plant scale

Three-dimensional point clouds collected from TLS and generated from VTLS were first used to estimate coarse indicators such as the plant height ( $H$ ) and width ( $W$ ), the volume of points cloud convex hull ( $V_{hull}$ ) and the area of the convex hull projection on the ground ( $S_{hull}$ ) (Table III.1). The 3D convex hulls and the associated volume and projected area were estimated using the rLiDAR

package of R [R Core Team, 2015]. Additionally, vertical crown profiles were plotted in order to visually compare TLS and VTLS lateral palm silhouettes (supplementary material Fig. III.13 page 85).

Orthographic views from TLS and VTLS were used for extracting other indicators related to the apparent plant area from the scanner viewpoint and characterizing crown structure. A first comparison was performed on the solid angle of vegetation ( $\Omega_{veg}$ ), which characterizes the area of the plant that would intercept light from a lateral viewpoint (Fig. III.3C). However, orthographic view generated from field TLS could be biased because additional 3D points could be detected on the edge of leaves depending on laser beam diameter. The laser beam

Table III.1: Indicators used to compare 3D mock-ups with field plants at individual scale (3D points clouds and TLS orthographic views) and plot scale (Hemispherical photographs (HP))

Data	Indicators	Definition	Units
3D points clouds	$H$	Plant height	m
	$W$	Crown maximal width	m
	$S_{hull}$	Projected area on soil of the 3D convex hull	m <sup>2</sup>
	$V_{hull}$	Volume of palm's 3D crown	m <sup>3</sup>
TLS views	$\Omega_{hull}$	Solid angle of palms 2D convex hull	sr
	$\Omega_{veg+}$	Solid angle of crown vegetation plus micro-gaps	sr
	$\Omega_{veg}$	Solid angle of crown vegetation	sr
	$f_{\Omega M}$	Fraction of macro-gaps into 2D convex hull	sr.sr <sup>-1</sup>
	$f_{\Omega \mu}$	Fraction of micro-gaps into crown vegetation	sr.sr <sup>-1</sup>
HP	GF	Gap fraction: ratio of sky pixels to total pixels	sr.sr <sup>-1</sup>

of the TLS apparatus used in our study has a diameter of 0.7 cm at its origin and a divergence of 0.35 mrad, leading to a diameter of 0.875 cm at a distance of 5m and 1.05cm at a distance of 10m (<http://www.riegl.com>). In order to address the possible bias induced by laser diameter, we corrected images by adding borders around vegetation pixels to mimic the effect of beam diameter. Given that up to 6 hits could be recorded for a single laser pulse with the RIEGL VZ400 equipment, we deduced that an occlusion of 1/6 of the beam could be sufficient for generating a return. Given the scanning configuration in field (with an average distance to the tree of 7m), we estimated additional returns when leaflet borders were distant to around half the of beam radius. We therefore corrected  $\Omega_{veg}$  for VTLS by applying a thin pixel border around original views as represented in supplementary material (Fig. III.11 page 83). The magnitude of correction varied between 4.5% and 8.5%, depending on virtual plants. Only values of corrected  $\Omega_{veg}$  are presented in the results.

We proposed to further characterize and compare plant structure with two additional indicators related to crown porosity: the fraction of micro-gaps ( $f_{\Omega \mu}$ ), which represent gaps within the crown, and the fraction of macro-gaps ( $f_{\Omega M}$ ), which represent the gaps outside the crown.  $f_{\Omega M}$  and  $f_{\Omega \mu}$  were given by the following equations:

$$f_{\Omega M} = \frac{\Omega_{hull} - \Omega_{veg+}}{\Omega_{hull}} \quad (\text{III.2})$$

$$f_{\Omega \mu} = \frac{\Omega_{veg+} - \Omega_{veg}}{\Omega_{veg+}} \quad (\text{III.3})$$

where:

$\Omega_{hull}$  corresponds to the solid angle of the crown envelope, defined as the lateral projection of the convex hull (Fig. III.3A)

$\Omega_{veg+}$  corresponds to the solid angle of vegetation estimated from an orthographic view generated considering a beam diameter large enough (3cm) to completely fill the micro-gaps (Fig. III.3B)

$\Omega_{veg}$  corresponds to the solid angle of vegetation (Fig. III.3C)

In order to more deeply assess the quality of the 3D structure of simulated palms, we complemented the analyses by the comparison of two profiles: 1) the relative number of pixels as a function of height that is related to the vertical and lateral extension of palm crowns and 2) the cumulated number of hits ( $Nb_{hits}$ ) as a function of their distance to the scanner position which is related to the foliage arrangement in depth, and enabled to approximate the profile of leaf area density within the crown

All these indicators (Table `retableIndicators`) were evaluated in the same way on the 11 plants that were scanned in the field (TLS) and their 11

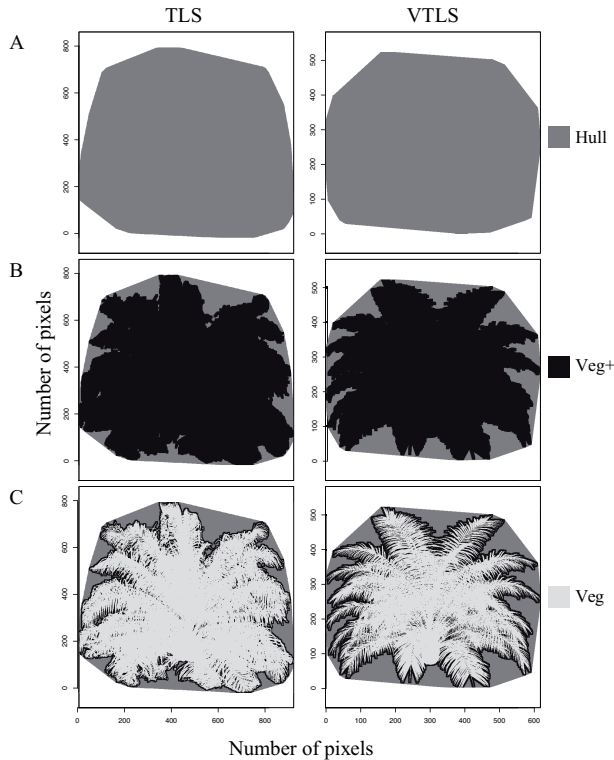


Figure III.3: Example of image processing from field TLS and 3D mock-up-derived TLS (VTLS) with representation of 2D convex hull (A), crown envelope (B) and vegetation pixels (C).

virtual counterparts (VTLS). After having evaluated the sensitivity of indicators to the azimuth of the scans (supplementary material, Table III.5 page 82), a single point of view was considered sufficient for tree to tree comparisons.

### HP-derived gap fraction for validations at plot scale

The optical centre and the projection function of the Fish-eye lens were calibrated according to the methodology proposed by Weiss and Baret [Weiss and Baret, 2010]. Gap fractions (GF) were solely analysed for elevations greater than  $20^\circ$  for precluding side effects of weeds and micro-topography in the camera field of view. As sky conditions may have changed between photographs, a specific threshold for differentiating sky from canopy in each image was estimated by an automated reclas-

sification approach (Fig. III.2B). The threshold was estimated from the histogram of frequencies of pixel values in the green colour, selecting the colour with the lowest frequency between canopy and sky colour peaks [Woodgate et al., 2015]. GF was then estimated as the fraction of sky pixels to total pixels. Subsets of pixels were selected depending on zenith angles ( $10^\circ$  to  $80^\circ$ ) to evaluate the evolution of GF from image centre to image periphery.

## 2.6 Assessment of light interception efficiency per progeny

### Light interception model and radiative conditions

Light interception was simulated on 3D mock-ups through the MMR model [Dauzat and Eroy, 1997, Dauzat et al., 2008] as described by Rey (2008). In this aim, the incident radiation was discretized into directional fluxes accounting for both direct and diffuse radiations. Then, for each direction, the plant components were projected in 2D with a Z-Buffer. The quantity of light intercepted by each plant component from each direction was obtained by counting the visible pixels. Finally, both the irradiation and area were attributed to each plant component in order to allow subsequent data extractions. Radiative conditions were simulated based on the meteorological data collected since 2012 for the studied site (Fig. III.4). A clearness index (Kt), defined as the ratio of the measured global irradiance to the corresponding irradiance above the atmosphere [Bristow and Campbell, 1984], was used first for splitting the incident radiation into its direct and diffuse components and, then, to estimate the flux density in the defined discrete directions. The seasonality of radiative conditions was accounted for by considering monthly averaged Kt values in the calculation of light interception. Consistently, the allometric-based approach allowed accounting for plant age and subsequently updating individual palm architecture every month (supplementary material, Fig. III.12 page 84).

### Calculation of radiative variables

Light calculations were performed on virtual plots including 20 stochastically generated mock-ups (i.e. generated with 20 different random seeds) disposed



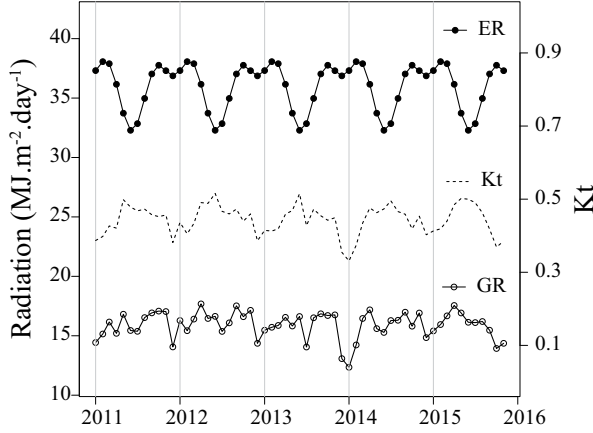


Figure III.4: Evolution of radiation in the Palembang region (*latitude* =  $-2.99^{\circ}$ ). Left axe: extraterrestrial radiation (ER) and global radiation (GR); right axe: clearness index (Kt).

in the triangular pattern previously described. Extractions of the area and the amount of light intercepted by the leaflets, the nervure (rachis and petioles) and the stem were achieved using AMAP-studio. At plant scale, the assessment the variability of light interception efficiency within progenies was studied through two different variables: the fraction of incident PAR intercepted by individual palms ( $f_{PARi}$ ) and the average leaf irradiance ( $LI$ ).  $f_{PARi}$  was obtained as the ratio of the total light intercepted by all components of a given plant on the incident light simulated on this plant, whereas  $LI$  was defined as the PAR intercepted by all its leaflets divided by their total area ( $A_{leaflets}$ ):

$$LI = \frac{PAR_{leaflets}}{A_{leaflets}} \quad (III.4)$$

At plot scale we defined light interception as the fraction of PAR intercepted by the whole canopy composed by several virtual plants ( $f_{PARc}$ ). LAI was also computed as the sum of areas of leaflets lamina in the scene divided by the scene ground area.

#### Correlation between VTLS and VHP-derived indicators and light interception

Finally virtual plots were generated from every reconstructed mock-up, and from 100 simulated

palms (20 plants x 5 progenies; generated with the stochastic approach in Vpalm) to enlarge variations in plant architecture. For each of the 111 virtual plants, radiative variables previously defined and related to light interception efficiency ( $f_{PARi}$  and  $LI$ ) were estimated and compared with the VTLS-derived indicators. Similarly, for each of the 15 virtual plots (5 progenies x 3 replicates) used to simulate the VHP, the correlations between mean GF and  $f_{PARc}$  were evaluated (Fig. III.1).

## 2.7 Statistical analyses

All statistical analyses were conducted on R software and all image processing (TLS and VLS orthographic views, HP and VHP) performed using the raster package of R. Root mean square errors (RMSE), normalized root mean square error (NRMSE) and bias were calculated for the comparison of TLS derived indicators between 3D mock-ups and simulated palms:

$$RMSE = \sqrt{\frac{\sum_{i=1}^n (s_i - m_i)^2}{n}}$$

$$NRMSE = \frac{RMSE}{\frac{\sum_{i=1}^n (m_i)}{n}}$$

$$Bias = \frac{\sum_{i=1}^n (s_i - m_i)}{n}$$

where  $s_i$  and  $m_i$  are respectively the values of indicators estimated from 3D mock-up and field TLS, and  $n$  represents the number of observations. Correlation between indicators estimated from VTLS and TLS and between VTLS or VHP indicators and light interception outputs ( $f_{PARi}$ ,  $f_{PARc}$ , and  $LI$ ) were evaluated with the Pearson coefficient  $r$ . A t-test was performed to test if the coefficient was significantly different from zero (cor.test procedure under R software).

The effect of camera position on GF estimated from HP (at zenith angle of  $80^{\circ}$ ) was studied to test if leaves were spreading in particular azimuth (North-South or East-West directions). Progeny effect on GF was studied to investigate the genetic influence on canopy closure. The significance of the two factors (camera position and progeny) on GF was tested by a two-way analysis of variances with interaction (ANOVA). Then for each factor,

a one-way ANOVA was applied to evaluate if GF was significantly different between HP and VHP. When ANOVA revealed significant difference, a post-hoc Tukeys test was performed to determine which modalities were significantly different.

The effect of progeny on light interception efficiency ( $f_{PARi}$  and  $LI$ ) was estimated by covariance analyses (ANCOVA) with clearness index, date and LAI as covariables to decipher architectural difference independently of environmental conditions or plant age. A post-hoc Tukey's test was performed to evaluate in detail which progenies were different from each other in November 2014, when TLS and HP data were collected.

### 3 Results

#### 3.1 Validation of 3D reconstructions at plant scale with TLS-derived indicators

##### Indicators from 3D points clouds

Palm height ( $H$ ) estimated from TLS was found to vary from 4.7 m to 6.3 m whereas  $H$  from VTLS varied from 5.3 m to 6.9 m (Fig. III.5). Comparisons showed a medium correlation value ( $r^2=0.61$ ; NRMSE=0.11), with nevertheless an average bias of 55 cm mainly due to an overestimation of  $H$  for small plants. Observed crown width ( $W$ ) varied from 7 to 8.6 m and had the same range of correlation with  $W$  of 3D mock-ups ( $r^2=0.60$ ) as  $H$ , with negligible errors and bias (RMSE= 35.68 cm, bias = 16.36 cm). The comparison of crown volume ( $V_{hull}$ ), and projected area on ground level ( $S_{hull}$ ), estimated from convex hull, had higher correlation coefficients between 3D mock-ups and simulated palms ( $r^2=0.77$  for  $V_{hull}$  and  $r^2=0.65$  for  $S_{hull}$ ). However volumes were overestimated in 3D mock-ups with an average error of 0.30 m<sup>3</sup> and a bias of 0.53 m<sup>3</sup> (Fig III.5).

##### Indicators derived from TLS and VTLS orthographic views

The comparison of solid angles of vegetation ( $\Omega_{hull}$ ,  $\Omega_{veg+}$  and  $\Omega_{veg}$ ) revealed little discrepancies between TLS and VTLS (Fig. III.5). Estimated

$\Omega_{hull}$  varied between 0.67 to 1.05 sr, with a correlation of 0.65 and little error between field and virtual views (NRMSE=0.13). Likewise, the  $\Omega_{veg}$  and  $\Omega_{veg+}$  indicators were correctly simulated, with a NRMSE of 0.14 and 0.13 respectively. Since  $\Omega_{veg}$  was unbiased, this indicator rendered the strong observed inter-individual variability (0.40 to 0.77 sr in TLS compared to 0.43 to 0.73 sr in VTLS).

The fraction of macro-gaps ( $f_{\Omega M}$ ) obtained from field TLS exhibited little variations among individuals ( $0.20 \pm 0.03$ ). VTLS simulations also produced stable  $f_{\Omega M}$  values, but with significant higher values than TLS on average ( $0.23 \pm 0.03$ ). Similarly micro-gap fractions ( $f_{\Omega \mu}$ ) exhibited low variability among plants.  $f_{\Omega \mu}$  was significantly overestimated in virtual views ( $0.22 \pm 0.04$ ) in comparison with field views ( $0.13 \pm 0.02$ ). An overestimation of  $f_{\Omega \mu}$  was still observed in VTLS ( $0.17 \pm 0.03$ ), even if it was markedly reduced by the correction process applied on  $\Omega_{veg}$  (supplementary material, Fig. III.11 page 83).

A visual analysis of the shape of crown profiles in height (supplementary material Fig. III.13 page 85) revealed that the largest discrepancies between TLS and VTLS views were mostly located in the lowest part of the tree crown. Remaining soil and weeds points during the cleaning process of the TLS point clouds is likely to explain the observed overestimation of  $f_{\Omega M}$  and  $f_{\Omega \mu}$ . TLS and VTLS profiles of cumulated  $Nb_{hits}$  with distance to scanner were visualized for the 11 studied individuals (Fig. III.6). Actual and virtual TLS exhibited close profiles for all individuals, with a steep linear portion followed by a portion where  $Nb_{hits}$  rapidly decreased with distance. The slope of the linear portion was visually similar between TLS and VTLS profiles but a lag could be noticed between profiles for two individuals (DY4-106-29 and DL7-107-20), probably due to the difficulty for positioning accurately the stem centre within the TLS point clouds.

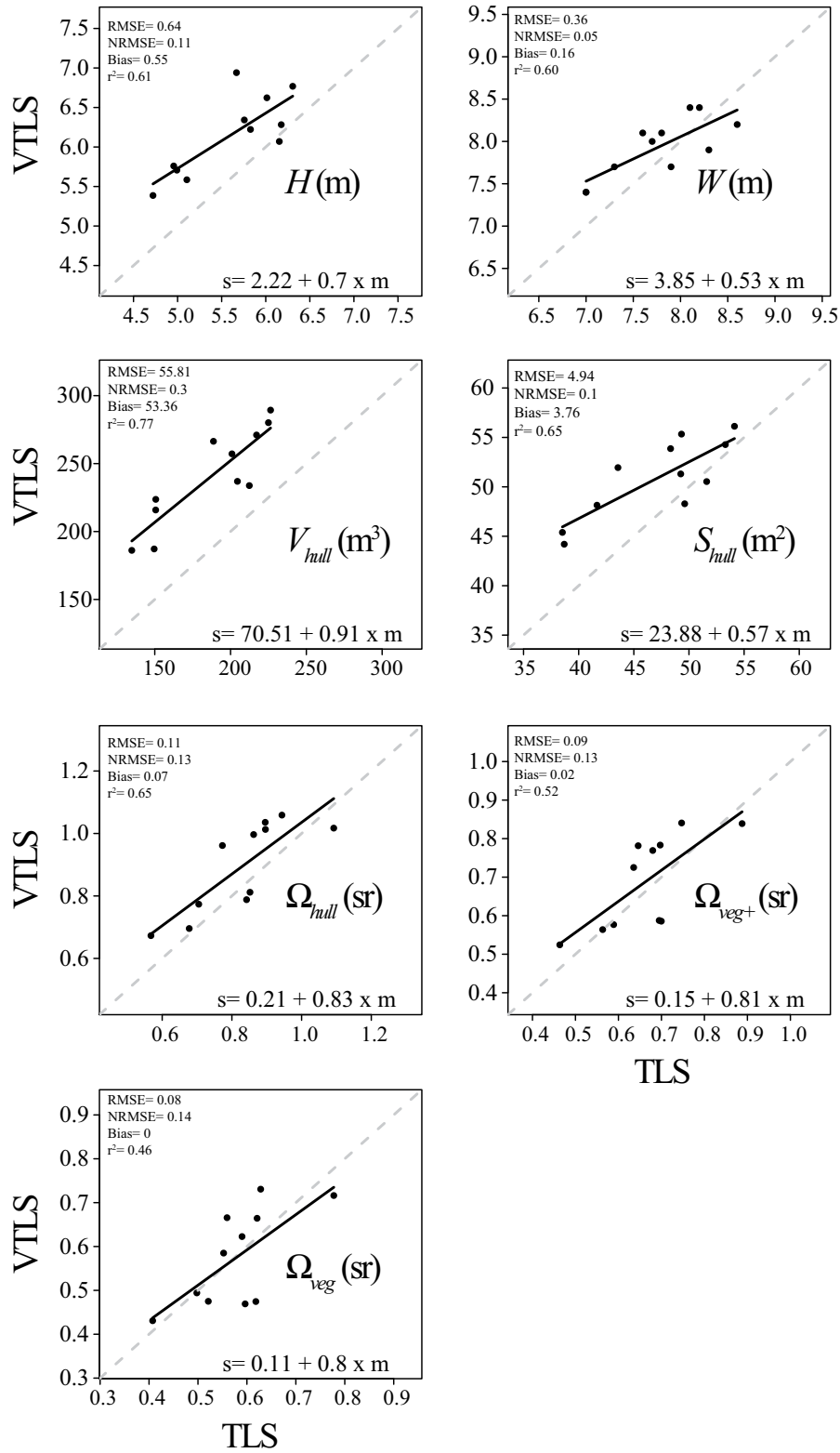


Figure III.5: Comparison of indicators derived from field TLS and virtual TLS (VTLS). Dotted lines represent the 1:1 line. See Table III.1 page 68 for abbreviations.



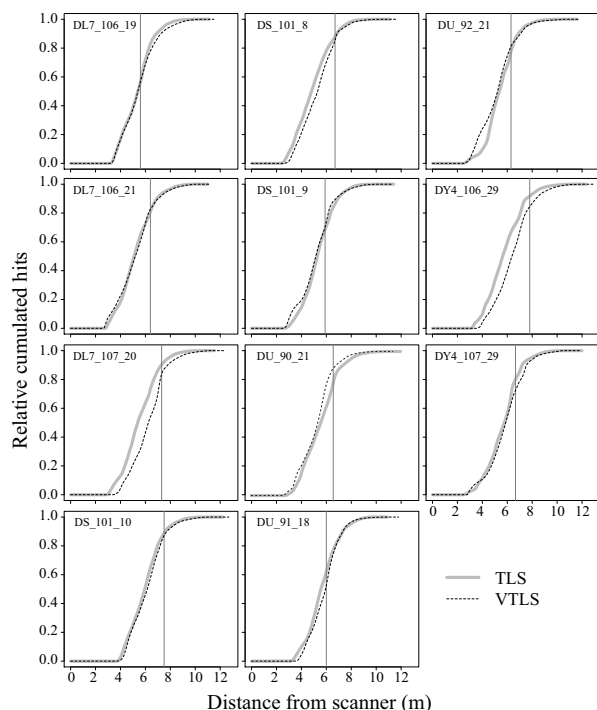


Figure III.6: Relative cumulated number of hits ( $Nb_{hits}$ ) depending on distance to scanner position for TLS and VTLS for the 11 studied plants. Vertical lines represent the estimated centre of palm stem base taken as reference for simulations.

### 3.2 HP-derived indicators to evaluate and validate architectural variabilities at plot scale

#### Influence of progeny and camera position on GF estimated from HP

The two-way ANOVA performed on GF highlighted the absence of camera position effect on the one hand and significant differences between progenies on the other hand (Fig. III.7A and Table III.2). Mean value of GF varied from 0.44 to 0.46 with three different camera positions whereas GF from 0.39 to 0.50 among progenies. The progeny effect explained 85% of the total variation. Progenies DA1 and DY4 presented lower GF (0.40 on average) than the three other progenies (0.48 on average), indicating lower canopy openness for those two progenies. The spatial variability of GF, estimated through the different positions of the camera within the plot,

was also contrasted within progenies, with a coefficient of variation varying from 7% (DS) to 16% (DA1).

#### Comparison of GFs estimated from HP and VHP

Regarding the effect of camera positioning, GF of VHP were in accordance with GF of HP since no significant difference could be detected between HP and VHP whatever the virtual plot (Fig. III.7A). Likewise, the overall variations among progenies were satisfactorily simulated, with 13 out of 15 VHP exhibiting no significant difference with the respective HP (Fig. III.7B). Progeny effect on VHP was significant for the three virtual plots although the ranking of progenies slightly differed from field results. Actually, in virtual plots 1 and 2, mean GF of progeny DA1 (0.39 and 0.33) were significantly lower than GF of progeny DY4 (0.45 and 0.42), whilst no difference was noted between these two progenies for HP as for VHP in virtual plot 3.

The consistency of virtual plots was also analysed through the evolution of GF depending on the zenith angle on HP and VHP (Fig. III.7C). Whatever the progeny and virtual plot, RMSE, NRMSE and bias were low: 0.049 to 0.076, 0.09 to 0.18 and -0.037 and 0.022, respectively. The trends of cumulated errors and bias vs. zenith angle appeared similar for all progenies, except for DA1 which presented slight dissimilarities. RMSE sharply increased from 20 to 60° before reaching a steady value whereas the absolute bias exhibited an increase followed by a decrease for highest zenith angles. These evolutions resulted from the images composition with mainly sky or vegetation pixels in their centre (zenith angle below 20°) or periphery (from 20° to 60°), respectively. Observed trends between 20 and 60 revealed an underestimation of GF in VHP, i.e. more vegetation visible in virtual plots whereas, in contrast, less vegetation was present in the peripheral zone of virtual views. Such difference was likely due to visible weeds in HP.

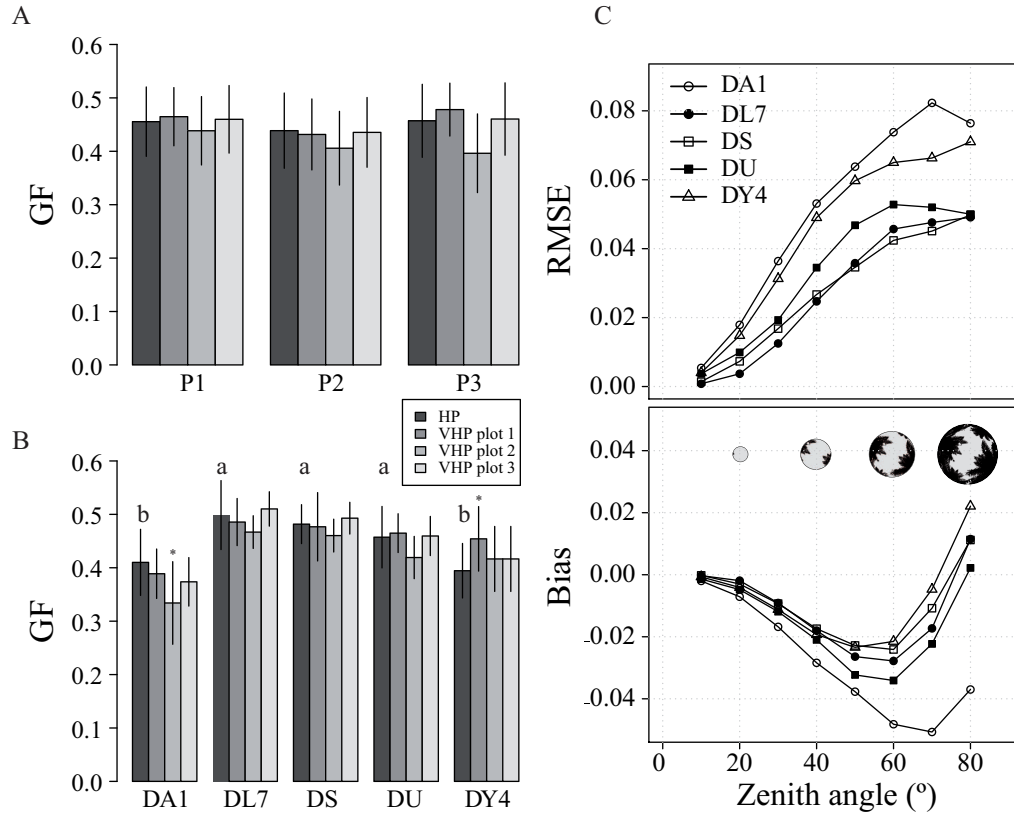


Figure III.7: Comparison of mean  $\pm$  standard deviation of gap fraction (GF) estimated from hemispherical photographs recorded in field (HP) and from virtual hemispherical photograph (VHP) with a zenith angle fixed at  $80^\circ$ . (A) Comparison for the three different camera positions in the plot. (B) Comparison for the 5 progenies. Different seeds were used to generate the 3 virtual plots (plot 1: seed 1 to 16; plot 2: seeds 17 to 32; plot 3: seeds 33 to 48). Letters indicate significant differences between HP and stars indicate VHP significantly different from the corresponding HP (Tukey's test  $p < 0.05$ ). (C) Evolution of RMSE and bias of gap fraction depending on progenies and zenith angle ( $n = 26$  pictures per progeny; outputs from plot 3).

Table III.2: ANOVA table of gap fraction (GF) estimated from field hemispherical photographs (zenith angle =  $80^\circ$ ). The ANOVA model is a two way with interactions (camera position  $\times$  progeny) model (n.s., non-significant; \*,  $p < 0.05$ ; \*\*,  $p < 0.01$ ; \*\*\*,  $p < 0.001$ ). The last column (% MS) is the relative contribution of the effect to the mean square sum.

Factor	Df	SS	MS	Fvalue	Pvalue	%MS
Progeny	4	0.2058	0.05144	16.468	***	85%
Position	2	0.0101	0.00505	1.618	n.s.	8%
Progeny $\times$ Position	8	0.0083	0.00104	0.333	n.s.	2%
Residuals	12	112	0.3498	0.00312		5%

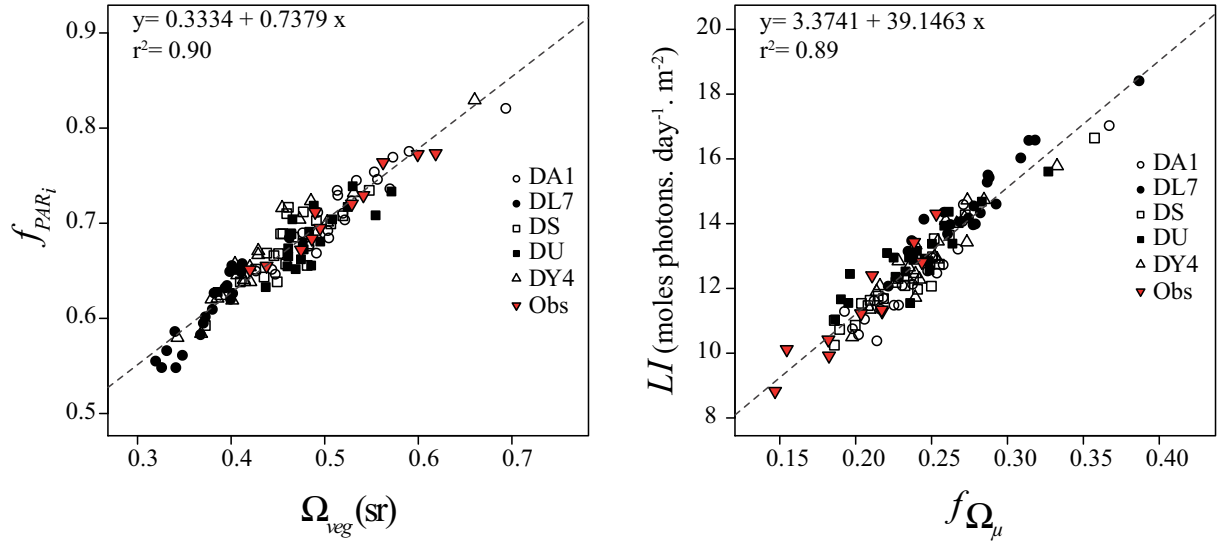


Figure III.8: Correlation between TLS indicators (solid angle of vegetation:  $\Omega_{veg}$ , fraction of micro-gaps  $f_{\Omega_m}$ ) and light interception variables ( $f_{PARi}$ ,  $LI$ ). Correlation was calculated on 20 random mock-ups per progeny plus the 11 mock-ups corresponding to the scanned plants (red triangles). Dotted lines represent the 1:1 line.

### 3.3 Correlation between simulated light interception and VTLS- and VHP-derived indicators

#### Light interception versus VTLS-derived indicators

All VTLS indicators, except  $H$ , were positively correlated with LAI,  $f_{PARi}$  and  $LI$  (Table III.3). Indicators related to crown dimensions ( $W$ ,  $S_{hull}$ ,  $V_{hull}$ ,  $\Omega_{hull}$ ,  $\Omega_{veg+}$  and  $\Omega_{veg}$ ) appeared highly correlated with the interception of incident PAR ( $f_{PARi}$ ) ( $r > 0.60$ ) whereas porosity indicators ( $f_{\Omega_M}$  and  $f_{\Omega_\mu}$ ) were correlated with LAI and  $LI$  ( $|r| > 0.8$ ).  $\Omega_{veg}$  presented the highest coefficient of correlation with  $f_{PARi}$  (0.97) and was correlated to the LAI, denoting the possibility to approximate total leaf area from lateral view. Similar results were obtained when testing those correlations with simulated palms, highlighting consistent relationships between TLS indicators and light interception for all the studied progenies and subsequently for an important range of architectural variability (Fig. III.8).

#### Light interception versus VHP-derived indicators

Regarding the relationships between GF and light interception, fair correlations were observed ( $|r| > 0.6$ ) (Table III.3). As expected, GFs obtained from VHP analyses provided relevant information about the light interception at canopy scale ( $r=0.87$  for  $f_{PARc}$ ). The overall results supported the soundness of HP for deriving valuable information at plot scale but also illustrated the interest of combining TLS and HP for getting a thorough evaluation of light interception relatively to leaf area.

#### Progeny effect on light interception efficiency

Monthly average of estimated  $f_{PARc}$  increased from 0.12 in January 2012 to 0.81 in December 2015 (Fig. III.9A). Trends of  $f_{PARc}$  over time were comparable for all progenies between 2 and 3 years (2012 to 2013), i.e. the first months after planting but differences among progenies tended to increase over years. This was especially the case for the progeny DL7 which presented a fraction of PAR interception significantly lower than the other progenies. Progeny DA1 intercepted more light than other

Table III.3: Correlation table (Pearson coefficient) between VTLS and VHP indicators with simulated radiative components, base on the 11 plants that were scanned. Mean values of LAI and LI were considered for correlations with gap fraction. Levels of significance correspond to the p-values of t-tests (n.s., non-significant; \*,  $p < 0.05$ ; \*\*,  $p < 0.01$ ; \*\*\*,  $p < 0.001$ ).

Data	Indicators	LAI	$f_{PARc}/f_{PARi}$	LI
3D points clouds (VTLS)	$H$	-0.05 n.s.	0.43 n.s.	0.20 n.s.
	$W$	0.23 n.s.	0.80**	-0.03 n.s.
	$S_{hull}$	0.22 n.s.	0.81**	0.00 n.s.
	$V_{hull}$	0.10 n.s.	0.68**	0.11 n.s.
VTLS views	$\Omega_{hull}$	0.17 n.s.	0.75**	0.03 n.s.
	$\Omega_{veg+}$	0.49 n.s.	0.94***	-0.28 n.s.
	$\Omega_{veg}$	0.74**	0.97***	-0.28 n.s.
	$f_{\Omega M}$	-0.80***	-0.44 n.s.	0.79**
	$f_{\Omega \mu}$	-0.90***	-0.42 n.s.	0.93***
VHP	GF	-0.78***	-0.87***	0.67***

progenies after four years after planting (2014). A significant progeny effect as well as the existence of interactions between progeny, plant age and LAI were highlighted by the analysis of variance performed at four years after planting, consistent with the fact that progenies have different dynamics of growth (Table III.3).

Four years after planting, the progeny effect on the fraction of light intercepted per individual was also significant (Fig. III.9B), for instance progeny DA1 captured on average 11% more of the incident light than progeny DL7 (Fig. III.9B and Fig. III.14 page 86 in supplementary material). Irrespective of the progeny, 98% of the light was intercepted by the lamina, the amount of light intercepted by the stem being negligible ( $<0.1\%$ ). In November 2014, differences in light interception were not only related to differences in LAI but also to other characteristic of progenies architecture representing 11% of the observed variance (supplementary material Table III.6 page 84). It is noteworthy that the  $f_{PARi}$  calculated from a scene composed by a unique mean individual per progeny (built with the mean value of progeny-specific parameters) was overestimated in comparison to the mean value of a population of virtual palms accounting for inter-individual variability.

A tendency to decrease over years was visible mainly because of the growth of the plant crown which increased leaf size and subsequently self and mutual shading. The effect of clearness index sea-

sonality was clearly visible on the evolution of estimated  $LI$  over time, with a decrease in  $LI$  around December and January, corresponding to the rainy season. The sharp decrease around January 2014 could be explained by an exceptional dry season due to “el niño” phenomenon, followed by important haze in the region, reducing consistently the global radiation (Fig. III.4). Progeny effect was highly significant and interactions between progeny, palm age and LAI were significant as well, indicating contrasted evolution of progeny crown structure and light interception efficiency over time (Table III.3).  $LI$  was steadily higher in DL7 (value) than in the other progenies, with an average difference of 2 moles of photons per day and per  $m^2$  of lamina in November 2014 (Fig. III.9D). The analysis of covariance of  $LI$  at that period pointed out that 18% of the observed variation was explained by progeny effect independently on their differences in LAI (supplementary material Table III.6 page 84). Inter-individual variations in  $LI$  were slightly different between progenies, with a coefficient of variation varying from 8% to 11%. Finally  $LI$  calculated from the mean individual showed some discrepancy in comparison with average values obtained from virtual population (mainly for progeny DS) (Fig. III.9D).

Table III.4: ANCOVA tables of radiative variables (n.s., non-significant; \*,  $p < 0.05$ ; \*\*,  $p < 0.01$ ; \*\*\*,  $p < 0.001$ ).  $\sqrt{f_{PARi}}$  was analysed in order to satisfy the homogeneity of the variances of model residuals.

Response	Factor/covariable	Df	SS	MS	Fvalue	Pvalue
$\sqrt{f_{PARi}}$	Progeny	4	1.13	0.28	227	***
	Kt	1	1.49	1.49	1200	***
	Date	1	137.36	137.36	110 400	***
	LAI	1	4.34	4.34	102 200	***
	Kt <sup>2</sup>	1	0.01	0.01	33	***
	Date <sup>2</sup>	1	2.56	2.56	6026	***
	LAI <sup>2</sup>	1	0.36	0.36	846	***
	Progeny x Kt	4	0.00	0.00	1	n.s.
	Progeny x Date	4	0.02	0.00	10	***
	Kt x Date	1	0.00	0.00	7	*
	Progeny x LAI	4	0.06	0.02	35	***
	Kt x LAI	1	0.00	0.00	2	n.s.
	Date x LAI	1	0.05	0.05	115	***
	Progeny x Kt <sup>2</sup>	4	0.00	0.00	0	n.s.
	Progeny x Date <sup>2</sup>	4	0.02	0.00	11	***
	Progeny x LAI <sup>2</sup>	4	0.03	0.01	17	***
	Progeny x Kt x Date	4	0.00	0.00	1	n.s.
	Progeny x Kt x LAI	4	0.00	0.00	1	n.s.
	Progeny x Date x LAI	4	0.05	0.01	27	***
	Kt x Date x LAI	1	0.00	0.00	0	n.s.
	Progeny x Kt x Date x LAI	4	0.00	0.00 0	n.s.	
	Residuals	4645	1.97	0.00		
<i>LI</i>	Progeny	4	2472	618	527	***
	Kt	1	3182	3182	2711	***
	Date	1	1133	1133	965	***
	LAI	1	2541	2541	4077	***
	Kt <sup>2</sup>	1	220	220	353	***
	Date <sup>2</sup>	1	81	81	130	***
	LAI <sup>2</sup>	1	324	324	519	***
	Progeny x Kt	4	33	8	13	***
	Progeny x Date	4	160	40	64	***
	Kt x Date	1	19	19	30	***
	Progeny x LAI	4	41	10	16	***
	Kt x LAI	1	20	20	32	***
	Date x LAI	1	43	43	70	***
	Progeny x Kt <sup>2</sup>	4	2	1	1	n.s.
	Progeny x Date <sup>2</sup>	4	37	9	15	***
	Progeny x LAI <sup>2</sup>	4	36	9	14	***
	Progeny x Kt x Date	4	4	1	1	n.s.
	Progeny x Kt x LAI	4	1	0	0	n.s.
	Progeny x Date x LAI	4	30	7	12	***
	Kt x Date x LAI	1	37	37	59	***
	Progeny x Kt x Date x LAI	4	4	1	2	***
	Residuals	4645	2895	1		

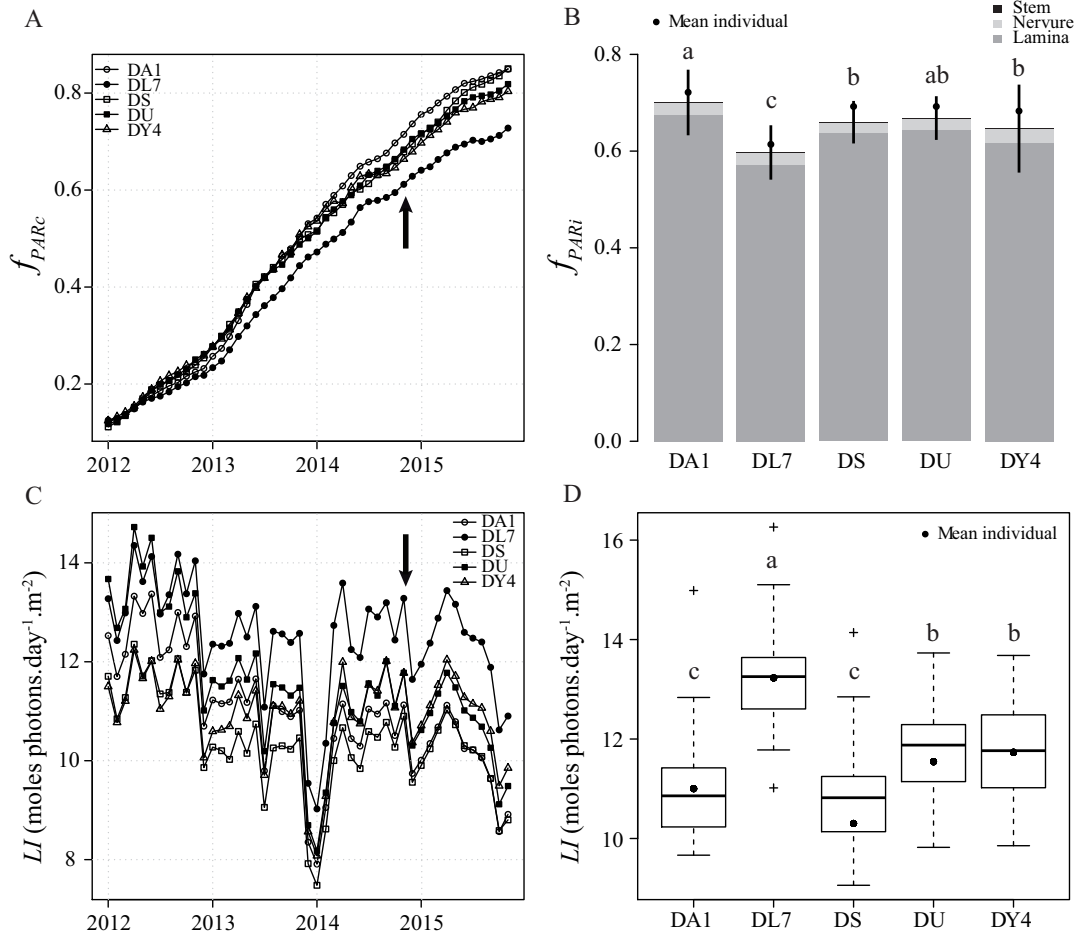


Figure III.9: A) Evolution of the fraction of PAR intercepted by the canopy (20 plants from two to six years after planting). Arrow indicates november 2014, when TLS were acquired. B) Fraction of PAR intercepted per plant four years old after planting (november 2014). Bars represents standard deviations for the 20 plants. C) Evolution of monthly average total leaf irradiance. D). Total leaf irradiance per plant four years after planting (november 2014). Letters indicate significant differences between progenies (Tukeys test  $p < 0.05$ )

## 4 Discussion

### 4.1 Scope of TLS and HP indicators for the assessment of 3D models

Up to recently HPs and PCA measurements were the popular methods for the evaluation of the consistency of virtual stands in comparison to actual ones. T-LiDAR technology is now opening wide opportunities for accessing to the 3D structure of plants. Ongoing research aims at reconstructing the

3D structure of plants through dedicated software developments [Côté et al., 2009, Hackenberg et al., 2015]. Such methods are presently not workable for palms because of their dense and intricate foliage, but various metrics can readily be extracted from LiDAR scans such as plant height or crown dimensions and volume [Moorthy et al., 2011]. We made use of such indicators ( $H$ ,  $W$ ,  $S_{hull}$  and  $V_{hull}$ ) and developed others ( $\Omega_{hull}$ ,  $\Omega_{veg+}$ ,  $\Omega_{veg}$ ) that were better correlated to both LAI and light interception. It is noteworthy that the use of TLS to validate 3D

mock-up was very suitable for palm trees since they provide a radial symmetry enabling the analysis of single view (supplementary Table III.5 page 82). More than a single viewpoint would be necessary to derive equivalent indicators on plants with more complex branching pattern, because branching element would likely greatly affect the values of solid angle depending on scanner position around the plant [Boudon et al., 2014].

Moreover, the use of TLS information enabled to evaluate 3D structure of virtual palms by detecting potential sources of bias, hardly perceived from simple geometric measurements. For instance, the comparison of crown volume ( $V_{hull}$ ) revealed an overestimation of crown expansion in 3D mock-ups, which could be explained by i) mismatches between periods of parameters calibration from morphometric measures and TLS acquisition, ii) inaccurate estimation of the altitude of stem base from TLS, iii) bias in leaves curvature modelling. This later discrepancies revealed the necessity to evaluate alteration in leaf geometry by time and environmental conditions (water availability), and subsequently the interest to integrate in our modelling approach interactions between environmental variations and 3D evolution of plant structure [Fourcaud et al., 2008].

The  $\Omega_{veg}$  and  $\Omega_{veg+}$  indicators reflected the apparent plant area as observed from a given viewpoint (here, from the scanner). In order to render these indicators independent from the scanning density, we used the notion of solid angles, i.e. apparent vegetation area from the TLS point of view, by creating TLS views with an orthographic projection comparable to the projection mode obtained with a perfect fisheye lens. First analyses of TLS views revealed that the apparent micro-gaps between leaflets were notably lower in TLS than in VTLS. The lower fraction of micro-gaps estimated from field TLS was likely attributable to the beam area of the laser recording additional hits on the edges of plant components. Similar observations were reported by Vaccari et al. [Vaccari et al., 2013] when comparing TLS views with HP views. For correcting such effect, these authors have proposed a method for “eroding” the pixels at the border of canopy gaps. By doing so, the gap size was enlarged and a better agreement between TLS and HP gap fractions was obtained. Here, we rectified VTLS

instead of correcting the data obtained from field TLS. By adding pixels in the edges of vegetation components, we simulated the effect of additional returns due to beam diameter and the biases in the fraction of micro-gaps were sharply reduced (supplementary material, Fig. III.11 page 83), but this raised questions about the calibration of the correcting process. Indeed, validation would be obtained by reproducing the TLS VZ400 specifications, but poor information was available on the laser beam diameter and on the receptor sensitivity.

Another source of error was the remaining soil and weeds pixels from TLS collected in field that resulted in an overestimation of vegetation area compared to virtual scans on which no soil was simulated (supplementary material, Fig. III.13 page 85). Such bias would no longer be a problem when working on older plants with crown high enough to easily set vegetation apart from ground.

## 4.2 Using HP and TLS indicators to validate the architecture modelling approach with respect to light interception

The analysis of the relationship between GF and radiative variables demonstrated significant correlations (Table III.3) and confirmed the interest of using GF for an integrative evaluation of light interception at canopy scale. The comparison of GF from HP and VHP emphasized that progeny effect on GF was consistently reproduced in virtual plots, DA1 and DY4 presenting a canopy closure 20% higher than other progenies. Given that the five progenies were planted at the time, such differences in canopy closure highlighted contrasted kinetic of crown development.

One way to assess the spatial heterogeneity of plots was to collect HP in various locations. Variability of the estimated GF allowed to depict inter-individual variability of space occupation, quantified by a coefficient of variation up to 15%. But, the location of cameras, in the intra- or in the inter-row of plots, did not significantly affect GF, suggesting a uniform development of the crown in all azimuths. The effect of intra-progeny variability on GF was visible when comparing the three different virtual plots of equivalent progeny, particularly for the progenies DA1 and DY4 for which the high-



est inter-individual variability was observed [Perez et al., 2016]. Indeed, since the virtual plots were represented by a limited number of plants (16 individuals), the presence of a plant with extreme size can deeply affect the variability GF within the plot.

A first validation of the virtual structures obtained from the architectural model was performed on detailed traits related to leaf and leaflets, and highlighted the consistency of the modelling approach to represent the exact geometry of organs [Perez et al., 2016]. However, the integrated spatial arrangement of plant components was set aside when evaluating organs geometry separately. The methodology proposed in this paper demonstrated that TLS provided relevant indicators to evaluate the quality of the integrative structure of individual crown.

At plant scale, the methodology proposed in this paper demonstrated that TLS provided relevant indicators to evaluate the quality of the integrative structure of individual crown. The analyses of correlations between observations and simulations of coarse indicators ( $H$ ,  $W$ ,  $S_{hull}$ ,  $V_{hull}$  and  $\Omega_{hull}$ ) revealed comparable crown size between actual trees and 3D mock-ups. Besides, the comparison of  $\Omega_{veg}$  and  $\Omega_{veg}$  between TLS and VTLS exhibited a similar density of leaflets within the crown, which is often considered as a key variable affecting light interception efficiency [Sonohat et al., 2002, Duursma et al., 2012]. Indeed, these indicators were closely linked to variables used in image-processing methods to compute light on virtual plant [Chen et al., 1993, Sonohat et al., 2002].

Even if comparisons were assessed for a unique side lateral view, TLS indicators revealed clear correlations with radiative variables (Table III.3). Only indicators related to vegetation area stressed a significant correlation with LAI and  $LI$ , contrarily to coarse indicators such as  $V_{hull}$ ,  $S_{hull}$  and  $\Omega_{hull}$ . Coarse indicators only rendered plant envelope connected to canopy openness, and thus provided information on relation to light interception at plot scale. However, at plant scale, envelopes alone were not sufficiently reliable for investigating light interception efficiency since they did not account for the disposition of leaves within structures. Several studies raised attention on considering variables such as leaf area density, leaf angle distribution and leaf clumping to estimate light interception [Van der

Zande et al., 2011, Louarn et al., 2012, Cerasuolo et al., 2013].  $\Omega_{veg}$  was satisfactory correlated with  $f_{PARi}$  and the LAI, for the 11 scanned individuals as for the 20 random individuals generated per progeny (Fig. III.8). As a result, TLS view centred on one individual palm was an excellent predictor of the total amount of light intercepted individually. Crown porosity indicators ( $f_{\Omega M}$  and  $f_{\Omega \mu}$ ), which characterized the arrangement of leaf surfaces within the crown, were correlated to  $LI$ , although discrepancies between actual and virtual plants were exhibited for these indicators. Deeper analyses should thus be performed to better explore the sources of such bias, as leaf irradiance is a key driver of photosynthesis.

### 4.3 Genetic effect on light interception

An originality of the investigated modelling approach was the study of architectural variability existing between individuals from a given progeny. Actually the large variability in light interception estimate among individuals of each progeny, likely related to heterogeneity in crown structure, supported the interest of an individual-based approach (Fig. III.8). We demonstrated that virtual scenes composed by unique mean individuals (simulated from average values of architectural parameters for a given progeny) did not generate the same  $f_{PARi}$  and  $LI$  as the ones obtained on average with a random population of individuals of the equivalent progeny (Fig. III.9). Besides, it is likely that using average parameters would be very sensitive to the number of plants observed for calibrating the model (particularly when only few plants are observed) and consequently could alter estimations of light intercepted by the canopy.

Various investigations showed differences in light interception among genotypes for both annual [Rey et al., 2008, Moeller et al., 2014] and perennial species [Jørgensen et al., 2003, Cerasuolo et al., 2013]. Our study highlighted clear differences among palm progenies with respect to light interception efficiency, both at plant ( $f_{PARi}$  and  $LI$ ) and plot scales ( $f_{PARc}$ ). Progenies with the largest crown dimensions showed fewer gaps in their canopy, leading to high values of  $f_{PARc}$ . Interestingly, the light interception efficiency was not exclusively ex-



plained by differences in LAI between the studied progenies, suggesting that specific combinations of geometric traits may optimize light interception for a given LAI (Table III.4). The differences found between progenies in crown structure, estimated four years after planting (November 2014), explained 11% of the variation in  $f_{PARi}$  and 18% of the variation in  $LI$ , independently of their difference in LAI (supplementary material Table III.6 page 84). The dynamic approach of our model also revealed distinct evolutions among progenies in the amount of light captured by the canopy, traducing different rapidity in canopy closure. This could be related to the observations made by breeders, who discriminated progenies with early bunch production (“quick starters”) from ones showing delayed production (“slow starters”) during the first years after planting (J-P. Caliman, personal communication).

Changes in plant architecture, in combination with agronomical practices, contributed to enhance plant productivity [Khush, 2001], and thus raised interest in studying the genetic control of plant architecture in various species [Wu and Stettler, 1998, Sakamoto and Matsuoka, 2004, Segura et al., 2008a, Truong et al., 2015]. Yield improvement was partly due to an enhancement in light interception [Koester et al., 2014], as a result, within an ideotype breeding context, sensitivity analyses of the 3D architectural model [Perez et al., 2016] in response to light interception could be useful for detecting the phenotypic traits optimizing light interception on oil palm and explore their relationships with plant productivity.

#### 4.4 Conclusion

New dedicated TLS indicators were derived for characterizing individual plant architecture whereas gap fractions derived from HP were used for assessing the variability of canopy structure at plot scale. The investigated indicators enabled to better detect sources of bias in the modelling approach, and the significant correlations established between indicators estimated from field measurements and from virtual scene provided a promising way for assessing 3D representation of plants, notably when the capacity of plants to intercept light is considered. Subsequently of the validation process, we used the 3D architectural model to assess light interception

efficiency of five progenies. Our result pointed out significant differences in the capacity of progenies to intercept light and raised attention to decipher the architectural traits responsible of such differences. Such prospect paves the way for further investigations aiming at defining varietal ideotype and unravelling the genetic determinism of oil palm structure.

#### Acknowledgements

The authors thank SMART Research Institute (SMARTRI, Smart Tbk.) for its financial support. We also thank Philippe Borianne for his constructive advice on images analysis.

## 5 Supplementary Material

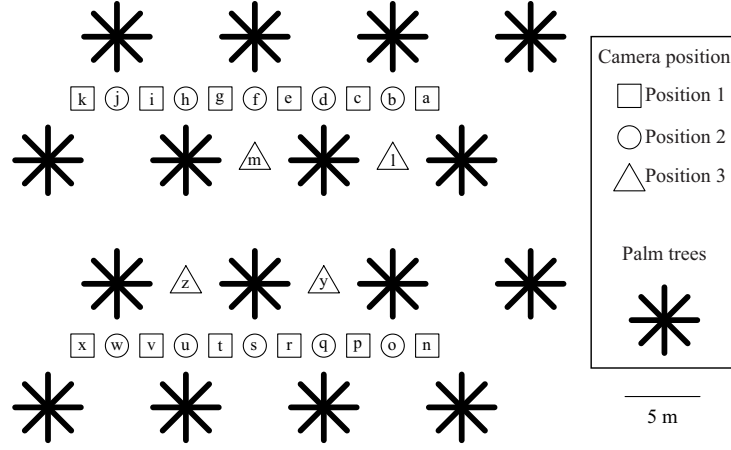


Figure III.10: Top view of the 26 hemispherical photographs positions within an elementary parcel.

Table III.5: Variation of indicators depending on equidistant positions of LiDAR (View) for an actual (TLS) and a virtual TLS (VTLS) (CV: coefficient of variation).

	View	$\Omega_{hull}$ (sr)	$\Omega_{veg+}$ (sr)	$\Omega_{veg}$ (sr)	$f_{\Omega M}$	$f_{\Omega \mu}$
TLS	1	0.78	0.64	0.55	0.18	0.13
	2	0.70	0.57	0.50	0.19	0.12
	3	0.82	0.68	0.59	0.16	0.14
<b>CV</b>		<b>0.08</b>	<b>0.09</b>	<b>0.09</b>	<b>0.07</b>	<b>0.04</b>
VTLS	1	0.86	0.63	0.46	0.26	0.28
	2	0.84	0.63	0.46	0.25	0.28
	3	0.85	0.62	0.45	0.28	0.28
	4	0.78	0.62	0.44	0.21	0.28
	5	0.82	0.60	0.44	0.27	0.28
	6	0.84	0.62	0.45	0.26	0.28
	7	0.84	0.61	0.45	0.28	0.26
	8	0.79	0.62	0.45	0.22	0.28
<b>CV</b>		<b>0.03</b>	<b>0.02</b>	<b>0.01</b>	<b>0.10</b>	<b>0.02</b>

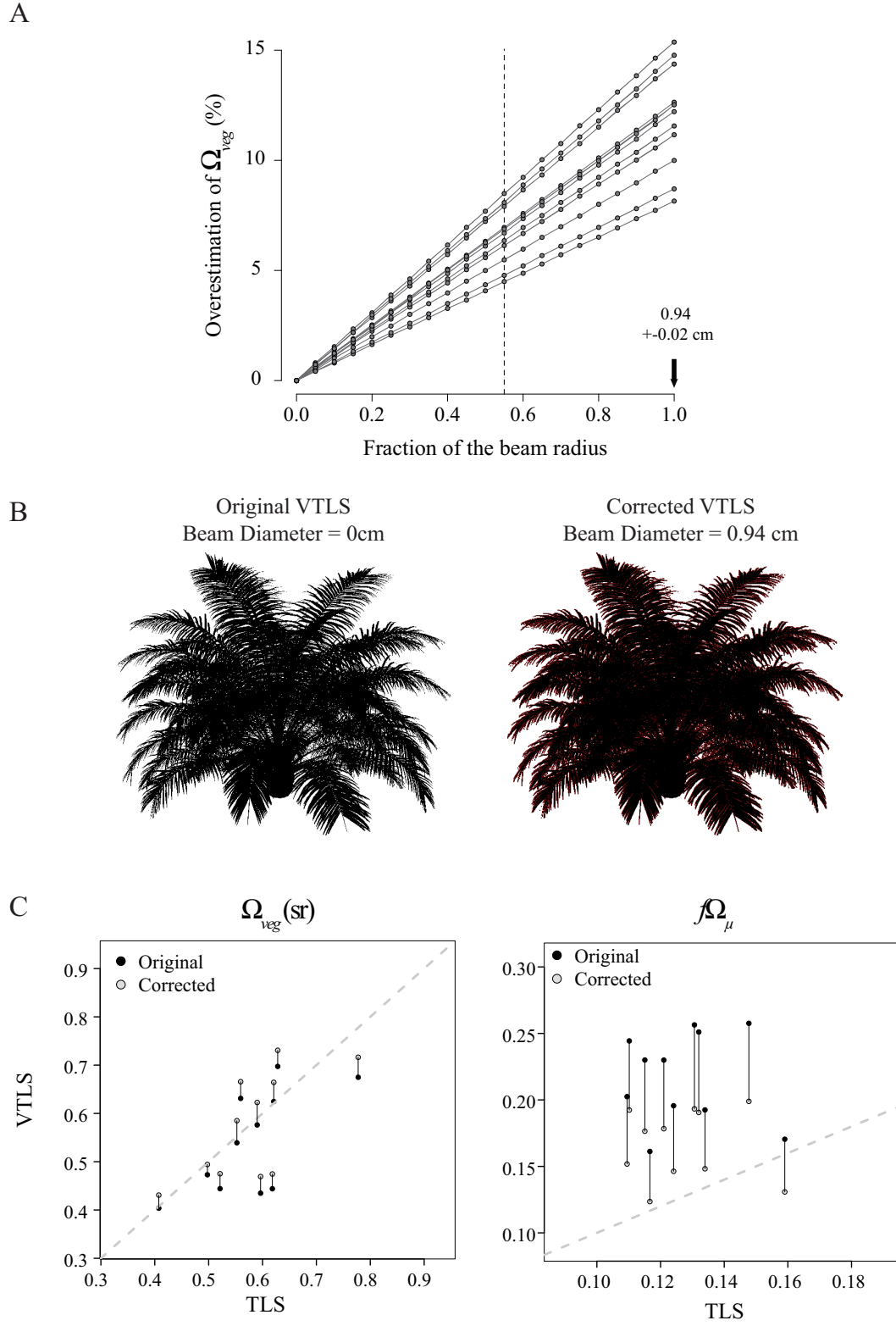


Figure III.11: A) Overestimation of  $\Omega_{veg}$  depending on the fraction of radius considered to correct each VTLS (solid lines with points). The dotted line corresponds to the fraction of beam retained to correct VTLS (0.55). B) Representation of a VTLS after correction for a radius of 0.94 cm. (C) Comparison of  $\Omega_{veg}$  and  $f\Omega_{\mu}$  before and after correction for a fraction of beam radius of 0.55

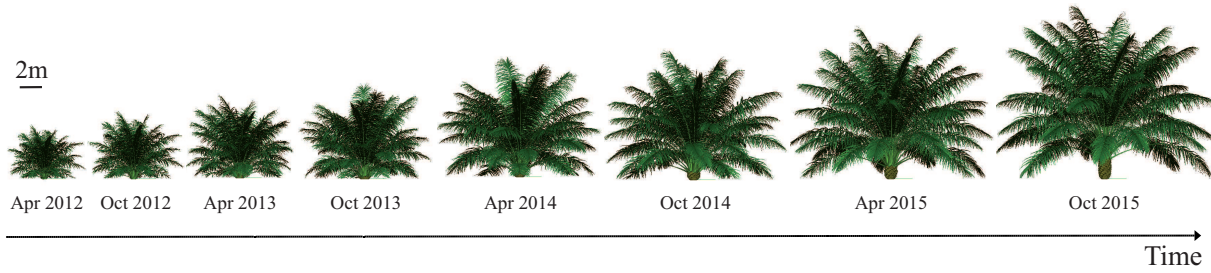


Figure III.12: Evolution of 3D mock-up architecture over time (exemple for the progeny DA1, seed 1).

Table III.6: ANCOVA tables of radiative variables in November 2014 (n.s, non significant; \*,  $p < 0.05$ ; \*\*,  $p < 0.01$ ; \*\*\*,  $p < 0.001$ ). The last column (% MS) is the relative contribution of the effect to the mean square sum.

Response	Factor	Df	Sum Sq	Mean Sq	F value	Pr(>F)	% MS
$f_{PARi}$	Progeny	4	0.11	0.03	20.08	0.0000***	11%
	LAI	1	0.24	0.24	167.14	0.0000***	89%
	Progeny:LAI	4	0.02	0.00	2.85	0.0284*	0%
	Residuals	90	0.13	0.00			0%
$LI$	Progeny	4	69.14	17.29	37.71	0.0000***	18%
	LAI	1	74.71	74.71	162.97	0.0000***	80%
	Progeny:LAI	4	4.93	1.23	2.69	0.0360*	1%
	Residuals	90	41.26	0.46			0%

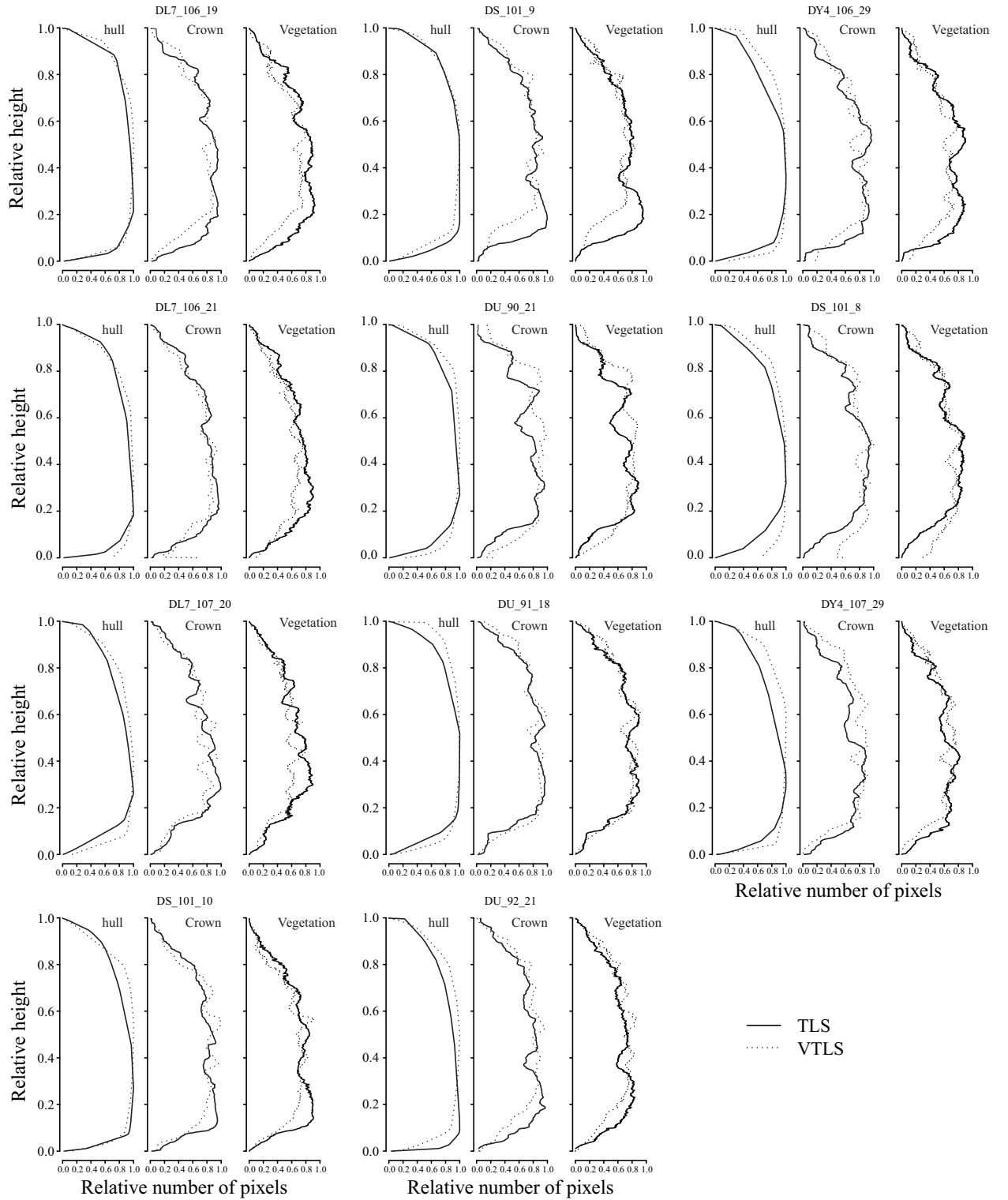


Figure III.13: Comparison of hull, crown (vegetation + microgaps) and vegetation profiles from TLS and VTLS orthographic views for the 11 studied palms. Number of pixels are expressed relatively to the number of pixels corresponding to the maximum width of the hull.



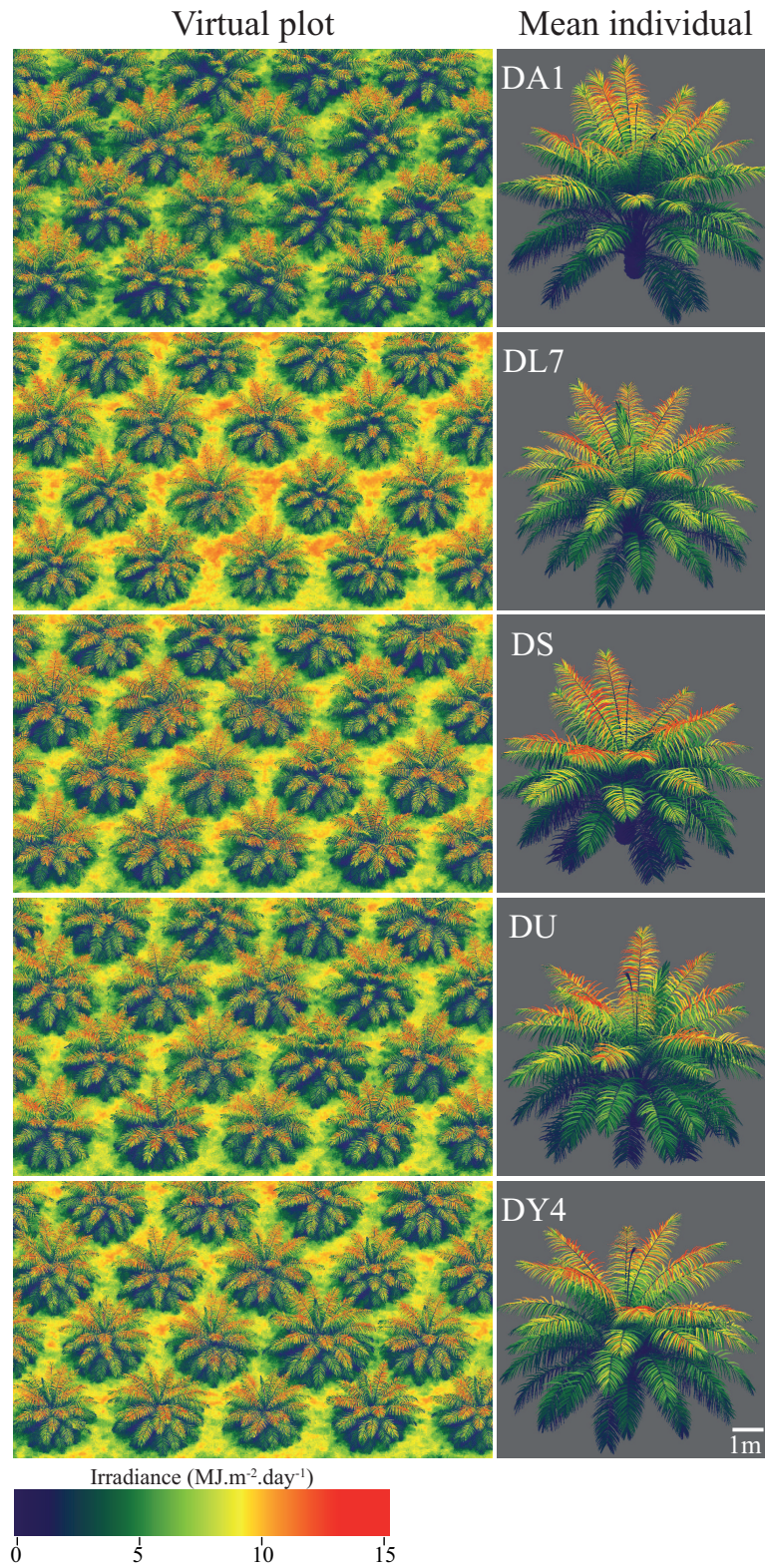


Figure III.14: Simulation of light interception on virtual 3D mock-ups for the five studied progenies (average daily value of irradiance in November 2014).

## Chapter IV

# Sensitivity analysis and Ideotype design

## Designing oil palm architectural ideotypes for optimal light interception and carbon assimilation through a sensitivity analysis of leaf traits

Raphaël P.A. Perez, Jean Dauzat, Benoît Pallas, Julien Lamour, Julien Heurtebize, Philippe Verley, Jean-Pierre Caliman, Evelyne Costes and Robert Faivre  
In preparation for *Annals of Botany*

### Abstract

**Background and Aims:** Enhancement of light harvesting in crops has successfully led to plant yield increase since the green revolution. Such an improvement has mainly been achieved by selecting plants with optimal canopy architecture for specific agronomic practices. Oil palm production has continuously increased over the past 50 years thanks to breeding programs based on fruit yield, but a yield ceiling tends to be reached under current agronomic practices. The aim of the present study was to explore potential improvement in light capture and carbon assimilation by manipulating oil palm leaf traits and propose architectural ideotypes.

**Methods:** We used a functional structural plant model (FSPM) recently developed for oil palm which takes into account genetic and inter-individual variability, in combination with sensitivity analyses based on the Morris method and a metamodeling approach, in order to virtually assess the impact of plant architecture on light interception efficiency and potential carbon acquisition.

**Key results:** The most sensitive parameters found over plant development were those related to leaf area (rachis length, number of leaflets, leaflets morphology), although fine attributes related to leaf geometry showed increasing influence when canopy got closed. In adult stands, optimized carbon assimilation was estimated on plants with a leaf area index (LAI) between 3.2 and 5.5 m<sup>2</sup>.m<sup>-2</sup>, with erect leaves, short rachis and petiole and high number of leaflet on rachis. Four architectural ideotypes for carbon assimilation were proposed based on specific combinations of organ dimensions and arrangement within the crown.

**Conclusions:** A rapid set-up of leaf area was critical at young stage to optimize light interception and

subsequently carbon acquisition. At the adult stage, carbon assimilation was optimized through specific combinations of architectural traits, which limit mutual shading and optimize light distribution within plant crown. The proposition of multiple morphotypes with comparable level of carbon assimilation opens the way to further investigation on ideotypes carrying optimal trade-off between carbon assimilation, plant transpiration and biomass partitioning.

**Key words:** *Elaeis guineensis*, FSPM, genetic variability, leaf area, light interception efficiency, meta-model, Morris method, plant architecture, progeny, shading.



# 1 Introduction

Great improvement in plant yield has been achieved since the green revolution by selecting plants adapted to specific agronomic practices [Khush, 2001]. This was particularly the case in crops for which breeding programs were designed to select key traits (morphological or physiological) defined through ideotypes [Thurling, 1991, Koester et al., 2014, Dingkuhn et al., 2015]. The concept of ideotype [Donald, 1968] relies on the possibility to combine traits of interest into an ideal plant to reach a specific purpose (yield potential, product quality) in a given environment. Seeking ideotypes thus relies on a clear understanding of how physiological and morphological characteristics control plant production on the one hand, and the possibility to combine the phenotypic traits associated to these characteristics by breeding strategies on the other hand. Improving resource use efficiency of plants by changing canopy architecture was one of the most successful strategies to enhance yields, notably for rice and wheat [Khush, 2001]. Plant architecture has thus been a criterion in the definition of ideotype for both annual [Peng et al., 2008] and perennial species [Lauri and Costes, 2005, Cilas et al., 2006].

Light interception efficiency has largely been studied since light is the source of energy that plants use to produce biomass. Light interception efficiency can be evaluated either by estimating the total amount of light intercepted by the canopy, or by focusing on the quantity of light intercepted relatively to the area of interception, or irradiance. The total amount of light intercepted, usually defined as the fraction of incident photosynthetically active radiation (PAR) intercepted, mainly results from the total leaf area disposed by the plant to intercept light. When considering irradiance, light interception efficiency relies on the trade-off between the area exposed and the quantity of light intercepted. As a result the way plants absorb light greatly depends on plant architecture, i.e. the geometrical and topological organisation of plant components [Godin et al., 1999]. Hence several studies focused on detecting the major architectural attributes that influence light interception efficiency [Pearcy et al., 2004, Sarlikioti et al., 2011, Da Silva et al., 2014]. Individual leaf area and leaf angles change light distribution

within the plant, and consequently greatly influence self-shading [Falster and Westoby, 2003]. The efficiency with which a plant intercepts solar radiation also depends on other architectural characteristics involved in the 3-dimensional (3D) arrangement of leaves, such as internode length [Dauzat et al., 2008, Da Silva et al., 2014], petiole length [Takenaka et al., 2001, Chenu et al., 2005] and branching patterns [Niinemets, 2007, Da Silva et al., 2014]. Plant architecture also impacts carbon assimilation by altering radiative and thermal conditions within the canopy [Niinemets, 2007, Chen et al., 2014]. Indeed, light intensity and temperature regulate stomatal conductance, which affects both CO<sub>2</sub> uptake and water loss [Damour et al., 2010] and subsequently the photosynthetic apparatus of leaves [Farquhar et al., 1980]. As a result, a specific spatial distribution of leaves within the canopy that optimizes carbon acquisition is likely to exist [Song et al., 2013, Chen et al., 2014]. Modelling approaches have typically been used to estimate light interception [Cerasuolo et al., 2013, Da Silva et al., 2013] and carbon assimilation of canopies [Buck-Sorlin et al., 2011, Sarlikioti et al., 2011, Chen et al., 2014] because they are roughly measurable in field.

The development of plant modelling opened new paths to explore plant performances and the possibility to build breeding strategies on predicted yield capacity rather than on recorded yield [Martre et al., 2014]. Functional-structural plant models (FSPM) allowed investigating the relationships between plant structure and physiological responses by explicitly representing plant architecture [Vos et al., 2010]. The development of a FSPM relies on the combination of an architectural model, which virtually describes the 3D architecture of the plant, with biophysical and physiological models (light interception, photosynthesis, transpiration, N allocation). FSPM are thus valuable tools for dissecting physiological traits into their constitutive components [Kang et al., 2014]. Sensitivity analyses performed on FSPM allow the evaluation of the relative contribution of each architectural trait as well as their interactions with variations in physiological responses [Da Silva et al., 2014]. Among sensitivity analyses, different methods can be applied according to the precision required to characterize parameter effects, from screening methods (global sorting among a large number of parameters) to

quantitative measures of parameters influences [Ioss, 2011, Faivre et al., 2013]. The exploration of FSPM behaviour with sensitivity analysis constitutes a step forward the virtual design of architectural ideotypes.

In this study we used a FSPM of oil palm to explore the impact of plant architecture on light interception efficiency and potential carbon acquisition. Indeed, oil palm production has continuously increased over the past 50 years through breeding programs based on fruit yield (bunch production and oil extraction rate) [Corley and Tinker, 2016], but a yield ceiling tends to be reached under present agronomic practices (see Figure I.9 page 31). So far little attention has been paid to the inter-connections between oil palm architecture and the physiological processes underlying oil palm productivity. The present study thus proposes alternative ways to improve oil palm performances through the enhancement of radiation use efficiency (RUE). Giving the hypothesis that oil palm architecture is heritable, which has already been shown for some architectural characteristics [Billotte et al., 2010, Barcelos et al., 2015, Perez et al., 2016], this study aimed at defining architectural ideotypes for light interception and carbon assimilation under current agronomic management. Based on a previous work which made possible to virtually generate 3D oil palm with a detailed description at organ scale [Perez et al., 2016], we tested different combinations of organ geometry in relation to light capture and carbon acquisition. Simulations reproduced the light environment of an industrial production system (planting density) under optimal radiative conditions. Sensitivity analyses based on architectural variations calibrated from five different oil palm progenies, allowed detecting the major architectural traits that should be taken into consideration to initiate breeding strategies based on architectural ideotypes.

## 2 Material and Method

### 2.1 Overall strategy

The methodological approach developed in the present study is divided in two consecutive sensitivity analyses. Both analyses explore the behaviour

of a FSPM that integrates an architectural model, a light interception model and a photosynthesis model. Responses in light interception and carbon assimilation are analysed depending on variations of architectural inputs. The first sensitivity analysis is a screening method, namely the Morris' method [Morris, 1991], which aims at identifying and hierarchizing the influence of a large number of architectural parameters (section 2.5). Given the relatively low cost in computation time, this first method enables to integrate the dynamic approach of the structural model, while designing comparable numerical experiments for six discrete steps of plant development (from 2 to 15 years old after planting). Hence it was possible to analyse the constancy of parameter influence over time and to detect the parameters with negligible effect. In a second step, these insensitive parameters are fixed to their mean value and a metamodeling approach is performed to estimate quantitative sensible indices for the most influential architectural parameters, at a given developmental stage. This overall methodological process combined R software scripts [R Core Team, 2015] with Java scripts on the Archimede platform (<http://amapstudio.cirad.fr/soft/archimed/start>). Simulations for both sensitivity analyses were run and achieved within two days thanks to the MBB cluster platform (<http://mbb.univ-montp2.fr/MBB/index.php>) (supplementary Fig. IV.9 page 111). Visualisations of 3D mock-ups were generated in the AMAPstudio platform [Griffon and de Coligny, 2014].

### 2.2 Architectural model

The present study relies on the so-called Vpalm model able to generate a detailed 3D architecture of palm trees [Perez et al., 2016]. The modelling approach was based on allometric relations that enabled to model the geometry of plant components (stem, leaves and leaflets) from spatial and temporal variables (Fig. IV.1). One specificity of the model is the possibility of modelling inter and intra-progeny variability through genetic-dependent parameters. Parameters used in allometric relationships were calibrated for five different progenies. In this study we paid attention to the architectural traits that significantly varied between progenies.

In order to limit the number of parameters consid-

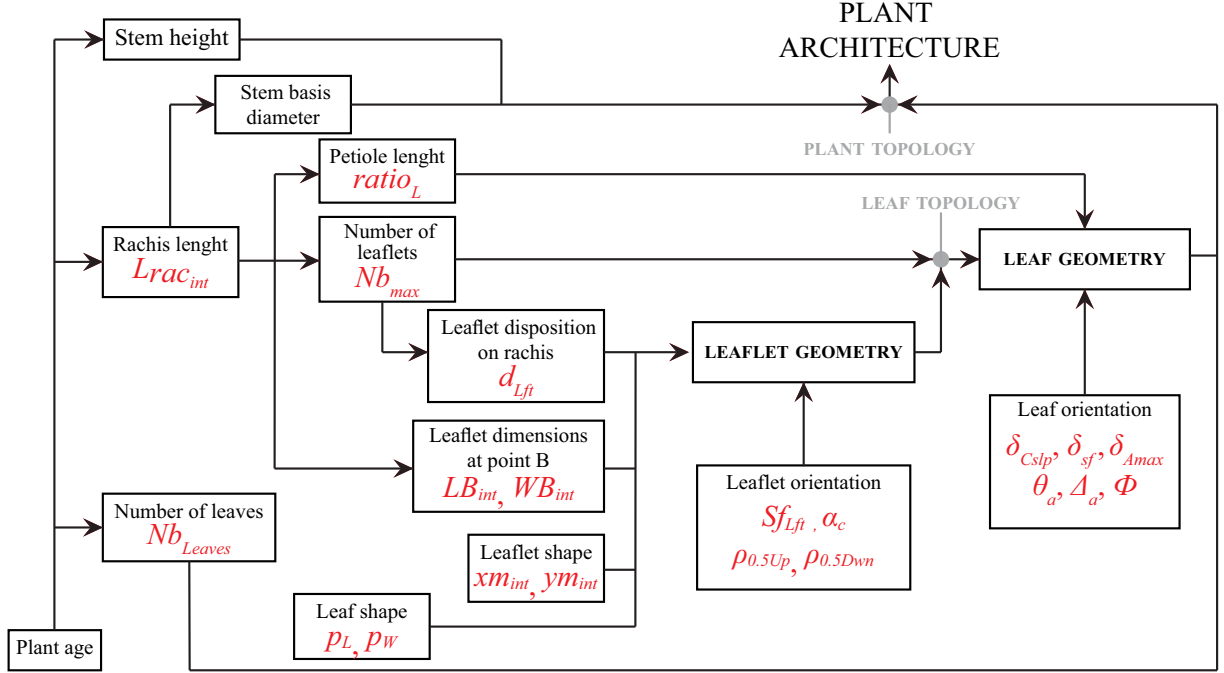


Figure IV.1: Allometric-based approach of the Vpalm model with relationships between the architectural parameters used in sensitivity analysis (see Table IV.1 page 92 for abbreviations).

ered in our study, a unique parameter per allometry was selected when the associated function was composed of several parameters. For instance, in a logistic function (number of leaflets depending on rachis length), only the parameter associated to curves maximal value was studied, the two others parameters being fixed to their mean values calibrated from field observations. Twenty-one parameters were finally selected according to their biological meaning and the facility to interpret their variations (Table IV.1). Among these 21 parameters, nine were related to leaf and leaflets morphology (supplementary material Fig. IV.10 page 112) whereas the others were linked to leaves and leaflets orientations, except for the number of leaves ( $Nb_{Leaves}$ ). The allometric-based formalism of the Vpalm model implied closed relationships between parameters (Fig. IV.1). As a result, changes in the range of variation of some parameters constrained the limits of variations of other ones. This was the case for all the parameters involved in allometric relationships based on rachis length. Indeed, rachis length

was calibrated from the parameter  $Lrac_{int}$ , which range of variation depended on plant age (defined through the number of leaves emitted from planting date ( $\Sigma_{leaves}$ ) (Fig. IV.2 and Table IV.2). Traits directly related to rachis length in the formalism, such as leaflets maximum width ( $W_{B_{int}}$ ) had subsequently their domain of variation changed according to plant age.

Six stages of development were chosen (namely 50, 100, 150, 250, 350 and 450 emitted leaves, corresponding approximately to 2 to 15 years after planting), to represent different levels of canopy closure. At young stages ( $\Sigma_{leaves} < 120$ ) the range of parameters values were calibrated using data collected in South Sumatra from five different progenies. The number of data used to determine the range of parameter variation depended on the difficulty of measuring the associated architectural traits. For instance, quick measurements such as rachis length, number of leaflets and leaflets length and width were collected on 25 plants per progeny, whereas tedious measurement such as leaflets orien-

Table IV.1: List of architectural parameters

Parameter	Units	Definition
<b>Crown scale</b>		
$Nb_{Leaves}$	-	Number of green leaves within the crown
$\delta_{Cslp}$	degrees.rank <sup>-1</sup>	Evolution of rachis declination angle at point C along the stem
$\phi$	degrees	Phyllotaxis
<b>Leaf scale</b>		
$Lrac_{int}$	cm	Rachis length
$ratio_L$	cm.cm <sup>-1</sup>	Ratio of petiole length to rachis length
$Nb_{max}$	-	Number of leaflets per leaf
$\delta_{sf}$	-	Evolution of rachis curvature along the rachis
$\delta_{Amax}$	degrees	Declination angle at rachis tip
$\theta_a$	degrees	Leaf twist at rachis tip
$\Delta_a$	degrees	Leaf deviation at rachis tip
$d_{Lft}$	-	Evolution of inter-leaflets distance along the rachis
<b>Leaflet scale</b>		
$L_{B_{int}}$	cm	Leaflets length at point B
$W_{B_{int}}$	cm	Leaflet maximum width at point B
$p_L$	-	Relative position of the longest leaflet on rachis
$p_W$	-	Relative position of the largest leaflet on rachis
$\alpha_c$	degrees	Leaflet axial insertion angle at point C
$xm_{int}$	-	Relative position of maximum width on leaflet
$ym_{int}$	-	Leaflet shape factor
$Sf_{Lft}$	-	Leaflet stiffness
$\rho_{0.5Up}$	degrees	Leaflet radial insertion angle of upper type leaflets
$\rho_{0.5Dwn}$	degrees	Leaflet radial insertion angle of lower type leaflets

tation and shape were sampled on four plants per progeny only (Chap. II). These data were also used to generate 80 calibrated mock-ups (20 per progeny) that were confronted to the ones generated during the sensitivity analysis at an equivalent age. At mature stage, only data related to leaf and leaflet dimensions and the number of leaflets per leaf were available from two other progenies. For detailed geometric variables, such as orientations of leaves and leaflets, one unique campaign of measurements was carried out (at plant age equivalent to around 110 leaves emitted). The relative range of parameter values was fixed and supposed constant all over plant development (Table IV.2).

Although the model enables to generate inter-individual variations within a progeny, simulations were performed on virtual plots including a unique 3D mock-up in order to better decipher the sensi-

tivity of parameters without dealing with model randomness. Virtual plants were placed in the plot according to the planting density used in the experimental site (136 palms.ha<sup>-1</sup>). This corresponded to a quincunx design where plants were spaced one from another by 9.2 meters. It is noteworthy that each virtual plot was replicated indefinitely in the periphery of its boundaries in order to avoid any border effects.

### 2.3 Radiative balance model

Virtual plots were generated on the Archimed platform, which enabled to estimate the light intercepted by plants thanks to the MMR (Mir-Musc-Radbal ) model [Dauzat and Eroy, 1997, Dauzat et al., 2008, Rey et al., 2008]. Radiative conditions were fixed using a daily average clearness index

Table IV.2: Range of values and relative mean deviation (RMD) of model parameters. †Parameters used in allometries related to rachis length and subsequently plant age.

Parameter	Age ( $\Sigma_{leaves}$ )	min	mean	max	RMD
<b>Crown scale</b>					
$Nb_{Leaves}$	All	35	40	45	0.12
$\delta_{Cslp}$ (degrees.rank <sup>-1</sup> )	All	0.92	1.59	2.64	0.48
$\phi$ (degrees)	All	136	137	139	0.01
<b>Leaf scale</b>					
$Lrac_{int}$ (cm)	50	87	118	141	0.23
	100	67	91	108	0.23
	150	114	154	185	0.23
	250	351	472	567	0.23
	350	460	619	743	0.23
	450	486	662	784	0.23
$ratio_L$ (cm.cm <sup>-1</sup> )	All †	0.10	0.23	0.39	0.59
$Nb_{max}$	All †	165	214	255	0.21
$\delta_{sf}$	All	-0.17	2.3	7.92	1.04
$\delta_{A_{max}}$ (degrees)	All	101	139	177	0.27
$\theta_a$ (degrees)	All	0	17	66	1
$\Delta_a$ (degrees)	All	0	5	33	1
$d_{Lft}$	All †	1.29	2.32	4.18	0.53
<b>Leaflet scale</b>					
$L_{B_{int}}$ (cm)	All †	4.42	30.93	47.28	0.83
$W_{B_{int}}$ (cm)	All †	1.32	2.37	3.84	0.49
$p_L$	All	0.25	0.49	0.85	0.55
$p_W$	All	0.35	0.61	0.85	0.42
$\alpha_c$ (degrees)	All	59	87	116	0.33
$xm_{int}$	All	0.14	0.24	0.40	0.47
$ym_{int}$	All	0.41	0.59	0.81	0.33
$Sf_{Lft}$	All	1000	5000	10000	0.82
$\rho_{0.5Up}$ (degrees)	All	5	31	67	0.86
$\rho_{0.5Down}$ (degrees)	All	-5	-7	-36	0.76

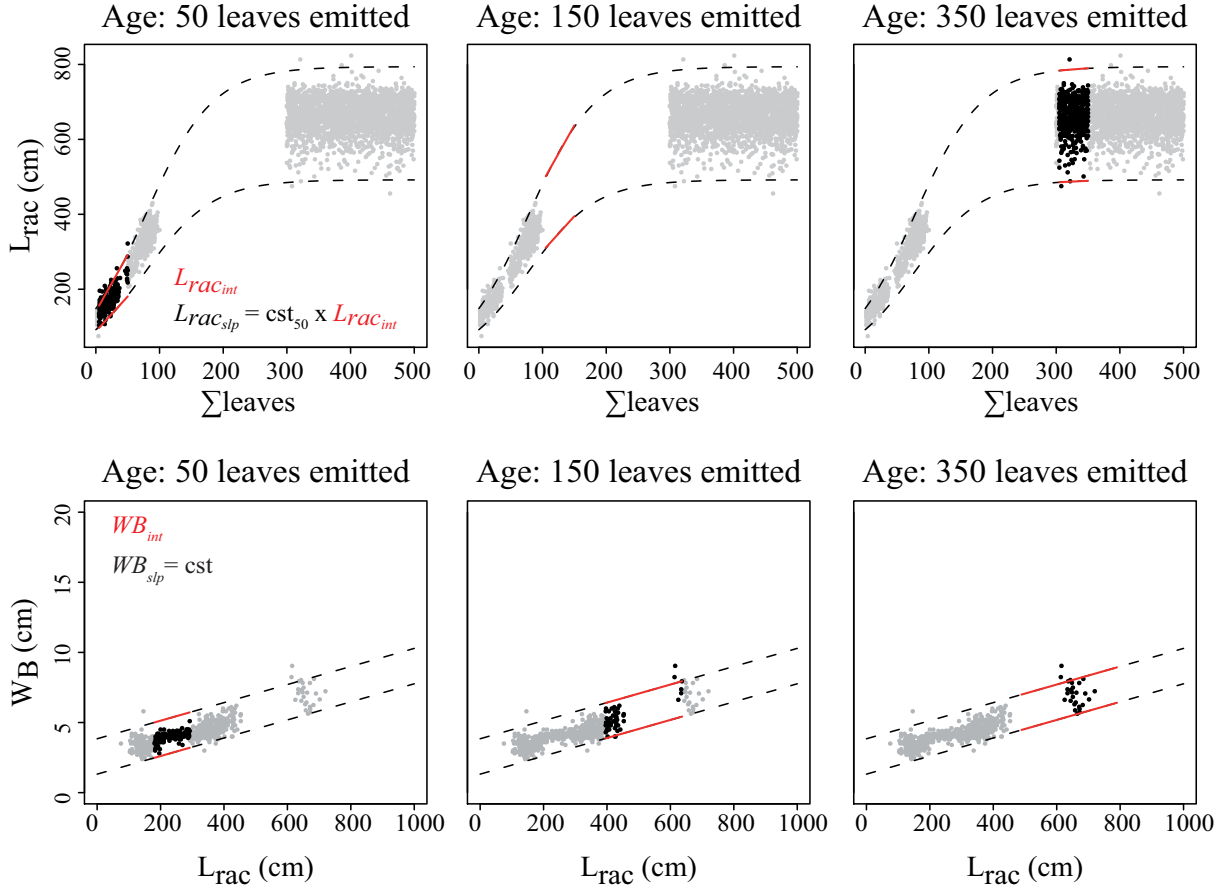


Figure IV.2: Parameters range variations (dotted lines) and observations (points) over plant development. Rachis length ( $L_{rac}$ ) follows a logistic evolution and was modeled as a succession of linear relationships with plant age. Leaflet maximum width at point B ( $W_B$ ) was expressed as a linear function of rachis length. Solid lines delimit the range for a given age and black points represent the observations carried out at the corresponding age.

(Kt), defined as the ratio of the measured global irradiance to the corresponding irradiance above the atmosphere [Bristow and Campbell, 1984]. Kt was calibrated from daily radiative data collected in the meteorological station of the studied site from 2011 to 2016 (Palembang, Sumatra latitude =  $-2.99^\circ$ ), and was fixed to its estimated upper limit ( $Kt = 0.5$ ) to perform simulation under local optimal conditions (close to clear sky). Regarding sun positioning and day length, simulations were done for a given day (November 1<sup>st</sup>, 2014), which corresponds to the month when detailed architectural measurements were performed. Light interception

was estimated every 30 mn of the day on every plant organ of the 3D mock-ups, each organ being represented by a 3D mesh. It was thus possible to estimate in detail the distribution of light within the plant canopy.

## 2.4 Carbon assimilation model

Irradiances, defined as the amount of light intercepted per unit leaf area, were determined for every organ composing the 3D mock-ups. Irradiances calculated on leaflets were then used together with a photosynthesis model of C3 leaves to estimate daily carbon assimilation (assimilation from



other components than leaflets were supposed negligible). Photosynthesis was modelled using the non-rectangular hyperbola (NRH) curve described as followed [Marshall and Biscoe, 1980, Thornley, 1998] (eq. IV.1):

$$A = \frac{\alpha PFD + A_{max} - \sqrt{(\alpha PFD + A_{max})^2 - 4\theta\alpha PFD A_{max}}}{2\theta} - Rd \quad (IV.1)$$

where:

$A$ : assimilation ( $\mu\text{mol.CO}_2.\text{m}^{-2}.\text{s}^{-1}$ )

$PFD$ : photon flux density or irradiance ( $\mu\text{mol photon.m}^{-2}.\text{s}^{-1}$ )

$A_{max}$ : maximum assimilation ( $\mu\text{mol.CO}_2.\text{m}^{-2}.\text{s}^{-1}$ )

$\alpha$ : photosynthetic efficiency ( $\mu\text{mol.CO}_2.\mu\text{mol photon}^{-1}$ )

$\theta$ : flux resistance of  $\text{CO}_2$  from the outside of the leaf to the chloroplasts

$Rd$ : mitochondrial respiration ( $\mu\text{mol.CO}_2.\text{m}^{-2}.\text{s}^{-1}$ )

This model enabled to render the non-linearity of photosynthetic response to light conditions. The model was parameterized from field gas exchange measurements (GFS 3000 Gas Exchange System, Walz, Germany) conducted on eight individuals under optimal conditions (clear sky and non-limiting water and nutrient supply). Constant conditions (considered as non-limiting for stomatal conductance) were controlled in the gas analyser chamber (temperature:  $28^\circ\text{C}$ ,  $\text{CO}_2$  concentration: 400 ppm; relative humidity: 70%) while the intensity of light was progressively changed ( $PFD$  from 1600 to 0  $\mu\text{mol photon.m}^{-2}.\text{s}^{-1}$ ) to draw response curve of assimilation vs. light. The experimental response curves were pooled together to fit an average NRH curve and to calibrate photosynthesis parameters (supplementary material Fig. IV.11 page 113). It is noteworthy that the carbon assimilation delivered by the NRH function must be considered as a potential assimilation since neither stomatal conductance regulation (from other limiting factor than light) nor nitrogen dependency were taken into account in our modelling approach. For all the simulations performed in this study, each photosynthetic parameter was fixed to its mean value calibrated in the average NRH curve.

## 2.5 Sensitivity analyses

### Model outputs

Parameter effects were studied in terms of both light interception and carbon assimilation at the plant scale. Light interception efficiency was determined through the fraction of incident light intercepted by palm canopies over a day ( $f_{PAR}$ , Table IV.3). A light extinction coefficient ( $k$ ) was also calculated as an indicator of the trade-off between light interception and leaf area index (LAI). Besides, plant mutual shading (MS) was estimated as the difference in the amounts of light intercepted by a single plant in plantation and by the same plant isolated under similar incident radiation. MS provided information about the level of competition for light between neighbourhood plants. Daily carbon assimilation ( $A_d$ ) was finally estimated by integrating the amount of carbon fixed by all leaflets along the day. Output variables investigated in this study are defined in Table IV.3.

### Morris method

The decision of replicating a unique individual in virtual scene rather than dealing with inter-individual variability offered the possibility to run the model in a deterministic way. The factorial screening method of Morris [Morris, 1991] was used in order to optimize the number of simulations for integrating the analysis over plant development. The Morris sensitivity analysis is a One at A Time (OAT) method, using discrete parameter values selected in a sampling design that decomposed each parameter in five possible values between its minimal and maximal value (normalized thereafter between 0 and 1 to make parameter ranges comparable). The analysis is based on sets of model runs called trajectories, a trajectory being composed of successive simulations differing by a unique parameter value, and each factor varying once in a trajectory. In our case, a trajectory was made of 22 simulations (an initial random run and 21 simulations to account for the successive variations of the 21 parameters). A total of 40 trajectories was performed for each stage of development (40 x 22 simulations x 6 stages) using the same sampling design with the sensitivity package of R software [R Core Team, 2015]. In this way 880 virtual plants

Table IV.3: Model outputs

Outputs	variables
$f_{PAR} = \frac{PAR_i - PAR_c}{PAR_i}$	$PAR_i$ : Incident PAR (MJ.day <sup>-1</sup> ) $PAR_c$ : PAR intercepted by the canopy (MJ.day <sup>-1</sup> )
$k = \frac{\ln(1-f_{PAR})}{-LAI}$	$LAI$ : leaf area index (m <sup>2</sup> .m <sup>-2</sup> )
$MS = \frac{PAR_{isol} - PAR_{stand}}{PAR_{isol}}$	$PAR_{isol}$ : PAR intercepted by the isolated plant (MJ.day <sup>-1</sup> ) $PAR_{stand}$ : PAR intercepted by the plant in stand (MJ.day <sup>-1</sup> )
$A_d = \sum_{t=0}^{24h} \sum_{l=0}^n NRH(PFD_{t,l})$	$PFD_{t,l}$ : irradiance of the leaflet $l$ at time $t$ (μmol.photon.m <sup>-2</sup> .s <sup>-1</sup> )
$PAR_{cumul} = \sum_{\Sigma leaves=50}^{450} PAR_c$	$PAR_c$ : PAR intercepted by the canopy (MJ.day <sup>-1</sup> )
$A_{cumul} = \sum_{\Sigma leaves=50}^{450} A_d$	$A_d$ : Daily assimilation (moles.CO <sub>2</sub> .day <sup>-1</sup> )

with contrasted architecture were followed over 6 stages of plant development (supplementary material Fig. IV.13 page 114). Analyses of model outputs were then performed for each date separately as well as for the whole period from 50 to 450 leaves emitted ( $PAR_{cumul}$  and  $A_{cumul}$  Table IV.3).

The Morris method enabled to estimate sensitivity indices for each  $X_p$  parameter ( $p = 1, \dots, 21$ ) by comparing model outputs between simulations that only differed from the value of the  $X_p$  parameter. For each trajectory, the difference in output between two successive simulations, differing from one another by the value of the parameter  $X_p$ , enabled to estimate the elementary effect of  $X_p$ . The mean value of the 40 elementary effects of the parameter  $X_p$  was then calculated to obtain a mean sensitive index  $\mu_p$ , which represented the mean influence of the parameter  $X_p$  on model outputs. The mean of absolute values of the elementary effects  $\mu_p^*$  was also used because effects could be positive or negative. The standard deviation of the elementary effect of the parameter  $X_p$ , noted  $\sigma_p$ , indicated if the parameter presents interactions with others parameters and/or if the response of model outputs to changes in  $X_p$  was linear or not. Normalized indices ( $\mu_{rel}$ ,  $\mu_{rel}^*$ ,  $\sigma_{rel}$ ), relatively to the most sensitive parame-

ter, were also calculated to better sort parameters sensitivity:

$$\mu_{p,rel} = \frac{\mu_p}{\max(\mu_p^*)} \quad (IV.2)$$

$$\mu_{p,rel}^* = \frac{\mu_p^*}{\max(\mu_p^*)} \quad (IV.3)$$

$$\sigma_{p,rel} = \frac{\sigma_p}{\max(\sigma_p)} \quad (IV.4)$$

### Metamodel

A second set of simulations was performed in order to get a deeper analysis of the parameter effects and interactions on adult palms ( $\Sigma leaves = 450$ ). We decided to focus on mature plants as this corresponds to the ontogenetic stage when crown architecture is steady over a long period of time (around 15 years) and plants reach their maximal fruit production [Corley and Tinker, 2016]. In this second sensitivity analysis, a reduced number of parameters (nine parameters) were selected according to their sensitivity estimated by the Morris method, the facility to calibrate them from field measurements and the heritability of the associated architectural traits as previously estimated (Chap. II). All the parameters which were not investigated



in this second analysis were fixed to their mean value (Table IV.2). The experimental design was based on orthogonal array-based latin hypercube (OA-LHS) [Tang, 1993], which enables to better explore the space of input parameter values and gives the possibility to estimate parameter interactions. The experimental design was generated from an array of discretized parameter values on which a latin hypercube sampling (LHS) was applied to generate randomness around the discretized parameters values. The array was designed to make possible the estimation of 3rd order interaction between the nine parameters, with 4 discretized values per parameter. These chosen criteria imposed a minimum and specific number of simulations (multiple of  $4^{(3+1)}$ ). The final design was carried out using the lhs and planor package of R, from which 8192 mock-ups with different combinations of the nine architectural parameters were generated.

A metamodeling approach based on these 8192 simulations was set up in order to model response curve of  $A_d$ . The choice of designing the metamodel on  $A_d$  rather than  $f_{PAR}$  was established to integrate the saturating nature of light-photosynthesis relationship and consequently better apprehend plant biomass production. Among metamodeling approaches [Faivre et al., 2013], we selected a quadratic polynomial model (eq. IV.5):

$$A_{di} = \theta_0 + \sum_{k=1}^9 \sum_{k' \neq k} (\theta_p X_{p,i} + \alpha_p X_{p,i}^2 + \beta_{p'p} X_{p',i} X_{p,i}) + \epsilon_i \quad (IV.5)$$

where  $\theta_0$  represents model intercept,  $X_{p,i}$  the value of the architectural parameter  $p$  ( $p=1, \dots, 9$ ) for the plant  $i$ ,  $\theta_p$  and  $\alpha_p$  model coefficient associated to the parameter  $p$ ,  $\beta_{p'p}$  coefficients associated to the interaction between parameters  $p$  and  $p$  ( $p \neq p'$ ) and  $\epsilon_i$  the residual error term. The metamodel allowed us to estimate sensitivity indices based on the coefficient of determination ( $r^2$ ). Those indices indicated the proportion of variance in  $A_d$  explained by each of the nine studied parameters, including their interaction.

### Identification of ideotypes

From the 8192 simulations obtained in the second sensitivity analysis, we proposed to compare four groups of plants which were defined according to their capacity to maximize (respectively minimize) light interception and carbon assimilation. The objective of comparing these four groups was to

pinpoint the architectural traits specifically influencing either light interception or carbon assimilation. First, we considered the 30 mock-ups with the highest value of  $A_d$ . Since the LAI greatly influenced  $f_{PAR}$  and  $A_d$ , the three other groups of 30 mock-ups, respectively with the lowest values of  $A_d$ , the lowest value of  $f_{PAR}$  and the highest value of  $f_{PAR}$ , were selected within the range of LAI defined by the first group. Analyses of variances (ANOVA) were conducted to assess which parameters and model outputs were significantly different. Tukey's tests were then used to compare mean values of the four groups. Composite traits such as leaf length, average leaf and leaflet area, frequency of leaflets on rachis ( $Fr_{QLft}$ ) and average ratio of leaflet length to leaflet maximal width ( $LW$  ratio) were also compared to better consider architectural specificities at leaf scale.

A second question was to know if, among the 30 mock-ups that revealed the highest  $A_d$ , there was a unique or several optimal combinations of architectural parameters. A principal component analysis (PCA) was thus performed on the nine parameters and the K-means clustering procedure of R software was used on projection values of the PCA to identify the possible distinct groups of parameter combinations (ideotypes) among the 30 virtual plants. Similarly to the analysis adopted to compare the four groups of mock-ups, ANOVAs and Tukey's tests were performed to determine which traits were stable or not among the identified ideotypes.

## 3 Results

### 3.1 Sensitivity of architectural parameters over plant age

The Morris method allowed exploring the sensitivity of model parameters over plant age for both light interception efficiency ( $f_{PAR}$ ) and carbon assimilation ( $A_d$ ) (Fig. IV.3A) (outputs for LAI,  $k$  and  $MS$  are presented in supplementary material Fig IV.14 page 115). Results highlighted constancy in the ranking of parameter sensitivity over plant development, both  $f_{PAR}$  and  $A_d$  being comparably influenced by the 21 parameters at the different ages investigated. Size-related parameters ( $Lrac_{int}$ ,

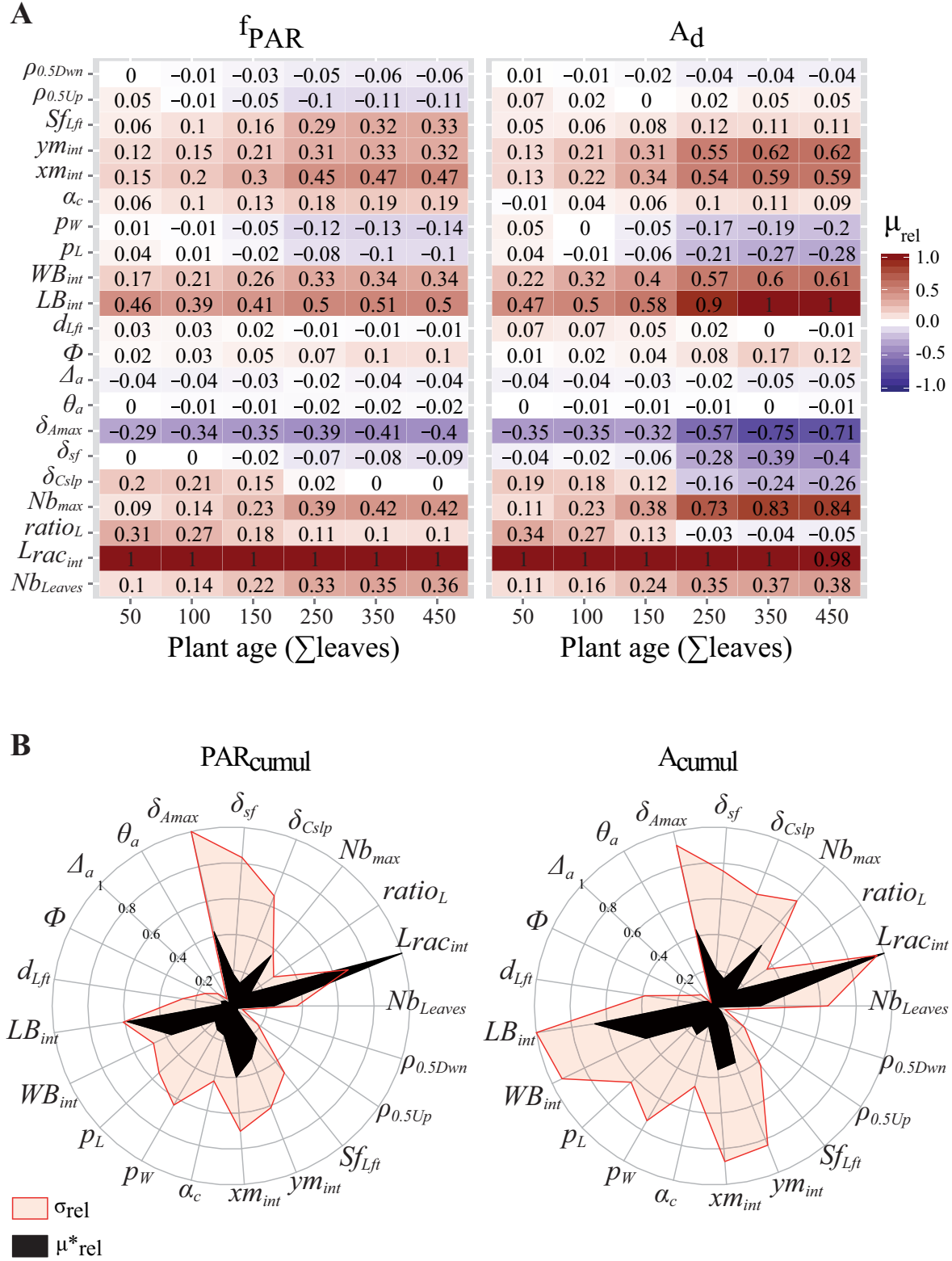


Figure IV.3: A) Heat map of relative mean values of elementary effects ( $\mu_{rel}$ ) for 6 ages over plants development, calculated for the fraction of PAR intercepted by the canopy ( $f_{PAR}$ ) and carbon assimilation ( $A_d$ ). Values are given relatively to the most sensitive parameter at a given age. B) Morris sensitivity indices for cumulated PAR intercepted ( $PAR_{cumul}$ ) and cumulated carbon assimilated ( $A_{cumul}$ ). Index values are relative to the most sensitive parameter,  $\mu^*_{rel}$  is the relative absolute mean value of elementary effects.

$Nb_{max}$ ,  $LB_{int}$ ,  $WB_{int}$ ) had positive impact ( $\mu_{rel} > 0$ ) on  $f_{PAR}$  and  $A_d$  whereas parameters related to leaf and leaflet orientation ( $\delta_{A_{max}}$ ,  $\delta_{sf}$ ,  $\delta_{Cslp}$ ,  $\rho$ ) reduced model outputs when increasing their values. The most sensitive parameter over plant age was  $Lrac_{int}$  ( $\mu_{rel}=1$ ) for both outputs, except for  $A_d$  at 450 leaves for which  $LB_{int}$  was the most sensitive parameter. In contrast, rachis twist ( $\theta_a$ ) and deviation ( $\Delta_a$ ) were the parameters with the lowest influence on model outputs at any given developmental stage of the plant. For  $f_{PAR}$  the elementary effect of  $Lrac_{int}$  was at least twice stronger than any other parameter whilst, for  $A_d$ , six parameters presented  $\mu_{rel} > 0.5$  ( $LB_{int}$ ,  $WB_{int}$ ,  $Nb_{max}$ ,  $\delta_{A_{max}}$ ,  $xm_{int}$  and  $ym_{int}$ ). In general, most of the sensitive parameters had greater sensitivity (relatively to the most sensitive parameter) with palm age. It was particularly the case for leaflets shape parameters ( $xm_{int}$  and  $ym_{int}$ ) and the parameter associated to leaf curvature at rachis tip ( $\delta_{A_{max}}$ ). Those geometrical attributes affected more  $A_d$  than  $f_{PAR}$  ( $\mu_{rel} > 0.5$  for  $A_d$  and  $\mu_{rel} < 0.5$  for  $f_{PAR}$  on advanced stages).

Sensitivity analysis based on the integrated variables over the six studied stages pointed out comparable results for  $PAR_{cumul}$  and  $A_{cumul}$  and was consistent with the analyses obtained at a given age (Fig IV.3B). Indeed, the ranking for elementary effects was conserved between  $PAR_{cumul}$  and  $A_{cumul}$ , and confirmed that the parameters related to leaf area ( $Lrac_{int}$ ,  $LB_{int}$ ,  $WB_{int}$  and  $Nb_{max}$ ) were the most sensitive. Variations in  $\delta_{A_{max}}$  revealed as well strong variations on output variables, indicating the significant improvement of erect leaves to maximize light capture and subsequently carbon assimilation. Regarding parameter interactions, the highest interaction ( $\sigma_{rel}=1$ ) was related to  $\delta_{A_{max}}$  for  $PAR_{cumul}$  while for  $A_{cumul}$  the highest value of  $\sigma_{rel}$  was estimated for  $LB_{int}$ . Also more parameters presented relatively high value of interaction ( $\sigma_{rel} > 0.6$ ) for  $A_{cumul}$  than for  $PAR_{cumul}$ . Such difference was very likely the consequence of the non-linear response of carbon assimilation to leaf irradiance (NRH model). Besides, model formalism implicated inter-connections between  $LB_{int}$ ,  $WB_{int}$ ,  $p_L$ ,  $p_W$ ,  $xm_{int}$  and  $ym_{int}$  on the one hand, and between  $\delta_{A_{max}}$ ,  $\delta_{sf}$  and  $\delta_{Cslp}$  on the other hand, which could explain the high values of  $\sigma_{rel}$  estimated for those parameters.

### 3.2 Comparing experimental vs. field calibrated mock-ups

Figure IV.4A presents the outputs predicted from the Morris mock-ups ( $100 \leq \Sigma_{leaves} \leq 150$ ) in comparison with the outputs estimated from the 80 mock-ups calibrated from field measurements on the five modelled progenies. Responses estimated for the calibrated mock-ups exhibited rough linear relationships with LAI, signifying that the architectural traits related to LAI largely affected light interception and carbon assimilation, at least at this developmental stage. As expected, the Morris mock-ups exhibited higher range of variation than calibrated mock-ups for all response variables investigated.  $f_{PAR}$  varied between 0.17 and 0.99 for the Morris mock-ups whilst it varied between 0.55 and 0.83 for the calibrated mock-ups. The virtual plants representing progenies showed MS values ranging from 0.11 to 0.26, whereas MS values varied between 0 and 0.60 in the sensitivity analysis. The coefficient of extinction ( $k$ ) varied between 0.43 and 0.71 for the calibrated mock-ups and between 0.19 and 1.03 for the others. For  $A_d$ , the mock-ups of progenies were closer to the upper limit than the lower limit defined by the virtual plants generated in the sensitivity analysis ( $56 < A_d < 93$  moles  $\text{CO}_2.\text{day}^{-1}$  for progenies and  $17 < A_d < 108$  moles  $\text{CO}_2.\text{day}^{-1}$  for Morris mock-ups). Such results illustrate that even if the limits of parameter values were restricted from the associated field observations, some combinations of architectural traits could provide potential improvement in light interception efficiency and carbon assimilation. For instance, for a LAI of  $2.1 \pm 0.21$  (average value of the 80 calibrated-mock-ups  $\pm 10\%$ ), the average  $A_d$  predicted from realistic mock-up was 68.3 moles  $\text{CO}_2.\text{day}^{-1}$  while it reached 74.5 moles  $\text{CO}_2.\text{day}^{-1}$  for virtual mock-ups, i.e. an average improvement in carbon assimilation of 9%.

### 3.3 Sensitivity analysis on adult stand

Given the stability of parameters sensitivity over plant development using the Morris method, we considered that the results obtained at a given palm age could be extrapolated to other ages. A second set of simulations was thus performed to better depict the

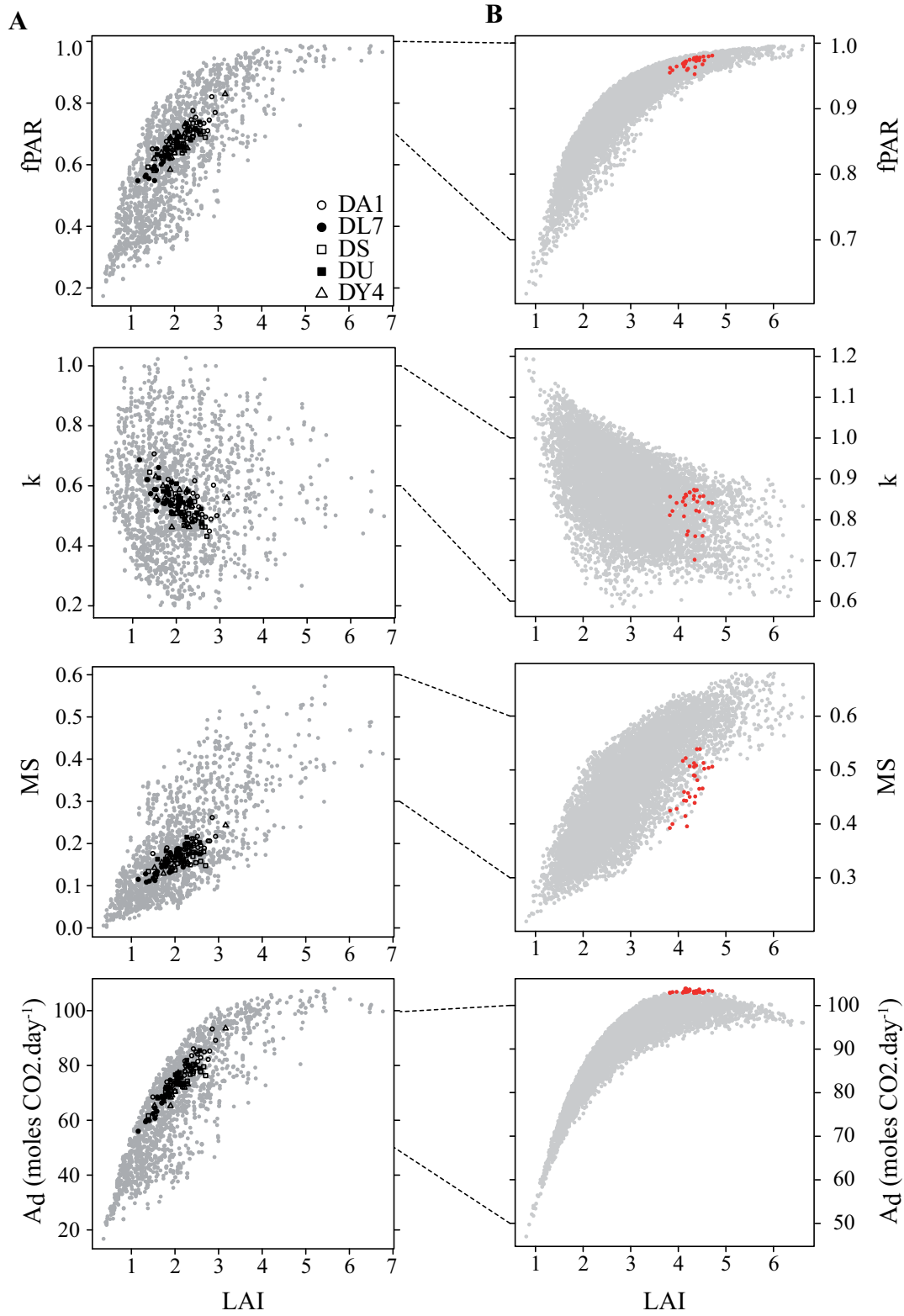


Figure IV.4: A) Dispersion of output variables for all the virtual plants generated with combinations of the 21 architectural parameters for the Morris analysis at 100 and 150 leaves emitted after planting (1760 mock-ups, grey points) and from mock-ups generated at equivalent age for the five studied progenies (20 individuals per progeny). B) Dispersion of output variables for all the virtual plants generated with combinations of the nine most sensitive architectural parameters at 450 leaves emitted (8192 mock-ups). Red points represents the 30 mock-ups with the highest values of  $A_d$

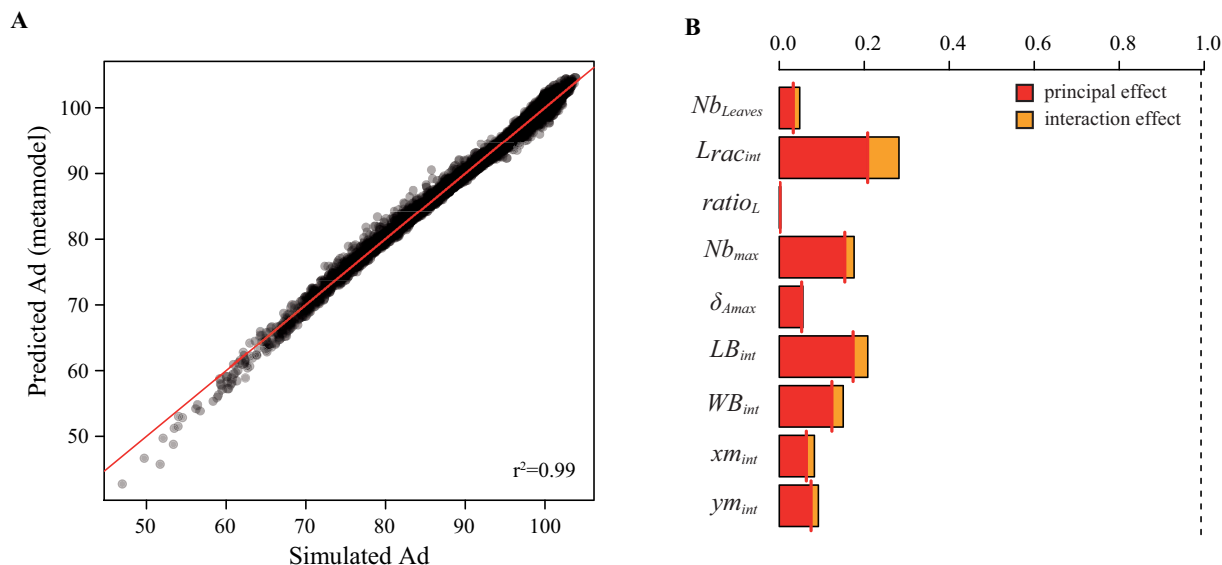


Figure IV.5: A) Quality of metamodel predictions of  $A_d$  (red line is the 1:1 line) B) Relative contribution of the nine architectural parameters to variation of  $A_d$  based on the polynomial metamodel (degree 2). The dotted line indicates the total variation explained by the metamodel.

influence of each parameter and their interaction on light interception efficiency and photosynthetic production. In the end, the eight most sensitive parameters identified using the Morris method were selected ( $Lrac_{int}$ ,  $Nb_{leaves}$ ,  $LB_{int}$ ,  $WB_{int}$ ,  $Nb_{max}$ ,  $ym_{int}$ ,  $xm_{int}$  and  $\delta_{Amax}$ ). A ninth parameter, the ratio of petiole length to rachis length ( $ratio_L$ ) was added since it was identified as the most heritable architectural trait between the five progenies (Chap. II).

The 8192 simulated mock-ups allowed us to estimate the effect of variations in mature palm architectures on potential physiological responses (Fig. IV.4B). Simulated LAI presented a coefficient of variation (CV) of 31% with values varying from 0.8 to  $6.6 \text{ m}^2 \cdot \text{m}^{-2}$ , denoting important changes in the leaf area between the investigated 3D mock-ups. As observed in the previous Morris analysis,  $f_{PAR}$  increases with LAI towards an upper limit of 1, corresponding to a total interception of incident light.  $f_{PAR}$  increased almost linearly for low values of LAI and reached a ceiling range of values varying from 0.91 to 1 for LAI superior to  $4 \text{ m}^2 \cdot \text{m}^{-2}$ . The overall CV of  $f_{PAR}$  was 7%. MS was linearly correlated with LAI ( $r = 0.82$ ) and presented the

highest CV (19%) with values varying from 0.22 to 0.68. Regarding  $A_d$ , a close relationship with LAI was as well highlighted.  $A_d$  increased with LAI until reaching a maximum value of 103 moles of  $\text{CO}_2 \cdot \text{day}^{-1}$ , and finally slightly decreased when LAI reached extreme values. Interestingly, the mock-ups with the highest values of  $A_d$  (quantile > 95%) only differed from each other on a maximum of 3.3 moles of  $\text{CO}_2$  per day whilst they presented variations in LAI between  $3.2$  and  $5.5 \text{ m}^2 \cdot \text{m}^{-2}$ .

Predictions in  $A_d$  from the metamodel were consistent with simulated  $A_d$ , as 99% of the variability in  $A_d$  was explained by the metamodel (Fig. IV.5A). Little bias was observed for values of  $A_d$  less than 65 moles  $\text{CO}_2 \cdot \text{day}^{-1}$ , which nevertheless represented less than 1% of the simulated values. The decomposition of variance explained by each parameter allowed ranking them according to their influence on  $A_d$  (Fig. IV.5B and supplementary Table IV.6 page 116). The most sensitive parameters were  $Lrac_{int}$ , which represent 20.7% of the total variance, followed by  $LB_{int}$  (17.3%),  $Nb_{max}$  (15.4%) and  $WB_{int}$  (12.4%). Interaction effects represented less than 10% of variations for each parameter,  $Lrac_{int}$  being the parameter that interacted the



most with the others parameters (7%). Besides, all interactions had positive effect, which meant that parameters intensified their mutual effects.

### 3.4 Ideotyping architecture (architectural traits) with regards to carbon assimilation

The 30 mock-ups exhibiting the highest  $A_d$  covered a LAI range of 3.8 to 4.7  $\text{m}^2 \cdot \text{m}^{-2}$ . Comparing these mock-ups with the 30 mock-ups exhibiting the highest  $f_{PAR}$ , and lowest  $A_d$  and  $f_{PAR}$  in this LAI range exhibited contrasted leaf geometry (Table IV.4). The similarity between plants that optimised  $f_{PAR}$  and  $A_d$  relied on the lowest values of  $ratio_L$  and  $\delta_{A_{max}}$ , i.e small petiole and erect leaves. A focus on the 30 mock-ups having the highest value of interception exhibits the importance of leaf area, since the highest values of LAI, individual leaf and leaflet area were found for this group. The parameter  $xm_{int}$ , linked to leaflet shape, was as well specifically high in comparison with the three other groups. The specificities of the plants that maximized  $A_d$  were the shortest leaves (Leaf length = 687 cm) due to short petiole and rachis, the highest number of leaflets on rachis ( $Nb_{max} = 244$  leaflets and  $Frq_{Lft} = 0.42$  leaflets.cm of rachis $^{-1}$ ) and the longest leaflets ( $LB = 41$  cm). It is noteworthy that the plants that optimized  $A_d$  exhibited the lowest values of mutual shading. All architectural parameters were significantly different between the 30 mock-ups with the highest values of  $A_d$  and the ones with the lowest values of  $A_d$  (except for  $xm_{int}$ ), which validated the high sensitivity of the selected parameters. The most contrasted difference between these two groups was the leaf curvature at rachis tip, with more erect leaves ( $\delta_{A_{max}} = 117^\circ$ ) for mock-ups having a low  $A_d$  than for mock-ups having a high  $A_d$  ( $\delta_{A_{max}} = 169^\circ$ ). At leaflet scale, plants that optimized assimilation presented longer and narrower leaflets ( $L = 41$ ,  $LW_{ratio} = 12.1$ ) than plants with low assimilation ( $L = 28$ ,  $LW_{ratio} = 11.3$ ). A contrasted distribution of light interception and assimilation within the crown was also revealed between the two groups (supplementary Fig. IV.12 page 113). In both cases, leaf irradiance and assimilation sharply decreased with leaf rank (except for the unfolded leaves; leaf rank < 2). Results showed that the gain of  $A_d$  was allowed by a more uniform

distribution of irradiance and assimilation within the crown, with higher values of both variables from rank 9 to 30.

PCA analysis performed on the nine parameter values for each of the 30 mock-ups having the highest  $A_d$  correctly gather the information into two principal components that explained 67% of the observed variance. The first component was positively correlated to  $Nb_{leaves}$ ,  $ratio_L$ ,  $xm_{int}$  and  $\delta_{A_{max}}$  and negatively correlated to  $Lrac_{int}$ . The second component explained less variance (17%) and was negatively correlated to  $ym_{int}$  and positively correlated to  $Nb_{max}$  (Fig. IV.6A). As a result the first axis allowed splitting virtual plants according to the length of their leaves against plants with specific crown structure (high number of short rachis with long petioles and bent leaves) while the second axis divides plants according to the detailed structure of their leaves (high number of narrow leaflets vs. low number of large leaflets). The projection of the 30 mock-ups on the two first components of the PCA and the clustering analysis enabled to discriminate four groups of virtual plants, hereafter designed as ideotypes (Fig. IV.6B). The mock-ups categorized according to PCA outputs highlighted the efficiency of the analysis to group comparable combination of parameters (Fig. IV.6C). The first group (ideotype A) presented plants with a relatively low number of leaves with long and erect rachis. Indeed, the specificities of ideotype A in comparison with the three other ideotypes (Table IV.5) were a significantly lower number of leaves, a longer rachis and leaves with shorter petiole. Ideotype A also exhibited the shortest and the narrowest leaflets but, interestingly, significantly higher leaflet area on average than other ideotypes, probably due to the combination of high values of  $ym_{int}$  and low values of  $xm_{int}$ . Ideotype B presented globally intermediate values of parameters in comparison with the other ideotypes, except for  $ym_{int}$  which presents the highest values together with ideotype A. Ideotype B displayed significantly shorter leaves than the other ideotypes. Ideotype C differed from the three other ideotypes by the highest number of leaves with long petiole and the shortest rachis. It presented as well the particularity of bent leaves at rachis tip (highest value of  $\delta_{A_{max}}$ ) and dense rachis, i.e short rachis with important number of leaflets (highest value of  $Frq_{Lft}$ ). In contrast with ideotype A, the leaflets

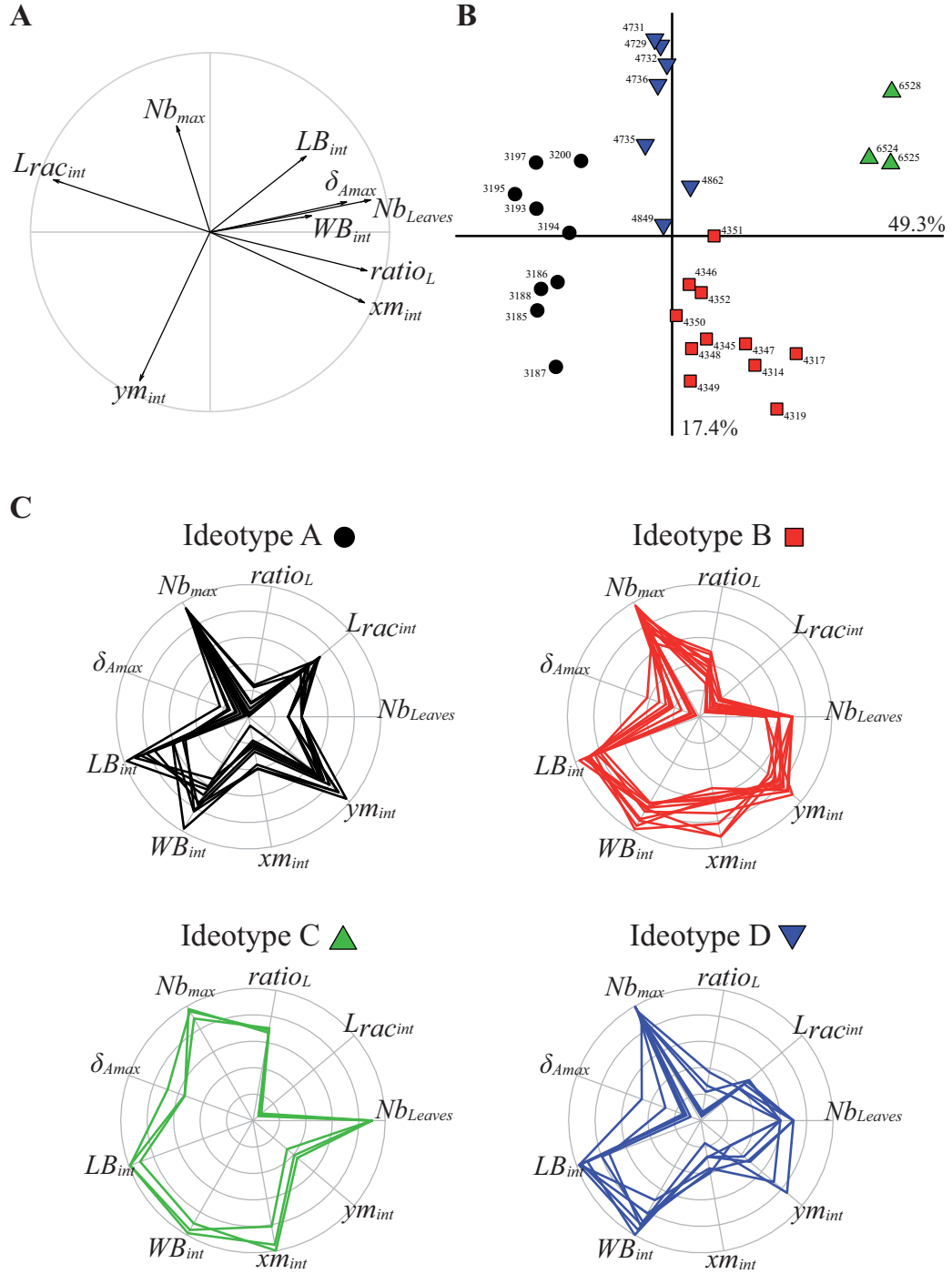


Figure IV.6: Principal component analysis (PCA) of the nine architectural parameters of the 30 mock-ups with the highest value of  $A_d$ . A) Projection of the nine parameters on the two first axes of the PCA. B) Projection of the 30 mock-ups on the two first axes of the PCA. Cluster analysis based on the two first components of the PCA revealed four contrasted ideotypes. C) Radial plots of the relative parameter values of the 30 mock-ups classified in the four ideotypes identified from the cluster analysis.



Table IV.4: Comparison of parameters, response variables and composite traits for the 30 mock-ups with the highest and the 30 mock-ups with the lowest values of  $f_{PAR}$  and  $A_d$  for LAI varying between 3.8 and 4.7  $\text{m}^2 \cdot \text{m}^{-2}$ . Letters correspond to significant differences between the four groups (Tukey's test,  $P < 0.05$ )

Variable	lowest $f_{PAR}$	highest $f_{PAR}$	lowest $A_d$	highest $A_d$
<i>Parameters</i>				
$Nb_{Leaves}$	41 ± 3 b	42 ± 2 ab	43 ± 2 a	41 ± 2 b
$Lrac_{int}(cm)$	641 ± 87 b	739 ± 33 a	755 ± 27 a	585 ± 69 c
$ratio_L$	0.29 ± 0.07 a	0.23 ± 0.08 b	0.29 ± 0.06 a	0.18 ± 0.06 b
$Nb_{max}$	228 ± 25 b	216 ± 24 bc	208 ± 25 c	244 ± 7 a
$\delta_{Amax}(^\circ)$	172 ± 3 a	114 ± 9 b	169 ± 5 a	117 ± 13 b
$L_{B_{int}}(cm)$	36 ± 7 ab	32 ± 10 bc	28 ± 11 c	41 ± 6 a
$W_{B_{int}}(cm)$	3.19 ± 0.64 a	3.06 ± 0.50 ab	2.72 ± 0.64 b	3.41 ± 0.30 a
$xm_{int}$	0.26 ± 0.08 b	0.32 ± 0.05 a	0.28 ± 0.06 b	0.27 ± 0.07 b
$ym_{int}$	0.67 ± 0.11 ab	0.63 ± 0.10 ab	0.61 ± 0.11 b	0.68 ± 0.08 a
<i>Model outputs</i>				
LAI	3.94 ± 0.09 c	4.59 ± 0.08 a	4.03 ± 0.19 c	4.27 ± 0.22 b
$f_{PAR}$	0.93 ± 0.01 d	0.98 ± 0.00 a	0.95 ± 0.01 c	0.97 ± 0.01 b
MS	0.50 ± 0.05 b	0.61 ± 0.02 a	0.59 ± 0.03 a	0.47 ± 0.04 c
k	0.68 ± 0.03 d	0.89 ± 0.02 a	0.74 ± 0.03 c	0.83 ± 0.04 b
$A_d$ (moles.CO <sub>2</sub> .day <sup>-1</sup> )	97 ± 2.5 c	100 ± 0.9 b	94 ± 0.5 d	103 ± 0.3 a
<i>Composite traits</i>				
Petiole length (cm)	181 ± 42 b	166 ± 61 b	221 ± 47 a	102 ± 26 c
Leaf lenght (cm)	822 ± 100 c	904 ± 67 b	976 ± 54 a	687 ± 57 d
Individual leaf area (m <sup>2</sup> )	7.11 ± 0.61 b	8.03 ± 0.54 a	6.96 ± 0.50 b	7.70 ± 0.53 a
FreqLft (leaflets.cm <sup>-1</sup> )	0.36 ± 0.07 b	0.29 ± 0.04 c	0.28 ± 0.03 c	0.42 ± 0.05 a
Individual leaflet area (cm <sup>2</sup> )	316 ± 44 b	376 ± 43 a	338 ± 41 b	316 ± 20 b
LW ratio (cm.cm <sup>-1</sup> )	12.0 ± 4.4 a	10.9 ± 4.3 a	11.3 ± 6.0 a	12.0 ± 2.1 a

of ideotype C were on average the longest and the largest but the lowest value of  $ym_{int}$  led to small leaflet area on average. The last ideotype (ideotype D) had intermediate rachis length with short petiole. Contrarily to other ideotypes, ideotype D presented low value for both  $xm_{int}$  and  $ym_{int}$ .

The representations of the four ideotypes (Fig. IV.7) allowed visualizing the overall architectural difference existing between them. Visualisation at leaflets scale highlighted the difference in term of size ( $L_{B_{int}}$  and  $W_{B_{int}}$ ) and shapes ( $xm_{int}$  and  $ym_{int}$ ). The specificities of leaflets geometry impacted on the geometry at leaf scale, together with rachis and petiole lengths and the number of leaflets on rachis that were notably different between the four leaves (Fig. IV.7B).

At plant scale, ideotype A, B and D looked similar except in term of crown dimensions, ideotype D exhibiting an intermediate size between ideotype A and B. Ideotype C presented a contrasted stature, mainly due to the important leaf bending. The top view of the four ideotypes in stand revealed different distribution of assimilation, with ideotype A and D exhibiting higher assimilation on the top of the canopy than B and C. This observation was confirmed with the detailed analysis of leaf assimilation depending on leaf rank, i.e. the topological position of the leaf on stem, from crown top to crown basis (Fig. IV.8). Indeed there is a clear sorting of ideotypes ( $A > D > B > C$ ) that assimilate more on the top leaves and the opposite sorting considering the ideotypes that assimilate more ef-

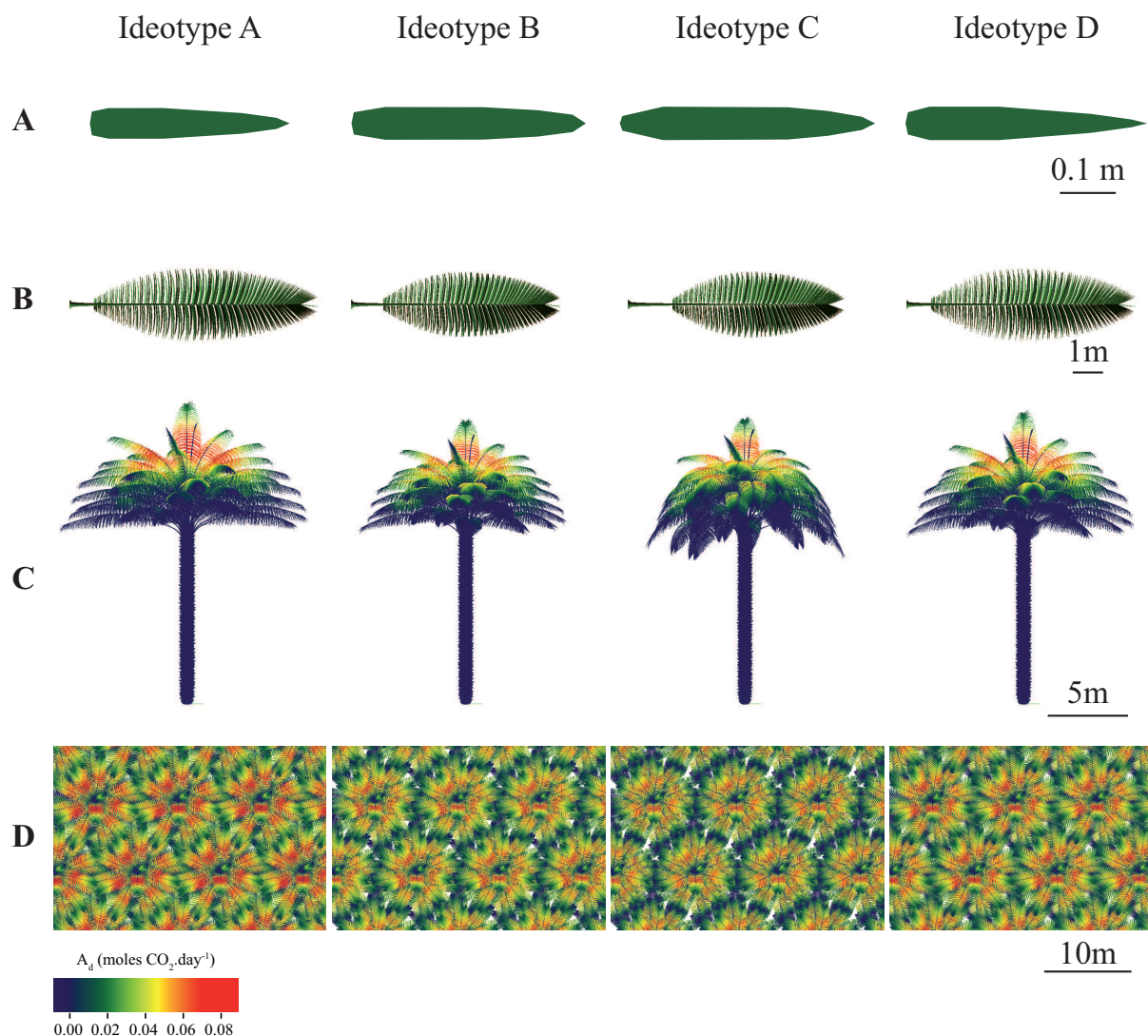


Figure IV.7: Virtual representation of architectural characteristics of the four defined ideotypes from leaflet to plot scale. Each 3D mock-up was generated from the mean values of the parameters associated to the mock-ups classified per ideotype (Fig. IV.6C). A) Top view of a leaflet at B point (flattened for better visualisation) B) Top view of a leaf (flattened for better visualisation) C) Lateral view of plants with daily assimilation per plant component. D) Top view of plants crown in homogeneous stands with daily assimilation per plant component.

ficiently in crown basis. Finally, even if the 30 mock-ups were comparable in term of potential assimilation, some dissimilarities in LAI,  $f_{PAR}$ , MS and  $k$  were evidenced (Fig. IV.4B and Table IV.5). Ideotype A had the highest values for all the studied responses, together with ideotype D. In contrast, ideotype B showed the lowest value of LAI,  $f_{PAR}$

and MS. Ideotype B presented the lowest value of LAI and consequently MS. Ideotype C presented significantly lower value of  $k$  than other ideotypes, as a consequence of a relatively important LAI ( $4.40 \text{ m}^2 \cdot \text{m}^{-2}$ ) with a relatively low  $f_{PAR}$  (0.96).

Table IV.5: Comparison of parameters, response variables and composite traits of the 4 ideotypes identified. Letters correspond to significant differences between ideotypes (Tukeys test,  $P < 0.05$ )

Variable	ideotype			
	A	B	C	D
<i>Parameters</i>				
$Nb_{Leaves}$	$39 \pm 1$ c	$41 \pm 1$ b	$44 \pm 0$ a	$41 \pm 1$ b
$Lrac_{int}(cm)$	$670 \pm 20$ a	$523 \pm 17$ c	$505 \pm 5$ c	$608 \pm 20$ b
$ratio_L$	$0.13 \pm 0.02$ c	$0.21 \pm 0.02$ b	$0.30 \pm 0.01$ a	$0.14 \pm 0.04$ c
$Nb_{max}$	$246 \pm 4$ a	$239 \pm 9$ a	$250 \pm 4$ a	$247 \pm 4$ a
$\delta_{Amax}(^\circ)$	$110 \pm 5$ b	$115 \pm 10$ b	$146 \pm 6$ a	$116 \pm 11$ b
$L_{B_{int}}(cm)$	$36 \pm 7$ b	$42 \pm 3$ a	$46 \pm 2$ a	$43 \pm 4$ a
$W_{B_{int}}(cm)$	$3.2 \pm 0.3$ b	$3.4 \pm 0.2$ ab	$3.7 \pm 0.1$ a	$3.5 \pm 0.3$ a
$xm_{int}$	$0.21 \pm 0.03$ c	$0.32 \pm 0.03$ b	$0.38 \pm 0.02$ a	$0.22 \pm 0.02$ c
$ym_{int}$	$0.72 \pm 0.04$ a	$0.73 \pm 0.03$ a	$0.57 \pm 0.02$ b	$0.61 \pm 0.08$ b
<i>Model outputs</i>				
LAI ( $m^2.m^{-2}$ )	$4.36 \pm 0.19$ a	$4.08 \pm 0.18$ b	$4.40 \pm 0.09$ a	$4.40 \pm 0.15$ a
$f_{PAR}$	$0.976 \pm 0.00$ a	$0.966 \pm 0.01$ b	$0.961 \pm 0.01$ b	$0.974 \pm 0.01$ a
MS	$0.52 \pm 0.01$ a	$0.43 \pm 0.03$ c	$0.45 \pm 0.01$ bc	$0.49 \pm 0.02$ ab
k	$0.85 \pm 0.02$ a	$0.83 \pm 0.03$ a	$0.74 \pm 0.03$ b	$0.83 \pm 0.04$ a
$A_d$ (moles.CO <sub>2</sub> .day <sup>-1</sup> )	$103 \pm 0.2$ a	$103 \pm 0.4$ a	$103 \pm 0.0$ a	$103 \pm 0.2$ a
<i>Composite traits</i>				
Petiole length (cm)	$86 \pm 16$ c	$110 \pm 13$ b	$152 \pm 4$ a	$87 \pm 23$ c
Leaf length (cm)	$757 \pm 24$ a	$633 \pm 27$ c	$657 \pm 8$ bc	$695 \pm 25$ b
Individual leaf area ( $m^2$ )	$8.30 \pm 0.36$ a	$7.24 \pm 0.29$ c	$7.33 \pm 0.15$ bc	$7.79 \pm 0.20$ b
FrqLft (leaflets.cm <sup>-1</sup> )	$0.37 \pm 0.01$ d	$0.46 \pm 0.03$ b	$0.49 \pm 0.01$ a	$0.41 \pm 0.02$ c
Individual leaflet area (cm <sup>2</sup> )	$338 \pm 15$ a	$303 \pm 14$ b	$294 \pm 11$ b	$315 \pm 7$ b
LW ratio (cm.cm <sup>-1</sup> )	$11.6 \pm 3.5$ a	$12.2 \pm 1.0$ a	$12.3 \pm 0.2$ a	$12.3 \pm 1.8$ a

## 4 Discussion

### 4.1 Viability, benefits and limitations of the modelling approach

Assessing the efficiency of oil palm in capturing light and assimilating carbon with respect to plant architecture was made possible through the implementation of a 3D architectural model, which precisely described organ geometry and allowed the estimation of photosynthesis at leaflet scale. The originality of the proposed approach was to study the sensitivity of architectural traits in combination, taking into account interactions between traits. Besides, all simulations were performed in agronomical

conditions with particular planting density and pattern, hence considering the effect of neighbouring plants on the radiative environment.

Our study showed the interest of using FSPM in combination with sensitivity analysis in order to precisely discriminate the influence of explicit architecture, which would not have been possible with a process-based model. The investigated architectural model was found suitable to perform sensitivity analysis as it involved a limited number of parameters with biological meaning. Besides, as the selected parameters were easily calibrated from field measurements, ranges of parameters variation, which are crucial when dealing with sensitivity analysis, were limited to variations observed

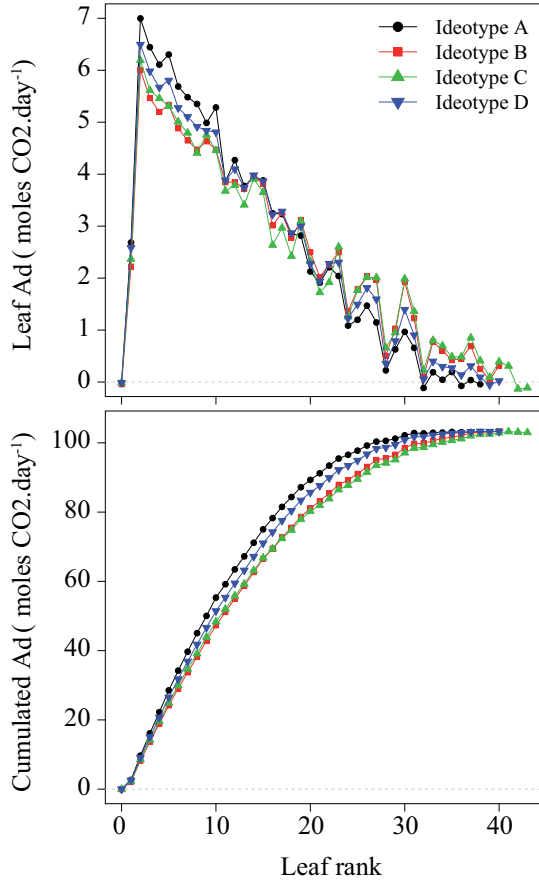


Figure IV.8: Daily leaf assimilation and accumulated assimilation with leaf rank for the mock-ups associated to the four identified ideotypes.

on contrasted genetic material (the five progenies modelled in Chap II and III).

The high interactions between architectural parameters pointed out by the Morris method ( $\sigma$ ) and by the metamodel (Fig. IV.3 and IV.5) were likely associated to the allometric-based formalism of the model, which takes into account correlations between parameters (Fig. IV.1). Plant components were interconnected in a way that changes in rachis length induced variability in leaf structure and consequently the way plants captured light and assimilated carbon. It was noteworthy that more parameters presented high values of  $\sigma_{rel}$  for  $A_d$  than for  $f_{PAR}$ , which is probably rather related to the non-linear response of  $A_d$  to irradiance than

to the intensity of interaction between parameters. The allometric-based approach of the architectural model also made possible to study architecture influence over plant development. However, the dynamics of plant growth (modelled through rachis length evolution over plant age) was only tested in a homothetic way (i.e. the plants with highest LAI in young stage stayed the plants with the highest LAI at adult stage; Fig. IV.2). Actually too many simulations would have been required to integrate additional developmental trajectories.

We chose to not include correlation constraints between architectural traits as it allowed exploring wider architectural possibilities. As a result the extreme values of LAI ( $LAI < 2\text{m}^2.\text{m}^{-2}$  and  $> 7\text{m}^2.\text{m}^{-2}$ ) obtained in our virtual experiment are probably unrealistic. Despite the fact that some virtual palms generated using the Morris method appeared quite unrealistic, it can be noticed that the outputs obtained for field calibrated for the five different progenies were strictly included within the range obtained for the virtual palms, whatever the variable considered ( $LAI$ ,  $f_{PAR}$ ,  $MS$ ,  $k$  or  $A_d$ ). The comparison between calibrated palms and other possible palms suggests that a promising potential exists for enhancing light interception and carbon assimilation through modifications of oil palm architecture (estimated around 10% on average for  $A_d$  on young plants).

Another particularity of our approach was to consider assimilation rather than light interception as criteria to design ideotypes. We justified this choice because investigating ideotype based on  $f_{PAR}$  would have pushed the selection of plants that maximize leaf area (Table IV.4) and conversely ideotype based on total irradiance (correlated to  $k$  in our study), or “silhouette to area ratio” (STAR; [Stenberg, 1996, Da Silva et al., 2014]) would have led to select the plants with the lowest leaf area. To our mind,  $A_d$  was an interesting trade-off between  $f_{PAR}$  and irradiance and it allowed optimal LAI between 4 and  $5\text{m}^2.\text{m}^{-2}$ , which is consistent with LAI of cultivated oil palms estimated between 4 and  $6\text{m}^2.\text{m}^{-2}$  in literature [Barcelos et al., 2015, Corley and Tinker, 2016]. The range of LAI with optimized assimilation was limited to  $4.7\text{m}^2.\text{m}^{-2}$  because exceeding shading on high LAI resulted in higher respiration than assimilation of leaves. Designing ideotype from  $A_d$  thus allow selecting the

architectures that confer an optimized distribution of light within the canopy by limiting self and mutual shading. Besides,  $A_d$  being calculated from cumulated values estimated every 30mn, optimized light distribution takes into account the different positions of the sun during the day.

The NHR carbon assimilation model was chosen in this study since its relative simplicity offered the possibility to reduced computational time. NHR curve parameters were calibrated from optimal field conditions for carbon assimilation (temperature: 28°C, CO<sub>2</sub> concentration: 400 ppm; relative humidity: 70%) and thus  $A_d$  estimated in the present paper must be considered as potential assimilation. However, dealing with potential assimilation does not question the validity of our approach since response curves of  $A_d$  to PFD are relatively homothetic under different conditions. Results obtained from calibration under unfavourable conditions would thus have been comparable (with a multiplicative factor  $<1$ ).

Our approach exclusively focused on architectural parameters, environmental and physiological parameters being fixed. However, various processes can reduce carbon assimilation of oil palm in field condition. The most important limitation of carbon assimilation is stomatal conductance ( $g_s$ ), closely related to climatic environment and soil water availability. Indeed, it has been proven that  $g_s$  was very sensitive to vapour pressure deficit (VPD) in oil palm [Dufrêne and Saugier, 1993]. Potential photosynthetic capacity is likely to depend on genetic origin [Lamade and Setiyo, 1996], as well as the behaviour of genotype against water deficit. Other studies also suggest that photosynthetic capacity is linked to the topological position of leaf within the crown (leaf age) [Corley, 1983, Dufrêne and Saugier, 1993]. The limited data set available in our study did not allow to sufficiently investigate the factor explaining the variation observed in light curve responses (supplementary Fig IV.11 page 113). Our simulation study highlighted important mutual shading in adult stand (around 50%) so that improving photosynthesis of shade leaves could be an option to gain higher canopy assimilation [Reynolds et al., 2000, Song et al., 2013, Gu et al., 2014]. As a result, investigating the influence of photosynthesis capacity in combination with architectural parameters would probably enlarge the

scope of potential improvement. Another limit of our study was that light quality was not considered [Chen et al., 2014, Dauzat et al., 2008], nor optical properties of leaves, which are likely to change the capture and the distribution of light within the crown [Sadras and Denison, 2016].

## 4.2 Designing architectural ideotypes for oil palm

Our results confirmed the close relationship existing between LAI, light interception and carbon assimilation [Barillot et al., 2014, Cerasuolo et al., 2016]. Indeed, the key parameters for both  $A_d$  and  $f_{PAR}$  were closely related to parameters defining leaf area, such as rachis length ( $L_{rac_{int}}$ ) and the number ( $Nb_{max}$ ), dimension ( $LB_{int}$  and  $WB_{int}$ ) and shape ( $xm_{int}$  and  $ym_{int}$ ) of leaflets. Comparable studies on plants with different branching pattern revealed that total leaf area had significant effect on light interception, together with leaf shape, internode length and branching pattern [Sarlikioti et al., 2011, Da Silva et al., 2014, Chen et al., 2014]. In our study, the strong influence of LAI-related parameters can be explained by the single-stem architecture of the oil palm, which mainly limits variations in its architecture to variations in leaf geometry. As a result, conversely to other plants that can alter their architecture acting on twigs number and geometry, oil palm cannot modulate its architecture independently of total leaf area.

Globally the ranking of parameter sensitivity was constant over plant age, suggesting that the most interesting architecture at young age should be the most interesting at mature stage. Nevertheless, most of the sensitive parameters had greater sensitivity (relatively to the most sensitive parameter) with palm age, suggesting that geometrical traits had higher influence when the canopy got closed. It was particularly the case for leaflets shape parameters ( $LB_{int}$ ,  $WB_{int}$ ,  $xm_{int}$  and  $ym_{int}$ ), and the parameter associated to leaf structure ( $Nb_{max}$ ) and curvature at rachis tip ( $\delta_{A_{max}}$ ) (Fig. IV.3A). We thus suggest that a rapid establishment of leaf area is critical at young stage to optimize light interception [Richter et al., 2010], but under high LAI, fine attributes related to leaf and leaflet arrangement within the crown influence more light capture by conditioning light distribution within the crown.



A focus in the virtual plants presenting a LAI between 3.8 and 4.7  $\text{m}^2.\text{m}^{-2}$  at mature stage revealed important discrepancies in  $A_d$  values whereas the range of  $f_{PAR}$  values was relatively narrow. This emphasized that assimilation at plant scale does not only depend on the quantity of light intercepted but also on the distribution of light within the crown. Indeed, the 30 mock-ups with the highest values of  $A_d$  were not the ones that intercepted light the most. Plants that optimized carbon assimilation displayed low mutual shading and high coefficient of extinction ( $k$ ) indicating high amount of light intercepted per unit leaf area [Duursma et al., 2012]. A detailed analysis at leaf scale revealed that light-saturated photosynthesis was reached in the upper leaves for plants with the lowest  $A_d$  (supplementary Fig. IV.12 page 113). Among the traits that allow light to penetrate deeper and more uniformly into the canopy, leaf angle has been shown of great influence [Falster and Westoby, 2003, Sarlikioti et al., 2011, Cerasuolo et al., 2013]. Our simulations also exhibited strong leaf angle effect, as plants with more erect leaves (low  $\delta_{A_{max}}$ ) presented the highest value of light interception and carbon assimilation. Another characteristic of the plants that optimized carbon assimilation was longer and narrower (low  $LW_{ratio}$ ) leaflets in comparison to plants with low assimilation. This result was consistent with results obtained in tomato [Sarlikioti et al., 2011]. The combination of all these traits participated in limiting foliage aggregation (clumping), which has been shown to decrease light interception efficiency in stands [Parveaud et al., 2008, Cerasuolo et al., 2013, Wang et al., 2014].

An unexpected result obtained in the present study was that four distinct ideotypes were revealed among the most interesting plants in term of assimilation. The four ideotypes presented comparable LAI except ideotype B that presented a significantly lower LAI. The four ideotypes had relatively short and erect leaves, which call to mind the ideotype developed in cereal crops to improve light harvest [Khush, 2001, Dingkuhn et al., 2015]. However, the discrepancies observed between the four identified ideotypes highlighted that several combinations of architectural traits were possible to enhance carbon assimilation. Ideotypes were distinguishable from their number of leaves, crown diameter (resulting from the combination of the three parameters

$ratio_L$ ,  $L_{rac}$  and  $\delta_{A_{max}}$ ), and leaflets geometry. For ideotypes A and D, there was an important inter-penetration of leaves between neighbouring plants, resulting in shaded rachis tips and overall higher values of mutual shading than the two other ideotypes. Ideotype B showed the shortest leaves while ideotype C had bent leaves. As a result all these characteristics involved contrasted contribution of the different leaves to the overall plant assimilation (Fig. IV.8): ideotype A and D optimized assimilation of leaves in crown top while ideotype B and C distributed assimilation to lower leaves. One particularity of the ideotype A, B and D was the horizontality of the leaves in crown basis. This kind of architecture is hardly visible in field, but the overall aspect of the canopy on mature stand tends to be comparable since harvesting process implies lower leaves pruning. Figure IV.8 showed that these crown bottom leaves had a negligible contribution to total plant assimilation. Integrating pruning practices in simulation (i.e. removing of leaves ranks  $> 33$ ) should not significantly modify the morphology of the ideotypes but reduced their LAI values.

### 4.3 Perspectives for oil palm breeding

From a theoretical point of view, this study addresses the question of the best arrangement of leaf area within plant crown. The responses curves obtained from simulations (Fig. IV.4) clearly exhibit envelope curve that delimit the optimal dispersion and density of oil palm leaves (at least for the model proposed). At young stage, results show that the studied progenies do not exhibit an optimal architecture. Without precise architectural characteristic of the same progenies at maturity, it is hard to evaluate their performance at more advanced stages of development. In fine, the trajectory of plants over years should be studied, since the major part of oil palm production occurs when the canopy is closed. As a result the kinetic of canopy closure would be a determinant criteria in breeding strategies.

With the four ideotypes selected in this study, we demonstrated that different balances between leaf dimensions, leaf structure and crown geometry could lead to comparable carbon assimilation rates. These different combinations of architectural

traits leading to efficient assimilation bring promising prospects for breeding. Different strategies of breeding could thus be considered from these various ideotypes as genetic resources and architectural traits heritability would probably limit the selection some of these theoretical ideotypes.

The ideotypes were defined in this work for a targeted environment characterized by the absence of resource limitation under current agronomic practices (density of 136 plants.ha<sup>-1</sup>). One interest of FSPM relies on the possibility to perform *in silico* experiments in order to investigate other ideotypes under innovative management practices. Testing new planting densities has raised interest from oil palm agronomists [Breure, 1988, Bonneau et al., 2014] and illustrated that leaf length was a critical trait to determine planting density [Barcelos et al., 2015]. Such experiments required substantial time and costs inputs for setting up experiments and these could be considerably reduced by using a modelling approach. However, such perspective raises attention on the need to integrate plant architectural plasticity in the modelling approach, as proposed for rice [Zhu et al., 2015, Kumar et al., 2017]. Other ideotypes could be identified under different planting pattern and density, but we can suppose that the variations obtained in comparison to the ideotype proposed in the present study would mainly rely on an adjustment of crown dimensions. Conversely, with a reverse approach, an interesting study would be to investigate optimized densities for given morphotypes.

We proposed here to define ideotypes that present optimal carbon assimilation, but these ideotypes could be different if a multi-objective approach is followed [Martre et al., 2014, Sadras and Denison, 2016]. Although genetical and environmental effect on carbon assimilation were not considered here, our study put forward interesting perspective in oil palm breeding notably regarding water deficit. Our simulation outputs revealed that architecture with relatively low values of LAI (close to 4 m<sup>2</sup>.m<sup>-2</sup>) presented level of potential assimilation comparable to plant with higher LAI (over 5 m<sup>2</sup>.m<sup>-2</sup>). Breeding strategies to limit water stress could thus rely on selecting architectures that confer an interesting trade-off between assimilation and LAI.

Similarly, trade-off between carbon assimilation and biomass investment in vegetative part to estab-

lish leaf area [Takenaka et al., 2001] would probably lead to different ideotypes with adapted LAI. Interestingly, our simulation study revealed an important range of LAI for comparable level of assimilation, which opens the path for defining new ideotypes by integrating further functional processes already developed in oil palm like carbon partitioning [Pallas et al., 2013a, Pallas et al., 2013b]. Indeed, integrative studies aimed at exploring several functioning processes highlighted the importance of biomass partitioning in yield variability [Lecoeur et al., 2011, Koester et al., 2014, Cerasuolo et al., 2016].

## Acknowledgements

The authors thank SMART Research Institute (SMARTRI, Smart Tbk.) for its financial support. We also thank Sebastien Griffon for his advise in the utilization of Xplo.



## 5 Supplementary Material

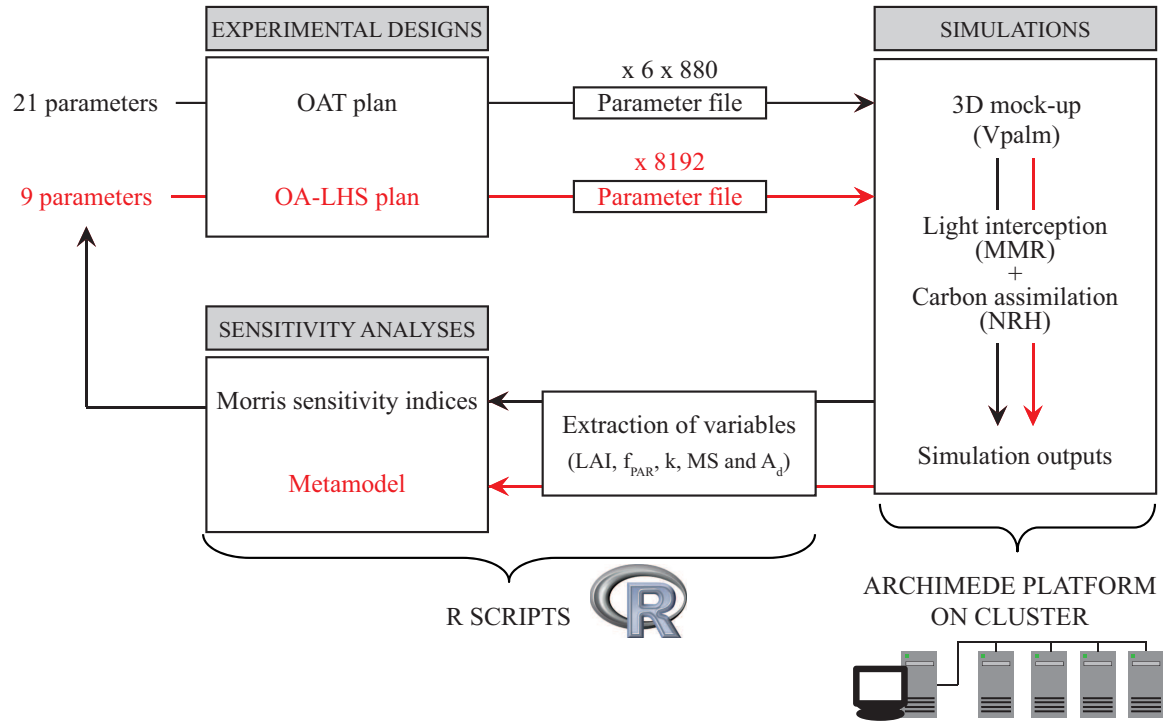


Figure IV.9: Schema of the overall approach with the different steps executed to perform Morris method and metamodeling. (OAT: one at a time; OA-LHS: orthogonal array-based latin hypercube; MMR: Mir-Musc-Radbal ; NRH: non-rectangular hyperbola; see Table IV.3 page 96 for variables abbreviations)

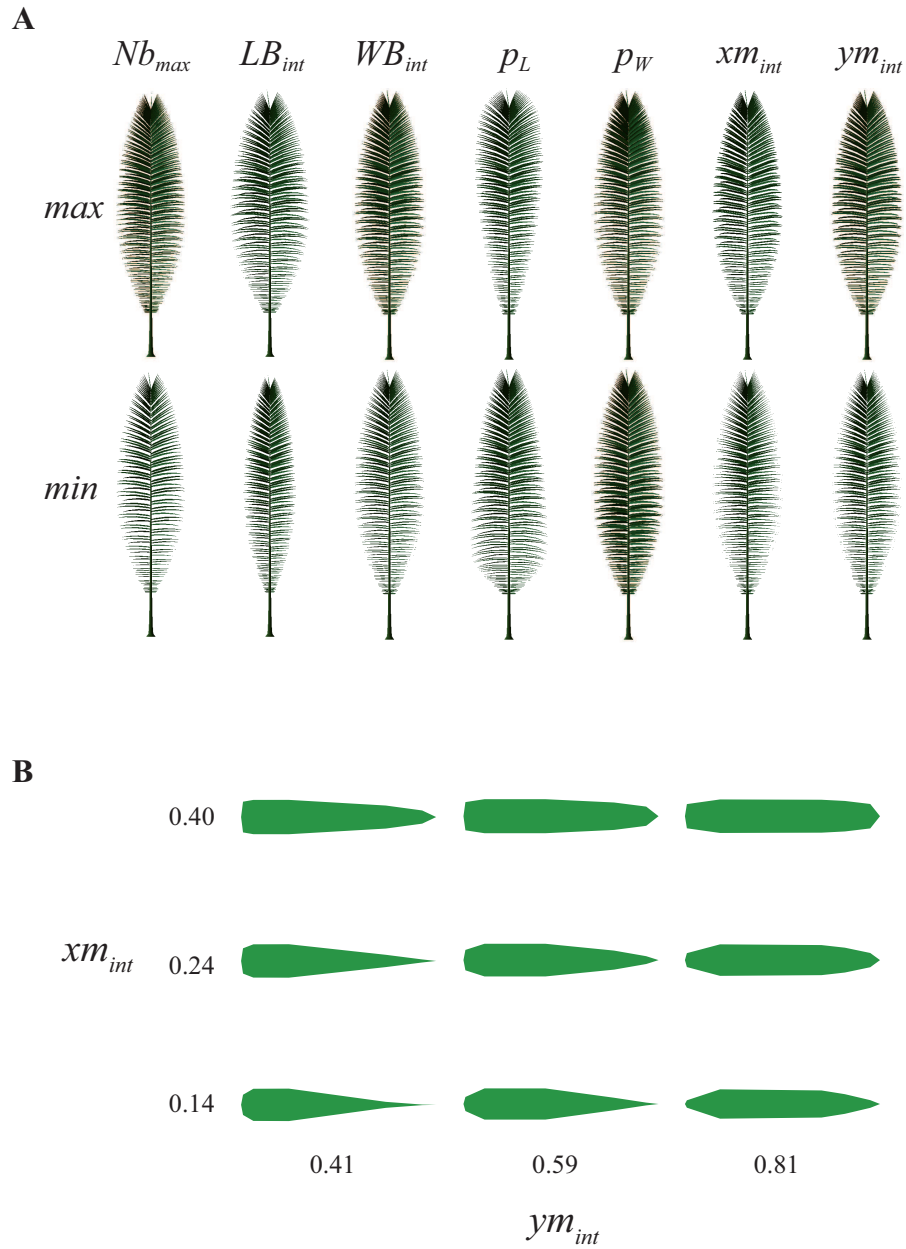


Figure IV.10: A) Leaf morphology depending on variation of morphometric-related parameters ( $Lrac_{int}$  and  $ratio_L$  are fixed to keep leaf length constant). B) Leaflet morphology depending on values of the parameters  $xm_{int}$  and  $ym_{int}$ .

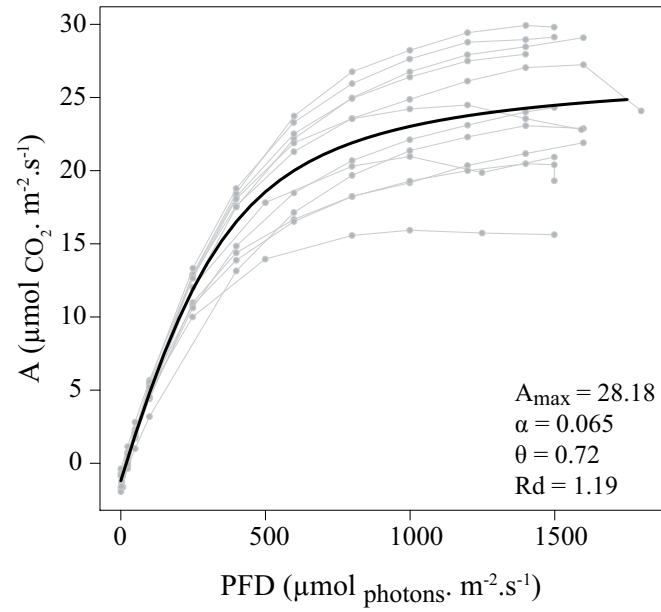


Figure IV.11: Calibration of non-rectangular hyperbola (NRH) curve for simulating leaf photosynthesis. Lines in grey represent the response curves measured on 12 different oil palm leaves (from 8 individuals, on leaflet at point B from leaf rank between 9 and 17). Black line represents average model adjustment (values of calibrated parameters are presented at bottom right of the graphic).

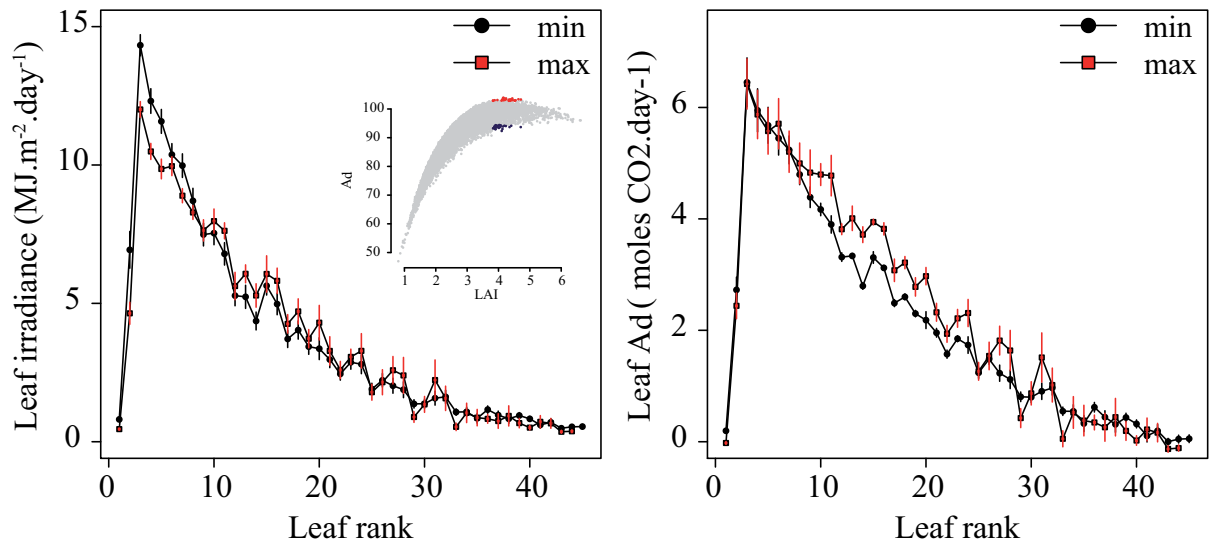


Figure IV.12: Daily leaf irradiance and assimilation for the 30 mock-ups with the highest and the 30 mock-ups lowest values of  $A_d$  for LAI varying between 3.8 and 4.7  $\text{m}^2 \cdot \text{m}^{-2}$ .

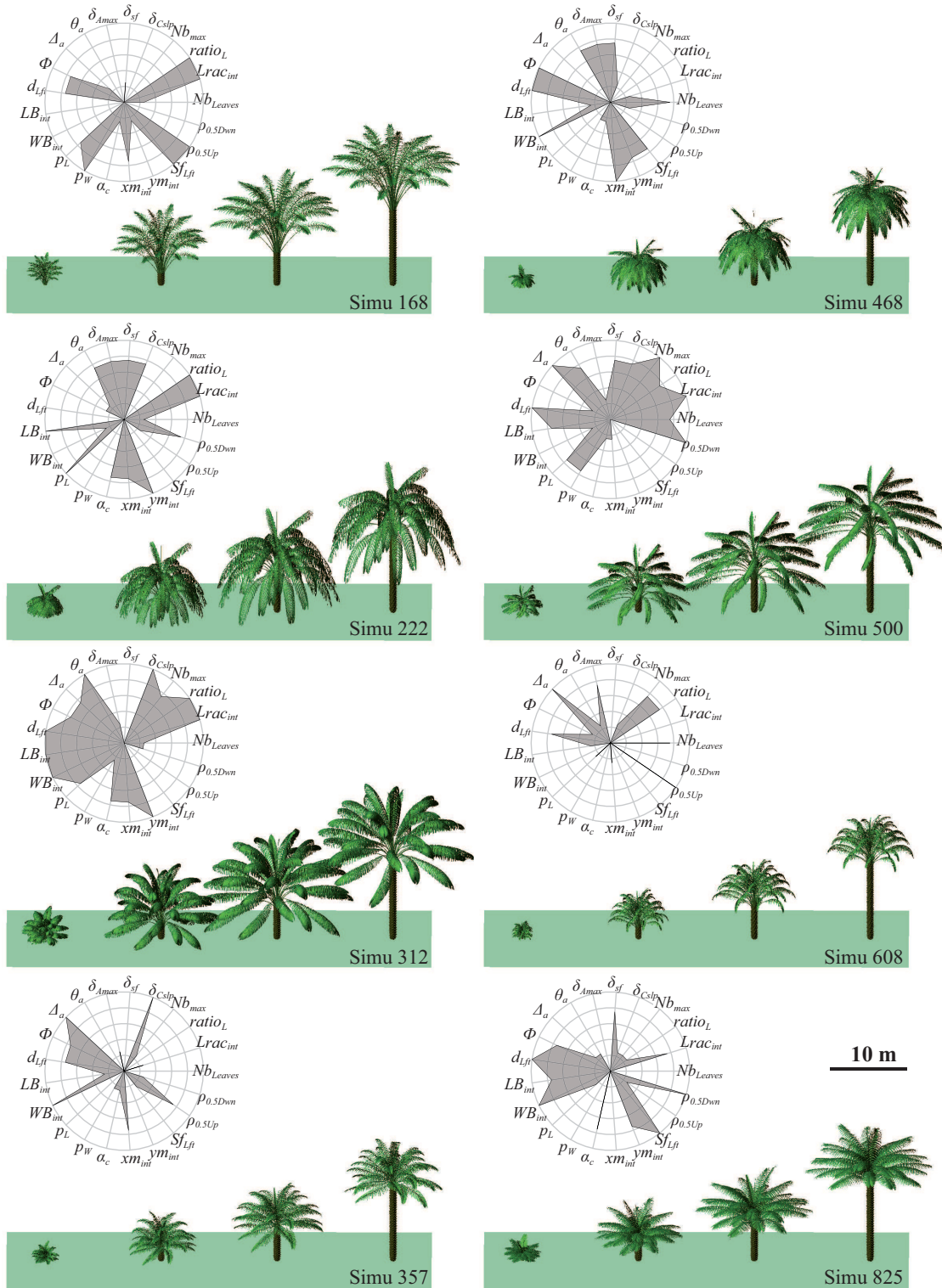


Figure IV.13: Sample of virtual plants generated during the Morris method with the associated relative values of architectural parameters. The four 3D mock-ups represent a similar combination of parameters at four different developmental stages (from left to right: 50, 150, 250 and 450 leaves emerged from planting date)

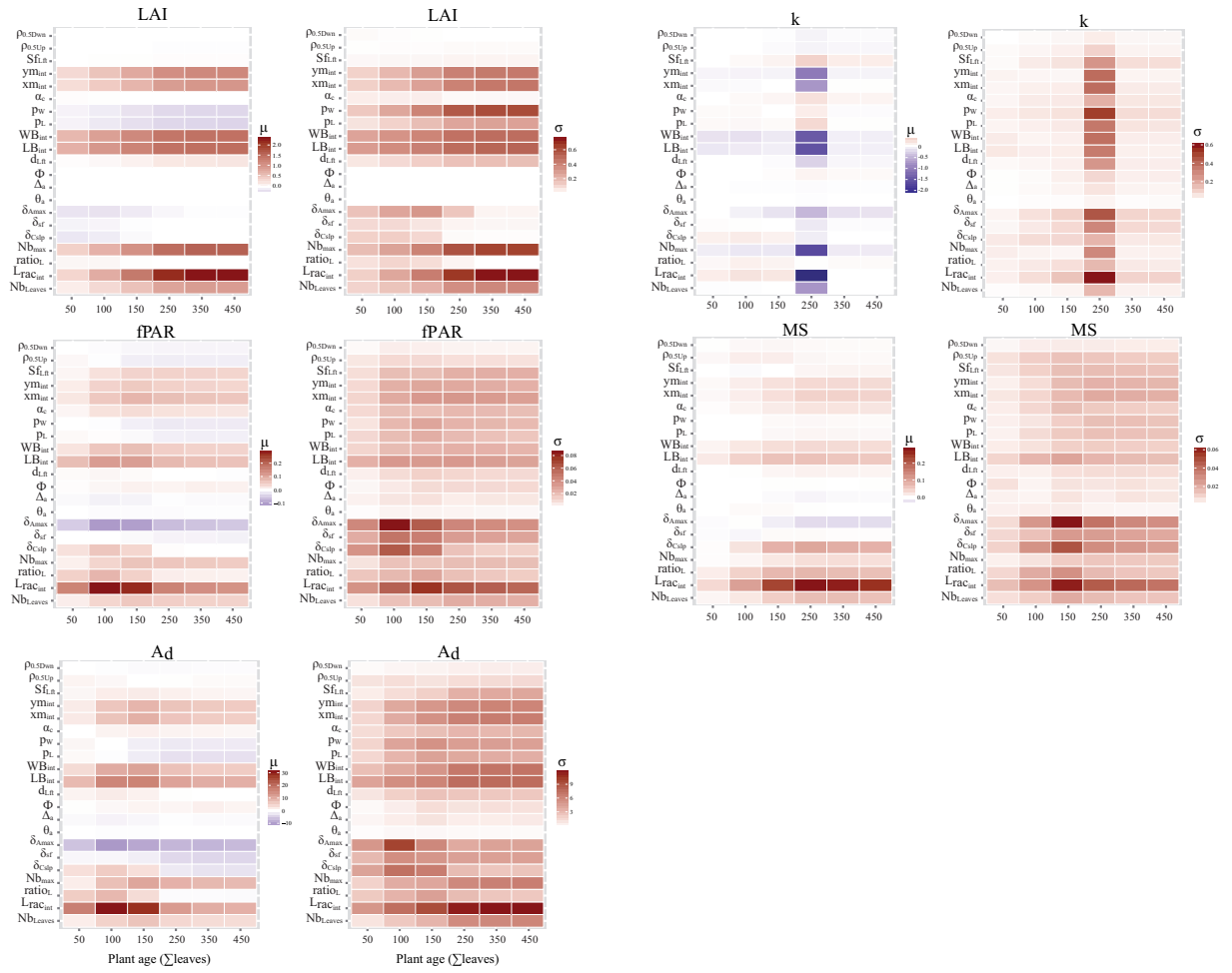


Figure IV.14: Heat map of elementary effects ( $\mu$ ) and interaction effects ( $\sigma$ ) for LAI and the four studied outputs over plant age (see Table IV.1 page 92 for parameter abbreviations and Table IV.3 page 96 for output calculation).

Table IV.6: Summary of metamodel adjustments to predict  $A_d$  with estimated values of the coefficients associated to parameters. Coefficients are ordered depending on their significance.

	Estimate	Std. Error	t value	Pr(> t )
(Intercept)	-561.6657	2.6638	-210.85	0.0000
$Lrac_{int}$	0.5894	0.0023	259.05	0.0000
$L_{B_{int}}$	2.1566	0.0133	162.75	0.0000
$Nb_{max}$	1.0274	0.0078	132.13	0.0000
$W_{B_{int}}$	34.5189	0.2277	151.61	0.0000
$ym_{int}$	157.0191	1.5436	101.73	0.0000
$xm_{int}$	303.5926	2.2966	132.19	0.0000
$\delta_{Amax}$	-0.0849	0.0085	-10.02	0.0000
$Nb_{Leaves}$	7.7733	0.0897	86.66	0.0000
$Lrac_{int}^2$	-0.0001	0.0000	-123.91	0.0000
$xm_{int}^2$	-129.4009	1.6322	-79.28	0.0000
$L_{B_{int}}^2$	-0.0032	0.0001	-54.97	0.0000
$Nb_{max}^2$	-0.0007	0.0000	-55.48	0.0000
$ratio_L$	32.2187	1.6662	19.34	0.0000
$W_{B_{int}}^2$	-0.7506	0.0165	-45.39	0.0000
$Nb_{Leaves}^2$	-0.0413	0.0010	-41.14	0.0000
$\delta_{Amax}^2$	-0.0004	0.0000	-24.62	0.0000
$ym_{int}^2$	-11.9180	0.6542	-18.22	0.0000
$ratio_L^2$	-6.3380	1.2590	-5.03	0.0000
$Lrac_{int}:L_{B_{int}}$	-0.0012	0.0000	-161.84	0.0000
$Lrac_{int}:W_{B_{int}}$	-0.0167	0.0001	-133.03	0.0000
$Lrac_{int}:Nb_{max}$	-0.0004	0.0000	-113.89	0.0000
$Lrac_{int}:Nb_{Leaves}$	-0.0031	0.0000	-99.88	0.0000
$ym_{int}:xm_{int}$	-79.5835	0.9235	-86.18	0.0000
$Lrac_{int}:xm_{int}$	-0.0990	0.0012	-79.33	0.0000
$Lrac_{int}:ym_{int}$	-0.0606	0.0008	-76.92	0.0000
$Nb_{max}:W_{B_{int}}$	-0.0272	0.0004	-65.46	0.0000
$L_{B_{int}}:Nb_{max}$	-0.0015	0.0000	-62.64	0.0000
$L_{B_{int}}:W_{B_{int}}$	-0.0535	0.0009	-61.22	0.0000
$Nb_{max}:xm_{int}$	-0.1922	0.0041	-46.69	0.0000
$Nb_{max}:ym_{int}$	-0.1201	0.0026	-46.16	0.0000
$L_{B_{int}}:ym_{int}$	-0.2397	0.0055	-43.83	0.0000
$W_{B_{int}}:xm_{int}$	-6.1906	0.1464	-42.30	0.0000
$W_{B_{int}}:ym_{int}$	-3.9172	0.0928	-42.20	0.0000
$W_{B_{int}}:Nb_{Leaves}$	-0.1523	0.0037	-41.41	0.0000
$L_{B_{int}}:Nb_{Leaves}$	-0.0088	0.0002	-40.42	0.0000
$L_{B_{int}}:xm_{int}$	-0.3322	0.0087	-38.15	0.0000
$Nb_{max}:Nb_{Leaves}$	-0.0035	0.0001	-34.09	0.0000
$ym_{int}:Nb_{Leaves}$	-0.7034	0.0231	-30.50	0.0000
$xm_{int}:Nb_{Leaves}$	-1.0840	0.0366	-29.58	0.0000
$Lrac_{int}:ratio$	-0.0261	0.0011	-23.94	0.0000
$L_{B_{int}}:\delta_{Amax}$	0.0006	0.0000	19.96	0.0000
$Lrac_{int}:\delta_{Amax}$	-0.0001	0.0000	-19.40	0.0000
$xm_{int}:\delta_{Amax}$	0.0895	0.0049	18.37	0.0000
$Nb_{Leaves}:ratio_L$	-0.5014	0.0320	-15.65	0.0000
$W_{B_{int}}:\delta_{Amax}$	0.0074	0.0005	15.02	0.0000
$ym_{int}:\delta_{Amax}$	0.0399	0.0031	12.92	0.0000
$Nb_{max}:\delta_{Amax}$	0.0002	0.0000	11.97	0.0000
$\delta_{Amax}:Nb_{Leaves}$	0.0014	0.0001	11.84	0.0000
$L_{B_{int}}:ratio_L$	0.0404	0.0076	5.31	0.0000
$ym_{int}:ratio_L$	2.5279	0.8079	3.13	0.0018

## Chapter V

# General discussion

## 1 Retrospect on the general problematic

### 1.1 Scientific framework

Nowadays, the major part of research studies in agronomy aims at working towards improving yields while taking into account agronomic system sustainability. By selecting plants adapted to specific conditions, plant breeding is one strategy to tackle such a problem. For cereals, genetic studies empirically revealed a close association between morphological traits and yielding ability. From these observations emerged the concept of ideotype proposed by Donald [Donald, 1968], who suggested that breeding strategies based on specific traits known to be related to yield would be more efficient than empirical breeding [Peng et al., 2008]. Following this concept, a great improvement of annual species productivity was achieved by altering plant architecture, in combination with agronomic practices [Khush, 2001]. Beyond improving yield, other objectives can be targeted when designing ideotypes, as for instance grain quality in cereals [Aguirrezábal et al., 2014, Martre et al., 2015]. In perennial plants, the definition of an ideotype largely depends on the system considered, i.e. forestry, horticultural or agricultural systems. As a result the development of tree ideotypes relies on the large diversity of the properties of interest, such as carbon sequestration, timber, fruit, kernel or oil production [Dickmann et al., 1994, Leakey and Page, 2006]. Architectural studies have contributed to the ideotype approach in trees, by considering architectural traits related to biomass accumulation in wood [Pile et al., 2016] or fruiting

productivity [Lauri and Costes, 2005, Cilas et al., 2006]. Ideotypes can be defined as “cultural” when they are designed through management practices (shoot pruning in orchards for instance [Willaume et al., 2004, Tang et al., 2015]) or as “varietal” when their conception relies on breeding programs [Laurens et al., 2000, Martre et al., 2014]. By analogy with these studies investigating plant performance through the definition of architectural ideotype, we proposed to investigate this strategy on oil palm because, to our knowledge, no equivalent study was addressed for this species.

Our study explored the ideotype approach applied on *Elaeis guineensis* architecture in the general context of improving sustainable yield in industrial oil palm plantations. This study thus proposed an upstream investigation of the potential improvement of oil palm yield by selecting specific plant architecture that could optimize light interception. Two reasons could explain why such study has not been intended in oil palm so far. First, conversely to annual and autogamous plants for which breeding program can be achieved in a few years due to the short generation time, oil palm is a perennial and allogamous plant that imposes to deal with a longer biological cycles and more complex breeding strategies. As a result, oil palm breeders mainly focused on integrated phenotypic traits directly related to yield (empirical method of “selection for yield”; [Martre et al., 2014]). Reciprocal recurrent selections between parental populations were conducted to test yield characteristics of progenies and subsequently define the best parents to cross.

The second reason was the difficulty to characterize and compare plant architectures, mainly for tall plants like oil palm. Indeed, conversely to



yield evaluation, phenotyping plants based on architectural description remains complex in breeding trials, but this phenotypic bottleneck is on the way to be overcome [Costes et al., 2004]. The recent development of biotechnology, mathematical tools and computational sciences has opened the way to innovative breeding strategies. Biotechnologies, with rapid technical advances in molecular markers mapping, quantitative trait loci (QTL) analysis and/or candidate gene approaches, now allow an integrative description of genotypes. The recent sequencing of oil palm genome [Singh et al., 2013b] allows performing QTL studies based on molecular markers (simple sequence repeat SSR or single nucleotide polymorphisms SNP) [Pootakham et al., 2015]. Besides, mathematical and computational science can facilitate phenotypic characterization and perform in-depth analyses of quantitative genetics. Hence these methodological breakthroughs enable to overcome empirical approach and test specific hypotheses. By opposition to mass selection leading to select experimentally the best plants without characterising genotypes, new breeding approaches rely on deciphering the phenotypic traits related to targeted physiological processes and investigating the genetic control of these traits. In this way it is now possible to breed for ideotypes.

## 1.2 Conceptual basis of an oil palm ideotype

Oil palm architecture can be considered as simple regarding the absence of a branching pattern, characterized by a single shoot that bears 30 to 40 green leaves, which is conserved during its entire lifespan. Conversely to plants with fluctuating branching patterns depending on ontogenetic stages and environment, the absence of axillary bud in oil palm gives a solitary stem, i.e. monopodial habit [Henderson, 2002], resulting in an architectural plasticity limited to variation in leaf morphology. As a result, architectural manipulation based on management practices appears as limited for the oil palm and consequently leads to consider varietal ideotype rather than cultural ideotype. In cereals, enhancement of production was partly achieved by selecting plants with reduced tillering capacity [Sakamoto and Matsuoka, 2004], thus demonstrating the benefit of the inability to adjust shoot branching for

cultivar performance [Kumar et al., 2017]. By analogy with the morphotypes designed by architectural manipulation in cereals, one could suggest that the single shoot structure of oil palm is advantageous in an agronomical context. So far stem height has been studied in breeding program to facilitate the harvesting process. Selection process enabled to slow down stem growth and QTLs related to stem height have recently been discovered [Pootakham et al., 2015], paving the way for further studies other oil palm vegetative characteristics such as crown structure. The organisation of leaves within the crown and their morphology is potentially a target for genetic-based architectural manipulation. In this context, the architectural ideotype of palm would rely on a specific crown structure (number of leaves, leaf shape and dimensions) conferring an optimal interception and distribution of light. Hence, we proposed a model-assisted phenotyping among different oil palm progenies in order to study the variations in the geometry and the spatial arrangement of leaves within the crown, with respect to the capacity of the plant to intercept light.

## 2 Three-dimensional representations of oil palm

### 2.1 Conception and formalism of the 3D modelling approach

In chapter II, we proposed a methodology to reconstruct the 3D architecture of oil palm with specific parameters related to progenies. The existence of segregation between genotypes within a progeny led to develop an individual based approach to simulate inter and intra-progeny variability. Indeed, progenies are hybrids obtained from breeding schemes based on crosses between contrasted populations (Chapter I section 1.4), leading to important genotypic variability.

The conception of the model relied on the identification of the architectural features required to virtually represent a plant. This first conceptual step was based on prior descriptions and simulation tools set up in the AMAP joint unit for coconut, oil palm and date palm ([Lecoustre and Jeager, 1989, Dauzat, 1990, Dauzat and Eroy, 1997, Julia, 2007], and Rey, personal communications). The

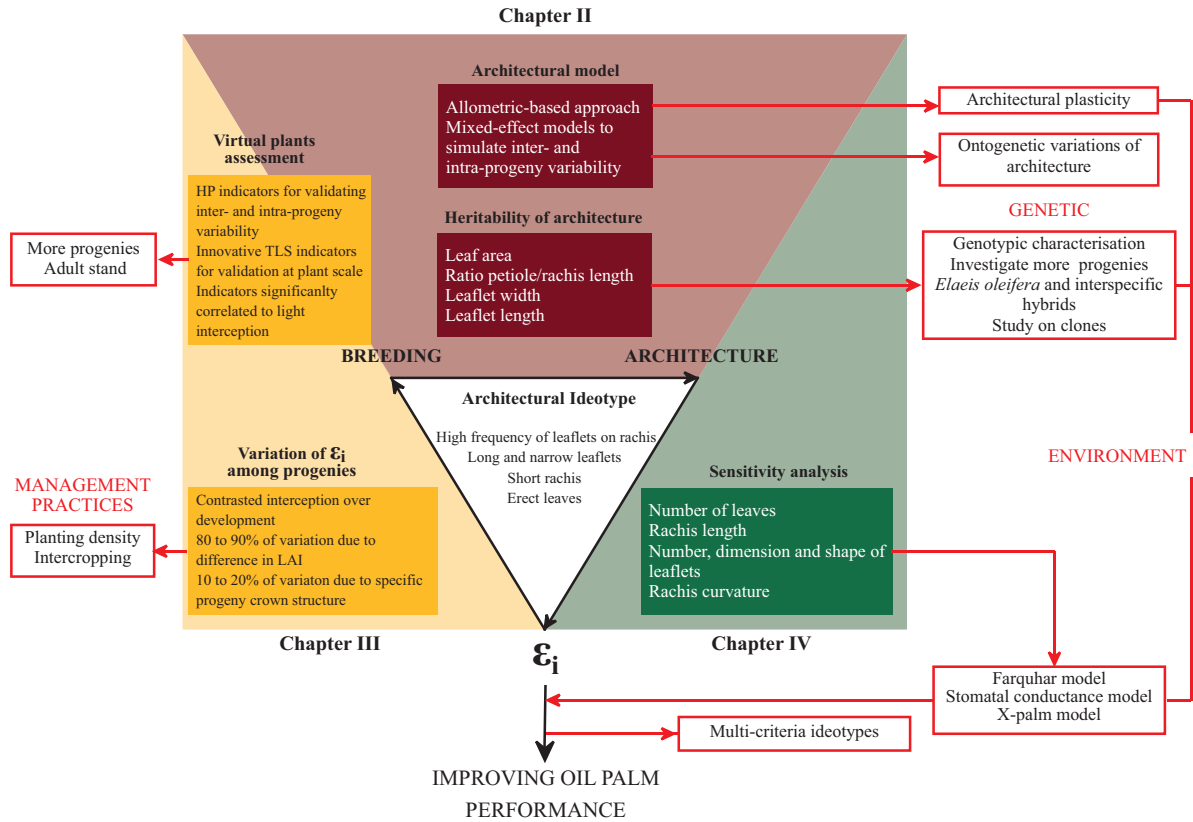


Figure V.1: Conclusions and perspectives of the study

description of several progenies involved the design of a protocol and an adapted sampling strategy for measuring these architectural traits, from leaflet to plant scales (appendix A page 129). This first step was crucial for the development of the architectural model and raised practical questions related to the level of accuracy required to reconstruct 3D mock-ups. Indeed, a first campaign of exhaustive field measurements enabled to evaluate the difficulty of performed architectural descriptions. The main issue in data collection was to characterize traits variability at different scale of organisation (plant, leaf and leaflets). First analyses led to a stratified sampling strategy: quick and simple measurements were done on a large number of individuals whereas detailed measurements were performed on a small number of individuals. The objective of the sampling strategy was to optimize a trade-off between the number of individuals described and the level

of detail of these descriptions for fine virtual reconstruction. Finally, a simplified protocol was set up on a limited number of architectural traits, considered practical to screen an important number of individuals over plant development, and which could be potentially used in breeding programs. However, these observations were set up to evaluate plants with limited height, which conferred accessibility to leaves without a destructive protocol. Hence, the protocol would have to be technically adapted to perform comparable phenotyping in mature stands.

Simulation of inter-individual architectural variability in 3D representations was made possible through the combination of an allometric-based approach with mixed-effect models. The allometric-based approach with fitting process performed on the collected data is a common tool to generate 3D modelling [Casella and Sinoquet, 2003, Sonohat et al., 2006, Iandolina et al., 2013], but the original-

ity of this study was the application of mixed-effect models to assess and virtually reproduce variability in plant architecture.

By using spatial and temporal variables to predict topological and geometrical attributes of plants, the allometric-based approach allowed the integration of ontogenetic and morphogenetic gradients in 3D mock-ups. Although the model does not account for functional processes driving the plant growth, it generates static architecture of a given plant over time (Fig. III.12 page 84). Simulation of plant ontogeny from allometric relationships was particularly adapted in our case since oil palm presents a single shoot with an indeterminate continuous growth (regular succession of phytomers over time). Hence a unique mathematical function was able to model the functioning of the meristem establishing the plant architecture. However, the validity of this developmental model depends on hypotheses, such as the stability of fine geometrical attributes over time (e.g. leaf curvature, leaflet orientations). In the absence of available data, the most parsimonious assumption was to not consider any variability due to plant ontogeny. This assumption is not likely to be true as morphogenetic gradients are generally observed over plant ontogeny [Barthélémy, 1991, Barthélémy and Caraglio, 2007]. Indeed, for oil palm gradients on leaf morphology can be observed on seedling with the gradual transition from a unique lamina to pinnate leaf, and it is likely that other changes appear when plants reach maturity. These hypotheses should be evaluated when the investigated plants will reach maturity.

The methodology developed in the present study could be applied to other species, but would be limited to species presenting particular architectures. By analogy with oil palm architecture, plant with a mono-axial structure, following the Corner or Holtum model [Hallé et al., 1978] could be virtually represented according to the approach established in this study. For plants with other branching patterns, different allometric relationships could be applied specifically on axis orders or category of axes to represent the contrasted morphogenetic differentiation of the meristems. For plants showing a mono-axial shoot with reiterated axes (e.g. date palm or banana trees), the repeating axes could potentially be modelled following comparable rules than the one applied to the first order axis, but

this would need further investigation notably on responses to environmental constraints [Negrón et al., 2013]. A second category of plants, which growth could be simulated similarly, gathers plants with equivalent and non-differentiated axes [Hallé et al., 1978], such as Tomlinson, Schoute, Chamberlain and Leeuwenberg models. In this case each category of axis or axis order could be modelled by different allometric relationships rendering the specific geometrical attributes of axes. However, applying allometric relationships and subsequently mixed-effect approach to represent plant structure would be limited by complex branching patterns and rhythmic growth of axes. Indeed, differentiation of axes and rhythmicity of growth would impose to deal with other mathematical formalisms that better depict subtle spatial and temporal series, such as Markov chains [Guédon et al., 2001]. For instance, this statistical approach allows the identification of dependency among successive node ranks and can also be applied to discriminate plant structure.

## 2.2 Assessing 3D mock-up of oil palm

The assessment of the 3D model developed in this study was performed through different quantitative approaches. First, we proposed to evaluate the quality of reconstruction by confronting different traits to field measurements. In agreement with the objective to simulate inter-individual variability, these assessments were examined by comparing for each progeny both mean and variance values of geometrical attributes between field observations and simulations. Results highlighted the capacity of the model to satisfactorily reproduce architectural characteristics at organ scale. In a second step, since the model was designed for rendering the variability among plants within a given progeny, we intended to evaluate the quality of 3D mock-ups with a more integrative approach at plant scale. The difficulty to assess virtual plant structure in its entirety depends on the capacity to develop practical indicators. We used terrestrial laser scans (TLS) to collect 3D data on field individuals and derived indicators related to space occupancy, such as 3D volume and lateral and vertical extension of crowns. These indicators were satisfactory correlated with equivalent indicators derived from 3D reconstruc-

tions. Indicators related to crown volume showed nevertheless some discrepancies between field plants and 3D mock-ups. The possibility to detect and quantify simulation bias allowed to propose ways of improving the architectural model. For instance, the integration of biomechanical models to simulate leaf curvature should be relevant in a view of better representing leaf geometry and its interactions with environment [Mouliia and Fournier, 2009].

In this study, we focused on indicators of plant structure related to light interception at plant scale. Similarly to hemispherical photographs estimating the light interception at canopy scale by deriving GFs [Jonckheere et al., 2004], we highlighted the adequacy of TLS to characterize single plant structure in relation to its capacity to intercept light (Chap. III). This study also highlighted the relevance of such indicators to rapidly estimate LAI. The originality of these indicators relied on their close relationship with leaf area density and leaf clumping that determine light interception efficiency [Parveaud et al., 2008, Duursma et al., 2012]. The TLS-derived indicators estimated from field acquisition and from simulation on 3D mock-up depicted a comparable area of interception at individual scale. Some discrepancies were nevertheless noticed when comparing the relative quantity of micro-gaps within crowns. The proposed innovative indicators for assessing 3D reconstruction are promising since TLS offers the possibility to rapidly generate huge amounts of field acquisitions. Besides the purpose of validating simulated palms, these indicators could be valuable for efficiently phenotyping individual palms in the field. Automated analysis of 3D TLS data were set up during this study but so far the limitation of the method remains the computational cleaning of 3D points clouds. Additional field TLS on a larger number of plants and progenies and for different plant ages would be interesting to better evaluate the validity of the method. Also aerial Lidar could be used to derive equivalent indicators and screen mature stands [Moorthy et al., 2011].

### 3 Enhancing light interception and potential carbon acquisition of oil palm

#### 3.1 Difference in light interception efficiency among progenies

In the literature, light interception efficiency is generally expressed through the fraction of incident light intercepted by the canopy cover ( $f_{PAR}$ , estimated generally at plot scale) since it can be derived from field measurements (HP or PCA). By doing so, the interception efficiency is mainly related to the LAI, and consequently plants are considered efficient to intercept light ( $f_{PAR}$  close to 1) when they dispose important area of leaves closing the canopy. In an agronomical context,  $f_{PAR}$  depends on the planting density and on the age of the plant. At planting time,  $f_{PAR}$  is close to 0, and tends to 1 more or less rapidly according to plant development, growth and planting density. In chapter III, the proposed modelling approach enables to simulate, for the five progenies investigated, the evolution of  $f_{PAR}$  from 2 to 6 years after planting, under a given planting density ( $136 \text{ palms.ha}^{-1}$ ). Although progenies presented a similar level of interception at planting,  $f_{PAR}$  diverged significantly over time between progenies. Differences in light interception over time were mainly due to different kinetics in crown expansion between progenies (rapid expansion for Deli x Avros material versus slow expansion for Deli x La Mé material). Four years after planting, 89% of the total variation in  $f_{PAR}$  was explained by differences in LAI while 11% was explained by other differences in progeny crown structure. These differences in LAI could be explained either by difference in phyllochron and/or in the size of leaves. According to field measurements (Chap. II), both phyllochron and leaf area were different between progenies. These results raise the question about the consequence of these contrasted developmental processes on production. For annual plants, a strategy for improving productivity via light interception efficiency was the extension of the growing season [Reynolds et al., 2000, Koester et al., 2014]. For perennial plants like oil palm, the period from planting to canopy closure represents a relatively short period compared to the lifespan of

a plantation (25-30 years). However, this growing period is likely to be crucial for the proper establishment of plants over years, and fruit pruning management is often performed until 3 years to enhance vegetative growth [Corley and Tinker, 2016]. At planting, young oil palms may be exposed to abiotic stresses such as excessive radiation or water deficit. A short growing period could thus be considered favourable to rapidly reach a closed canopy and stabilized microclimate conditions [Hardwick et al., 2015]. The differences observed between progenies in the dynamics of crown expansion would be very interesting to be related with production data. Furthermore, as we do not have any information regarding the development of roots; the strategy of biomass investment may differ between plants, with plants investing more biomass in the root compartment than others investing more in the aerial compartment. The estimation of root biomass is laborious and is still a bottle-neck [Jourdan and Rey, 1997a, Jourdan and Rey, 1997b].

Another interesting question is to investigate if these progenies with different kinetics of light interception during the growing phase will reach equivalent maximal values of LAI in mature stands. The potential advantage of maintaining vegetative vigour to capture light in young stages could become a drawback in mature stands (with the assumption of homothetic vigour between young and adult stages). Indeed, experiments in planting density clearly demonstrated a decrease in productivity when LAI exceeded  $6 \text{ m}^2 \cdot \text{m}^{-2}$ , mainly explained by respiration cost [Corley and Tinker, 2016].

The contrasted evolutions of canopy structures with respect to light interception raise multiple questions related to their impact on production and offer the possibility to imagine different strategies of potential production. For instance, a strategy based on rapid return on investment, with plants that rapidly produce after planting, would be favourable for smallholders. Conversely, industrial estates would rather have a long-term vision and would look for plant material that maximizes the production over the whole generation.

### 3.2 Designing ideotypes to optimise light interception and carbon assimilation

At plant scale, light interception efficiency can be estimated with FSPM approaches thanks to integrative variables such as the silhouette to area ratio (STAR [Stenberg, 1996]). In this study light interception by individual plants was assessed within a stand, i.e. individuals surrounded by other plants laid in a given arrangement and density. The comparison of light interception among the calibrated 3D representations of the five progenies (Chap. III) stressed significant differences among progenies, explaining 18% of the variability in light interception efficiency (LI) independently of their difference in LAI. This result confirmed that light interception is mainly driven by the total leaf area developed by a plant, but also stressed the non-negligible impact of finer geometrical differences in progenies crown structure. To better decipher these structural differences, the sensitivity analysis developed in chapter IV aimed at identifying the main architectural traits governing light interception. Global sensitivity analysis stressed the influence of the architectural traits related to area of individual leaves such as the rachis length, the number and dimensions of leaflets (width and length), but also the shape of leaflets. Similar traits were considered critical for light interception efficiency in other species with compound leaves like tomato [Sarlikioti et al., 2011].

Significant variations in light interception were also determined by rachis curvature, which emphasizes the positive impact of “erectophile” canopies in light distribution, under the investigated planting density. This confirmed the negative impact of pending leaves in light interception efficiency obtained in other palm species [Chazdon, 1985]. In this study, I realized that a critical point of the proposed approach was to determine a criteria (model responses) to establish the notion of light interception efficiency. Actually, by considering the total amount of light intercepted by an individual ( $f_{PARi}$ ), the most efficient plant tends to be the one exposing the maximum leaf area, and conversely, by considering light interception per unit area ( $LI, k$ ), the most efficient plant tends to be the one exposing the most reduced leaf area. Hence, in



a breeding context, optimizing light interception relies on a trade-off between the quantity of light intercepted and the leaf area developed, high values of LAI reducing the biological efficiency with respiration cost. This led me to perform a detailed analysis within a given range of LAI, consistently with actual LAI reported in literature [Corley and Tinker, 2016, Barcelos et al., 2015]. This analysis allowed detecting some attributes that were not considered influential in the global analysis, such as the ratio of petiole to rachis length. In fine, we suggested that the distribution of light within the crown was a relevant criterion and proposed to use plant carbon assimilation as an integrative indicator of light distribution within the crown. Indeed, potential carbon assimilation was calculated in order to assess the implications of non-linearity in the light-response curve. Conversely to an integrated value of irradiance at plant scale, plant assimilation enabled to take into account the intensity of organ irradiance and its variation over a day.

We have identified four ideotypes (or morphotypes) that present different combinations of leaf geometrical attributes for comparable level of plant assimilation. Our results showed that a given potential carbon assimilation can be achieved with quite different  $f_{PAR}$  values. Actually, the best morphotypes are those that can achieve the most evenly distributed light over time (along the day) and space (within their crown). The similarity among ideotypes relies on their total leaf area, an important number of leaflets on rachis as well as long and narrow leaflets. This high density of narrow leaflets within the crown is an optimal configuration that allows light to penetrate deeper and uniformly while limiting self- and mutual-shading [Takenaka, 1994]. This vertical distribution of light within crown derived from narrow leaflets and steep leaf angle has been shown to be crucial to reduce high light exposure [Falster and Westoby, 2003, Pearcy et al., 2005, Sarlikioti et al., 2011]. Results also revealed that ideotypes differ in crown diameter (resulting from a particular combination of petiole length, rachis lengths and leaf curvature) and the number of leaves composing the crown. The fact that the ideotypes exhibited different features is particularly interesting in a breeding context, since genetic resources and heritability of architectural traits are likely to limit the development of some

combination of traits.

Further analyses will be needed to evaluate to what extent results can be affected by the photosynthesis model used in simulations. It is likely that some photosynthesis parameters will just have a scale effect, i.e. changing the absolute value of assimilation without changing the ranking of morphotypes. But other parameters altering the shape of light-response curve would probably lead to different ideotypes.

### 3.3 Improving the carbon assimilation model

The carbon assimilation model used in this study (NRH model [Marshall and Biscoe, 1980]) has some limitations. The major one is the absence of consideration of stomatal conductance regulation. Given the high sensitivity of oil palm to stomatal conductance (notably due to VPD; [Dufrêne, 1989]), the consideration of a photosynthesis-stomatal conductance submodel is required for predicting assimilates supply under fluctuating environmental conditions. A dedicated study aimed at developing and calibrating on oil palm the Farquhar's model [Farquhar et al., 1980] together with a stomatal conductance model [Ball et al., 1987, Leuning, 1995] was initiated during this thesis with the work of Lamour [Lamour et al., 2014]. The proposed model enabled to account for the temperature dependency of Farquhar's model parameters [Baldocchi and Harley, 1995, Leuning, 2002] and nitrogen dependency [Prieto et al., 2012]. Lamour developed a method to jointly calibrate the parameters of the photosynthesis model and the stomatal conductance model from  $CO_2$  and light response curves measured in field conditions. Analyses of leaf nitrogen content were also conducted to characterize the spatial distribution of nitrogen within the crown and subsequently link it to photosynthesis capacity. Results highlighted the capacity of the model to accurately predict carbon assimilation at leaf scale. Results also highlighted positive correlations between photosynthesis capacity and nitrogen content.

A topological gradient of photosynthesis capacity was also observed since higher nitrogen concentrations were measured in young leaves than in older ones. The model showed, however, some discrepancies notably in the prediction of stomatal con-

ductance, that could be overcome by integrating the effect of soil water deficit on stomatal regulation [Damour et al., 2010]. Further experiments would also be required to evaluate the genetic dependency of photosynthesis and stomatal conductance parameters [Lamade and Setiyo, 1996], which raise nowadays more and more interest in the climate change context.

### 3.4 Genetic control of oil palm architecture

The experimental site chosen for this study was interesting to investigate the relationship between plant architecture and genetics thanks to the diversity of the progenies available. Another way to decipher genetic influence on plant architecture would have been to assess architectural variability among clones, but only few clones were available on the studied site. Indeed, clones present higher value of inbreeding coefficient than progenies [Cros, 2015], allowing a more precise estimation of traits heritability, but somatic propagation of clones still faces the issue of “mantled” abnormality, which limit their exploitation [Corley and Tinker, 2016]. The important molecular and biochemical research initiated to unravel somaclonal variation are nevertheless promising for the future development of clones [Rival et al., 2008, Rival et al., 2013]. Whatever the breeding strategy performed, either based on progeny or clone, the development of new phenotypic traits remains crucial.

Architectural differences among progenies were studied in order to evaluate the soundness of breeding based on architectural characteristics. For each architectural trait investigated, the comparison of allometric adjustments among progenies and within progenies allowed estimating individual and progeny effects on traits variability. Subsequently, the significance of progeny/individual effects determined the level of variability to generate in 3D representations. Progeny variances estimated by the mixed-effect models were used to calculate broad-sense heritabilities ( $H^2$ ) and hence target the traits that could potentially be interesting to focus on in a specific genetic study. Among these traits, the ratio of petiole to rachis length, leaf area and leaflets width and length presented high values of  $H^2$ . An important limitation of this study was the low number of pro-

genies investigated and the incapacity to precisely characterize genotypes, and consequently to decipher the sources of the variations observed (genetic, environmental and their interaction).

One way to account for environmental variations would have been to screen the progenies in different environments. Obviously such investigation would have set aside the possibility to make detailed and time-consuming observations (e.g morphogenetic gradients of leaflets along the rachis) and subsequently generate precise 3D reconstructions. However, some coarse architectural measurements (rachis length and number of leaflets on rachis) were performed on all the plants of each replicate of the experimental site. I took advantage of this available dataset to evaluate the representativeness of i) the plants sampled for our study among all the plants of the same replicate and ii) the studied replicate among the other replicates (appendix B page 143). By doing so, architectural differences among progenies were analysed taking into account replicate effect, corresponding to micro-environmental variations (mainly related to soil composition). Although the significant effect of the replicates was stressed, significant differences on coarse architectural traits were also highlighted among progenies.

Regarding genetic effect, our analysis was limited to the study of plants identified through progenies, without any information about the segregation of character within these families. For a deeper investigation of the genetic control of palm architecture, a study on a higher number of progenies, with available pedigree or molecular data to estimate genealogical co-ancestry, would be required. Indeed, the possibility to link individuals according to their pedigree would enable to better estimate their genotypic value, traits heritabilities and potentially identify parents with interesting breeding values with respect to architecture. The use of molecular markers to characterize genotypes could also help in identifying potential QTL associated to architectural traits [Pootakham et al., 2015]. However, beyond genetic characterization, fine phenotypic data would be necessary for such a study.

Using the results of the sensitivity analysis of the architectural model (Chap. IV), we proposed to focus on the potential architectural traits that could be linked to light interception and potential carbon assimilation and thus be interesting for



breeding. Consequently this study permits to anticipate future genetic studies on palm architecture by proposing a limited number of traits to investigate and which are easy to measure on a high number of individuals.

The integration in genetic trials of new phenotypic traits related to plant architecture, as the one revealed in the sensitivity analysis, could be interesting to i) unravel the correlation between architecture and productivity and ii) determine breeding values of parents based on architectural traits. While breeding value from production traits can only be estimated on *tenera* and *dura* due to the infertility of *pisifera* fruits, breeding value from architectural traits could be interestingly estimated on *pisifera* parents. The characterization of the interspecific variability of these traits on *Elaeis oleifera* and *guineensis* x *oleifera* hybrids is a very interesting prospect [Barcelos et al., 2015]. Indeed, studies on *E. oleifera* would enable to screen wider genetic resources. The contrasted stem and crown structures of this species in comparison with *E. guineensis* offer the possibility to found other interesting combinations of morphological traits.

The recent development of genomic selection for oil palm paves the way for predicting the best material to cross for enhancing plant production [Cros, 2015]. Genomic selection raises interest as it enables to sharply reduce the time of breeding programs, by limiting the number of generations of progeny to test. Genomic selection based on architectural criteria could be promising in combination with FSPM to predict and select plants adapted to specific environmental conditions or specific agronomical practices. However, the use of model-assisted phenotyping with genomic selection, also called “virtual breeding”, is just emerging for annual crops and faces some scientific and technical issues to be routinely applied [Martre et al., 2014, Xu et al., 2011]. Indeed, the difficulty of such approach is the robustness of models to inferred physiological processes. Consequently, given the complexity of oil palm physiology and genetics, such a strategy is a long-term perspective. In fine, plant modelling is an explorative tool and its applicability requires validation from field experiments to harness the complexity of plant phenotypic plasticity, which can be defined as genotype x environment interactions [Sultan, 2000].

## 4 Towards a FSPM simulating yield of oil palm

The main limit of our study to investigate oil palm performance in relation to light interception was the absence of reproductive organ in the FSPM approach, and subsequently the absence of yield prediction. This results from the initial choice to investigate 3-years-old plants that started to produce bunches during the thesis. Besides, additional field-work to set a protocol, to collect data relative to production and to analyze them was hardly feasible given the schedule of the thesis. Our investigation was rather a preliminary approach of the potential enhancement of plant performance from the improvement in light interception. Consequently in this part we propose an outlook on the work that should be done to complement the FSPM initiated in this study toward a model able to predict yield.

Conversely to annual crops that produce usually once in their lifespan, perennial plants present rhythmic productions. As a result, under environmental constraints, annual and perennial plant develop opposed fitness strategies: annual plants may enter in a reproductive phase to generate seeds while perennial plants will limit their production to stock reserves [Vilela et al., 2008]. The difficulty to obtain consistent annual yield in perennial plants is driven by fruit load, which limit vegetative growth and limit production months or years afterwards [Smith and Samach, 2013]. From a modelling point of view, this uncontrolled rhythmic production in perennial plants encourages the development of individual-based approaches to predict yield, conversely to annual crops that can be modelled as a unique system harvested once. Experiments were thus set up to investigate the individual behaviour of oil palm by studying effect of trophic imbalances on production [Legros, 2008]. Based on these studies, Pallas [Pallas et al., 2013c] developed an individual-based approach of carbon partitioning in the oil palm (X-palm).

The work developed in this thesis contributes to establish the structural basis of a FSPM to be coupled with the functional X-palm model. The X-palm model is specifically structured to simulate the biomass partitioning at individual scale, with an explicit representation of plant topology and a

decomposition of each typology of organ (leaves, bunches, fruits). Assimilate supply is estimated using the Monteith formalism and Beer-Lambert law, which simulate carbon supply at plot scale. The work developed in this thesis could thus provide an opportunity to give finer estimation of assimilate supply at individual scale, in relation to the detailed structure of the plant. The combination of the architectural model, the light interception model and an improved carbon assimilation model would enable to estimate assimilate supply at leaf scale. A validation step of the carbon assimilation model would be required, either from nitrogen measurements as proposed by Prieto [Prieto et al., 2012] or from biomass data after coupling the model with X-palm. Additional formalisms to link leaf and stem structure to their biomass would need to be found and calibrated for each progeny investigated. Similarly biomass data relative to inflorescences and bunch would be required to calibrate the competition index ( $I_c$ , ratio between carbon supply and demand) developed in the X-palm approach.

Following the work initiated by Pallas on source:sink imbalance [Pallas et al., 2013b], further experiments would need to be carried out to determine the genetic variability of yield components (number of inflorescences and sex ratio, number of fruit per bunch, spikelet number and weight, individual fruit weight) and their potential interaction with abiotic constraints such as water deficit [Cros et al., 2013]. A challenge would be to apprehend the sensitive phases of production in relation to climatic conditions, and integrate genetic characteristic of production in the modelling approach. Indeed, the difference in production between Deli x La Mé material, which shows a high number of small bunches, and Deli x Avros material, which bears a lower number of heavy bunches [Cros, 2015], demonstrates the potential genetic control of carbon partitioning processes. The quantification of these physiological processes and their genetic inheritance using simulation tools could pave the way for designing other ideotypes of oil palm and supporting innovative breeding strategies [Rötter et al., 2015].

## 5 Conclusions

In conclusion, the present study highlighted how plant modelling and analytical tools can be used to virtually explore plant biology. In our case, the 3D model of oil palm, in its conception and its application, enabled to detect the architectural traits which are genetically determined and influence light interception. The morphological traits of the proposed ideotype could guide further breeding experiments. Nevertheless, an important work remains to be done in order to integrate functional processes allowing the evaluation of the relation between architecture, light interception and plant performances. This could be achieved on the short term by coupling our model with the modelling approaches previously developed. The ongoing characterization of plant architecture at the experimental site, following the protocol set up during this thesis, will be crucial to get a more global vision of the ontogenetic gradients of plant architecture and establish their relationship with production.

The proposed ideotypes were designed under a given environment and under specific management practices, but other ideotypes could be developed in different contexts. Future ideotypes could be designed for different purposes, addressed by various actors of the sector, such as smallholders, industrials and consumers [Rival and Levang, 2014]. For instance smallholders would prefer plant material that optimize heavy individual bunch weight because they are paid out on the basis of bunch weight. Conversely, for palm oil mills, ideotypes would consist in plants that produce fruit with high oil extraction rate. Millers will search for plants with regular and predictable frequency of production to better organize production and transformations chains. Finally, consumers will push to design ideotypes with particular oil composition.

The modelling approach initiated in this study could be developed to test different scenarios, for instance in a climate change context with low radiations or drought conditions. Similarly, the model could be used to investigate different planting patterns and intercropping systems [Mao et al., 2016]. This could be achieved using other available 3D plant models (teak, acacia, coffee and cacao trees) or adapting the 3D modelling approach developed in this study to plants with an architecture relatively

close to oil palm (such as banana or papaya trees). Optimising intercropping systems with respect to light interception could be particularly interesting for family farmers who possess limited areas and would like to diversify their production, notably to get outcome from young plantations before palms produce. Besides, changes in agronomical practices with integration of agro-ecological process such as intercropping could also provide interesting advantages notably regarding pests and diseases. All these perspectives will be however possible with further studies dedicated to better understand the interactions between plants and their environment.

In the short term, the best strategy to tackle the agronomic issue addressed in introduction will rely on the accessibility of improved material to smallholders, which represent half of the global palm oil production. There is an undoubted requirement to keep on improving plant material taking into account new challenges of sustainability and future climate constraints. This continuous improvement will depend on a better comprehension of agroecosystems, and FSPM are likely to play a key role in this comprehension. Indeed, beyond its agronomical purposes, our study aimed at investigating deeper on the biology of oil palm, notably from an architectural point of view. The precise characterization of palm morphology with a focus on its potential connection to genetic and physiological processes can raise many scientific questions. The application of the proposed methodology to other species of palms enlarges the scope of our study. In an evolutionary and ecological context, the comprehension of relationship between architecture and functioning of palm species is promising, given that palms are among the most abundant, diverse and economically important families of plants of tropical and subtropical regions of the world [Henderson, 2002].



## Appendix A

# Protocol for measuring aerial architectural traits of *Elaeis guineensis* Jacq.

### Material and methodology

#### Material

#### Angles measurements

##### Al-Kashi method

Several ways of measuring angles were tested in field using different methods but one has been retained for its simplicity and its possible application for almost all the required angles. This methodology is based on the Al-Kashi theorem as presented Figure A.1.

The methodology enables to calculate an angle measuring a length. Indeed fixing the values of  $c=b=L$ , the value of the angle  $\alpha$  is directly calculated through the  $a$  value according to the equation (A.1):

$$\alpha = \arccos \left( 1 - \frac{a^2}{2L^2} \right) \quad (\text{A.1})$$

A tool has thus been designed to measure angles in field using this methodology. The device is made with two identical rulers (similar  $L$  length) stucked together with adhesive tape (see Figure A.2). Then the measurement lies on fitting the tool with the angle of interest and measure the distance between the extremities of the rulers (representing  $a$ , the

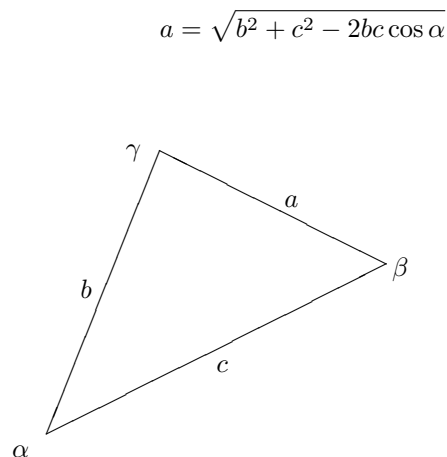


Figure A.1: Al-Kashi theorem

distance measured by the yellow soft ruler in the Figure A.2). This method is particularly useful for the determination of leaflets angles and frond torsion. The rulers should not be too long and not too wide to make easier the measurements (20 cm length x 2 cm width is satisfactory).

Table A.1: *Material listing*

Measured parameters	Material
Axial, radial and rotation angles	2 rulers with a common length a soft ruler (2m) a bubble level a rope with plumb
Bending and lateral deviation	a bar (3.5m) with two supports a soft ruler (4m) a transparent adhesive tape a rope (2m) with plumb a T-square ruler
Frond length	a soft ruler (4m) a ruler (1m) transparent adhesive tape
Spear length Spear diameter	a bar (4m) a soft ruler (4m) a slide caliper (mm graduation)
Leaflet length, width and height	a slide caliper (mm graduation) a soft ruler (1m)
Phyllotaxy	a compass
Stem diameter Stem height	a slide caliper (1.50m) a soft ruler (4m) transparent adhesive tape

### Pythagore method

For the frond bending and frond deviation an other technic was adopted because the reference axe has to be conserved all along the nervure position (for leaflets angles the reference depends on the nervure axe and thus varies along the nervure position). Figure A.3 is a representative scheme of the device. The frond bending angle is then obtained measuring the projections of the rachis control points (1, 2 and n) on the  $x, y$  plan (Figure A.4a). The frond deviation is calculated by projecting those points in the  $x, z$  plan (Figure A.4b). For both angle the Pythagore theorem gives the following equations ((A.2) for bending and (A.3) for deviation):

$$\beta = \arctan \left( \frac{y_n - y_{n-1}}{x_n - x_{n-1}} \right) \quad (\text{A.2})$$



Figure A.2: Device for angle measurement

$$\delta = \arctan \left( \frac{z_n - z_{n-1}}{x_n - x_{n-1}} \right) \quad (\text{A.3})$$

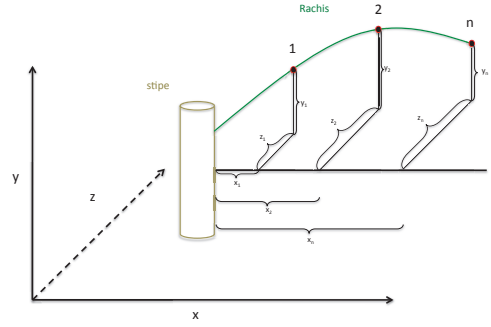


Figure A.3: Device for frond bending and deviation

⚠ This method is not accurate if the control points along the nervure are too distant from each other. Indeed as the angle is estimated by the tangent (the hypotenuse in that case) it is important to look at the length and the amplitude of frond bending/deviation before doing the measurement. Usually ten control points are supposed to

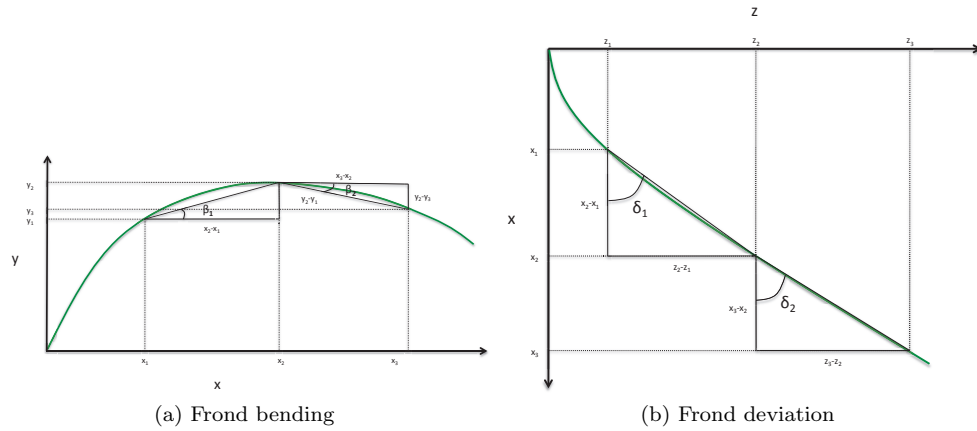


Figure A.4: Projections of frond bending and deviation

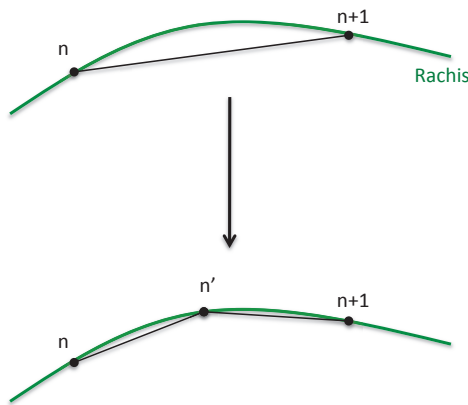


Figure A.5: Adding control point for an accurate estimation of angles

be sufficient to assess consistently the frond bending/deviation but if the angles vary sharply between two consecutive points it is appropriate to increase the number of control points along the frond (see Figure A.5).

## General observations

### Tree identification

Before collecting any data, it is important to identify the tree on which the data will be collected. Each form begins with a tabular **identification** to fill as describe Figure A.17 page 139. In the cell **Al-Kashi method**,  $L$  is the length (in cm) of the rulers used for measuring **all the angles** of the corresponding form.

### Vegetative observation

#### Numbering fronds

The first observation is to identify the frond rank 1 as well as the order 8 parastiche and numbering the other fronds thanks to the latter (as describe Figure A.6). The frond rank 1 is define as the one almost fully open (just some leaflets at the frond base are not yet open). Clearly paint or write with a permanent marker the frond rank in each petiole. The number of frond on the crown (green ones) is then reported.

#### Parastiches direction

The parastiche direction is given by observing the order 8 parastiche. The direction is also given by the position of the frond rank 4 from the frond



rank 1: if the latter is at the right from the rank 1 the parastiche goes to the right (trigonometric direction), if it is at the left from the rank 1 the parastiche goes to the left (clockwise direction). The **clockwise** direction is written down **+1** in the data collection form and the **trigonometric** direction is noted **-1** (see Figure A.6).

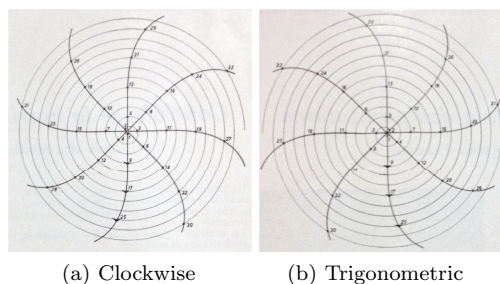


Figure A.6: Phyllotaxy and parastiche directions (top view)

### Stump number

The stump number can be reported directly after counting them but an estimation is usually easier. To estimate the stump number, select the oldest crown frond (green one) and follow the corresponding 8<sup>th</sup> parastiche until reaching the soil. The estimated number of stump is then obtained subtracting the frond rank from the latest stump rank:

$$Nb_{stumps} = Rank_{LowerFrond} - Rank_{LowerStump}$$

### Spears

Count the spears and identify the higher one. In the latter measure its length, its diameter at the base (with a slide caliper) and the spear axial angle from the vertical. The angle is determined with the Al-Kashi method taking one ruler along the spear from the base and the other one along the vertical obtained with a level or a plumb rope (see Figure A.7).

### Torsion rate

The torsion represents the angle due to the nervure rotation as described in Figure A.8. The torsion di-

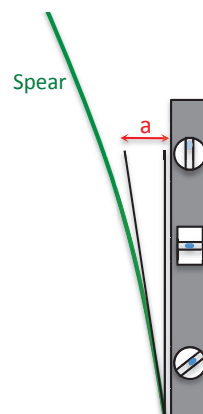


Figure A.7: Measuring the axial spear angle. The measurement consists in reporting the value  $a$  (in cm) that will be used to calculate the angle as described in Figure A.1

rection (looking front to the stem) can be either clockwise (+1) or trigonometric (-1). The torsion rate is the proportion of fronds with a clockwise torsion. After a quick observation of the frond crown, assess this proportion and report the proportion of clockwise torsion and trigonometric torsion.

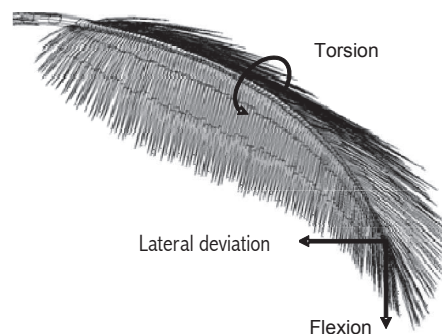



Figure A.8: Frond torsion

 All the data previously measured are reported in the tabular **vegetative observation** presented in the form Figure A.17 page 139.

## Stem

### Phyllotaxy

Once the order 8 parastiche is located in the stem, azimuths of the frond rank 1, 9, 17, 25, and 33 are measured thanks to a compass targeting the orientation given by the petiole base. The phyllotaxic angle is then calculated thanks to the equation (A.4):

$$\alpha = \frac{n * 360 \pm (A_i - A_{p+i})}{p} \quad (\text{A.4})$$

where:

$\alpha$  = phyllotaxic angle

$n$  = number of tour between the two fronds

$\pm$  = + if the parasitic direction is trigonometric;  
– if the direction is clockwise

$A_i$  = azimuth of the frond rank  $i$


$A_{p+i}$  = azimuth of the frond rank  $p + i$

$p$  = number of fronds between the two studied fronds

**Stem height** On the same fronds used for the phyllotaxy, measure the height from the soil to the frond insertion (I point, see Figure A.9).

**Stem diameter** The stem diameter is measured on those fronds thanks to a 1.50-meter caliper. Make sure to measure only the stem without including any petiole. The measurement is done around the frond insertion (I point).

**Axial insertion angle** For each frond of the order 8 parastiche, using the same technic as describe in the Figure A.7, measure the frond insertion angle placing the two rulers as close as possible to the I point.

 All the data related to the stem are reported in the tabular **stem** presented in the form Figure A.17 page 139.

## Reproductive components

While observing every frond insertions on the stem, report the presence of a male inflorescence (M), a female inflorescence (F) or a bunch (B) and note the

corresponding frond rank. Count the total number of each of them and report that number in the tabular **reproductive observations** (Figure A.17 page 139).

## Frond geometry

### Nervure length

Place a ruler as deep as possible toward the insertion point and note the petiole length (from I point to C point, see Figure A.9). Then place a soft ruler (4m) from the C point to the A point and stick it to the frond nervure with the transparent adhesive tape. Note the distance (in cm) from the C point and the B point and from the C point to the A point. Let the frond at its initial position, focus the position of the nervure point at the maximum height and report the distance between that particular point and the C point.

**Control points** Divide the rachis length (C to A distance) by 10 and report this value (in cm) in the cell **10%**. From the C point toward the A point, mark every 10% the control points thanks to a dark tape, a piece of rope or even painting a sign on the rachis. Add a mark below the C point toward the I point (that will correspond to the -10% control point). Finally 11 control points are indicated in the nervure: -10%, 0% (= C point), and 10% to 90%.

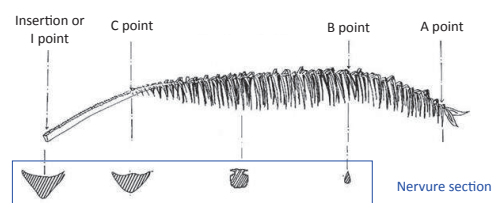


Figure A.9: Reference points on the frond nervure

## Torsion

The torsion is sometimes difficult to measure mainly nearby the A point because of frond flexion (see Figure A.8). A way to avoid misleading measurement is to deal with the normal to the frond plane rather

than the frond plane itself. Indeed measuring the angle between the normal to the frond plane and the absolute vertical is equivalent to measure the angle between the frond plane and the absolute horizontal. But because of frond flexion, it turns out to be easier to take the vertical as reference. Using the Al-Kashi method, the torsion is directly measured putting one ruler as the normal to the frond plane and the other ruler as the vertical thanks to the gravity (see Figure A.10). According to the direction of the torsion, the distance between the two rulers ( $a$ ) will be reported as positive (clockwise direction) or negative (trigonometric direction). Reported the value (in cm) of each  $a$  distance from the C point to the 90% control point.



Figure A.10: Torsion measurement. One ruler is the normal to the frond plane and the other is the absolute vertical.

## Bending and deviation


Frond bending and lateral deviation are determined thanks to the device previously presented Figure A.3 page 130. The crucial point relies on

the well setting up of the device before doing the measurements. Firstly the 3.5 meter bar has to be positioned in the azimuth define by the petiole basis. It is useful to take this azimuth and take care that it is conserved all along the bar once positioned. Then it is really important to check with the bubble level that the bar stays horizontal, moving the supports if necessary. Make sure that the bar is located below all the control points. Fix the bar to the supports and the petiole with an adhesive tape. Stick as well the soft ruler on the bar with a transparent tape.


Next the 3 distances of interest ( $x$ ,  $y$  and  $z$ ) can be measured at each control point. Place the plumb rope just underneath the rachis and let it hang down until it stays still (do not fix the rope to the nervure when the plumb blends the frond). Slide the square ruler along the bar until reaching the rope and then report the  $x$  and  $z$  distances. The  $z$  distance is either positive if the deviation goes to the right or either negative if the deviation moves to the left. The last parameter  $y$  is reported by measuring the rope from the rachis to the square ruler (Figure A.12).

## Nervure section

The nervure section is measured thanks to a slide caliper. The height and the width of the nervure are taken at each control point (-10%, C point, 10%, 20%, ..., 90%) as presented Figure A.13.

 All the data related to the frond geometry have to be reported in the form **frond geometry** presented Figure A.17. The length position (in centimeter) has to be reported to check where the control points are. In the case of additional control points for measurements it is important to note this position as well.

## Frond description

 Before describing the frond, make sure that the frond geometry form has been completed because the following descriptions imply manipulations of the frond that usually modify its initial shape.

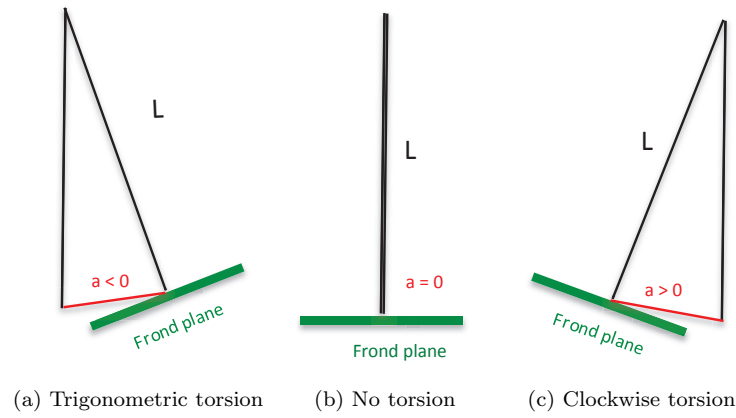


Figure A.11: Torsion directions. The frond plane refers to the plane done by the nervure and the leaflets without radial angle. The distance  $a$  is reported with a positive (clockwise) sign or a negative sign (trigonometric).

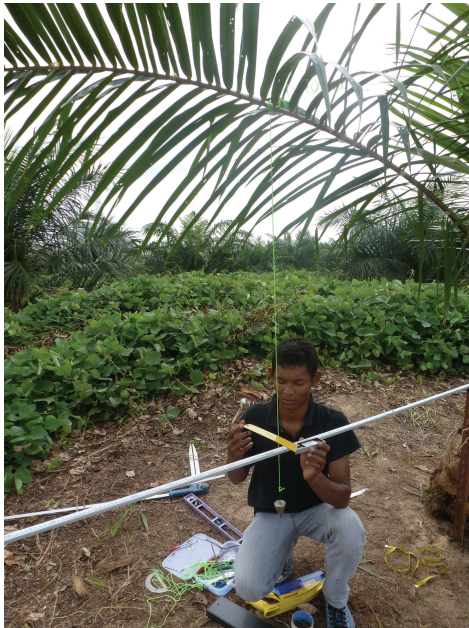


Figure A.12: Bending and deviation measurement. The bar gives the  $x$  value, the square ruler the  $z$  value and the rope gives the  $y$  value, all in centimeters.

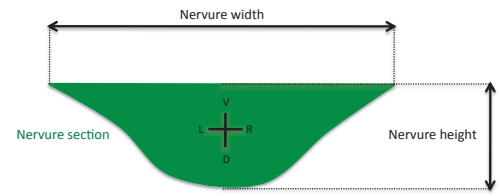


Figure A.13: Nervure section height and width. (V=ventral, D=dorsal, R=Right, L=Left).

### Metric position of the leaflets

As it has been done for positioning the control points, stick the soft ruler from the C point to the A point. To define the right left orientation of the frond, stand at the A point and look toward the frond insertion, the right side of the frond is then given by your right arm.

Select one side and report directly the observation in the corresponding tabular (semi-frond left or right, see Figure A.17 page 139). The metric position corresponds to the distance from the C point to the pinnae. Begin by the first one, near the C point, and report the distance of every pinnae until the A point.

👉 Do those observations on both semi-fronds.

## Group position

While or after reporting the metric position, assess the orientation of the leaflet according to its radial insertion on the frond nervure. There are three different positions, as described in Figure A.14:

- the superior position, noted **+1**
- the medium position, noted **0**
- the inferior position, noted **-1**

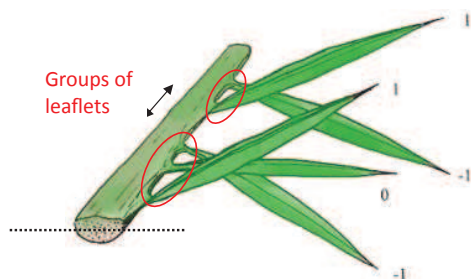


Figure A.14: Representation of the groups of leaflet with the different positions +1, 0 and -1 according to their radial insertion on the nervure. Two groups are represented, one of 2 leaflets and one of 3 leaflets.

The difference between the 0 and the -1 position is most of the time not easy to distinct. The best way to deal with that problem is to look at the groups in a first time. Indeed there are four possible groups:

- group of one leaflet: **0**
- group of 2 leaflets: **1 -1**
- group of 3 leaflets: **+1 0 -1**
- group of 4 leaflets: **+1 0 0 -1**

Then looking at the distance between consecutive leaflets, the intra group distance helps to define if the leaflet is -1 or 0. For instance if there are 3 leaflets but the distance between the second and the third one is very important compare to the two first leaflets, then it is better to consider two groups (**1 -1** and **0**) than one group (**+1 0 -1**).

## Leaflet length

Once the metric position is reported and the groups are defined, measure the leaflet length (column **max length** Figure A.17 page 139) of all the leaflets from the A point to the C point (measuring toward the C point avoids misleading measurements due to the difficulty to describe the first pinnae around the C point). The measurement is done with a soft ruler from the leaflet insertion in the nervure.

Do this measure on both semi-fronds.

All the data related to the frond description have to be reported in the form **frond description** presented in Figure A.17 page 139.

There are 3 consecutive forms per frond, make sure to report the data correctly.

## Leaflet geometry

### Selection of groups

Around each control point, select one group of leaflets on each side (at least a group of two leaflets (**1 -1**) but if possible a group three leaflets (**+1 0 -1**)) and identify every leaflet by marking its position **+1**, **0** or **-1**. This will define the groups of leaflets noted **G10** to **G90** as visible in the form Figure A.17 page 139. The group terminal **GT** is defined as the three last leaflets (A point). The following parameters presented in the next sections are measured in every leaflets of every groups.

### Leaflet width and height

Starting from the **G10** (because there is no leaflet around the C point), measure the length of the leaflet from its insertion in the nervure. Divide this value per three and report with a permanent marker the position  $1/3$  and  $2/3$  as defined in Figure A.15b.

**Half-width** Measure thanks to the slide caliper the leaflet half-width at the  $1/3$  position ( $W_{1/3}$ ) and at the  $2/3$  position ( $W_{2/3}$ ).



**Height** Similarly to the width measurements, measure with the caliper and report the height at the two positions:  $H_{1/3}$  and  $H_{2/3}$  (Figure A.15a).

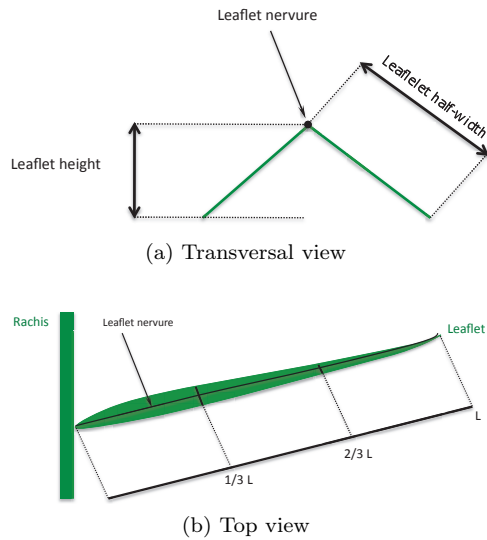


Figure A.15: Segmentation of the leaflet for width and height measurements.

## Leaflet angles

### Axial insertion angle

The axial insertion angle is the angle visible from the top between the leaflet and the rachis (see Figure A.16a). The measurement is done thanks to the Al-Kashi method by fitting the rulers with the leaflet insertion.

✎ If the orientation of the leaflet is toward the A point, the angle is reported positively. If the orientation is toward the C point (rare), the angle is reported negatively.

**Radial insertion angle** The radial insertion angle is the angle given by the leaflet and the rachis from the transversal view. The measurement is done thanks to the Al-kashi method by placing one ruler along the leaflet and the other in the frond plane, as presented Figure A.16b.

✎ For the leaflet **+1** the radial angle is reported positively. It is reported negatively for the leaflet **-1**. The leaflet **0** can be either positive or negative according to its position from the frond plane.

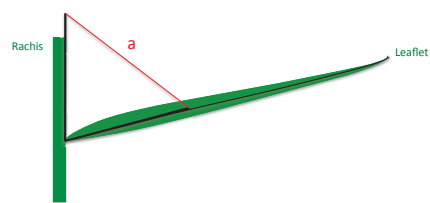
### Rotation angle

The rotation angle is associated to how the leaflet is inserted on the rachis. It depends on the position of the leaflet (**-1**, **0**, or **+1**) but is sometimes difficult to define. For the measurement, place the common summit of the two rulers in order to pinch the leaflet. In that way one ruler is above the leaflet and the other must fit the rachis axis while being under the leaflet (see Figure A.16c)

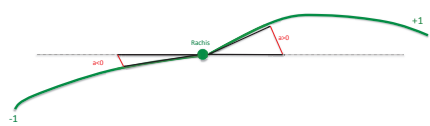
✎ For the leaflet **+1** the rotation angle is reported positively. It is reported negatively for the leaflet **-1**. The leaflet **0** can be either positive or negative according to its insertion (positively if the direction is toward the A point and negatively if the direction is toward the C point).

✎ All the data related to the leaflet geometry have to be reported in the form **leaflet geometry** presented Figure A.17 page 139.

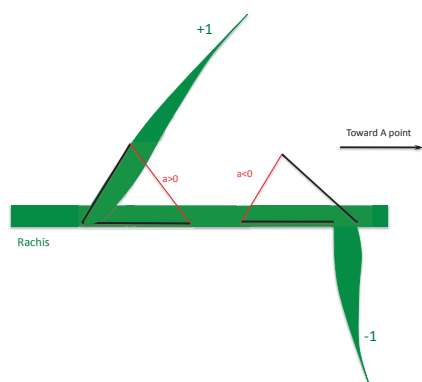
☞ Make sure to report the data in the form that corresponds to the side of the frond under observation (one form for each side).



(a) Axial insertion angle (top view)



(b) Radial insertion angle (transversal view)



(c) Rotation angle (lateral view)

Figure A.16: Representation and measurements of the leaflet angles.



Date						<b>Reproductive observations</b> <b>Type (B, F, M)</b> rank	
<b>Identification</b> Trial Repetition Property Tree number			<b>AI kashl method (AK)</b> Length of 1. (cm)			B=bunch F=Inflo Female M=Inflo Male	
<b>Vengetative observations</b> Number of Fronds Parastiche direction Stump number Number of spars Linear base diameter Spear axial angle (AK cm) Spear length % of leaves with torsion Tors. 1 clockwise +1							
GENERAL & STEM	<b>Stem</b> Frond rank Azimuth Height from soil Axial insertion angle (AK cm) Stem diameter		1	9	17	25	33

(a) General observations form

Data		AI haashi method (AK)				
Identification		Length of L				
Title						
Description						
Property						
Time running						
Found rank						
		010	020	030	040	050
counted L = 100						
all L (1)						
all L (2)						
all L (3)						
all L (4)						
all L (5)						
Actual angle						
Ideal angle						
Location angle						
		060	070	080	090	01
counted L = 100						
all L (1)						
all L (2)						
all L (3)						
all L (4)						
Actual angle						
Ideal angle						

(b) Leaflet geometry

<b>Date</b>	
-------------	--

Identification	
Trial	
Repetition	
Progeny	
Tree number	
Frend rank	

Nervure length (cm)	
Petiol (I to C)	
C to max frend heigth	
C to B	
Rachis (C to A)	

Al kashi method (AK)	
Length of L	

→

10% =

Torsion		
Relative position	Length Position(cm)	Torsion angle (AK)
0 (=C point)		
10%		
20%		
30%		
40%		
50%		
60%		
70%		
80%		
90%		

← trigo=-  
clockwise= +

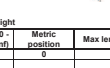
Bending and deviation			
Relative position	Length Position(cm)	x	y
0(=C point)			
10%			
20%			
30%			
40%			
50%			
60%			
70%			
80%			
90%			

to the left=-  
to the right= +

Nervure section			
Relative position	Length Position(cm)	width (cm)	height (cm)
-10%			
0(=C point)			
10%			
20%			
30%			
40%			
50%			
60%			
70%			
80%			
90%			

(c) Frond geometry form

Date													
<table border="1"> <tr> <th colspan="2">Identification</th> </tr> <tr> <td>Thall</td> <td></td> </tr> <tr> <td>Repetition</td> <td></td> </tr> <tr> <td>Progeny</td> <td></td> </tr> <tr> <td>Tree number</td> <td></td> </tr> <tr> <td>Froned rank</td> <td></td> </tr> </table>		Identification		Thall		Repetition		Progeny		Tree number		Froned rank	
Identification													
Thall													
Repetition													
Progeny													
Tree number													
Froned rank													
<table border="1"> <tr> <th colspan="2">Nervure length (cm)</th> </tr> <tr> <td>Petiol (I to C)</td> <td></td> </tr> <tr> <td>C to max height</td> <td></td> </tr> <tr> <td>C to B</td> <td></td> </tr> <tr> <td>Rachis (C to A)</td> <td></td> </tr> </table>		Nervure length (cm)		Petiol (I to C)		C to max height		C to B		Rachis (C to A)			
Nervure length (cm)													
Petiol (I to C)													
C to max height													
C to B													
Rachis (C to A)													



Semi-frond left			
Pinnae rank	Position + Ø - (sup med inf)	Metric position	Max length
C	-	Ø	
1			
2			
3			
4			
5			
6			
7			
8			
9			
10			
11			
12			
13			
14			
15			
16			
17			
18			
19			
20			
21			
22			
23			
24			
25			
26			
27			
28			
29			
30			
31			
32			
33			
34			
35			
36			
37			
38			
39			
40			
41			
42			
43			
44			
45			
46			
47			
48			
49			

Semi-frond right			
Pinnae rank	Position + Ø - (sup med inf)	Metric position	Max length
C	-	Ø	
1			
2			
3			
4			
5			
6			
7			
8			
9			
10			
11			
12			
13			
14			
15			
16			
17			
18			
19			
20			
21			
22			
23			
24			
25			
26			
27			
28			
29			
30			
31			
32			
33			
34			
35			
36			
37			
38			
39			
40			
41			
42			
43			
44			
45			
46			
47			
48			
49			

(d) Frond description form

Figure A.17: Data forms.

## Simplified protocol

### General notation

#### Tree identification

- Progeny: progeny reference
- TreeNumber: Identification of the individual from location in plot (row x column)
- Date: date of the observation (dd/mm/yy)

#### Leaf identification

- **LeafNumber**: number of leaf that refers to the phyllochron (LeafNumber = -10 mean that 10 leaves have been emitted from the beginning of the monitoring). Every 2 months a screening of the experimental trees is carry out to number the new emitted fronds.
- **LeafRank**: agronomic rank that refers to the spatial position of the leaf in the crown at a given time. Rank 1 is the youngest leaf totally open with a visible rachis basis (visible C point).

### Stem and crown observations

1. **Circumference**: Stem basis circumference measured with a rope (in centimetres)
2. **Height**: Stem height from the soil. The top reference is the insertion of leaf rank 17 (in centimetres)
3. **TotalLeaves**: number of leaves in the crown (not yet dry)
4. **Angle C**: Bending angle (Y) and twist angle (X) at C point measured with a clinometer (in degrees) (Figure A.18)
5. **Angle A**: Bending angle (Y) and twist angle (X) of rachis tip measured with a clinometer (in degrees)

6. **Leaf curvature**: Cartesian coordinates (X, Y, Z) along leaf midrib (from C point to A point) that enable the assessment of rachis bending and rachis deviation (in centimetres) (Figure A.5 page 131)

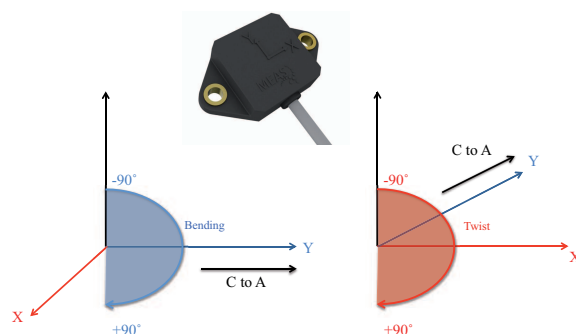


Figure A.18: Clinometer device for measuring bending and twist leaf angles

### Leaf and leaflet observations

Measurements done on the rank 17 every 2 months (Figure A.20)

7. **PetioleLength**: distance from leaf insertion (I point) to C point (in centimetres)
  8. **BPosition**: distance from C to B point (in centimetres)
  9. **RachisLength**: distance from C to A point (in centimetres)
  10. **BLength and BWidth**: leaflet length and maximal width at B point (in centimetres)
- Leaflet sample: divide the rachis in 10 even length sections. For each section, mark a reference leaflet around the middle section.
11. **NbLeaflets**: number of leaflets per section (in one side)
  12. **LeafletRefPosition and LeafletRefRank**: for each leaflet sampled, measure the distance (in centimetres) from C point to leaflet insertion on the rachis and number its rank. Leaflet rank 1 is the first leaflet after C point.

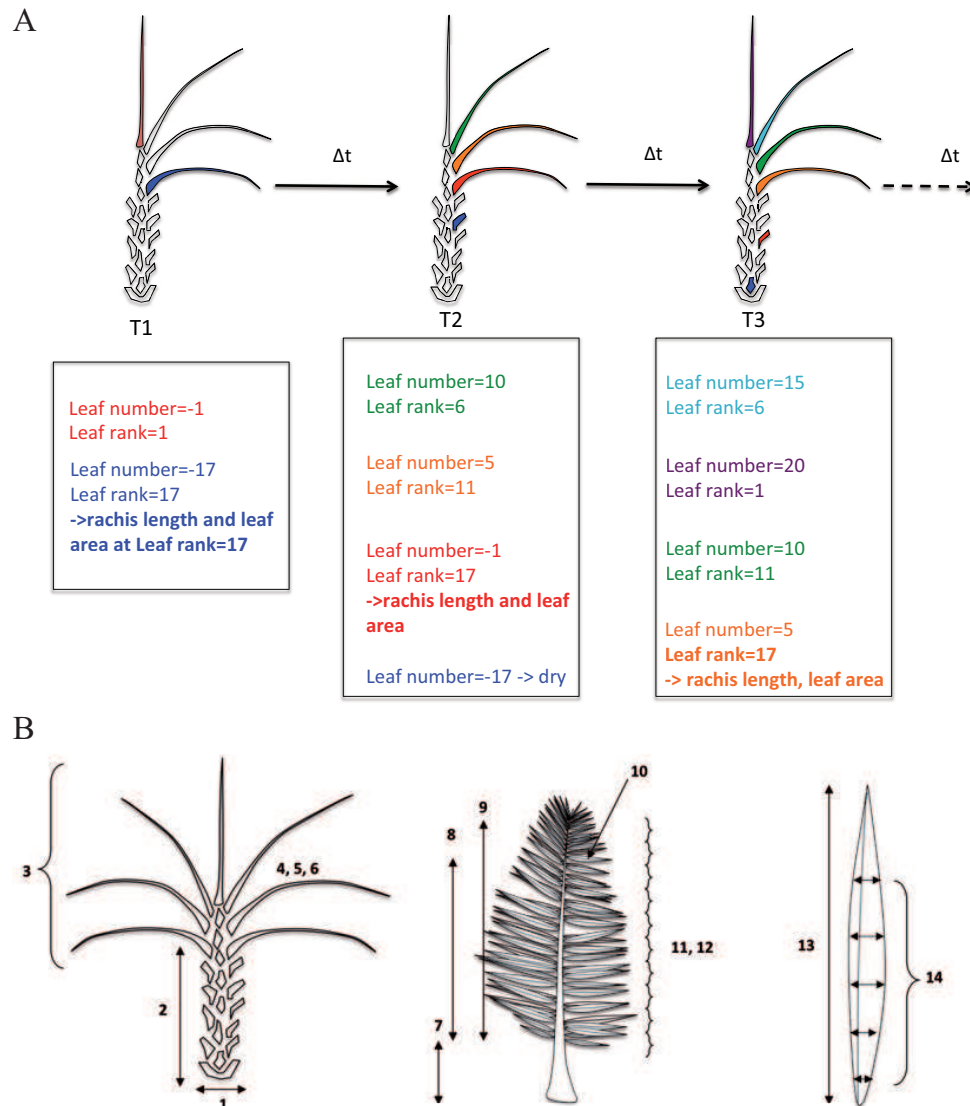


Figure A.19: A) Monitoring of rachis dimension measurement. B) Observation at tree scale (left scheme), leaf scale (middle scheme) and leaflet scale (right scheme).

13. **LeafletLength:** for each leaflet sampled, measure its length (in centimetres)
14. **LeafletWidth:** for each leaflet sampled, measure width in 5 positions along leaflet midrib (PositionOnLeaflet). The last position on leaflet is leafletLength, the corresponding LeafletWidth is therefore 0 (in centimetres)

[illegible]

TreeNumber	LeafNumber	LeafRank	AngleC		AngleA	
			Bending (Y)	Twist(X)	Bending (Y)	Twist(X)

TreeNumber	LeafNumber	Leaf Rank	AngleC		AngleA	
			Bending (Y)	Twist(X)	Bending (Y)	Twist(X)

D

Date
LeafNumber

[illegible]

Date		Progeny	TreeNumber		
LeafNumber	LeafRank	Position	X	Y	Z
		C			
		1			
		2			
		3			
		4			
		5			
		6			
		7			
		8			
A					
		C			
		1			
		2			
		3			
		4			
		5			
		6			
		7			
		8			
A					
		C			
		1			
		2			
		3			
		4			
		5			
		6			
		7			
		8			
A					
		C			
		1			
		2			
		3			
		4			
		5			
		6			
		7			
		8			
A					
		C			
		1			
		2			
		3			
		4			
		5			
		6			
		7			
		8			
A					

142

## Appendix B

# Field replicates comparison and sampling assessment

Table B.1: ANOVA table of rachis length and number of leaflets 30 months after planting. The ANOVA model is a two way with interactions ( progeny x replicate) model (n.s., non-significant; \*,  $p < 0.05$ ; \*\*,  $p < 0.01$ ; \*\*\*,  $p < 0.001$ ).

Variable	Factor	Df	Sum Sq	Mean Sq	F value	Pr(>F)
Rachis lenght	Progeny	4	55464.91	13866.23	30.10	0.0000***
	Replicate	6	43875.81	7312.64	15.88	0.0000***
	Progeny x Replicate	24	58596.83	2441.53	5.30	0.0000***
	Residuals	745	343159.29	460.62		
Number of leaflets	Progeny	4	7861.33	1965.33	49.74	0.0000***
	Replicate	6	5516.24	919.37	23.27	0.0000***
	Progeny x Replicate	24	17551.85	731.33	18.51	0.0000***
	Residuals	745	29436.96	39.51		

Table B.2: ANOVA table of rachis length and number of leaflets 30 months after planting. The ANOVA model is a two way with interactions ( progeny x sample) model (n.s., non-significant; \*,  $p < 0.05$ ; \*\*,  $p < 0.01$ ; \*\*\*,  $p < 0.001$ ).

Variable	Factor	Df	Sum Sq	Mean Sq	F value	Pr(>F)
Rachis length	Progeny	4	54961.98	13740.49	24.75	0.0000***
	Sample	1	1448.86	1448.86	2.61	0.1066 n.s.
	Progeny x Sample	4	4985.28	1246.32	2.24	0.0626 .
	Residuals	829	460292.67	555.24		
Number of leaflets	Progeny	4	7540.59	1885.15	28.75	0.0000***
	Sample	1	76.24	76.24	1.16	0.2812 n.s.
	Progeny x Sample	4	2269.87	567.47	8.66	0.0000***
	Residuals	829	54349.43	65.56		

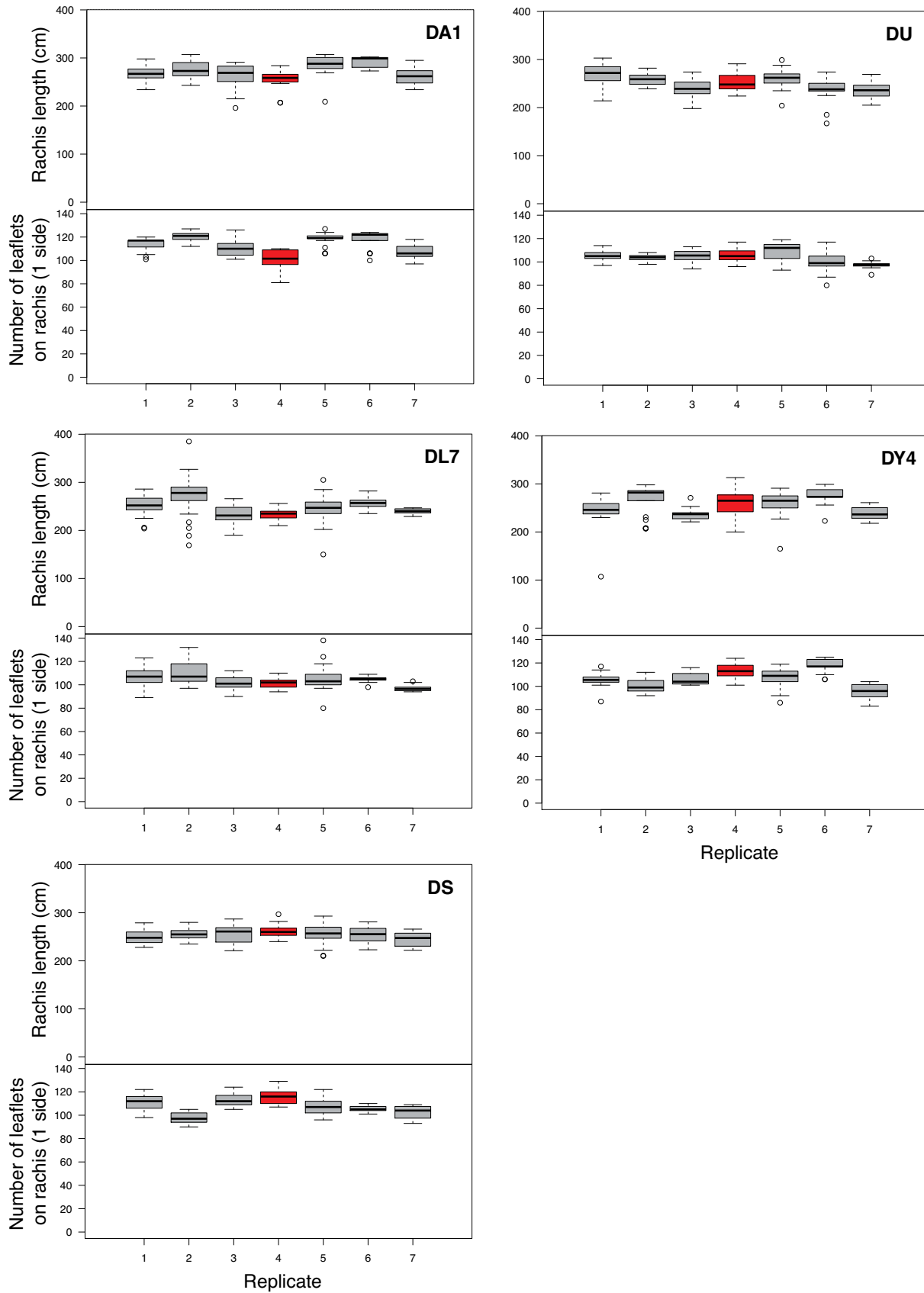


Figure B.1: Coarse architectural traits measurements (rachis length and number of leaflets) for the 7 replicates of the experimental site, for the 5 studied progenies (30 months after planting). Replicate 4 (in red) is the replicate on which detailed measurements for 3D reconstructions were performed.

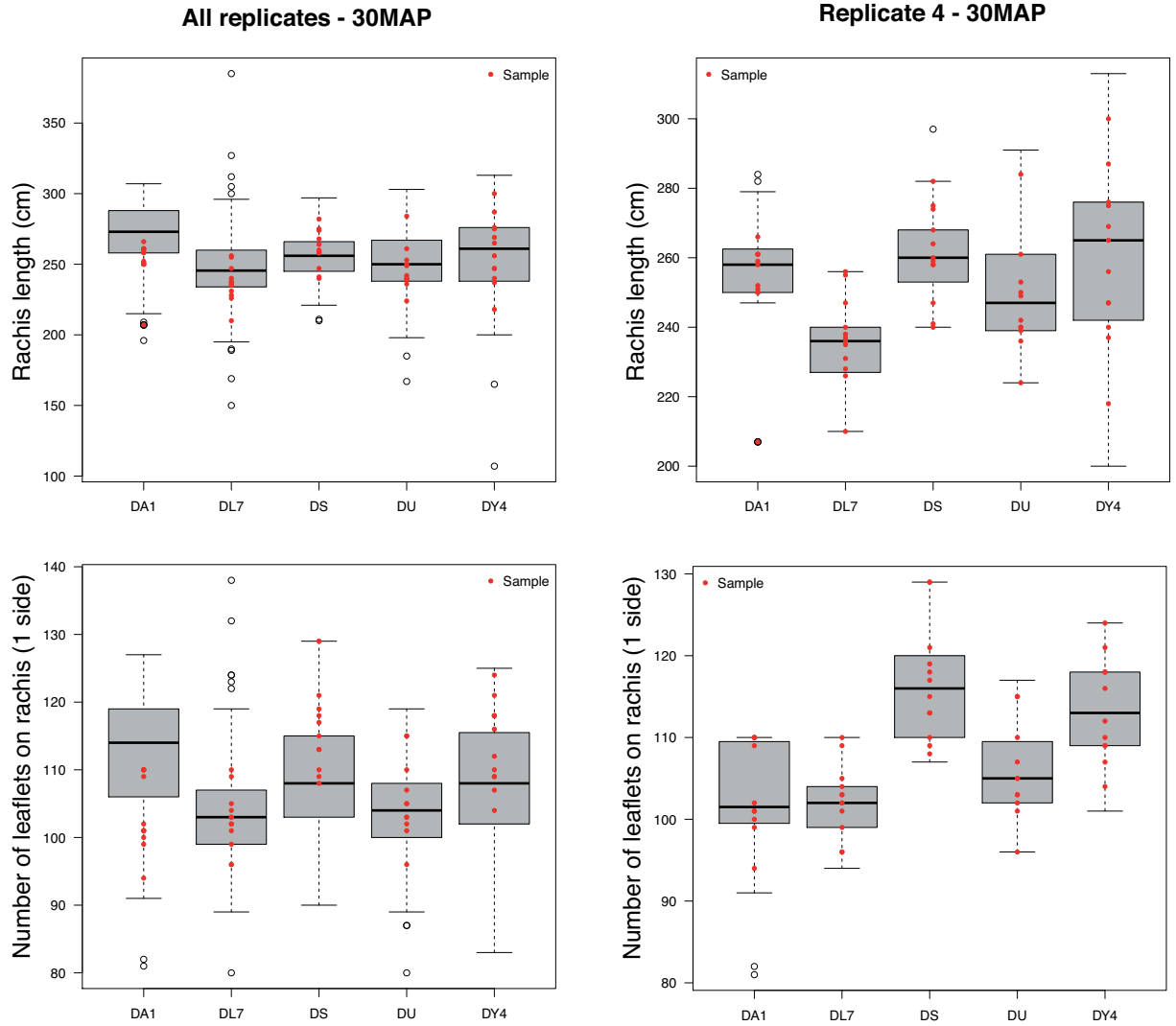


Figure B.2: Coarse architectural traits measurements (rachis length and number of leaflets) for the 5 studied progenies in all replicates 30 months after planting. Red points indicate plants on which detailed measurements for 3D reconstructions were performed.



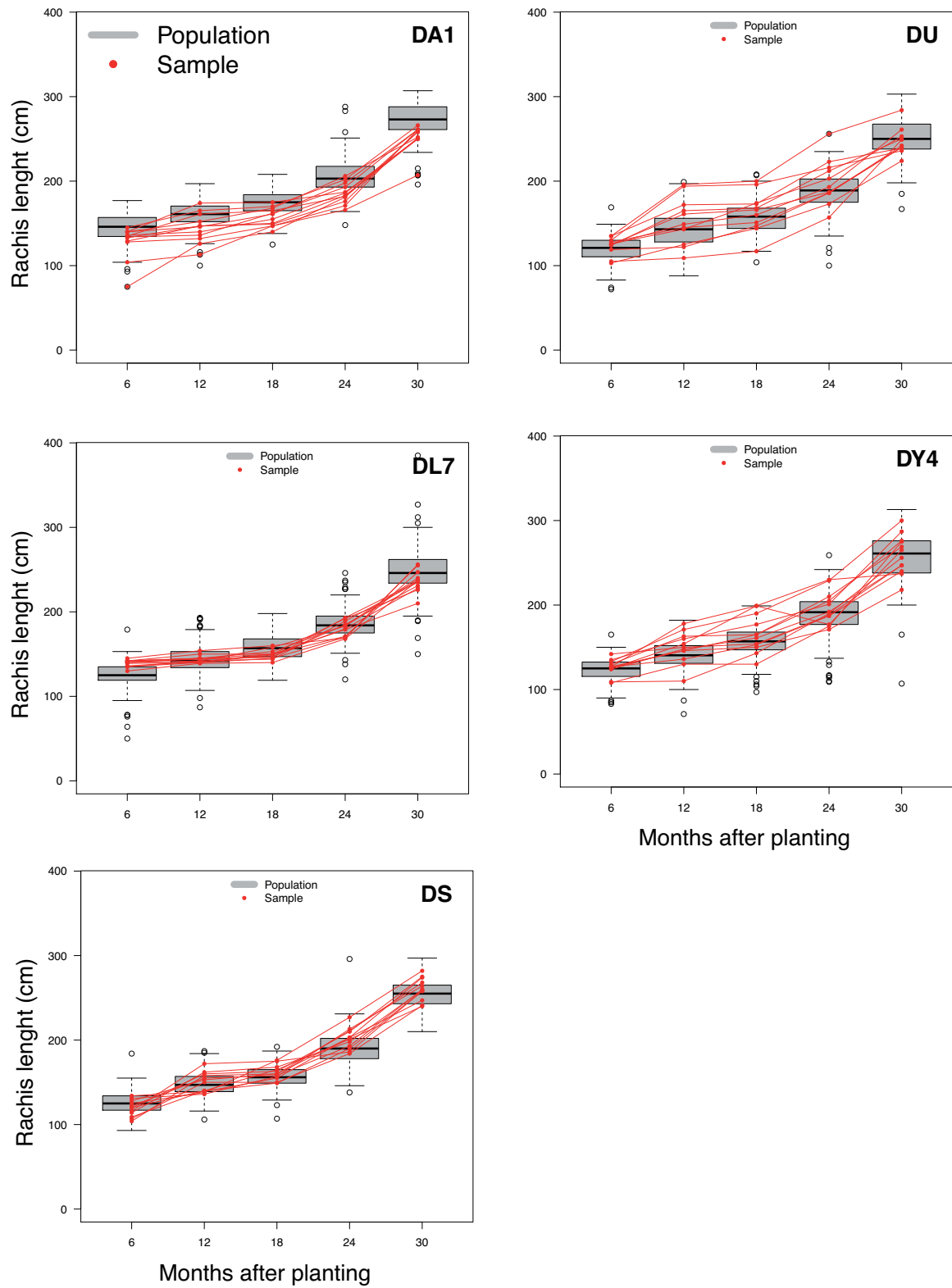


Figure B.3: Evolution of rachis length (leaf rank 17) over plant development for replicate 4

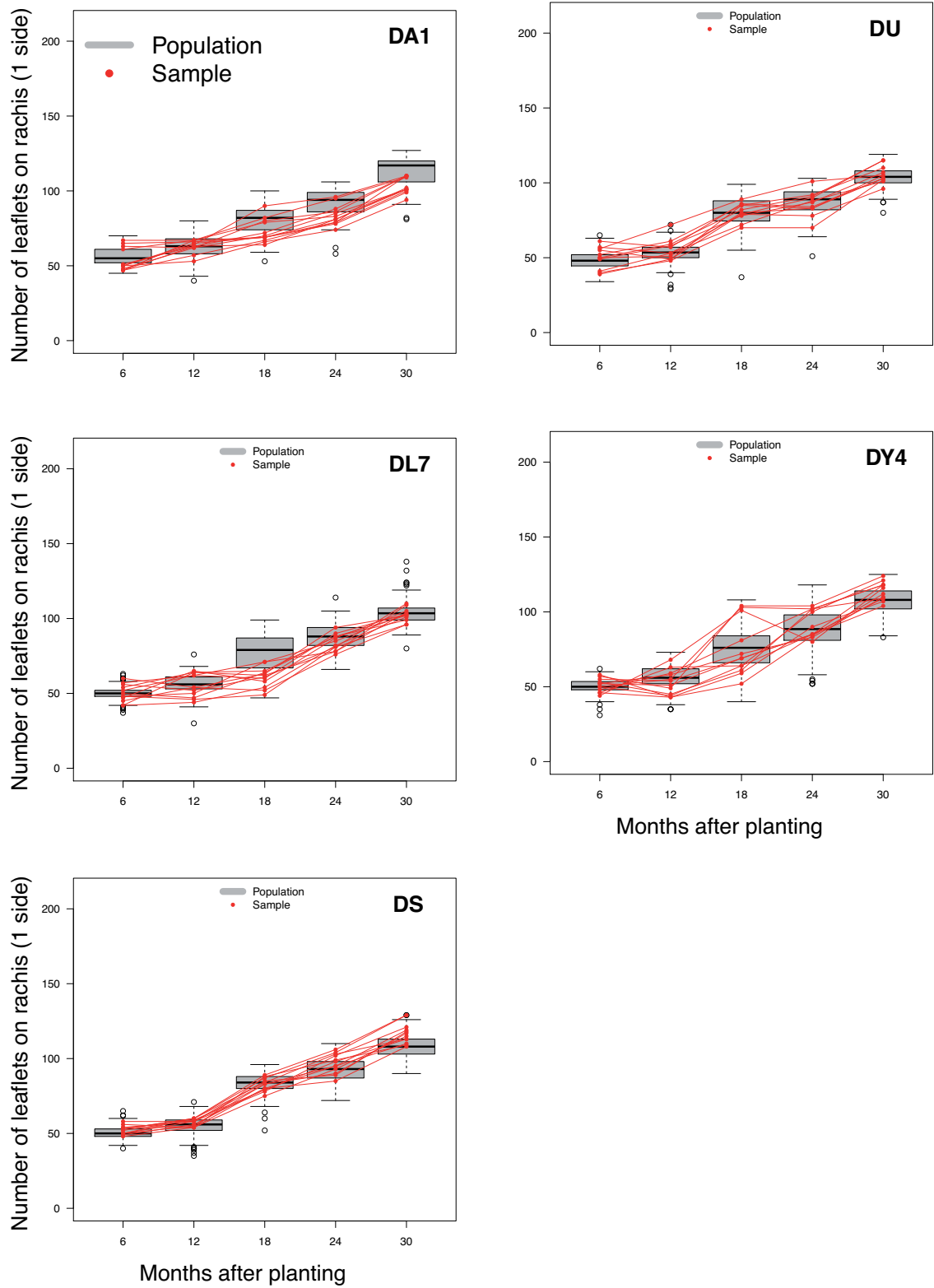


Figure B.4: Evolution of leaflets number on rachis (1 side; leaf rank 17) over plant development for replicate 4



# Bibliography

- [Adam et al., 2011] Adam, H., Collin, M., Richaud, F., Beulé, T., Cros, D., Omoré, A., Nodichao, L., Nouy, B., and Tregear, J. W. (2011). Environmental regulation of sex determination in oil palm: current knowledge and insights from other species. *Annals of Botany*, 108(8):1529–1537.
- [Aguirrezábal et al., 2014] Aguirrezábal, L., Martre, P., Pereyra-Irujo, G., Mercedes Echarte, M., and Izquierdo, N. (2014). *Crop Physiology: Applications for Genetic Improvement and Agronomy*, chapter Improving grain quality: ecophysiological and modeling tools to develop management and breeding strategies. London Academic Press.
- [Baey et al., 2013] Baey, C., Didier, A., Sébastien, L., Maupas, F., and Cournède, P.-H. (2013). Modelling the inter-individual variability of organogenesis in sugar beet populations using a hierarchical segmented model. *Ecological Modelling*, 263:56–63.
- [Baldocchi, 1994] Baldocchi, D. (1994). An analytical solution for coupled leaf photosynthesis and stomatal conductance models. *Tree Physiology*, 14:1069–1079.
- [Baldocchi and Harley, 1995] Baldocchi, D. and Harley, P. (1995). Scaling carbon dioxide and water vapour exchange from leaf to canopy in a deciduous forest. ii. model testing and application. *Plant, Cell & Environment*, 18(10):1157–1173.
- [Ball et al., 1987] Ball, J. T., Woodrow, I. E., and Berry, J. A. (1987). *Progress in Photosynthesis Research*. Springer.
- [Barcelos et al., 2015] Barcelos, E., Rios, S. d. A., Cunha, R. N., Lopes, R., Motoike, S. Y., Babiychuk, E., Skirycz, A., and Kushnir, S. (2015). Oil palm natural diversity and the potential for yield improvement. *Frontiers in Plant Science*, 6(190).
- [Barczi et al., 2008] Barczi, J.-F., Rey, H., Caraglio, Y., De Reffye, P., Barthélémy, D., Fourcaud, T., and Dong, Q. X. (2008). Amapsim: an integrative whole-plant architecture simulator based on botanical knowledge. *Annals of Botany*, 101(8):1125–1138.
- [Barillot et al., 2014] Barillot, R., Escobar-Gutiérrez, A. J., Fournier, C., Huynh, P., and Combes, D. (2014). Assessing the effects of architectural variations on light partitioning within virtual wheat–pea mixtures. *Annals of Botany*, page mcu099.
- [Barthélémy, 1991] Barthélémy, D. (1991). Levels of organization and repetition phenomena in seed plants. *Acta Biotheoretica*, 39(3-4):309–323.
- [Barthélémy and Caraglio, 2007] Barthélémy, D. and Caraglio, Y. (2007). Plant architecture: A dynamic, multilevel and comprehensive approach to plant form, structure and ontogeny. *Annals of Botany*, 99:375–407.

- [Baudouin et al., 1997] Baudouin, L., Baril, C., Clément-Demange, A., Leroy, T., and Paulin, D. (1997). Recurrent selection of tropical tree crops. *Euphytica*, 96:101–114.
- [Beirnaert and Vanderweyen, 1941] Beirnaert, A. and Vanderweyen, R. (1941). Contribution à l'étude génétique et biométrique des variétés d'*Elaeis guineensis* Jacq. *Publ. Inst. Nat. Etude Agron. Congo Belge. Ser. Sci.*, 27:1–101.
- [Ben Sadok et al., 2013] Ben Sadok, I., Moutier, N., Garcia, G., Dosba, F., Grati-Kamoun, N., Rebai, A., Khadari, B., and Costes, E. (2013). Genetic determinism of the vegetative and reproductive traits in an fl olive tree progeny. *Tree Genetics and Genomes*, 9:205–221.
- [Bernacchi et al., 2001] Bernacchi, C. J., Singsaas, E. L., Pimentel, C., Portis, A. R., and Long, S. P. (2001). Improved temperature response functions for models of rubisco-limited photosynthesis. *Plant, Cell and Environment*, 24:253–259.
- [Billotte et al., 2010] Billotte, N., Jourjon, M. F., Marseillac, N., Berger, A., Flori, A., Asmady, H., Adon, B., Singh, R., Nouy, B., Potier, F., Cheah, S., Rohde, W., Ritter, E., Courtois, B., Charrier, A., and Mangin, B. (2010). Qtl detection by multi-parent linkage mapping in oil palm (*Elaeis guineensis* Jacq.). *Theor Appl Genet*, 120:1673–1687.
- [Bonneau et al., 2014] Bonneau, X., Vandessel, P., Buabeng, M., and Erhahuyi, C. (2014). Early impact of oil palm planting density on vegetative and oil yield variables in West Africa. *OCL*, 21(4).
- [Boudon et al., 2014] Boudon, F., Preuksakarn, C., Ferraro, P., Diener, J., Nacry, P., Nikinmaa, E., and Godin, C. (2014). Quantitative assessment of automatic reconstructions of branching systems obtained from laser scanning. *Annals of botany*, 114(4):853–862.
- [Bradshaw and Stettler, 1995] Bradshaw, H. J. and Stettler, R. (1995). Molecular genetics of growth and development in populus. iv. mapping QTLs with large effects on growth, form, and phenology traits in a forest tree. *Genetics*, 139:963–973.
- [Bréda, 2003] Bréda, N. J. J. (2003). Groundbased measurements of leaf area index: a review of methods, instruments and current controversies. *Journal of Experimental Botany*, 54(392):2403–2417.
- [Breure, 1988] Breure, C. (1988). The effect of palm age and planting density on the partitionning of assimilates in oil palm. *Experimental Agriculture*, 24:53–66.
- [Bristow and Campbell, 1984] Bristow, K. L. and Campbell, G. S. (1984). On the relationship between incoming solar radiation and daily maximum and minimum temperature. *Agricultural and Forest Meteorology*, 31:159–166.
- [Buck-Sorlin et al., 2011] Buck-Sorlin, G., de Visser, P. H. B., Henke, M., Sarlikioti, V., van der Heijden, G. W. A. M., Marcelis, L. F. M., and Vos, J. (2011). Towards a functional-structural plant model of cut-rose: simulation of light environment, light absorption, photosynthesis and interference with the plant structure. *Annals of Botany*, 108:1121–1134.
- [Byrne et al., 1997] Byrne, M., Murrell, J. C., Kriedemann, J. V. O. P., Williams, E. R., and Moran, G. F. (1997). Identification and mode of action of quantitative trait loci affecting seedling height and leaf area in *Eucalyptus nitens*. *Theor Appl Genet*, 94:674–681.
- [Casadebaig et al., 2011] Casadebaig, P., Guilioni, L., Lecoeurb, J., Christophe, A., Champolivier, L., and Debaeke, P. (2011). Sunflo, a model to simulate genotype-specific performance of the sunflower crop in contrasting environments. *Agricultural and Forest Meteorology*, 151:163–178.

- [Casella and Sinoquet, 2003] Casella, E. and Sinoquet, H. (2003). A method for describing the canopy architecture of coppice poplar with allometric relationships. *Tree Physiology*, 23:1153–1170.
- [Cerasuolo et al., 2013] Cerasuolo, M., Richter, G. M., Cunliff, J., Purdy, S., Shield, I., and Karp, A. (2013). A pseudo-3d model to optimise the target traits of light interception in short-rotation coppice willow. *Agricultural and Forest Meteorology*, 173:127–138.
- [Cerasuolo et al., 2016] Cerasuolo, M., Richter, G. M., Richard, B., Cunliff, J., Girbau, S., Shield, I., Purdy, S., and Karp, A. (2016). Development of a sink-source interaction model for the growth of short-rotation coppice willow and *in silico* exploration of genotype x environment effects. *Journal of Experimental Botany*, 67(3):961–977.
- [Chazdon, 1985] Chazdon, R. (1985). Leaf display, canopy structure, and light interception of two understory palm species. *American Journal of Botany*, 72:1493–1502.
- [Chelle and Andrieu, 1998] Chelle, M. and Andrieu, B. (1998). The nested radiosity model for the distribution of light within plant canopies. *Ecological Modelling*, 111(1):75 – 91.
- [Chen et al., 1993] Chen, S. G., Impens, I., Ceulemans, R., and Kockelbergh, F. (1993). Measurement of gap fraction of fractal generated canopies using digitalized image analysis. *Agricultural and Forest Meteorology*, 65:245–259.
- [Chen et al., 2014] Chen, T.-W., Nguyen, T. M. N., Kahlen, K., and Stützel, H. (2014). Quantification of the effects of architectural traits on dry mass production and light interception of tomato canopy under different temperature regimes using a dynamic functional-structural plant model. *Journal of Experimental Botany*, 65(22):6399–6410.
- [Chenu et al., 2009] Chenu, K., Chapman, S. C., Tardieu, F., McLean, G., Welcker, C., and Hammer, G. L. (2009). Simulating the yield impacts of organ-level quantitative trait loci associated with drought response in maize: A “gene-to-phenotype” modeling approach. *Genetics*, 183:1507–1523.
- [Chenu et al., 2005] Chenu, K., Franck, N., Dauzat, J., Barczi, J.-F., Rey, H., and Lecoeur, J. (2005). Integrated responses of rosette organogenesis, morphogenesis and architecture to reduced incident light in *Arabidopsis thaliana* results in higher efficiency of light interception. *Functional Plant Biology*, 32:1123–1134.
- [Cilas et al., 2006] Cilas, C., Bar-Hen, A., Montagnon, C., and Godin, C. (2006). Definition of architectural ideotypes for good yield capacity in *Coffea canephora*. *Annals of Botany*, 97:405–411.
- [Cochard et al., 2009] Cochard, B., Adon, B., Rekima, S., Billotte, N., de Chenon, R. D., Koutou, A., Nouy, B., Omoré, A., Purba, A. R., Glazsmann, J.-C., and Noyer, J.-L. (2009). Geographic and genetic structure of african oil palm diversity suggests new approaches to breeding. *Tree Genetics and Genomes*, 5:493–504.
- [Combres et al., 2013] Combres, J. C., Pallas, B., Rouan, L., Mialet-Serra, I., Caliman, J. P., and Braconnier, S. (2013). Simulation of inflorescence dynamics and estimation of environment-sensitive phases : a model based analysis. *Functional Plant Biology*, 40:263–279.
- [Corbeil and Searle, 1976] Corbeil, R. and Searle, S. (1976). Restricted maximum likelihood (REML) estimation of variance components in the mixed model. *Technometrics*, 18:31–38.
- [Corley, 1983] Corley, R. (1983). Photosynthesis and age of oil palm leaves. *Photosynthetica*, 17(1):97–100.

- [Corley et al., 1971] Corley, R., Gray, B., and Kee, N. S. (1971). Productivity of the oil palm (*Elaeis guineensis* Jacq.) in Malaysia. *Experimental Agriculture*, 7(2):129–136.
- [Corley and Tinker, 2003] Corley, R. and Tinker, P. (2003). *The oil palm*. Blackwel Science Ltd, 9600 Garsington Road, Oxford, OX4 2DQ , UK, fourth edition.
- [Corley and Tinker, 2016] Corley, R. and Tinker, P. (2016). *The oil palm*. Blackwel Science Ltd, Oxford, UK, fifth edition.
- [Costes et al., 2004] Costes, E., Lauri, P., Laurens, F., Moutier, N., Belouin, A., Delort, F., Legave, J., and Regnard, J. (2004). Morphological and architectural traits on fruit trees which could be relevant for genetic studies: a review. *Acta Horticulturae*, 663:349–355.
- [Costes et al., 2008] Costes, E., Smith, C., Renton, M., Guédon, Y., Prusinkiewicz, P., and Godin, C. (2008). Mapplet: simulation of apple tree development using mixed stochastic and biomechanical models. *Functional Plant Biology*, 35:936–950.
- [Côté et al., 2009] Côté, J.-F., Widlowski, J.-L., Fournier, R. A., and Verstraete, M. M. (2009). The structural and radiative consistency of three-dimensional tree reconstructions from terrestrial lidar. *Remote Sensing and Environment*, 113:1067–1081.
- [Cros, 2015] Cros, D. (2015). *Etude des facteurs contrôlant l’efficacité de la sélection génomique chez le palmier à huile (Elaeis guineensis Jacq.)*. PhD thesis, SIBAGHE.
- [Cros et al., 2013] Cros, D., Flori, A., Nodichao, L., Omoré, A., and Nouy, B. (2013). Differential response to water balance and bunch load generates diversity of bunch production profiles among oil palm crosses (*Elaeis guineensis*). *Tropical plant biology*, 6:26–36.
- [Da Silva et al., 2013] Da Silva, D., Han, L., and Costes, E. (2013). Light interception efficiency of apple trees: A multiscale computational study based on MAppleT. *Ecological Modelling*, 290:45–53.
- [Da Silva et al., 2014] Da Silva, D., Han, L., Faivre, R., and Costes, E. (2014). Influence of the variation of geometrical and topological traits on light interception efficiency of apple trees: sensitivity analysis and metamodeling for ideotype definition. *Annals of Botany*, 114(4):739–752.
- [Damour et al., 2010] Damour, G., Simonneau, T., Cochard, H., and Urban, L. (2010). An overview of models of stomatal conductance at the leaf level. *Plant, Cell and Environment*, 33:1419–1438.
- [Danson et al., 2007] Danson, F. M., Hetherington, D., Morsdorf, F., Koetz, B., and Allgöwer, B. (2007). Forest canopy gap fraction from terrestrial laser scanning. *IEEE Geoscience and remote sensing letters*, 4(1):157–160.
- [Dauzat, 1990] Dauzat, J. (1990). *Simulation des transferts radiatifs sur maquettes informatiques d’Elaeis guineensis*. IRHO Laboratoire de modélisation du Gerdar, rapport atp n°222 CIRAD edition.
- [Dauzat et al., 2008] Dauzat, J., Clouvel, P., Luquet, D., and Martin, P. (2008). Using virtual plants to analyse the light-foraging efficiency of a low-density cotton crop. *Annals of Botany*, 101(8):1153–1166.
- [Dauzat and Eroy, 1997] Dauzat, J. and Eroy, M. (1997). Simulating light regime and inter-crop yields in coconut based farming systems. *European Journal of Agronomy*, 7:63–74.
- [De Reffye et al., 1997] De Reffye, P., Fourcaud, T., Blaise, F., Barthélémy, D., and Houllier, F. (1997). A functional model of tree growth and tree architecture. *Silva Fennica*, 31:297–311.



- [DeJong et al., 2011] DeJong, T. M., Silva, D. D., Vos, J., and Escobar-Gutiérrez, A. J. (2011). Using functional-structural plant models to study, understand and integrate plant development and ecophysiology. *Annals of Botany*, 108:987–989.
- [Dickmann et al., 1994] Dickmann, D. I., Gold, M. A., and Flore, J. A. (1994). The ideotype concept and the genetic improvement of tree crops. *Plant Breed. Rev.*, 12:163–193.
- [Dingkuhn et al., 2015] Dingkuhn, M., Laza, M. R. C., Kumar, U., Mendez, K. S., Collard, B., Jagadish, K., Singh, R. K., Padolina, T., Malabayabas, M., Torres, E., Rebolledo, M. C., Manneh, B., and Sow, A. (2015). Improving yield potential of tropical rice: Achieved levels and perspectives through improved ideotypes. *Field Crops Research*, 182:43–59.
- [Donald, 1968] Donald, C. (1968). The design of a wheat ideotype. *Finlay, KW and Shepherd*.
- [Dufrêne, 1989] Dufrêne, E. (1989). *Photosynthèse, consommation en eau et modélisation de la production chez le palmier à huile*. PhD thesis, Université of Paris-Sud Orsay.
- [Dufrêne et al., 1992] Dufrêne, E., Dubos, B., Rey, H., Quencez, P., and Saugier, B. (1992). Changes in evapotranspiration from an oil palm stand (*Elaeis guineensis* Jacq.) exposed to seasonal soil water deficits. *Acta Oecologica*, 13:299–314.
- [Dufrêne et al., 1990] Dufrêne, E., Ochs, R., and Saugier, B. (1990). Oil palm photosynthesis and productivity linked to climatic factors. *Oléagineux*, 45:345–355.
- [Dufrêne and Saugier, 1993] Dufrêne, E. and Saugier, B. (1993). Gas exchange of oil palm in relation to light, vapour pressure deficit, temperature and leaf age. *Functional Ecology*, 7:97–104.
- [Durand-Gasselin et al., 1999] Durand-Gasselin, T., Noiret, J., Kouamé, K., Cochard, B., and Adon, B. (1999). Availability of quality pollen for improved oil palm (*Elaeis guineensis* Jacq.) seed production. *Plantations, Recherche, Développement*, 6(4):264–276.
- [Duursma et al., 2012] Duursma, R. A., Falster, D. S., Valladares, F., Sterck, F. J., Pearcy, R. W., Lusk, C. H., Sendall, K. M., Nordenstahl, M., Houter, N. C., Atwell, B. J., Kelly, N., Kelly, J. W. G., Liberloo, M., Tissue, D. T., Medlyn, B. E., and Ellsworth, D. S. (2012). Light interception efficiency explained by two simple variables: a test using a diversity of small- to medium-sized woody plants. *New Phytologist*, 193:397–408.
- [Edelin, 1977] Edelin, C. (1977). *Images de l’architecture des conifères*. PhD thesis, Université Montpellier II.
- [Faivre et al., 2013] Faivre, R., Iooss, B., Mahévas, S., Makowski, D., and Monod, H. (2013). *Analyse de sensibilité et exploration de modèles. Application aux sciences de la nature et de l’environnement*. Quae edition.
- [Falster and Westoby, 2003] Falster, D. S. and Westoby, M. (2003). Leaf size and angle vary widely across species: what consequences for light interception? *New Phytologist*, 158(3):509–525.
- [Fan et al., 2015] Fan, Y., Rounsard, O., Bernoux, M., Maire, G. L., Panferov, O., Kotowska, M. M., and Knohl, A. (2015). A sub-canopy structure for simulating oil palm in the community land model (CLM-Palm): phenology, allocation and yield. *Geoscientific Model Development*, 8:3785–3800.
- [Farquhar et al., 1980] Farquhar, G., von Caemmerer, S., and Berry, J. (1980). A biochemical model of photosynthetic CO<sub>2</sub> assimilation in leaves of C<sub>3</sub> species. *Planta*, 149:78–90.

- [Fourcaud et al., 2008] Fourcaud, T., Zhang, X., Stokes, A., Lambers, H., and Körner, C. (2008). Plant growth modelling and applications: The increasing importance of plant architecture in growth models. *Annals of Botany*, 101(8):1053–1063.
- [Frary et al., 2004] Frary, A., Fritz, L. A., and Tanksley, S. D. (2004). A comparative study of the genetic bases of natural variation in tomato leaf, sepal, and petal morphology. *Theor Appl Genet*, 109:523–533.
- [Frazer et al., 2001] Frazer, G. W., Fournier, R. A., Trofymow, J., and Hall, R. J. (2001). A comparison of digital and film fisheye photography for analysis of forest canopy structure and gap light transmission. *Agricultural and Forest Meteorology*, 109:249–263.
- [Gallais, 1990] Gallais, A. (1990). *Théorie de la sélection en amélioration des plantes*. Masson.
- [Gastellu-Etchegorry et al., 1996] Gastellu-Etchegorry, J.-P., Demarez, V., Pinel, V., and Zagolski, F. (1996). Modeling radiative transfer in heterogeneous 3-D vegetation canopies. *Remote sensing of environment*, 58(2):131–156.
- [Godin and Caraglio, 1998] Godin, C. and Caraglio, Y. (1998). A multiscale model of plant topological structures. *Journal of Theoretical Biology*, 191:1–46.
- [Godin et al., 1999] Godin, C., Costes, E., and Sinoquet, H. (1999). A method for describing plant architecture which integrates topology and geometry. *Annals of Botany*, 84:343–357.
- [Griffon and de Coligny, 2014] Griffon, S. and de Coligny, F. (2014). Amapstudio: An editing and simulation software suite for plants architecture modelling. *Ecological Modelling*, 290:3–10. Special Issue of the 4th International Symposium on Plant Growth Modeling, Simulation, Visualization and Applications (PMA’12 ) Special Issue of PMA’12.
- [Gu et al., 2014] Gu, J., Yin, X., Zhang, C., Wang, H., and Struik, P. C. (2014). Linking ecophysiological modelling with quantitative genetics to support marker-assisted crop design for improved yields of rice (*Oryza sativa*) under drought stress. *Annals of Botany*, 114(3):499–511.
- [Guédon et al., 2001] Guédon, Y., Barthélémy, D., Caraglio, Y., and Costes, E. (2001). Pattern analysis in branching and axillary flowering sequences. *Journal of Theoretical Biology*, 212(4):481–520.
- [Hackenberg et al., 2014] Hackenberg, J., Morhart, C., Sheppard, J., Spiecker, H., and Disney, M. (2014). Highly accurate tree models derived from terrestrial laser scan data: A method description. *Forests*, 5:1069–1105.
- [Hackenberg et al., 2015] Hackenberg, J., Spiecker, H., Calders, K., Disney, M., and Raunonen, P. (2015). Simpletree—an efficient open source tool to build tree models from TLS clouds. *Forests*, 6(11):4245–4294.
- [Hall and Bailey, 2001] Hall, D. B. and Bailey, R. L. (2001). Modeling and prediction of forest growth variables based on multilevel nonlinear mixed models. *Forest Science*, 47(3):311–321.
- [Hallé and Oldeman, 1970] Hallé, F. and Oldeman, R. (1970). *Essai sur l’architecture et la dynamique de croissance des arbres tropicaux*. IRD, 6, Masson et Cie, Paris, France.
- [Hallé et al., 1978] Hallé, F., Oldeman, R., and Tomlinson, P. (1978.). *Tropical trees and forests*. Springer-Verlag, Berlin.
- [Hammer et al., 2010] Hammer, G. L., van Oosterom, E., McLean, G., Chapman, S. C., Broad, I., Harland, P., and Muchow, R. C. (2010). Adapting APSIM to model the physiology and genetics of complex adaptive traits in field crops. *Journal of Experimental Botany*, 61(8):2185–2202.

- [Hardwick et al., 2015] Hardwick, S. R., Toumi, R., Pfeifer, M., Turner, E. C., Nilus, R., and Ewers, R. M. (2015). The relationship between leaf area index and microclimate in tropical forest and oil palm plantation: Forest disturbance drives changes in microclimate. *Agricultural and Forest Meteorology*, 201(0):187 – 195.
- [Henderson, 2002] Henderson, A. (2002). *Evolution and ecology of palms*. New York Botanical Garden Press New York.
- [Henry, 1958] Henry, P. (1958). Croissance et développement chez *Elaeis Guineensis* Jacq. de la germination à la première floraison. *Rev. Gen. Bot.*, 66:5–34.
- [Hill, 2010] Hill, W. G. (2010). Understanding and using quantitative genetic variation. *Philosophical transactions of the Royal Society of London, series B Biological Sciences*, 365(73-85).
- [Hoffmann et al., 2014] Hoffmann, M., Vera, A. C., van Wijk, M., Giller, K., Oberthür, T., Donough, C., and Whitbread, A. (2014). Simulating potential growth and yield of oil palm (*Elaeis guineensis*) with PALMSIM: Model description, evaluation and application. *Agricultural Systems*, 131(0):1 – 10.
- [Hosoi and Omasa, 2007] Hosoi, F. and Omasa, K. (2007). Factors contributing to accuracy in the estimation of the woody canopy leaf area density profile using 3D portable lidar imaging. *Journal of Experimental Botany*, 58(12):3463–3473.
- [Hung et al., 2012] Hung, H.-Y., Browne, C., Guill, K., Coles, N., Eller, M., Garcia, A., Lepak, N., Melia-Hancock, S., Oropeza-Rosas, M., Salvo, S., Upadyayula, N., Buckler, E., Flint-Garcia, S., McMullen, M., Rocheford, T., and Holland, J. (2012). The relationship between parental genetic or phenotypic divergence and progeny variation in the maize nested association mapping population. *Heredity*, 108:490–499.
- [Huth et al., 2014] Huth, N. I., Banabas, M., Nelson, P. N., and Webb, M. (2014). Development of an oil palm cropping systems model: Lessons learned and future directions. *Environmental Modelling and Software*, 62:411–418.
- [Iandolina et al., 2013] Iandolina, A., Percy, R., and Williams, L. (2013). Simulating three-dimensional grapevine canopies and modelling their light interception characteristics. *Australian Journal of Grape and Wine Research*, 19:388–400.
- [Ioss, 2011] Ioss, B. (2011). Review of global sensitivity analysis of numerical models. *Journal de la Société Française de Statistique*, 151(1):3–25.
- [Jaligot and Rival, 2015] Jaligot, E. and Rival, A. (2015). Applying epigenetics in plant breeding: Balancing genome stability and phenotypic plasticity. In *Advances in Plant Breeding Strategies: Breeding, Biotechnology and Molecular Tools*, pages 159–192. Springer International Publishing.
- [Jonckheere et al., 2004] Jonckheere, I., Fleck, S., Nackaerts, K., Muys, B., Coppin, P., Weiss, M., and Baret, F. (2004). Review of methods for *in situ* leaf area index determination: Part I. Theories, sensors and hemispherical photography. *Agricultural and Forest Meteorology*, 121(1–2):19 – 35.
- [Jones, 1997] Jones, L. (1997). The effects of leaf pruning and other stresses on sex determination in the oil palm and their representation by a computer simulation. *J. theor. Biol.*, 187:241–260.
- [Jørgensen et al., 2003] Jørgensen, U., Mortensen, J., and Ohlsson, C. (2003). Light interception and dry matter conversion efficiency of miscanthus genotypes estimated from spectral reflectance measurements. *New Phytologist*, 157:263–270.

- [Jourdan and Rey, 1997a] Jourdan, C. and Rey, H. (1997a). Architecture and development of the oil-palm (*Elaeis guineensis* Jacq.) root system. *Plant and Soil*, 189:33–48.
- [Jourdan and Rey, 1997b] Jourdan, C. and Rey, H. (1997b). Modelling and simulation of the architecture and development of the oil-palm (*Elaeis guineensis* Jacq.) root system. *Plant and Soil*, 120:217–233.
- [Julia, 2007] Julia, C. (2007). Modélisation et simulation de l’architecture du palmier à huile afin de calculer l’interception lumineuse par le couvert vegetal. Rapport the master, ENITA Clermont-Ferrand.
- [Kang et al., 2014] Kang, F., Cournède, P.-H., Lecoeur, J., and Letort, V. (2014). Sunlab: A functional–structural model for genotypic and phenotypic characterization of the sunflower crop. *Ecological Modelling*, 290:21–33.
- [Kawamura et al., 2013] Kawamura, K., Oyant, L. H.-S., Foucher, F., Thouroude, T., and Loustau, S. (2013). Kernel methods for phenotyping complex plant architecture. *Journal of Theoretical Biology*, 342:83–92.
- [Khush, 2001] Khush, G. S. (2001). Green revolution: the way forward. *Nature Genetics*, 2:815–821.
- [Koester et al., 2014] Koester, R. P., Skoneczka, J. A., Cary, T. R., Diers, B. W., and Ainsworth, E. A. (2014). Historical gains in soybean (*Glycine max* Merr.) seed yield are driven by linear increases in light interception, energy conversion, and partitioning efficiencies. *Journal of Experimental Botany*, 65(12):3311–3321.
- [Kumar et al., 2017] Kumar, U., Laza, M. R., Soulié, J.-C., Pasco, R., Mendez, K. V., and Dingkuhn, M. (2017). Analysis and simulation of phenotypic plasticity for traits contributing to yield potential in twelve rice genotypes. *Field Crops Research*, 202:94–107.
- [Kurth and Sloboda, 1997] Kurth, W. and Sloboda, B. (1997). Growth grammars simulating trees-an extension of L-systems incorporating local variables and sensitivity. *Silva Fennica*, 31(3):285–295.
- [Lamade and Setiyo, 1996] Lamade, E. and Setiyo, E. (1996). Variation in maximum photosynthesis of oil palm in Indonesia: comparison of three morphologically contrasting clones. Plantations, recherche, développement.
- [Lamanda et al., 2008] Lamanda, N., Dauzat, J., Jourdan, C., Martin, P., and Malézieux, E. (2008). Using 3D architectural models to assess light availability and root bulkiness in coconut agroforestry systems. *Agroforestry Systems*, 72:63 – 74.
- [Lamour et al., 2014] Lamour, J., Moguédéc, G. L., Perez, R. P., Fabre, D., and Dauzat, J. (2014). Modelling carbon assimilation of *elaeis guineensis* jacq.: From field protocol to statistical analyses. Master’s thesis, Ecole Nationale Supérieur Agronomique de Montpellier.
- [Laurens et al., 2000] Laurens, F., Audergon, J., Claverie, J., Duval, H., Germain, E., Kervella, J., Le Lezec, M., Lauri, P., and Lespinasse, J. (2000). Integration of architectural types in french programmes of ligneous fruit species genetic improvement. *Fruits*, 55(2):141–152.
- [Lauri and Costes, 2005] Lauri, E. and Costes, E. (2005). Progress in whole-tree architectural studies for apple cultivar characterization at INRA, france - contribution to the ideotype approach. *Acta Horticulturae*, 663:357–362.
- [Le Bec et al., 2015] Le Bec, J., Courbaud, B., Le Moguédéc, G., and Péliissier, R. (2015). Characterizing tropical tree species growth strategies: Learning from inter-individual variability and scale invariance. *PloS ONE*, 10(3):e0117028.

- [Leakey and Page, 2006] Leakey, R. and Page, T. (2006). The 'ideotype concept' and its application to the selection of cultivars of trees providing agroforestry tree products. *Forests, Trees and Livelihoods*, 16(1):5–16.
- [Lecoeur et al., 2011] Lecoeur, J., Poiré-Lassus, R., Christophe, A., Pallas, B., Casadebaig, P., Debaeke, P., Vear, F., and Guillioni, L. (2011). Quantifying physiological determinants of genetic variation for yield potential in sunflower. SUNFLO: a model-based analysis. *Functional Plant Biology*, 38(246-259).
- [Lecoustre and Jeager, 1989] Lecoustre, R. and Jeager, M. (1989). *Modélisation de l'architecture et de la géométrie d'Elaeis guineensis Jacq.* IRHO Laboratoire de modélisation du Gerdar, rapport atp n°222 CIRAD edition.
- [Legros, 2008] Legros, S. (2008). *Ajustement de la phénologie, de la croissance et de la production du palmier à huile (Elaeis Guineensis Jacq.) face à des environnements variables: mécanismes de la plasticité phénotypique*. PhD thesis, SIBAGHE.
- [Legros et al., 2009a] Legros, S., Mialet-Serra, I., Caliman, J. P., Siregar, F., Clément-Vidal, A., and Dingkuhn, M. (2009a). Phenology and growth adjustments of oil palm (*Elaeis guineensis*) to photoperiod and climate variability. *Annals of Botany*, 104:1171–1182.
- [Legros et al., 2009b] Legros, S., Mialet-Serra, I., Caliman, J.-P., Siregar, F. A., Clement-Vidal, A., Fabre, D., and Dingkuhn, M. (2009b). Phenology, growth and physiological adjustments of oil palm (*Elaeis guineensis*) to sink limitation induced by fruit pruning. *Annals of Botany*, 104:1183–1194.
- [Legros et al., 2009c] Legros, S., Miallet-Serra, I., Clement-Vidal, A., Caliman, J., Siregar, F., Fabre, D., and Dingkuhn, M. (2009c). Role of transitory carbon reserves during adjustment to climate variability and source–sink imbalances in oil palm (*Elaeis guineensis*). *Tree Physiology*, 29:1199–1211.
- [Letort et al., 2008] Letort, V., Mahe, P., Cournède, P.-H., de Reffye, P., and Courtois, B. (2008). Quantitative genetics and functional–structural plant growth models: Simulation of quantitative trait loci detection for model parameters and application to potential yield optimization. *Annals of Botany*, 101:1243–1254.
- [Leuning, 1995] Leuning, R. (1995). A critical appraisal of a combined stomatal-photosynthesis model of C3 plants. *Plant, Cell and Environment*, 18:339–355.
- [Leuning, 2002] Leuning, R. (2002). Temperature dependence of two parameters in a photosynthesis model. *Plant, Cell and Environment*, 25:1205–1210.
- [Li et al., 2015] Li, C., Li, Y., Shi, Y., Song, Y., Zhang, D., Buckler, E. S., Zhang, Z., Wang, T., and Li, Y. (2015). Genetic control of the leaf angle and leaf orientation value as revealed by ultra-high density maps in three connected maize populations. *PloS ONE*, 10(3):e0121624.
- [Lin and West, 2016] Lin, Y. and West, G. (2016). Retrieval of effective leaf area index (LAIe) and leaf area density (LAD) profile at individual tree level using high density multi-return airborne lidar. *International journal of Applied Earth Observation and Geoinformation*, 50:150–158.
- [Lindenmayer, 1968] Lindenmayer, A. (1968). Mathematical models for cellular interaction in development, parts I and II. *J. Theor. Biol*, 18:280–315.
- [Lopez et al., 2008] Lopez, G., Favreau, R. R., Smith, C., Costes, E., Prusinkiewicz, P., and DeJong, T. M. (2008). Integrating simulation of architectural development and source–sink behaviour of peach trees by incorporating Markov chains and physiological organ function submodels into L-PEACH. *Functional Plant Biology*, 35:761–771.

- [Louarn et al., 2008] Louarn, G., Lecoeur, J., and Lebon, E. (2008). A three-dimensional statistical reconstruction model of grapevine (*Vitis vinifera*) simulating canopy structure variability within and between cultivar/training system pairs. *Annals of Botany*, 101(8):1167–1184.
- [Louarn et al., 2012] Louarn, G., Silva, D. D., Godin, C., and Combes, D. (2012). Simple envelope-based reconstruction methods can infer light partitioning among individual plants in sparse and dense herbaceous canopies. *Agricultural and Forest Meteorology*, 166(167):98–112.
- [Luquet et al., 2006] Luquet, D., Dingkuhn, M., Kim, H., Tambour, L., and Clement-Vidal, A. (2006). Ecomeristem, a model of morphogenesis and competition among sinks in rice. 1. concept, validation and sensitivity analysis. *Functional Plant Biology*, 33:309–323.
- [Maddonni et al., 2001] Maddonni, G., Chelle, M., Drouet, J.-L., and Andrieu, B. (2001). Light interception of contrasting azimuth canopies under square and rectangular plant spatial distributions: simulations and crop measurements. *Field Crops Research*, 70:1–13.
- [Mao et al., 2016] Mao, L., Zhang, L., Evers, J. B., Henke, M., van der Werf, W., Liu, S., Zhang, S., Zhao, X., Wang, B., and Li, Z. (2016). Identification of plant configurations maximizing radiation capture in relay strip cotton using a functional-structural plant model. *Field Crops Research*, 187:1–11.
- [Marshall and Biscoe, 1980] Marshall, B. and Biscoe, P. (1980). A model for C3 leaves describing the dependence of net photosynthesis on irradiance. *Journal of Experimental Botany*, 31(120):29–39.
- [Martre et al., 2015] Martre, P., He, J., Le Gouis, J., and Semenov, M. A. (2015). In silico system analysis of physiological traits determining grain yield and protein concentration for wheat as influenced by climate and crop management. *Journal of experimental botany*, page erv049.
- [Martre et al., 2014] Martre, P., Quilot-Turion, B., Luquet, D., Ould-Sidi, M.-M., Memmah, Chenu, K., and Debaeke, P. (2014). *Crop Physiology: Applications for Genetic Improvement and Agronomy*, chapter 14 Model-assisted phenotyping and ideotype design, pages 323–373. London Academic Press.
- [Moeller et al., 2014] Moeller, C., Evers, J. B., and Rebetzke, G. (2014). Canopy architectural and physiological characterization of near-isogenic wheat lines differing in the tiller inhibition gene *tin*. *Frontiers in Plant Science*, 5(617).
- [Monsi and Saeki, 2005] Monsi, M. and Saeki, T. (2005). On the factor light in plant communities and its importance for matter production. *Annals of Botany*, 95:549–567.
- [Monteith, 1977] Monteith, J. (1977). Climate and the efficiency of crop production in britain. *Phylosophical transactions of the Royal Society of London, series B Biological Sciences*, 281:277–294.
- [Moorthy et al., 2011] Moorthy, I., Miller, J. R., Berni, J. A. J., Zarco-Tejada, P., Hu, B., and Chen, J. (2011). Field characterization of olive (*Olea europaea* L.) tree crown architecture using terrestrial laser scanning data. *Agricultural and Forest Meteorology*, 151:204–214.
- [Moorthy et al., 2008] Moorthy, I., Miller, J. R., Hu, B., Chen, J., and Li, Q. (2008). Retrieving crown leaf area index from an individual tree using ground-based lidar data. *Can. J. Remote Sensing*, 34(3):320–332.
- [Morcillo et al., 2013] Morcillo, F., Cros, D., Billotte, N., Ngando-Ebongue, G.-F., Domonh  do, H., Pizot, M., Cu  llar, T., Esp  out, S., Dhouib, R., Bourgis, F., Claverol, S., Tranbarger, T., Nouy, B., and Arondel, V. (2013). Improving palm oil quality through identification and mapping of the lipase gene causing oil deterioration. *Nature communication*, 4(2160).

- [Morris, 1991] Morris, M. D. (1991). Factorial sampling plans for preliminary computational experiments. *Technometrics*, 33(2):161–174.
- [Mouliia and Fournier, 2009] Mouliia, B. and Fournier, M. (2009). The power and control of gravitropic movements in plants: a biomechanical and systems biology view. *Journal of Experimental Botany*, 60(2):461–486.
- [Murchie et al., 2009] Murchie, E. H., Pinto, M., and Horton, P. (2009). Agriculture and the new challenges for photosynthesis research. *New Phytologist*, 181:532–552.
- [Negrón et al., 2013] Negrón, C., Contador, L., Lampinen, B. D., Metcalf, S. G., Guédon, Y., Costes, E., and DeJong, T. M. (2013). Differences in proleptic and epicormic shoot structures in relation to water deficit and growth rate in almond trees (*Prunus dulcis*). *Annals of botany*, page mct282.
- [Niinemets, 2007] Niinemets, Ü. (2007). Photosynthesis and resource distribution through plant canopies. *Plant, Cell and Environment*, 30:1052–1071.
- [Niinemets et al., 2004a] Niinemets, Ü., Al Afas, N., Cescatti, A., Pellis, A., and Ceulemans, R. (2004a). Petiole length and biomass investment in support modify light interception efficiency in dense poplar plantations. *Tree Physiology*, 24(2):141–154.
- [Niinemets et al., 2004b] Niinemets, Ü., Cescatti, A., and Christian, R. (2004b). Constraints on light interception efficiency due to shoot architecture in broad-leaved *Nothofagus* species. *Tree Physiology*, 24(6):617–630.
- [Niklas, 1988] Niklas, K. J. (1988). The role of phyllotatic pattern as a ”developmental constraint” on the interception of light by leaf surfaces. *Evolution*, 42:1–16.
- [Niklas, 1995] Niklas, K. J. (1995). Size-dependent allometry of tree height, diameter and trunk taper. *Annals of Botany*, 75:217–227.
- [Nothdurft et al., 2006] Nothdurft, A., Kublin, E., and Lappi, J. (2006). A non-linear hierarchical mixed model to describe tree height growth. *Eur J Forest Res*, 125:281–289.
- [OECD/FAO, 2014] OECD/FAO (2014). *OECD-FAO Agricultural Outlook 2014*. OECD/FAO, Paris, FRANCE.
- [Onoda et al., 2014] Onoda, Y., Saluñga, J. B., Akutsu, K., ichiro Aiba, S., Yahara, T., and Anten, N. P. R. (2014). Trade-off between light interception efficiency and light use efficiency: implications for species coexistence in one-sided light competition. *Journal of Ecology*, 102:167–175.
- [Osorio et al., 2001] Osorio, L. F., White, T. L., and Huber, D. A. (2001). Age trends of heritabilities and genotype-by-environment interactions for growth traits and wood density from clonal trials of *Eucalyptus grandis* HILL ex MAIDEN. *Silvae Genetica*, 50(1):30–37.
- [Pallas et al., 2013a] Pallas, B., Clément-Vidal, A., Rebolledo, M.-C., Soulié, J.-C., and Luquet, D. (2013a). Using plant growth modeling to analyze c source-sink relations under drought: inter- and intraspecific comparison. *Frontiers in Plant Science*, 4(437).
- [Pallas et al., 2013b] Pallas, B., Mialet-Serra, I., Rouan, L., Clément-Vidal, A., Caliman, J.-P., and Dingkuhn, M. (2013b). Effect of source/sink ratios on yield components, growth dynamics and structural characteristics of oil palm (*Elaeis guineensis*) bunches. *Tree Physiology*, 33:409–424.



- [Pallas et al., 2013c] Pallas, B., Soulié, J.-C., Aguilar, G., Rouan, L., and Luquet, D., editors (2013c). *X-Palm, a functional structural plant model for analysing temporal, genotypic and inter-tree variability of oil palm growth and yield*. 7th International Conference on Functional-Structural Plant Models. Saariselkä, Finland, Risto Sievänen and Eero Nikinmaa and Christophe Godin and Anna Lintunen and Pekka Nygren.
- [Parveaud et al., 2008] Parveaud, C.-E., Chopard, J., Dauzat, J., Courbaud, B., and Auclair, D. (2008). Modelling foliage characteristics in 3D tree crowns: influence on light interception and leaf irradiance. *Trees*, 22(1):87–104.
- [Pearcy et al., 2005] Pearcy, R., Muraoka, H., and Valladares, F. (2005). Crown architecture in sun and shade environments: assessing function and trade-offs with a three-dimensional simulation model. *New Phytologist*, 166:791–800.
- [Pearcy et al., 2004] Pearcy, R., Valladares, F., Wright, S., and de Paulis, E. (2004). A functional analysis of the crown architecture of tropical forest psychotria species: do species vary in light capture efficiency and consequently in carbon gain and growth? *Oecologia*, 139(2):163–177.
- [Peng et al., 2008] Peng, S., Khush, G. S., Virk, P., Tang, Q., and Zou, Y. (2008). Progress in ideotype breeding to increase rice yield potential. *Field Crops Research*, 108:32–38.
- [Perez et al., 2016] Perez, R. P., Pallas, B., Mogueédec, G. L., Rey, H., Griffon, S., Caliman, J.-P., Costes, E., and Dauzat, J. (2016). Integrating mixed-effect models into an architectural plant model to simulate inter- and intra-progeny variability: a case study on oil palm (*Elaeis guineensis* Jacq.). *Journal of Experimental Botany*, page erw203.
- [Perttunen et al., 1996] Perttunen, J., Sievänen, R., Nikinmaa, E., Salminen, H., and Saarenmaa, H. (1996). Lignum: a tree model based on simple structural units. *Annals of Botany*, 77(1):87–98.
- [Phattaralerphong and Sinoquet, 2005] Phattaralerphong, J. and Sinoquet, H. (2005). A method for 3d reconstruction of tree crown volume from photographs: assessment with 3d-digitized plants. *Tree Physiology*, 25:1229–1249.
- [Pile et al., 2016] Pile, L. S., Maier, C. A., Wang, G. G., Yu, D., and Shearman, T. M. (2016). Responses of two genetically superior loblolly pine clonal ideotypes to a severe ice storm. *Forest Ecology and Management*, 360:213–220.
- [Pinheiro and Bates, 2000] Pinheiro, J. C. and Bates, M. (2000). *Mixed-Effects Models in S and S-PLUS*. Springer.
- [Plomion et al., 1996] Plomion, C., Durel, C.-E., and O’Malley, D. M. (1996). Genetic dissection of height in maritime pine seedlings raised under accelerated growth conditions. *Theor Appl Genet*, 93:849–858.
- [Pootakham et al., 2015] Pootakham, W., Jomchai, N., Ruang-areerate, P., Shearman, J. R., Sonthirod, C., Sangsrakru, D., Tragoonrung, S., and Tangphatsornruang, S. (2015). Genome-wide SNP discovery and identification of QTL associated with agronomic traits in oil palm using genotyping-by-sequencing (GBS). *Genomics*, 105(5):288–295.
- [Prieto et al., 2012] Prieto, J., Louarn, G., Perez Peña, J., Ojeda, H., Simonneau, T., and Lebon, E. (2012). A leaf gas exchange model that accounts for intra-canopy variability by considering leaf nitrogen content and local acclimation to radiation in grapevine (*Vitis vinifera* L.). *Plant, Cell and Environment*, 35(7):1313–1328.

- [Prusinkiewicz, 2004] Prusinkiewicz, P. (2004). Modeling plant growth and development. *Current Opinion in Plant Biology*, 7:79–83.
- [Prusinkiewicz and Lindenmayer, 1990] Prusinkiewicz, P. and Lindenmayer (1990). *The algorithmic beauty of plants*. Prusinkiewicz, P, springer-verlag edition.
- [Prusinkiewicz et al., 2001] Prusinkiewicz, P., Muendermann, L., Karwowski, R., and Lane, B. (2001). The use of positional information in the modeling of plants. In *Proceedings of SIGGRAPH*, Los Angeles, California.
- [R Core Team, 2015] R Core Team (2015). *R: A Language and Environment for Statistical Computing*. R Foundation for Statistical Computing, Vienna, Austria.
- [Ramirez et al., 2013] Ramirez, F. A., Armitage, R. P., and Danson, F. M. (2013). Testing the application of terrestrial laser scanning to measure forest canopy gap fraction. *Remote Sensing*, 5:3037–3056.
- [Rance et al., 2001] Rance, K., Mayes, S., Price, Z., Jack, P., and Corley, R. (2001). Quantitative trait loci for yield components in oil palm (*Elaeis guineensis* Jacq.). *Theor Appl Genet*, 103:1302–1310.
- [Raumonen et al., 2013] Raumonen, P., Kaasalainen, M., Akerblom, M., Kaasalainen, S., Kaartinen, H., Vastaranta, M., Holopainen, M., Disney, M., and Lewis, P. (2013). Fast automatic precision tree models from terrestrial laser scanner data. *Remote Sensing*, 5:491–520.
- [Rees, 1964] Rees, A. (1964). The apical organization and phyllotaxis of the oil palm. *Annals of Botany*, 28:57–69.
- [Rey et al., 2008] Rey, H., Dauzat, J., Chenu, K., Barczi, J.-F., Dosio, G., Guillermo, A., and Lecoecur, J. (2008). Using a 3-d virtual sunflower to simulate light capture at organ, plant and plot levels: Contribution of organ interception, impact of heliotropism and analysis of genotypic differences. *Annals of Botany*, 101:1139–1151.
- [Reymond et al., 2003] Reymond, M., Muller, B., Leonardi, A., Charcosset, A., and Tardieu, F. (2003). Combining quantitative trait loci analysis and an ecophysiological model to analyze the genetic variability of the responses of maize leaf growth to temperature and water deficit. *Plant Physiology*, 131(2):664–675.
- [Reynolds et al., 2000] Reynolds, M. P., van Ginkel, M., and Ribaut, J.-M. (2000). Avenues for genetic modification of radiation use efficiency in wheat. *Journal of Experimental Botany*, 51:459–473.
- [Richter et al., 2010] Richter, G., Acutis, M., Trevisiol, P., Latiri, K., and Confalonieri, R. (2010). Sensitivity analysis for a complex crop model applied to Durum wheat in the Mediterranean. *European Journal of Agronomy*, 32:127–136.
- [Rival et al., 2013] Rival, A., Ilbert, P., Labeyrie, A., Torres, E., Doubeau, S., Personne, A., Dussert, S., Beulé, T., Durand-Gasselin, T., and Tregear, J. W. (2013). Variations in genomic dna methylation during the long-term in vitro proliferation of oil palm embryogenic suspension cultures. *Plant cell reports*, 32(3):359–368.
- [Rival et al., 2008] Rival, A., Jaligot, E., Beulé, T., and Finnegan, E. J. (2008). Isolation and expression analysis of genes encoding MET, CMT, and DRM methyltransferases in oil palm (*Elaeis guineensis* Jacq.) in relation to the ‘mantled’ somaclonal variation. *Journal of Experimental Botany*, 59(12):3271–3281.
- [Rival and Levang, 2014] Rival, A. and Levang, P. (2014). *Palms of controversies: Oil palm and development challenges*. CIFOR, Bogor, Indonesia.

- [Rötter et al., 2015] Rötter, R., Tao, F., Höhn, J., and Palosuo, T. (2015). Use of crop simulation modelling to aid ideotype design of future cereal cultivars. *Journal of Experimental Botany*, page erv098.
- [Roupsard et al., 2008] Roupsard, O., Dauzat, J., Nouvellon, Y., Deveau, A., Feintrenie, L., Saint-André, L., Mialet-Serra, I., Braconnier, S., Bonnefond, J.-M., Berbigier, P., Epron, D., Jourdan, C., Navarro, M., and Bouillet, J.-P. (2008). Cross-validating sun-shade and 3d models of light absorption by a tree-crop canopy. *Agricultural and Forest Meteorology*, 148:549–564.
- [Sadras and Denison, 2016] Sadras, V. O. and Denison, R. F. (2016). Neither crop genetics nor crop management can be optimised. *Field Crops Research*, 189:75–83.
- [Sakamoto and Matsuoka, 2004] Sakamoto, T. and Matsuoka, M. (2004). Generating high-yielding varieties by genetic manipulation of plant architecture. *Current Opinion in Biotechnology*, 15:144–147.
- [Sarlikioti et al., 2011] Sarlikioti, V., de Visser, P. H. B., Buck-Sorlin, G. H., and Marcelis, L. F. M. (2011). How plant architecture affects light absorption and photosynthesis in tomato: towards an ideotype for plant architecture using a functional–structural plant model. *Annals of Botany*, 108:1065–1073.
- [Segura et al., 2008a] Segura, V., Cilas, C., and Costes, E. (2008a). Dissecting apple tree architecture into genetic, ontogenetic and environmental effects: mixed linear modelling of repeated spatial and temporal measures. *New Phytologist*, 178:302–314.
- [Segura et al., 2006] Segura, V., Cilas, C., Laurens, F., and Costes, E. (2006). Phenotyping progenies for complex architectural traits: a strategy for 1-year-old apple trees (*Malus x domestica* Borkh.). *Tree Genetics and Genomes*, 2:140–151.
- [Segura et al., 2008b] Segura, V., Ouangraoua, A., Ferraro, P., and Costes, E. (2008b). Comparison of tree architecture using tree edit distances: application to 2-year-old apple hybrids. *Euphytica*, 161:155–164.
- [Seidel et al., 2015] Seidel, D., Ammer, C., and Puettmann, K. (2015). Describing forest canopy gaps efficiently, accurately, and objectively: New prospects through the use of terrestrial laser scanning. *Agricultural and Forest Meteorology*, pages 23–32.
- [Serrano-Cartagena et al., 1999] Serrano-Cartagena, J., Robles, P., Ponce, M. R., and Micol, J. L. (1999). Genetic analysis of leaf form mutants from the *Arabidopsis* information service collection. *Molecular and General Genetics*, 261:725–739.
- [Singh et al., 2013a] Singh, R., Low, E.-T. L., Ooi, L. C.-L., Ong-Abdullah, M., Ting, N.-C., Nagappan, J., Nookiah, R., Amiruddin, M. D., Rosli, R., Manaf, M. A. A., et al. (2013a). The oil palm SHELL gene controls oil yield and encodes a homologue of SEEDSTICK. *Nature*, 500(7462):340–344.
- [Singh et al., 2013b] Singh, R., Ong-Abdullah, M., Low, E.-T. L., Manaf, M. A. A., Rosli, R., Nookiah, R., Ooi, L. C.-L., Ooi, S.-E., Chan, K.-L., Halim, M. A., et al. (2013b). Oil palm genome sequence reveals divergence of interfertile species in old and new worlds. *Nature*, 500(7462):335–339.
- [Sinoquet et al., 1997] Sinoquet, H., Rivet, P., and Godin, C. (1997). Assessment of the three-dimensional architecture of walnut trees using digitising. *Silva Fennica*, 31:265–273.
- [Sinoquet et al., 2001] Sinoquet, H., Roux, X. L., Adam, B., Ameglio, T., and Daudet, F. (2001). RATP: a model for simulating the spatial distribution of radiation absorption, transpiration and photosynthesis within canopies: application to an isolated tree crown. *Plant, Cell and Environment*, 24:395–406.
- [Smith et al., 2005] Smith, A., Cullis, B., and Thompson, R. (2005). The analysis of crop cultivar breeding and evaluation trials: an overview of current mixed model approaches. *Journal of Agricultural Science*, 143:449–462.

- [Smith and Samach, 2013] Smith, H. M. and Samach, A. (2013). Constraints to obtaining consistent annual yields in perennial tree crops. I: Heavy fruit load dominates over vegetative growth. *Plant Science*, 207:158–167.
- [Song et al., 2013] Song, Q., Zhang, G., , and Zhu, X.-G. (2013). Optimal crop canopy architecture to maximise canopy photosynthetic CO<sub>2</sub> uptake under elevated CO<sub>2</sub> – a theoretical study using a mechanistic model of canopy photosynthesis. *Functional Plant Biology*, 40:109–124.
- [Sonohat et al., 2006] Sonohat, G., Sinoquet, H., Kulandaivelu, V., Combes, D., and Lescourret, F. (2006). Three-dimensional reconstruction of partially 3D-digitized peach tree canopies. *Tree Physiology*, 26(3):337–351.
- [Sonohat et al., 2002] Sonohat, G., Sinoquet, H., Varlet-Grancher, C., Rakocevic, M., Jacquet, A., Simon, J., and Adam, B. (2002). Leaf dispersion and light partitioning in three-dimensionally digitized tall fescue–white clover mixtures. *Plant, Cell and Environment*, 25:229–238.
- [Stenberg, 1996] Stenberg, P. (1996). Simulations of the effects of shoot structure and orientation on vertical gradients in intercepted light by conifer canopies. *Tree Physiology*, 16(1-2):99–108.
- [Sultan, 2000] Sultan, S. E. (2000). Phenotypic plasticity for plant development, function and life history. *Trends in plant science*, 5(12):537–542.
- [Takenaka, 1994] Takenaka, A. (1994). Effects of leaf blade narrowness and petiole length on the light capture efficiency of a shoot. *Ecological Research*, 9:109–114.
- [Takenaka et al., 1998] Takenaka, A., Inui, Y., , and Osawa, A. (1998). Measurement of three-dimensional structure of plants with a simple device and estimation of light capture of individual leaves. *Functional Ecology*, 12:159–165.
- [Takenaka et al., 2001] Takenaka, A., Takahashi, K., and Kohyamas, T. (2001). Optimal leaf display and biomass partitioning for efficient light capture in an understorey palm, *Licuala arbuscula*. *Functional Ecology*, 15:660–668.
- [Talliez and Koffi, 1992] Talliez, B. and Koffi, C. B. (1992). A method for measuring oil palm leaf area. *Oléagineux*, 47:537–545.
- [Tang, 1993] Tang, B. (1993). Orthogonal array-based latin hypercubes. *Journal of the American statistical association*, 88(424):1392–1397.
- [Tang et al., 2015] Tang, L., Hou, C., Huang, H., Chen, C., Zou, J., and Lin, D. (2015). Light interception efficiency analysis based on three-dimensional peach canopy models. *Ecological Informatics*, 30:60–67.
- [Tardieu, 2003] Tardieu, F. (2003). Virtual plants: modelling as a tool for the genomics of tolerance to water deficit. *Trends in Plant Science*, 8(1):9 – 14.
- [Thornley, 1998] Thornley, J. (1998). Dynamic model of leaf photosynthesis with acclimation to light and nitrogen. *Annals of Botany*, 81:421–430.
- [Thurling, 1991] Thurling, N. (1991). Application of the ideotype concept in breeding for higher yield in the oilseed brassicas. *Field Crops Research*, 26:201–219.
- [Tisné et al., 2015] Tisné, S., Denis, M., Cros, D., Pomiès, V., Riou, V., Syahputra, I., Omoré, A., Durand-Gasselin, T., Bouvet, J.-M., and Cochard, B. (2015). Mixed model approach for IBD-based QTL mapping in a complex oil palm pedigree. *BMC Genomics*, 16(798).

- [Truong et al., 2015] Truong, S. K., McCormick, R. F., Rooney, W. L., and Mullet, J. E. (2015). Harnessing genetic variation in leaf angle to increase productivity of sorghum bicolor. *Genetics*, 201:1229–1238.
- [Vaccari et al., 2013] Vaccari, S., van Leeuwen, M., Calders, K., Coops, N. C., and Herold, M. (2013). Bias in lidar-based canopy gap fraction estimates. *Remote Sensing Letters*, 4(4):391–399.
- [Valladares and Brites, 2004] Valladares, F. and Brites, D. (2004). Leaf phyllotaxis: Does it really affect light capture? *Plant Ecology*, 174(1):11–17.
- [Valladares et al., 2002] Valladares, F., Skillman, J. B., and Pearcy, R. W. (2002). Convergence in light capture efficiencies among tropical forest understory plants with contrasting crown architecture: a case of morphological compensation. *American Journal of Botany*, 89(8):1275–1284.
- [Van der Zande et al., 2011] Van der Zande, D., Stuckens, J., Verstraeten, W. W., Mere, S., Muys, B., and Coppin, P. (2011). 3D modeling of light interception in heterogeneous forest canopies using ground-based LiDAR data. *International journal of Applied Earth Observation and Geoinformation*, 13:792–800.
- [Van Kraalingen et al., 1989] Van Kraalingen, D., Breure, C., and Spitters, C. (1989). Simulation of oil palm growth and yield. *Agricultural and Forest Meteorology*, 46:227–244.
- [Vilela et al., 2008] Vilela, A., Cariaga, R., González-Paleo, L., and Ravetta, D. (2008). Trade-offs between reproductive allocation and storage in species of *Oenothera* L. (Onagraceae) native to argentina. *Acta Oecologica*, 33(11):85–92.
- [Vos et al., 2010] Vos, J., Evers, J. B., Buck-Sorlin, G. H., Andrieu, B., Chelle, M., and de Visser, P. H. B. (2010). Functional-structural plant modelling: a new versatile tool in crop science. *Journal of Experimental Botany*, 61(8):2101–2115.
- [Wang et al., 2014] Wang, N., Huang, Q., Sun, J., Yan, S., Ding, C., Mei, X., Li, D., Zeng, X., Su, X., and Shen, Y. (2014). Shade tolerance plays an important role in biomass production of different poplar genotypes in a high-density plantation. *Forest Ecology and Management*, 331:40–49.
- [Wang and Li, 2005] Wang, Y. and Li, J. (2005). The plant architecture of rice (*Oryza sativa*). *Plant Molecular Biology*, 59(1):75–84.
- [Weiss and Baret, 2010] Weiss, M. and Baret, F. (2010). *CAN-EYE user manual*.
- [Welham et al., 2002] Welham, C. V. J., Turkington, R., and Sayre, C. (2002). Morphological plasticity of white clover (*Trifolium repens* L.) in response to spatial and temporal resource heterogeneity. *Oecologia*, 130:231–238.
- [Willaume et al., 2004] Willaume, M., Lauri, P.-É., and Sinoquet, H. (2004). Light interception in apple trees influenced by canopy architecture manipulation. *Trees*, 18(6):705–713.
- [Woodgate et al., 2015] Woodgate, W., Jones, S. D., Suarez, L., Hill, M. J., Armston, J. D., Wilkes, P., Soto-Berelov, M., Haywood, A., and Mellor, A. (2015). Understanding the variability in ground-based methods for retrieving canopy openness, gap fraction, and leaf area index in diverse forest systems. *Agricultural and Forest Meteorology*, pages 83 – 95.
- [Wu and Stettler, 1998] Wu, R. and Stettler, R. (1998). Quantitative genetics of growth and development in populus. iii. phenotypic plasticity of crown structure and function. *Heredity*, 81:299–310.
- [Xu et al., 2011] Xu, L., Henke, M., Zhu, J., Kurth, W., and Buck-Sorlin, G. (2011). A functional-structural model of rice linking quantitative genetic information with morphological development and physiological processes. *Annals of Botany*, page mcq264.

- [Xue et al., 2015] Xue, H., Han, Y., Li, Y., Wang, G., Feng, L., Fan, Z., Du, W., Yang, B., Cao, C., and Mao, S. (2015). Spatial distribution of light interception by different plant population densities and its relationship with yield. *Field Crops Research*, 184:17–27.
- [Yang et al., 2016] Yang, W.-W., Chen, X.-L., Saudreau, M., Zhang, X.-Y., Zhang, M.-R., Liu, H.-K., Costes, E., and Han, M.-Y. (2016). Canopy structure and light interception partitioning among shoots estimated from virtual trees: comparison between apple cultivars grown on different interstocks on the Chinese Loess Plateau. *Trees*, pages s00468–016–1403–8.
- [Yang and Hwa, 2008] Yang, X.-C. and Hwa, C.-M. (2008). Genetic modification of plant architecture and variety improvement in rice. *Heredity*, 101:396–404.
- [Yin et al., 1999] Yin, X., Kropff, M. J., and Stam, P. (1999). The role of ecophysiological models in qtl analysis: the example of specific leaf area in barley. *Heredity*, 82:415–421.
- [Zhu et al., 2015] Zhu, J., van der Werf, W., Anten, N. P. R., Vos, J., and Evers, J. B. (2015). The contribution of phenotypic plasticity to complementary light capture in plant mixtures. *New Phytologist*, 207:1213–1222.







## Abstract

The development of new breeding strategies to find more sustainable and productive systems is a major challenge to cope with ceaseless increasing demands for vegetable oils, notably palm oil. Optimizing plant architecture to increase radiation interception efficiency could be an option for enhancing potential oil palm production. Indeed, studies in cereals showed great improvement of yields by altering plant architecture, in combination with agronomic practices. By analogy, we proposed to investigate the influence of oil palm architecture on the capacity of the plant to intercept light, by using 3D reconstructions and model-assisted evaluation of radiation-use efficiency. The first objective of this study was to analyse and model oil palm architecture and light interception taking into account genetic variability. A second objective was to explore the potential improvement in light capture and carbon assimilation by manipulating oil palm leaf traits and propose architectural ideotypes.

Data were collected in Sumatra, Indonesia, on five progenies (total of 60 palms), in order to describe the aerial architecture from leaflet to crown scales. Allometric relationships were applied to model these traits according to ontogenetic gradients and leaf position within the crown. The methodology allowed reconstructing virtual oil palms at different stages over plant development. Additionally, the allometric-based approach was coupled to mixed-effect models in order to integrate inter and intra progeny variability through progeny-specific parameters. The model thus allowed simulating the specificity of plant architecture for a given progeny while including observed inter-individual variability. The architectural model, once parameterized for the different progenies, was then implemented in AMAPstudio to generate 3D mock-ups and estimate light interception efficiency, from individual to stand scales.

Model validations were performed at different scales. Firstly at organ scale, the geometry of the stem, the leaves and the leaflets were compared between virtual mock-ups and actual plants measured in the field. Secondly, at plant scale with indicators derived from terrestrial laser scanning (TLS) to assess crown dimensions and porosity. These indicators integrated topological and geometrical information related to the amount of light intercepted by an individual. Finally, validations were performed at plot scale using hemispherical photographs (HP) to assess the variability of canopy openness for the five studied progenies.

Significant differences in leaf geometry (petiole length, density of leaflets and rachis curvature) and leaflets morphology (gradients of leaflets length and width) were detected between and within progenies, and were accurately simulated by the modelling approach. The comparison of plant area obtained from TLS and virtual TLS highlighted the capacity of the model to generate realistic 3D mock-ups. The architectural variabilities observed at plot scale between and within progenies were also satisfactory simulated. Finally, light interception estimated from the validated 3D mock-ups showed significant variations among the five progenies.

Sensitivity analyses (Morris method and metamodeling approach) were then performed on a subset of architectural parameters in order to identify the architectural traits impacting light interception efficiency and potential carbon assimilation over plant development. Daily carbon assimilation was estimated with a photosynthesis model coupled to the radiative balance model, which enabled to integrate the temporal and spatial variations of photosynthetic organ irradiances.

The most sensitive parameters over plant development were those related to leaf area (rachis length, number of leaflets, leaflets morphology), although fine attribute related to leaf geometry showed increasing influence when canopy got closed. In adult stand, optimized carbon assimilation was estimated on plants presenting a leaf area index (LAI) between 3.2 and 5.5  $\text{m}^2.\text{m}^{-2}$ , with erect leaves, short rachis and petiole and high number of leaflet on rachis. Four ideotypes were identified with respect to carbon assimilation, exhibiting specific geometrical features that optimize light distribution within plant crown and reduce mutual shading among plants.

In conclusion, this study highlighted how a functional-structural plant model (FSPM) can be used to virtually explore plant biology. In our case, the 3D model of oil palm, in its conception and its application, enabled the detection of the architectural traits genetically determined and influencing light interception. The limited number of traits revealed in the sensitivity analysis and the combination of traits proposed through ideotypes could guide future breeding programs. Forthcoming work will be dedicated to integrate in the modeling approach other physiological processes such as stomatal conductance and carbon partitioning. The improved FSPM could then be used to test different scenarios, for instance in climate change context with low radiations or frequent drought events. Similarly, the model could be used to investigate different planting patterns and intercropping systems and propose new multi-criteria ideotypes of oil palm.

**Keywords:** carbon assimilation, FSPM, hemispherical photographs, ideotype, light interception efficiency, mixed-effect model, plant architecture, progeny, terrestrial LiDAR, three-dimensional reconstruction, sensitivity analysis

